Metabolic engineering approaches reveal widespread physiological functions of membrane lipids for *Saccharomyces cerevisiae*

Vom Fachbereich Biologie der Technischen Universität Darmstadt

zur Erlangung des akademischen Grades

eines *Doctor rerum naturalium*

genehmigte Dissertation von

M.Sc. Daniel Degreif

aus Mainz

1. Referent: Prof. Dr. Adam Bertl

2. Referent: Prof. Dr. Gerhard Thiel

Tag der Einreichung: 05.12.2017

Tag der mündlichen Prüfung: 25.01.2018

Darmstadt 2018

D 17

Summary

The lipid composition of biological membranes can differ significantly between organisms and even between organelles of the same cell in terms of lipid compounds and specific ratios of lipid classes. Referring to this, every membrane features a characteristic lipid composition that is thought to regulate its physicochemical properties and cellular function by providing lipid environments supporting the integrity of membrane-localized protein machinery and membrane-associated processes. **Chapter I** gives a brief overview of the interlinkage between the chemical nature of membrane lipids, the structural and functional organization as well as the physicochemical properties of lipid bilayers and their influence on membrane-embedded proteins.

Studies to gain detailed knowledge on how membrane lipid composition influences the physiology of cells and regulates cellular processes require tools to manipulate lipid composition *in vivo*. By employing metabolic engineering approaches based on titratable gene expression tools, sets of *Saccharomyces cerevisiae* strains in which membrane lipid composition is under experimental control were engineered. The study described in **Chapter II** addresses *OLE1*, encoding for the sole fatty acid desaturase of budding yeast, to control the extent of acyl unsaturation of fatty acids incorporated in phospholipids. This approach revealed cellular roles for the physical state of cell membranes, so called membrane fluidity, on yeast flocculation and hypoxic growth. It is shown, how the endogenous lipid homeostasis machinery of budding yeast is adapted to carry out a broad response to oxygen limitation (hypoxia) and how it activates a non-canonical yeast flocculation pathway involving *FLO1*, which encodes for cell wall glycoproteins that mediate cell-cell-interactions by binding cell wall mannose residues of adjacent cells.

In **Chapter III**, the previously generated strain in which expression of *OLE1* is under experimental control was used as a cellular platform to assay the activity of heterologously expressed stearoyl-CoA desaturases (SCDs). Putative SCDs from human pathogens *T. brucei* and *T. cruzi* were functionally expressed in *S. cerevisiae*, thereby additionally confirming their SCD activity *in vivo*. The presented assay might also provide a tool to screen for inhibitors of SCDs, which are interesting drug targets in the treatment of bacterial and parasitic infections in humans.

The study presented in **Chapter IV** addresses *ERG9*, an essential gene involved in the ergosterol biosynthetic pathway and used a metabolic engineering approach to achieve control over the total sterol biosynthetic activity of the cell. Cells that allowed for manipulating the native sterol homeostasis were employed to unveil physiological effects of ergosterol and total sterol depletion on the cell's general viability as well as on fundamental

membrane associated processes such as protein sorting and endo- and exocytosis. By combining this metabolic engineering approach and the powerful method of marker-free CRISPR/Cas9-mediated gene tagging, it was possible to establish a cellular system for investigating the impact of sterol depletion on the lateral distribution pattern of lipid-raft associated GFP-tagged membrane proteins within the plasma membrane of yeast.

Chapter V introduces a novel set of all-in-one constitutive and inducible CRISPR/Cas9 vectors that allow for a very easy and highly convenient application of the technology in *S. cerevisiae*. The simplicity of the inducible system is based on the possibility of introducing a desired gRNA targeting sequence with homologous recombination-mediated assembly of overlapping single-stranded oligonucleotides. The inducible Cas9 expression approach also introduces the novel concept of chronologically separating the cloning procedure from the actual genome editing step by preloading cells with an all-in-one CRISPR/Cas9 plasmid. This way, CRISPR/Cas9-supported genome editing can be obtained with high efficiency and effectivity by just transforming a desired preloaded target strain with donor DNA to be genomically integrated without the need of co-introducing any of the CRISPR system components. These novel CRISPR/Cas9 systems will help to overcome limitations often observed for challenging metabolic and genetic engineering approaches that can be e.g. used for following studies to reveal physiological roles of membrane lipids for budding yeast.

Zusammenfassung

Biologische Membranen unterschiedlicher Organismen, aber auch von Zellen des gleichen Organismus und sogar Organellen der gleichen Zelle können sich hinsichtlich ihrer spezifischen Lipidzusammensetzung deutlich voneinander unterscheiden. Jede Membran weist dabei eine charakteristische Lipidkomposition auf, die sowohl die physikochemischen Eigenschaften als auch die biologische Funktion dieser Membran maßgeblich bestimmt, indem spezifische Lipid-Umgebungen zur Verfügung gestellt werden, die für die Integrität der Membran-lokalisierten Protein-Maschinerie und Membran-assoziierter zellulärer Prozesse essentiell ist. **Kapitel I** gibt einen kurzen Überblick über die chemische Struktur prominenter Membranlipide, die damit eng verbundenen physikochemischen Eigenschaften membranärer Lipid-Bilayer, sowie die Beeinflussung der Funktion Membran-inkorporierter Proteine durch diese Membrancharakteristika.

Studien zur Aufklärung des Einflusses der Lipidkomposition auf die allgemeine Zellphysiologie sowie Regulation zellulärer Prozesse benötigen effiziente Methoden zur Manipulation der Lipidkomposition *in vivo*. Metabolic Engineering Ansätze in Verbindung mit Methoden zur Regulation von Genexpression wurden dabei genutzt, um *Saccharomyces cerevisiae* Stämme zu generieren, die eine gezielte und experimentell kontrollierbare Veränderung ihrer Lipidkomposition erlauben. Die in **Kapitel II** beschriebene Studie adressiert dabei die einzige in *S. cerevisiae* vorkommende Fettsäure-Desaturase (codiert durch *OLE1*), um experimentelle Kontrolle über den Sättigungsgrad Phospholipid-inkorporierter Fettsäuren und somit der Gesamtheit des Hefelipidoms zu erlangen. Dieser Ansatz offenbarte zelluläre Funktionen eines wichtigen physikalischen Membranparameters, der sogenannten Membranfluidität, für Prozesse wie die Ausbildung eines Flockulierungsphänotypes sowie Anpassung an hypoxische Wachstumsbedingungen. Die präsentierte Studie zeigt, wie die Hefe-endogene Lipid-Homöostase-Maschinerie dazu genutzt wird, eine umfangreiche zelluläre Antwort auf Sauerstoff-limitierende Umgebungsbedingungen (Hypoxie) einzuleiten und Zell-Zell-Aggregation in Form von Flo1p-vermittelter Flockulierung zu induzieren. Dieser Aggregationsphänotyp basiert dabei auf der von Flo1p als Zellwand-verankertes Glykoproteins vermittelten Fähigkeit zur spezifischen Bindung der von der Zellwand benachbarter Hefezellen präsentierten Mannosylseitenketten.

Die in **Kapitel III** beschriebene Studie nutzt die zuvor generierten Stämme mit experimentell kontrollierbarer *OLE1*-Expression als zelluläre Plattform zum Nachweis der enzymatischen Aktivität heterolog exprimierter Stearoyl-CoA-Desaturasen (SCDs). Mutmaßliche SCDs der beiden humanpathogenen Parasiten *T. brucei* und *T. cruzi* wurden dabei funktional in *S. cerevisiae* exprimiert und auf diese Weise gleichsam ihre Stearoyl-CoA Desaturase-

Aktivität *in vivo* nachgewiesen. Das vorgestellte Assay eignet sich daher ebenfalls als Werkzeug zum Hefe-basierten Screening von SCD-Aktivität inhibierenden Substanzen, die als vielversprechende Medikamente zur Behandlung bakterieller und parasitärer Infektionen des Menschen gelten und teilweise bereits Einsatz finden.

Kapitel IV beschreibt die Nutzung eines *ERG9*-adressierenden Metabolic Engineering Ansatzes, um experimentelle Kontrolle über die Sterol-Biosythese-Aktivität von *S. cerevisiae* zu erlangen. *ERG9* codiert für eine Squalen-Synthase, die als sogenanntes „Gate-Keeper Enzym" den Metabolit-Flux in Richtung des linearen Ergosterol-Biosyntheseweges zu regulieren in der Lage ist. Zellen mit manipulierbarer Sterol-Homöostase und verringertem Ergosterol-Gehalt wurden dazu genutzt, um den Einfluss von Membransterolen auf die generelle Zell-Viabilität aber auch auf fundamentale Zellmembran-assoziierte Prozesse wie Protein Sorting sowie Endo- und Exocytose zu untersuchen. Durch Kombination dieses Metabolic Engineering Ansatzes und CRISPR/Cas9-vermittelter Marker-freier Genom-Editierung war es zudem möglich, ein zelluläres System zur Untersuchung des Einflusses einer Verarmung von Membransterolen auf das laterale Verteilungsmuster Lipid-Raft-assoziierter GFP-getaggter Membranproteine in der Plasmamembran der Bäckerhefe zu etablieren.

In **Kapitel V** wird ein neuartiges, induzierbares oder konstitutives *all-in-one* CRISPR/Cas9-Plasmidsystem zur einfachen und komfortablen Anwendung dieser Technologie in *S. cerevisiae* vorgestellt. Die Einfachheit des vorgestellten induzierbaren Systems liegt dabei in der Möglichkeit zur bequemen Einklonierung einer gewünschten, in der gRNA codierenden Sequenz enthaltenen Protospacer-Sequenz begründet. Die Einführung der Protospacer-Sequenz beruht dabei alleine auf einer wenig arbeitsintensiven homologen Rekombinations-vermittelten Assemblierung von einzelsträngigen DNA-Oligonukleotiden *in vivo*. Gleichsam führt das vorgestellte induzierbare CRISPR/Cas9-System, mit dem zu modifizierende Zellen vor dem eigentlichen Genom-Editierungsschritt vorgeladen werden können, ein neuartiges Konzept der chronologischen Separierung essentieller Arbeitsschritt (Plasmidklonierung, Genom-Editierung), gepaart mit hoher Transformationseffizienz sowie einfacher Anwendbarkeit, ein. Eine hohe Effizienz und Effektivität der Genom-Editierung wird dadurch gewährleistet, dass Komponenten des CRISPR/Cas9-Systems sowie die genomisch zu integrierende Donor-DNA zeitlich getrennt in die Zelle eingeschleust werden können, wodurch eine multiplikative Verknüpfung unvorteilhafter Einzeltransformationseffizienten umgegangen wird. Dieses neuartige Plasmid-basierte CRISPR/Cas9-System eignet sich folglich dazu, Transformationseffizienz-bedingte Limitierungen von Metabolic und Genetic Engineering Ansätzen zu überwinden, die wiederum für nachfolgende Studien zur Aufklärung physiologischer Funktionen von Membranlipiden von Nutzen sind.

Table of contents

Chapter I

General introduction

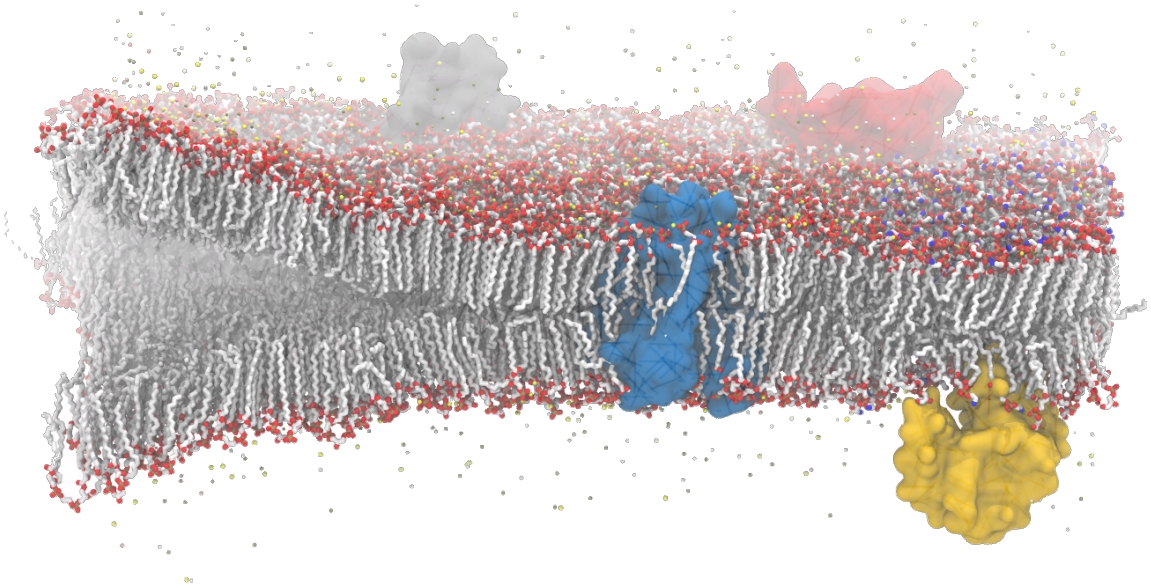

1. Chapter I: General introduction

1.1. Biological membranes

Biological membranes are essential structures of cellular systems. Their primary function consists in the physical separation of cell internal structures from the external environment [1]. Due to their physicochemical properties, they build up an almost impermeable barrier for hydrophilic and charged molecules and ions. Specialized membrane embedded proteins or fusion and fission of membrane material are required to mediate and control the exchange of substances and energy between cells and their environment by active or passive transport processes, thereby emphasizing the regulatory function of biological membranes [2]. In an equivalent manner, cell membranes are involved in the exchange of information, perception of extracellular signals and cell-cell communication [1]. Specialized proteins within biological membranes register specific messenger molecules [3] and immaterial signals and stimuli such as electromagnetic radiation (light [4], infrared (thermal) radiation [5]) or electric potential differences [6] and respond in a coordinated manner by undergoing changes in protein conformation or spatial organization in order to transmit signals into the cell's interior. Eukaryotic cells feature additional internal membrane structures, thereby constituting separated cellular compartments that enable to spatially segregate chemical reactions for the purpose of providing optimal reaction conditions to ensure maximal biochemical efficiency as well as restricted dissemination of generated reaction products [2].

From a chemical point of view, cellular membranes are constituted by amphiphilic (amphipathic) lipids that form a double layer (bilayer) in which membrane proteins are embedded in by means of hydrophobic, electrostatic or non-covalent interactions. Lipid bilayers are typically ~40 Å thick, however, the exact thickness depends on the composition of the membrane and varies between organelles [7]. The principle organization of biological membranes as lipid bilayers was already hypothesized in 1925 by Gorter and Grendel [8]. However, this model did not take into account that biological membranes are equipped with proteins that determine the biological function of the membrane. The fluid mosaic model by Singer and Nicolson from 1972 [9] described biological membranes as a fluid lipid bilayer in which membrane proteins can be fully embedded in (integral proteins), are associated with or only penetrate peripheral regions of the bilayer (peripheral proteins) or are anchored to the membrane as they are covalently attached to strongly hydrophobic molecules such as lipids (lipid anchored proteins). Proteins and lipids can freely diffuse within the two dimensional bilayer, thus forming a homogenous protein-lipid mixture. Although, the fluid

mosaic model is still a well-accepted model [10], it cannot be fully correct as it will be discussed later.

The structured organization of membrane lipids in bilayers is guaranteed by their hydrophilic and lipophilic properties which allows them to undergo a thermodynamically/entropically driven spontaneous self-association in an aqueous milieu. The hydrophobic moieties of membrane lipids face to the interior of the bilayer thereby forming a hydrophobic core of the membrane whereas lipophobic parts of membrane lipids face towards to hydrophilic external milieu and constitute the surface of the membrane. The driving force of this spontaneous self-assembly is the interaction of hydrophilic parts of the lipids with the aqueous milieu and not the association of their non-polar structural elements. This effect referred to as “hydrophobic effect” [11] originates from the fact that non-polar molecules are not able to form hydrogen bonds with water, thereby disrupting the hydrogen bonding network between water molecules in the aqueous phase [12]. Water molecules in close contact of hydrophobic elements of membrane lipids are reoriented in order to minimize the disruption of the hydrogen bonding network. Due to this reorientation and additional limitation of interaction partners at the non-polar surface to form hydrogen bonds, water molecules get caged and feature restricted translational and rotational degrees of freedom thus leading to an overall reduced entropy of the system which makes the process unfavorable in terms of free energy. From thermodynamics, it is therefore favorable to reduce the amount of hydrophobically hydrated non-polar molecules, or rather that non-polar molecules reduce the area exposed to water e.g. by self-aggregation. Thus, self-assembly of membranous bilayers with hydrophobic parts of lipid molecules interacting with each other allows to effectively maximize the free energy of the system [13]. This way, polar structural elements of membrane lipids shield the hydrophobic core of the bilayer from the aqueous solvent.

1.2. Membrane lipids

The main lipids of cellular membranes are glycerophospholipids, sphingolipids, sterols and cardiolipins [1]. Glycerophospholipids contain a central glycerol moiety whose hydroxyl groups in *sn-1* and *sn-2* position are esterified with two fatty acids. The hydroxyl group in *sn-3* position is esterified to a phosphoric acid group that can be further esterified to different alcohols that determine the functional and physicochemical properties of the polar head group. Alcohols often found to be incorporated in glycerophospholipid head groups are ethanolamine, serine, choline glycerol and inositol but also a free phosphate group exists as in case of phosphatidic acid [1]. The enormous diversity of this class of membrane lipids arises from the combination of different head group alcohols and glycerophospholipid-incorporated fatty acids with different length and degree of unsaturation as well as the

specific positions of double bonds. Fatty acids in bacteria can even feature branched acyl chains [14]. The most abundant glycerophospholipids of *S. cerevisiae* are phosphatidic acid (PA), phosphatidylcholine (PC), phosphatidylethanolamine (PE), phosphatidylinositol (PI) and phosphatidylserine (PS) (Fig. I-1A). The fatty acid composition of these lipids is mostly limited to palmitic acid (C16:0), palmitoleic acid (C16:1), stearic acid (C18:0) and oleic acid (C18:1) and only traces of fatty acids with shorter and longer carbon chains are found [15].

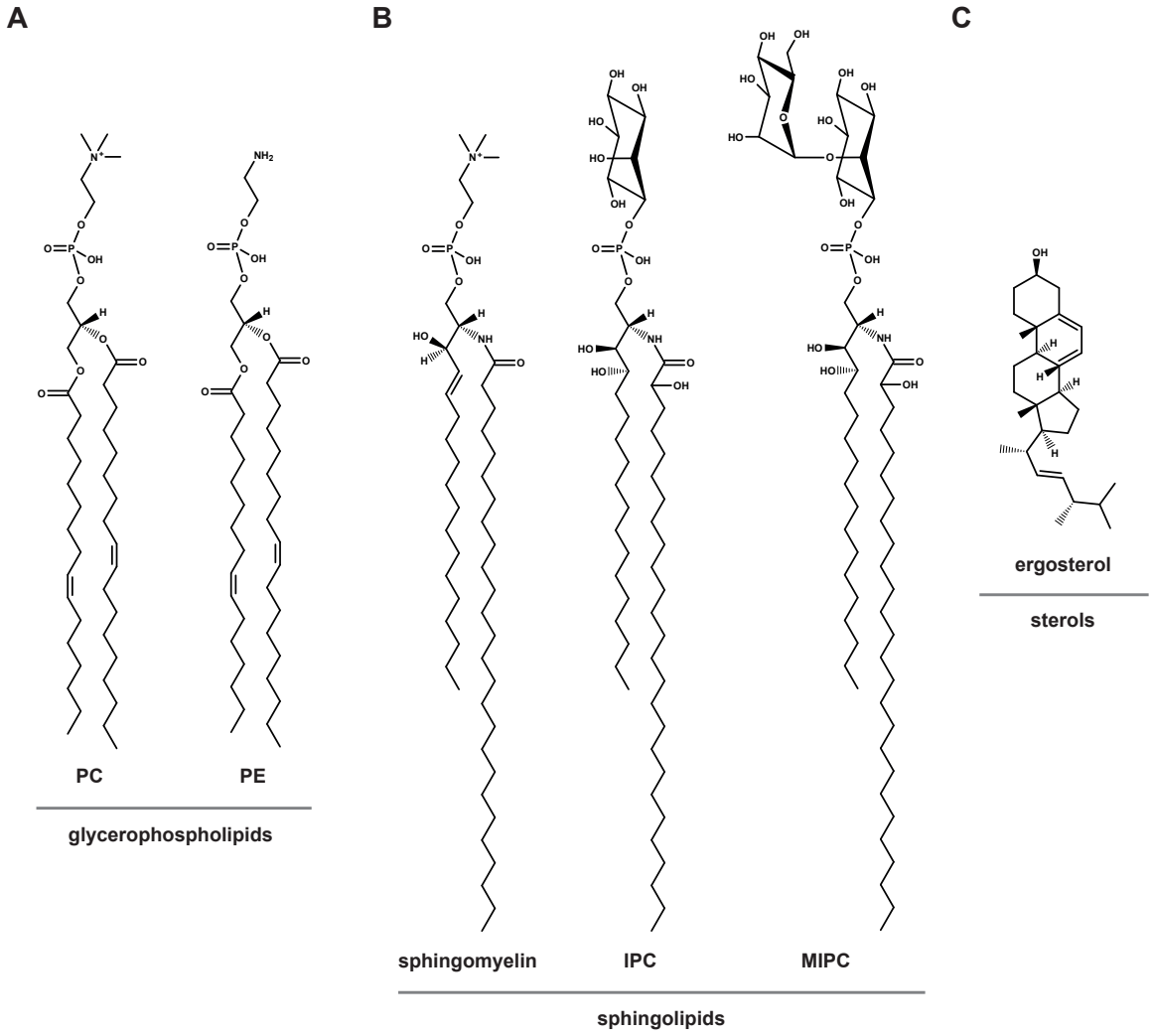

Fig. I-1: Chemical structures of representatives from abundant membrane lipid classes of *S. cerevisiae*. (A) Indicated are representatives of glycerophospholipids featuring different head groups. Glycerophospholipids contain a central glycerol moiety that is esterified with two fatty acids and a phosphoric acid group that is further esterified with an alcohol such as choline (phosphatidylcholine (PC)) or ethanolamine (phosphatidylethanolamine (PE)). Phospholipids from *S. cerevisiae* often contain monounsaturated fatty acids with a chain length of 16- and 18- carbon atoms (C16:1 and C18:1). **(B)** Sphingolipids are composed of a central sphingosine molecule that is linked to a mostly very long chain saturated fatty acid (e.g. C26:0) via an amide bond. Sphingomyelins feature head groups identical to glycerophospholipids (phosphocholine or phosphoethanolamine) and are therefore ranked among the class of phospholipids. Abundant sphingolipids of *S. cerevisiae* are inositol-phosphorylceramid (IPC) and mannosyl-inositol-phosphorylceramide (MIPC). These sphingolipids contain phytoshingosine as long chain base (instead of sphingosine) which is further linked to a α-hydroxylated very long chain fatty acid. **(C)** Ergosterol is the most prominent sterol of yeast cells. Chemical structures were generated with the LIPID MAPS Online Tools [16] and visualized by MoleculeSketch (version 1.6.2).

Sphingolipids feature a sphingosine (or derivatives) backbone that already contains a long saturated hydrocarbon chain (therefore called long chain bases) and is further linked to a primary saturated fatty acid via an amide bond. The C1 hydroxyl group of the central sphingosine backbone can be, similar to glycerophospholipids, esterified to a phosphoric acid group that can be also further esterified to different alcohols (mainly ethanolamine and choline) [1]. Due to this characteristic architecture, these sphingomyelines (Fig. I-1B) are ranked among the group of phospholipids. In contrast to that, ceramides feature an unmodified sphingosine C1 hydroxyl group, whereas the respective HO group is glycosidically linked to single sugars or sugar chains in glycosphingolipids (cerebrosides and gangliosides). The yeast sphingolipidome mainly consists of inositol-phosphorylceramide (IPC), mannosyl-inositol-phosphorylceramide (MIPC) and mannosyl-di-(inositolphosphoryl)ceramide ($M(IP)_2C$). The ceramide backbone of these sphingolipids contains phytosphingosine (instead of sphingosine) which is linked to a very long chain fatty acid (mostly α-hydroxylated C26:0) via an amide bond [15] (Fig. I-1B).

Another class of membrane lipid that is found in almost all eukaryotic cellular membranes and even in membranes of some prokaryotes are sterols. The most prominent sterol of animal cells is cholesterol, whereas fungi such as *S. cerevisiae* synthesize a highly similar sterol, ergosterol, instead (Fig. I-1C). All membrane sterols feature similar physicochemical properties and play therefore identical roles for the organization of biological membranes. The hydrophobic, planar chemical structure of sterols allows them to intercalate between phospholipids and to favorably interact with their hydrocarbon chains. The hydroxyl group of membrane sterols is typically faced towards the polar surface of the bilayer thereby allowing to interact with the polar head groups of phospholipids via hydrogen bonds. According to the umbrella model [17], sterols preferentially interact with sphingolipids whose head groups physically shield them from the aqueous phase on both sides of the bilayer. Since sphingolipids contain saturated, *trans*-configured hydrocarbon chains, they are able to form taller cylinders that can pack more tightly compared the glycerophospholipids containing unsaturated, stably *cis*-configured fatty acids. Sterols intercalating between the straight hydrocarbon chains of sphingolipid-rich membrane areas break up their tight packing, thus functioning as fluidizers in tightly packed membranes [2, 18]. On the other hand, sterols condense loosely-packed membranes by reducing the average area covered by each molecule within the lipid bilayer [19, 20] and increasing membrane surface density and rigidity [21], which affects e.g. the water permeability of the bilayer [22]. The condensing effect is closely related to the so-called ordering effect of sterols on fluid phase membranes. This effect is characterized by a reduced content of sterically hindering *gauche* and *eclipse* conformations and an increased percentage of stabilized *trans* conformations of the C-chains torsion angles within the long hydrocarbon chains of saturated fatty acids when

interacting with the smooth α-faces of sterols [23]. This way, straightened hydrocarbon chains can pack more tightly thereby rigidifying highly fluid membranes and reducing the average volume of a lipid molecule. These opposite functions emphasize the dual nature of membrane sterols and their roles for regulating membrane fluidity and phase behavior as well as broadening the temperature range in which transition between the solid-ordered (solid-gel) and liquid-disordered (liquid-crystalline) phase behavior takes place [24].

1.3. Lipid domains and phase behavior

The phase behaviors of biological membranes are determined to a great extent by the chemical structures of their components as well as by their thermal energization.

At low temperatures, the hydrocarbon chains of fully saturated fatty acids are as much expanded as possible, with sterically preferable all single C-C bonds in *trans* conformation (all-*trans*; also *anti* conformation) thereby maximizing van-der-Waals intermolecular interactions. The high proportion of straightened fatty acyl chains as well as the network of van-der-Waals interactions lead to a densely packed, highly ordered membrane structure [25]. These bilayers are characterized by a high order parameter of their lipids as well as an extremely small lateral (translational) diffusion coefficient (D_T = ~10^{-3} $\mu m^2 \cdot s^{-1}$) [2], therefore impeding lateral diffusion of membrane lipids and embedded proteins. This lipid phases are designated as solid-ordered (s_o; solid gel) phases which is thought to not support biological function in general, although proteins such as the Ca^{2+}-ATPase can show low activities in gel phase lipid bilayers [26].

With increasing temperature (higher than the thermotropic phase transition temperature T_m), solid-ordered membrane phases are converted into membranes with so-called liquid-disordered (L_d; liquid-crystalline) phase behavior [25]. This conversion results from rotations of C-atoms around the C-C single bond axes within the hydrocarbon chains of saturated fatty acids, the so-called *trans-gauche* isomerization [27] (Fig. I-2A). These rotations are accompanied by thermodynamically unfavorable, sterically hindering *gauche* and *eclipse* conformations that are facilitated in a higher energized (thermal energy) system. C-C single bonds with *eclipse*/*gauche* conformation are pseudo *cis*-configured, thus introducing a kinked structure of fatty acid hydrocarbon chains which strongly impedes a dense lipid packing and ordering. Such liquid-disordered membranes are therefore characterized by a low ordering parameter and a high lateral diffusion coefficient (D_T = ~1 $\mu m^2 \cdot s^{-1}$) [2], thus enabling fast translational and rotational diffusion of membrane components (Fig. I-2B) which is considered to be essential for the integrity of membrane associated biological processes.

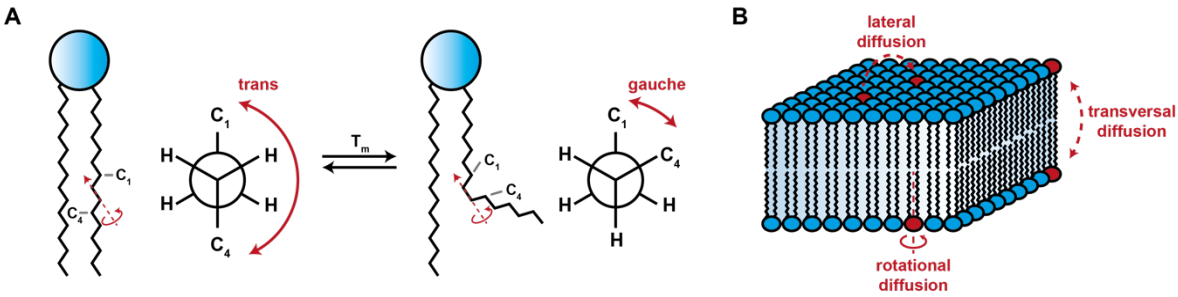

Fig. I-2: Schematic illustration of the dynamics of membrane lipids. (A) Straight fatty acid chains of fully saturated fatty acids with all-*trans* conformation undergo thermally induced conformational changes (*trans-gauche* isomerization). C-C single bonds with *gauche* conformation induce a kinked structure of the fatty acids acyl chains which strongly impedes a dense lipid packing and ordering. Temperatures higher than the thermotropic phase transition temperature (T_m) strongly affect the conformational order of lipid molecules thereby inducing a transition of the phase state of biological membranes. Newman projections of C-C single bonds with *trans* and *gauche* conformations are shown as an example. Blue circles represent the head groups of phospholipids and jagged lines depict the hydrocarbon chains of phospholipid-incorporated fatty acids. **(B)** Lipids in biological bilayers undergo lateral, rotational and transversal diffusion. Lateral and rotational diffusion rates of lipids depend on the phase state of the bilayer. Highly-ordered bilayers impede lateral and rotational diffusion whereas fluid-disordered membranes allow lipid molecules to diffuse quickly. Adapted from [25].

Besides thermal energy, the phase behavior of biological membranes is determined to a great extent by the chemical character of the membrane lipids and their included fatty acids. Unsaturated fatty acids with *cis*-configured C-C double bonds possess conformationally stable kinked structures that are equivalent to those resulting from C-C single bonds with *eclipse* conformation but do not depend on the thermal energization of the membranous system. The incorporation of unsaturated fatty acids in membrane lipids can thus maintain a liquid-disordered phase state of membranes even at temperatures that do not support *eclipse* configured rotameric structures.

Unsaturated fatty acids are mostly found in membrane glycerophospholipids so that these tend to form and be enriched in liquid-disordered phases, whereas sphingolipids that mostly contain long, saturated hydrocarbon chains adopt solid-ordered phases. Moreover, sphingolipids tend to segregate together because of thermodynamically favorable van-der-Waals and hydrophobic interactions between their straight hydrocarbon chains [28]. Interactions between their polar, oligosaccharide-containing head groups can enhance this auto-assembly process [29] thus emphasizing the high tendency of sphingolipids to form solid-ordered lipid phases [30]. However, since sphingolipid-enriched membrane parts often contain sterols that do not form bilayer phases by themselves, no real solid-ordered but rather a third type of membrane phase, the liquid-ordered phase (L_o) is constituted [18]. This phase combines properties of the previously described solid and fluid membrane phases and is characterized by the high conformational order of a solid [31] but still features the high lateral mobility [32, 33] of a liquid (D_T = ~1 $\mu m^2 \cdot s^{-1}$) [2]. In other words, the liquid-ordered phase features characteristics of a transition phase between a solid-order and a liquid-disordered phase.

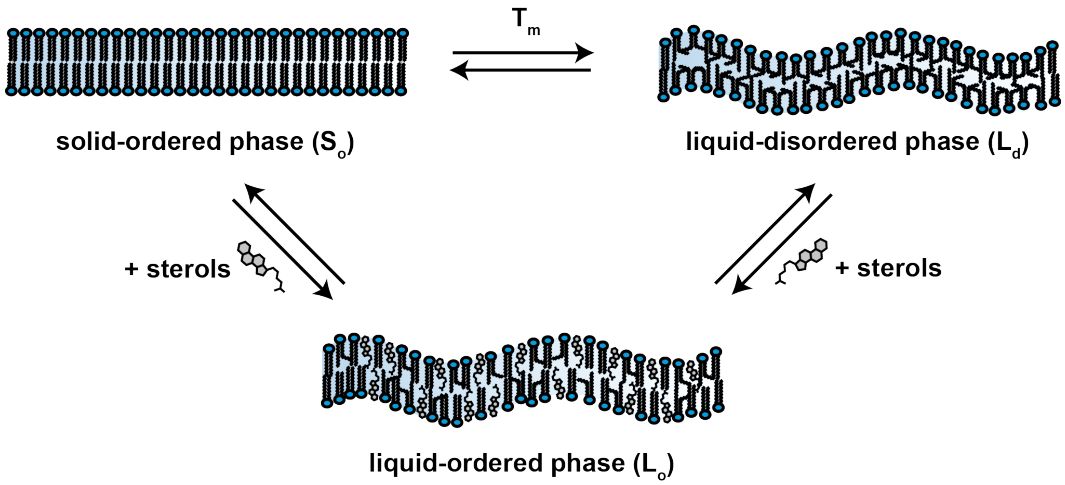

Fig. I-3: Physical membrane states adopted by lipid bilayers in biological systems. A solid-ordered phase state (S_o) is characterized by a highly-ordered and dense lipid packing. Increasing temperatures induce conformational changes in the fatty acid acyl chains of membrane lipids thereby impeding a dense lipid packing. The resulting phase is designated as liquid-disordered (L_d) phase. Liquid-disordered phase behavior of biological bilayers is not only thermally induced but also occurs due to incorporating unsaturated fatty acids in membrane lipids. Liquid-ordered phases (L_o) feature characteristics of both previously mentioned phase states as they are characterized by a high conformational order (ordered) but still support fast lateral diffusion (liquid). Solid-ordered and liquid-disordered membranes can be converted to liquid-ordered membranes by the incorporation of membrane sterols. Integration of sterols into highly-ordered bilayer breaks up their tight packing, thus functioning as fluidizers of membranes with solid-ordered phase state. In contrast, sterols condense loosely-packed membranes by straightening the fatty acid hydrocarbon chains, thus increasing the order parameter of a disordered bilayer. Adapted from [25].

1.4. Membrane fluidity and its significance for biological processes

Membrane fluidity can be described as the extent of molecular disorder within a bilayer and its capability to support lateral and rotational motion of membrane components such as membrane lipids and membrane proteins. Membrane fluidity is therefore closely linked with the previously described phase behaviors of differently composed and energized bilayers. The fact that organisms have evolved means to maintain physiological membrane fluidity that supports the proper function of membrane associated processes, so called homeoviscous adaption [34], emphasizes that membrane fluidity plays an important role in cellular functions. Homeoviscous adaption is preferentially important for poikilothermic organisms such as bacteria, plants, and fungi. Common means to maintain physiological membrane fluidity are based on altering the membrane lipid composition as e.g. changing the degree of fatty acid unsaturation thereby directly influencing lipid packing and order [35].

Membrane proteins are mobile within a fluid lipid environment that supports translational and rotational motion, although lateral diffusion of membrane proteins is slower than expected by theory due to protein crowding in the membrane and restrictions caused by the aqueous phase on both sides of the lipid bilayer [36]. However, dynamics of membrane proteins is supported by their lipid environment as it is essential for their biological function.

Diffusion-based processes within biological membranes benefit from the 2D organization of their matrix since reduction of dimensionality enhances the likelihood for collisional encounters [36]. This means, on the other hand, that membrane fluidity and the lipid environment of participating membrane proteins have to support their lateral mobility. Under diffusion limiting conditions (such as in biological membranes), collisional encountering can become the rate limiting step of the overall reaction, which is why membrane-associated signal transduction processes are often diffusion-controlled [37]. In contrast to that, there are diffusion coupled membrane processes that are not controlled by the diffusion of interacting partners. Those reactions often contain interaction partners and mediating elements whose mobility is not restricted within the bilayer so that other steps of the reaction get rate limiting. An example for this phenomenon is the mitochondrial electron transport chain involving fast-diffusing ubiquinones that transfer electrons between the diffusion-restricted respiratory complexes [38].

Another aspect of membrane protein dynamics is their conformational flexibility. Membrane proteins are no rigid structures but possess a certain conformational flexibility so that their actual structure is more a superposition of a countless number of different conformational substates [39]. An intrinsic property of enzymatically acting proteins is the continuous interconversion from one conformational substate to another. Additionally, motion of small substrate molecules into the inside of an enzyme might only be possible due to these conformational fluctuations [40]. It was shown, that the viscosity of the solvent influences the activation energy required for protein conformation changes [39] emphasizing that the lipid environment of proteins can influence the kinetics of protein conformational changes in a viscosity-dependent manner [41]. Proteins that carry out their function and thereby undergo changes in shape have to move at least some of their parts in the lipid solvent thus experiencing frictional forces. These frictional forces are directly linked with the viscosity of the lipid solvent, or its inverse, the fluidity of the lipid bilayer. The balance of the frictional forces and the mechanical restoring forces of the solvent (lipid bilayer) directly influence the mode of molecular motion of the protein (part) in the bilayer. Changes in prevailing frictional forces can thereby affect molecular vibrations within the protein and favor either overdamped (high frictional forces) or underdamped (low frictional forces) molecular motions [42]. These findings underline furthermore that membrane viscosity and thus membrane fluidity have a major impact on the conformational flexibility of membrane proteins which is crucial for their proper function. Membrane lipids might provide an environment to induce the optimal conformation for catalytic activity and breaks in the Arrhenius plots of membrane-embedded enzymes might be directly linked to the fluidity of the surrounding membrane [36]. Moreover, conformational interconversions and flexibility

was found to influence protein folding dynamics [43, 44], thereby emphasizing an essential role of the lipid environment for the kinetics of membrane protein constitution.

Another membrane parameter that is closely related the chemical structure of membrane lipids (fatty acid unsaturation) and thus membrane fluidity is the thickness of the bilayer: Highly ordered membranes are significantly thicker as compared to bilayers featuring a low ordering parameter [45, 46]. Integral membrane proteins interact with the lipophilic core of the bilayer by means of the hydrophobic surface structures of their trans-bilayer parts whereas the hydrophilic protein parts interact with the polar lipid head-groups as well as with the aqueous milieu on both sides of the bilayer. Reducing the thickness of the membrane simultaneously decreases the hydrophobic interaction area between the bilayer core and the membrane protein so that non-polar parts of the protein get exposed to a polar environment. This way, proteins can be distorted [47] or can be forced to unfavorable conformations that can be further accompanied by a total or partial loss of function as shown for the Na^+-K^+-ATPase [48] and other membrane proteins [49, 50]. Alternatively, membrane proteins might be directed to membrane parts that provide optimal bilayer thickness in order to maximizing beneficial hydrophobic protein-bilayer interactions and preventing hydrophobic mismatches [51]. This way, membrane proteins with longer bilayer spanning parts would preferably locate in physiologically active membranes with liquid-ordered phase behavior. Alternatively, it is suggested that rather the lipid bilayer is distorted in order to match the hydrophobic region of a membrane protein and thus to minimize hydrophobic mismatches [7, 52, 53].

Besides membrane fluidity and the thickness of the bilayer, lipid head groups and their differences in hydrogen bonding potential as well as their shape and the closely linked membrane curvature and lateral pressure profiles of the membrane might be important factors in determining the effects of lipids on protein activities [42].

1.5. Sensing of membrane fluidity by the OLE pathway of *S. cerevisiae*

Homeoviscous adaption and maintenance of physiological membrane fluidity is essential for cell viability. One of the key factors that determines fluidity and phase behavior of membranes in living cellular systems is the proportion of saturated and unsaturated fatty acids that are incorporated in glycerophospholipids [35]. The mechanism and system that regulates the synthesis of unsaturated fatty acids in order to adapt the extent of membrane lipid unsaturation to environmental conditions (e.g. temperature, oxygen availability) was extensively studied in the model organism *S. cerevisiae*. This system was referred to as “OLE pathway” [54] and includes all components that are required to sense membrane lipid unsaturation as well as to synthesize unsaturated fatty acids *de novo* if required. Key

players of the system are Ole1p, a stearoyl-CoA desaturase which is the sole fatty acid desaturase found in yeast that is essential to synthesize Δ9 monounsaturated fatty acids [55]. Other components of the system are the transcription activators Spt23p and Mga2p, ER membrane-resident proteins that function as membrane fluidity sensors [56].

Spt23p and Mga2p possess a transmembrane helix (TMH) that anchors both proteins, respectively, within the ER membrane. Both proteins form homo-dimers which is a prerequisite for sensing of membrane fluidity and lipid packing. Helix-helix interactions are facilitated by the high proportion of aromatic amino acids situated within the TMHs presumably forming intermolecular interactions by pi stacking [56]. The sensing mechanism of dimeric Mga2p is based on the structure of its TMHs and involves rotational TMH motions which leads to a continuum of alternative TMH-TMH interfaces [54]. A bulky tryptophan residue is atypically positioned deep within the membrane bilayer and important for sensing. Voluminous tryptophan residues are usually located close to the membrane-water interface [57]. In a loosely packed, fluid membrane, this bulky amino acid side chain can be easily accommodated in the lipid environment so that a high proportion a Mga2p dimers and their TMHs features a characteristic rotational orientation to each other with both tryptophan residues facing outwards. This relative orientation of both TMHs represents the off-state of the sensor and indicates physiological membrane fluidity. In contrast, increasing membrane packing and decreasing membrane fluidity favor an inward rotation of the bulky tryptophan residue, thus stabilizing an alternative relative TMH orientation that hides both residues in the dimer interface. This relative rotational orientation marks the on-state of the sensor. Importantly, the different rotational orientations seem not to be separated by high energy barriers so that even very little changes in membrane lipid unsaturation can be effectively sensed by the system [35, 56]. The on-conformation further allows Rsp5p-mediated ubiquitination of Mga2p at a position close to the ER membrane which is suggest to be the signal for subsequent proteolytic processing by the cytosolic 26S proteasome. Proteasome-dependent activation involves the cleavage of the protein thereby releasing the N-terminal soluble p90 fragment. The activated p90 domains translocate to the nucleus and upregulate the expression of a number of genes involved in various cellular processes such as the central carbon and lipid metabolism, ribosome biogenesis, flocculation and mating [58, 59]. Although Mga2p90 and Spt23p90 do not contain any known DNA binding domain, they seem to control transcription by chromatin remodeling [58, 60]. Prominent targets of Mga2p90 are *OLE1* and *ERG1* that encodes for an essential enzyme involved in the biosynthesis of ergosterol. The upregulation of *OLE1* leads to increased fatty acid unsaturation thus eventually fluidizing the ER membrane and closing the end-product feedback regulation loop to maintain physiological membrane fluidity.

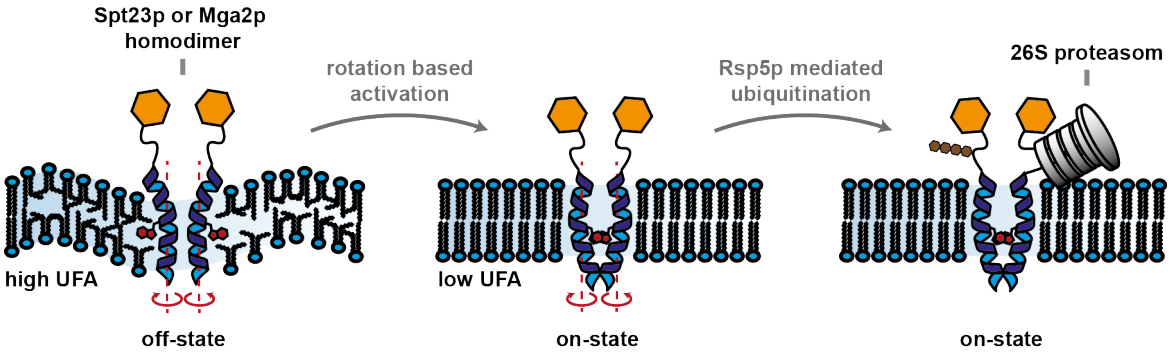

Fig. I-4: Sensing of lipid packing and membrane fluidity by Spt23p and Mga2p. Homodimers of Spt23p or Mga2p use their transmembrane helices (TMH) to sense the lipid packing of the bilayer. A loosely packed bilayer stabilizes a relative rotational orientation of both TMHs that allows to bury their bulky tryptophan residue (red) deep within the lipid bilayer. This relative TMH orientation refers to the off-state of the sensor. In contrast, highly ordered lipid bilayers do not allow the tryptophan residue to be rotated outwards and favors a relative rotational orientation of the TMHs in which both tryptophan residues face towards the dimer interface. This orientation characterizes the on-state of the sensors and supports Rsp5p-mediated ubiquitination of both monomers. Ubiquitination serves as the signal for subsequent proteolytic processing by the cytosolic 26s proteasome which activates the sensor. Activation involves protein cleavage, thus releasing a soluble p90 fragment (orange) which translocates to the nucleus and serves as a transcription activator. Adopted from [54].

Other organisms have evolved different mechanisms to sense the composition of their membranes. The DesK/DesR system from *B. subtilis* measures the thickness of the membrane for deducing the unsaturation degree and viscosity of the bilayer. Increased bilayer thickness eventually leads to the activation of *des*, encoding for a lipid desaturase [61]. Another prominent example of transcriptional regulation of genes involved in lipid metabolism is mediated by the metazoan SREBPs (sterol response element binding proteins). These proteins measure the content of sterols in the membrane and get activated upon sterol depletion [62].

1.6. Membrane sterols and the lipid raft concept

According to the fluid mosaic model of biological membrane organization [9], all membrane lipids and membrane embedded proteins form a homogenous two-dimensional fluid in which its components can laterally diffuse without restriction. Although the general description of cell membrane organization has proven to be correct, findings from the last three decades strongly contradict the theory of biological membranes as homogenous phases. The mere fact that cellular membranes contain a high proportion of sphingolipids and sterols that tend to segregate into lipid clusters with a more ordered phase behavior within a fluid-disordered glycerophospholipid-rich phase is not in accordance with a uniform lipid bilayer. These sterol- and sphingolipid-enriched lipid clusters turned out to be more resistant against non-ionic detergents and seemed to provide an environment in which certain proteins preferably move into due to an intrinsic affinity [63]. These findings gave rise to a concept of lipid rafts which were defined as “small (10-200 nm), heterogeneous,

highly dynamic sterol- and sphingolipid-enriched domains that compartmentalize cellular processes" [64].

Specific association of proteins with lipid rafts was firstly reported for GPI-anchored proteins [63]. Besides that, some other membrane-anchoring protein modifications such as myristoylation and palmitoylation have been suggested to be associated with protein targeting to lipid rafts [65, 66]. However, also proteins without fatty acid conjugation were discovered in lipid rafts, indicating that proteinous elements must be responsible for raft localization. Both, transmembrane [67] as well as intra- [68] and extracellular domains [69] were identified to targeting signals, although no consensus protein-based raft targeting sequences could be determined. Additionally, protein domains with sphingolipid-binding activity were already discovered [70]. However, forces that drive proteins to segregate into different lipid environments are still poorly understood. Another mechanism that directs proteins to lipid rafts could be based on membrane thickness and the length of transmembrane domains of membrane proteins. Liquid-ordered, sterol containing bilayers are considerably thicker than liquid-disordered ones [71, 72] thereby making it energetically favorable for a protein to enter and stay within a membrane whose thickness matches the length of its membrane spanning part [73]. This way, membrane proteins with longer transmembrane domains would preferably segregate into lipid rafts in order to prevent hydrophobic mismatches [51]. In line with that theory, it could already be shown that the ratio of membrane thickness and length of transmembrane domains influences protein sorting to the plasma membrane. The concentration of sphingolipids and sterols increase along the way from the ER to the plasma membrane thus also increasing the membrane thickness [74] and proteins with longer TMHs (~20 aa) are preferably addressed to the plasma membrane whereas Golgi proteins feature usually shorter TMHs (~15 aa) [75]. It has also been hypothesized that so-called "lipid shells" can confer membrane proteins an affinity for lipid rafts. Lipid shells consist of ~80 sterol/sphingolipid molecules that surround the transmembrane domain of membrane proteins due to physical interactions and direct proteins to lipid rafts in a thermodynamically-driven lipid-mediated manner as sterols and sphingolipids themselves have an affinity for preexisting raft domains [76].

Similarly, it is not well understood how raft or non-raft localization of membrane proteins can affect their function. However, it is known that proteins can exist in different states depending on their lipid environment. For example, glutamate receptors were found to be in a low affinity state when embedded in a sterol-depleted membrane whereas the receptor changes its conformation in sterol-rich bilayers with liquid-ordered phase behavior and switches to a high-affinity state [77]. This way, it could be suggested that the lipid environment directly influences the conformation of proteins and the most functional conformation is only supported in raft domains. Following the previously mentioned theory,

an unfavorable ratio of membrane thickness and the length of transmembrane domains could force proteins into an unfavorable conformation in order to prevent hydrophobic mismatches, thus negatively affecting protein function [49]. Alternatively, protein function could be affected by the lipid environment in a similar way as shown for the lipid packing sensors Spt23p and Mga2p from *S. cerevisiae* [56]. Large bulky amino acid side chains of transmembrane domains could affect protein motion [75] (e.g. rotation) in different lipid environments as liquid-ordered and liquid-disordered membrane domains differ significantly in their order parameter and packing density.

Proteomics on lipid raft-resident proteins was used to identified biological processes that might be closely associated with lipid rafts. These analyses identified raft localization of cell signaling proteins such as heterotrimeric G proteins, tyrosine kinases, phosphatases [78] and support the long-time evidence that lipid rafts are associated with cell signaling [79]. Additionally, cytoskeletal and adhesion proteins (e.g. actin, myosin, vinculin) [78, 80, 81] were found in lipid raft preparations thereby suggesting lipid rafts interact with the cytoskeleton. For *S. cerevisiae*, lipid rafts have been discussed to be involved in protein sorting, development of cell polarity [82, 83], cell growth, drug-mediated cell death [84] and membrane compartmentation [85].

1.7. References

1. **Berg JM, Held A, Stryer L, Lange C, Mahlke K et al.** *Stryer Biochemie*: Springer Berlin Heidelberg; 2015.
2. **van Meer G, Voelker DR, Feigenson GW**. Membrane lipids: where they are and how they behave. *Nat Rev Mol Cell Biol* 2008;9(2):112-124.
3. **Uings IJ, Farrow SN**. Cell receptors and cell signalling. *Mol Pathol* 2000;53(6):295-299.
4. **Kouyama T, Kouyama AN, Ikegami A**. Bacteriorhodopsin is a powerful light-driven proton pump. *Biophys J* 1987;51(5):839-841.
5. **Gracheva EO, Cordero-Morales JF, Gonzalez-Carcacia JA, Ingolia NT, Manno C et al.** Ganglion-specific splicing of TRPV1 underlies infrared sensation in vampire bats. *Nature* 2011;476(7358):88-91.
6. **Catterall WA**. Ion channel voltage sensors: structure, function, and pathophysiology. *Neuron* 2010;67(6):915-928.
7. **Mitra K, Ubarretxena-Belandia I, Taguchi T, Warren G, Engelman DM**. Modulation of the bilayer thickness of exocytic pathway membranes by membrane proteins rather than cholesterol. *Proc Natl Acad Sci U S A* 2004;101(12):4083-4088.
8. **Gorter E, Grendel F**. On Bimolecular Layers of Lipoids on the Chromocytes of the Blood. *J Exp Med* 1925;41(4):439-443.
9. **Singer SJ, Nicolson GL**. The fluid mosaic model of the structure of cell membranes. *Science* 1972;175(4023):720-731.
10. **Nicolson GL**. The Fluid-Mosaic Model of Membrane Structure: still relevant to understanding the structure, function and dynamics of biological membranes after more than 40 years. *Biochim Biophys Acta* 2014;1838(6):1451-1466.
11. **Blokzijl W, Engberts JBFN**. Hydrophobe Effekte – Ansichten und Tatsachen. *Angewandte Chemie* 1993;105(11):1610-1648.
12. **Silverstein TP**. The Real Reason Why Oil and Water Don't Mix. *Journal of Chemical Education* 1998;75(1):116.
13. **Clarke S**. The hydrophobic effect: Formation of micelles and biological membranes, 2nd edition (Tanford, Charles). *Journal of Chemical Education* 1981;58(8):A246.
14. **Kaneda T**. Fatty acids of the genus Bacillus: an example of branched-chain preference. *Bacteriol Rev* 1977;41(2):391-418.
15. **Klose C, Surma MA, Gerl MJ, Meyenhofer F, Shevchenko A et al.** Flexibility of a eukaryotic lipidome--insights from yeast lipidomics. *PLoS One* 2012;7(4):e35063.
16. **Fahy E, Sud M, Cotter D, Subramaniam S**. LIPID MAPS online tools for lipid research. *Nucleic Acids Res* 2007;35(Web Server issue):W606-612.
17. **Huang J, Feigenson GW**. A microscopic interaction model of maximum solubility of cholesterol in lipid bilayers. *Biophys J* 1999;76(4):2142-2157.
18. **Ipsen JH, Karlstrom G, Mouritsen OG, Wennerstrom H, Zuckermann MJ**. Phase equilibria in the phosphatidylcholine-cholesterol system. *Biochim Biophys Acta* 1987;905(1):162-172.
19. **Alwarawrah M, Dai J, Huang J**. A molecular view of the cholesterol condensing effect in DOPC lipid bilayers. *J Phys Chem B* 2010;114(22):7516-7523.
20. **Yeagle PL**. Cholesterol and the cell membrane. *Biochim Biophys Acta* 1985;822(3-4):267-287.
21. **Marsh D, Smith IC**. An interacting spin label study of the fluidizing and condensing effects of cholesterol on lecithin bilayers. *Biochim Biophys Acta* 1973;298(2):133-144.
22. **Kai L, Kaldenhoff R**. A refined model of water and CO(2) membrane diffusion: effects and contribution of sterols and proteins. *Sci Rep* 2014;4:6665.
23. **Rog T, Pasenkiewicz-Gierula M**. Cholesterol effects on the phosphatidylcholine bilayer nonpolar region: a molecular simulation study. *Biophys J* 2001;81(4):2190-2202.
24. **Rog T, Pasenkiewicz-Gierula M, Vattulainen I, Karttunen M**. Ordering effects of cholesterol and its analogues. *Biochim Biophys Acta* 2009;1788(1):97-121.
25. **Eeman M, Deleu M**. From biological membranes to biomimetic model membranes. *Biotechnol Agron Soc Environ* 2010;14(4):719-736.
26. **Lee AG**. Lipid-protein interactions in biological membranes: a structural perspective. *Biochim Biophys Acta* 2003;1612(1):1-40.

27. **Yellin N, Levin IW**. Hydrocarbon trans-gauche isomerization in phospholipid bilayer gel assemblies. *Biochemistry* 1977;16(4):642-647.

28. **Ramstedt B, Slotte JP**. Membrane properties of sphingomyelins. *FEBS Lett* 2002;531(1):33-37.

29. **Rock P, Allietta M, Young WW, Jr., Thompson TE, Tillack TW**. Organization of glycosphingolipids in phosphatidylcholine bilayers: use of antibody molecules and Fab fragments as morphologic markers. *Biochemistry* 1990;29(36):8484-8490.

30. **Wang T-Y, Leventis R, Silvius JR**. Fluorescence-Based Evaluation of the Partitioning of Lipids and Lipidated Peptides into Liquid-Ordered Lipid Microdomains: A Model for Molecular Partitioning into “Lipid Rafts”. *Biophysical Journal* 2000;79(2):919-933.

31. **Gally HU, Seelig A, Seelig J**. Cholesterol-induced rod-like motion of fatty acyl chains in lipid bilayers a deuterium magnetic resonance study. *Hoppe Seylers Z Physiol Chem* 1976;357(10):1447-1450.

32. **Almeida PF, Vaz WL, Thompson TE**. Percolation and diffusion in three-component lipid bilayers: effect of cholesterol on an equimolar mixture of two phosphatidylcholines. *Biophys J* 1993;64(2):399-412.

33. **Filippov A, Oradd G, Lindblom G**. The effect of cholesterol on the lateral diffusion of phospholipids in oriented bilayers. *Biophys J* 2003;84(5):3079-3086.

34. **Sinensky M**. Homeoviscous adaptation--a homeostatic process that regulates the viscosity of membrane lipids in Escherichia coli. *Proc Natl Acad Sci U S A* 1974;71(2):522-525.

35. **Ernst R, Ejsing CS, Antonny B**. Homeoviscous Adaptation and the Regulation of Membrane Lipids. *J Mol Biol* 2016;428(24 Pt A):4776-4791.

36. **Lenaz G**. Lipid fluidity and membrane protein dynamics. *Biosci Rep* 1987;7(11):823-837.

37. **Rimon G, Hanski E, Braun S, Levitzki A**. Mode of coupling between hormone receptors and adenylate cyclase elucidated by modulation of membrane fluidity. *Nature* 1978;276(5686):394-396.

38. **Lenaz G, Fato R**. Is ubiquinone diffusion rate-limiting for electron transfer? *J Bioenerg Biomembr* 1986;18(5):369-401.

39. **Walser R, van Gunsteren WF**. Viscosity dependence of protein dynamics. *Proteins* 2001;42(3):414-421.

40. **Beece D, Eisenstein L, Frauenfelder H, Good D, Marden MC et al.** Solvent viscosity and protein dynamics. *Biochemistry* 1980;19(23):5147-5157.

41. **Sekhar A, Latham MP, Vallurupalli P, Kay LE**. Viscosity-dependent kinetics of protein conformational exchange: microviscosity effects and the need for a small viscogen. *J Phys Chem B* 2014;118(17):4546-4551.

42. **Lee AG**. How lipids affect the activities of integral membrane proteins. *Biochim Biophys Acta* 2004;1666(1-2):62-87.

43. **Hagen SJ**. Solvent viscosity and friction in protein folding dynamics. *Curr Protein Pept Sci* 2010;11(5):385-395.

44. **Maurya SR, Chaturvedi D, Mahalakshmi R**. Modulating lipid dynamics and membrane fluidity to drive rapid folding of a transmembrane barrel. *Sci Rep* 2013;3:1989.

45. **Dufourc EJ**. Sterols and membrane dynamics. *J Chem Biol* 2008;1(1-4):63-77.

46. **Thurmond RL, Niemi AR, Lindblom G, Wieslander A, Rilfors L**. Membrane thickness and molecular ordering in Acholeplasma laidlawii strain A studied by 2H NMR spectroscopy. *Biochemistry* 1994;33(45):13178-13188.

47. **Williamson IM, Alvis SJ, East JM, Lee AG**. Interactions of phospholipids with the potassium channel KcsA. *Biophys J* 2002;83(4):2026-2038.

48. **Johannsson A, Smith GA, Metcalfe JC**. The effect of bilayer thickness on the activity of (Na+ + K+)-ATPase. *Biochim Biophys Acta* 1981;641(2):416-421.

49. **Pilot JD, East JM, Lee AG**. Effects of bilayer thickness on the activity of diacylglycerol kinase of Escherichia coli. *Biochemistry* 2001;40(28):8188-8195.

50. **Froud RJ, Earl CR, East JM, Lee AG**. Effects of lipid fatty acyl chain structure on the activity of the (Ca2+ + Mg2+)-ATPase. *Biochim Biophys Acta* 1986;860(2):354-360.

51. **Sprong H, van der Sluijs P, van Meer G**. How proteins move lipids and lipids move proteins. *Nat Rev Mol Cell Biol* 2001;2(7):504-513.

52. **Engelman DM**. Membranes are more mosaic than fluid. *Nature* 2005;438(7068):578-580.

53. **Petrache HI, Zuckerman DM, Sachs JN, Killian JA, Koeppe RE et al.** Hydrophobic Matching Mechanism Investigated by Molecular Dynamics Simulations. *Langmuir* 2002;18(4):1340-1351.

54. **Ballweg S, Ernst R**. Control of membrane fluidity: the OLE pathway in focus. *Biol Chem* 2017;398(2):215-228.

55. **Stukey JE, McDonough VM, Martin CE**. The OLE1 gene of Saccharomyces cerevisiae encodes the delta 9 fatty acid desaturase and can be functionally replaced by the rat stearoyl-CoA desaturase gene. *J Biol Chem* 1990;265(33):20144-20149.

56. **Covino R, Ballweg S, Stordeur C, Michaelis JB, Puth K et al.** A Eukaryotic Sensor for Membrane Lipid Saturation. *Mol Cell* 2016;63(1):49-59.

57. **Sharpe HJ, Stevens TJ, Munro S**. A comprehensive comparison of transmembrane domains reveals organelle-specific properties. *Cell* 2010;142(1):158-169.

58. **Auld KL, Brown CR, Casolari JM, Komili S, Silver PA**. Genomic association of the proteasome demonstrates overlapping gene regulatory activity with transcription factor substrates. *Mol Cell* 2006;21(6):861-871.

59. **Degreif D, de Rond T, Bertl A, Keasling JD, Budin I**. Lipid engineering reveals regulatory roles for membrane fluidity in yeast flocculation and oxygen-limited growth. *Metab Eng* 2017;41:46-56.

60. **Zhang S, Skalsky Y, Garfinkel DJ**. MGA2 or SPT23 is required for transcription of the delta9 fatty acid desaturase gene, OLE1, and nuclear membrane integrity in Saccharomyces cerevisiae. *Genetics* 1999;151(2):473-483.

61. **Cybulski LE, Ballering J, Moussatova A, Inda ME, Vazquez DB et al.** Activation of the bacterial thermosensor DesK involves a serine zipper dimerization motif that is modulated by bilayer thickness. *Proc Natl Acad Sci U S A* 2015;112(20):6353-6358.

62. **Rawson RB**. The SREBP pathway--insights from Insigs and insects. *Nat Rev Mol Cell Biol* 2003;4(8):631-640.

63. **Brown DA, Rose JK**. Sorting of GPI-anchored proteins to glycolipid-enriched membrane subdomains during transport to the apical cell surface. *Cell* 1992;68(3):533-544.

64. **Pike LJ**. Rafts defined: a report on the Keystone Symposium on Lipid Rafts and Cell Function. *J Lipid Res* 2006;47(7):1597-1598.

65. **Zacharias DA, Violin JD, Newton AC, Tsien RY**. Partitioning of lipid-modified monomeric GFPs into membrane microdomains of live cells. *Science* 2002;296(5569):913-916.

66. **Smotrys JE, Linder ME**. Palmitoylation of intracellular signaling proteins: regulation and function. *Annu Rev Biochem* 2004;73:559-587.

67. **Scheiffele P, Roth MG, Simons K**. Interaction of influenza virus haemagglutinin with sphingolipid-cholesterol membrane domains via its transmembrane domain. *EMBO J* 1997;16(18):5501-5508.

68. **Crossthwaite AJ, Seebacher T, Masada N, Ciruela A, Dufraux K et al.** The cytosolic domains of Ca2+-sensitive adenylyl cyclases dictate their targeting to plasma membrane lipid rafts. *J Biol Chem* 2005;280(8):6380-6391.

69. **Yamabhai M, Anderson RG**. Second cysteine-rich region of epidermal growth factor receptor contains targeting information for caveolae/rafts. *J Biol Chem* 2002;277(28):24843-24846.

70. **Mahfoud R, Garmy N, Maresca M, Yahi N, Puigserver A et al.** Identification of a common sphingolipid-binding domain in Alzheimer, prion, and HIV-1 proteins. *J Biol Chem* 2002;277(13):11292-11296.

71. **Smondyrev AM, Berkowitz ML**. Molecular dynamics simulation of the structure of dimyristoylphosphatidylcholine bilayers with cholesterol, ergosterol, and lanosterol. *Biophys J* 2001;80(4):1649-1658.

72. **Nezil FA, Bloom M**. Combined influence of cholesterol and synthetic amphiphillic peptides upon bilayer thickness in model membranes. *Biophys J* 1992;61(5):1176-1183.

73. **Mouritsen OG, Bloom M**. Mattress model of lipid-protein interactions in membranes. *Biophys J* 1984;46(2):141-153.

74. **Dumas F, Lebrun MC, Tocanne JF**. Is the protein/lipid hydrophobic matching principle relevant to membrane organization and functions? *FEBS Lett* 1999;458(3):271-277.

75. **Bretscher MS, Munro S**. Cholesterol and the Golgi apparatus. *Science* 1993;261(5126):1280-1281.

76. **Anderson RG, Jacobson K**. A role for lipid shells in targeting proteins to caveolae, rafts, and other lipid domains. *Science* 2002;296(5574):1821-1825.

77. **Eroglu C, Brugger B, Wieland F, Sinning I**. Glutamate-binding affinity of Drosophila metabotropic glutamate receptor is modulated by association with lipid rafts. *Proc Natl Acad Sci U S A* 2003;100(18):10219-10224.

78. **Foster LJ, De Hoog CL, Mann M**. Unbiased quantitative proteomics of lipid rafts reveals high specificity for signaling factors. *Proc Natl Acad Sci U S A* 2003;100(10):5813-5818.

79. **Simons K, Toomre D**. Lipid rafts and signal transduction. *Nat Rev Mol Cell Biol* 2000;1(1):31-39.

80. **Nebl T, Pestonjamasp KN, Leszyk JD, Crowley JL, Oh SW et al.** Proteomic analysis of a detergent-resistant membrane skeleton from neutrophil plasma membranes. *J Biol Chem* 2002;277(45):43399-43409.

81. **Chichili GR, Rodgers W**. Cytoskeleton-membrane interactions in membrane raft structure. *Cell Mol Life Sci* 2009;66(14):2319-2328.

82. **Bagnat M, Simons K**. Lipid rafts in protein sorting and cell polarity in budding yeast Saccharomyces cerevisiae. *Biol Chem* 2002;383(10):1475-1480.

83. **Bagnat M, Keranen S, Shevchenko A, Shevchenko A, Simons K**. Lipid rafts function in biosynthetic delivery of proteins to the cell surface in yeast. *Proc Natl Acad Sci U S A* 2000;97(7):3254-3259.

84. **Mollinedo F**. Lipid raft involvement in yeast cell growth and death. *Front Oncol* 2012;2:140.

85. **Grossmann G, Opekarova M, Novakova L, Stolz J, Tanner W**. Lipid raft-based membrane compartmentation of a plant transport protein expressed in Saccharomyces cerevisiae. *Eukaryot Cell* 2006;5(6):945-953.

Chapter II

Lipid engineering reveals regulatory roles for membrane fluidity in yeast flocculation and oxygen-limited growth

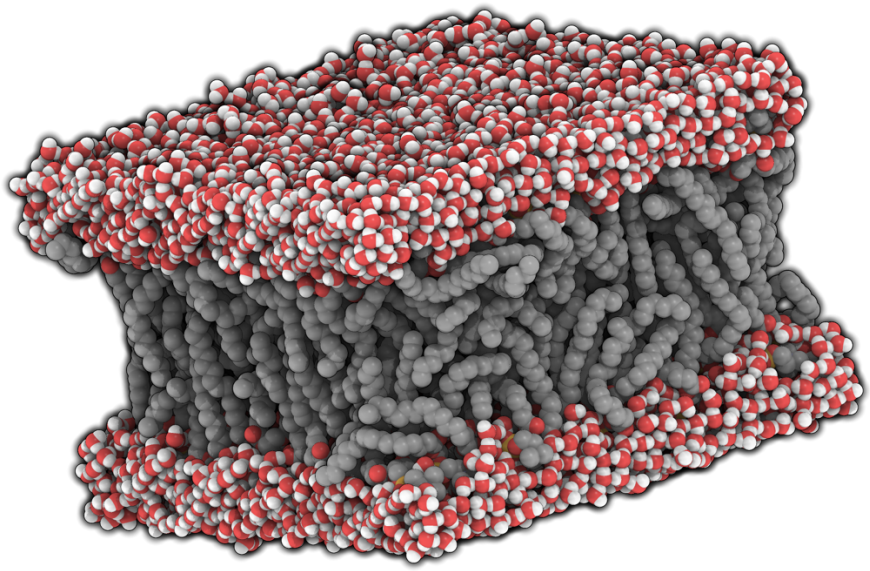

2. Chapter II: Lipid engineering reveals regulatory roles for membrane fluidity in yeast flocculation and oxygen-limited growth

2.1. Abstract

Cells modulate lipid metabolism in order to maintain membrane homeostasis. Here a metabolic engineering approach was used to manipulate the stoichiometry of fatty acid unsaturation, a regulator of cell membrane fluidity, in *Saccharomyces cerevisiae*. Unexpectedly, reduced lipid unsaturation triggered cell-cell adhesion (flocculation), a phenomenon characteristic of industrial yeast but uncommon in laboratory strains. It was found that ER lipid saturation sensors induce expression of *FLO1* – encoding a cell wall polysaccharide binding protein – independently of its canonical regulator. In wild-type cells, Flo1p-dependent flocculation occurs under oxygen-limited growth, which reduces unsaturated lipid synthesis and thus serves as the environmental trigger for flocculation. Transcriptional analysis shows that *FLO1* is one of the most highly induced genes in response to changes in lipid unsaturation, and that the set of membrane fluidity-sensitive genes is globally activated as part of the cell's long-term response to hypoxia during fermentation. The results presented here show how the lipid homeostasis machinery of budding yeast is adapted to carry out a broad response to an environmental stimulus important in biotechnology.

2.2. Introduction

The lipid composition of cellular compartments is thought to control the physicochemical properties of their membranes and thus could act as a broad regulator of membrane-localized cellular machinery. Lipid composition can vary tremendously between cells, organelles, and tissues, potentially reflecting differing constraints that molecular processes hosted by these membranes place [1]. For example, in budding yeast (*Saccharomyces cerevisiae*), global lipid analysis by mass spectrometry has shown that the cellular lipidome changes during growth and is dependent on carbon source [2]. However, understanding functional roles for differences in lipid composition remains a challenge because a limited set of tools is available for studying lipid composition *in vivo*. Standard genetic approaches, e.g. gene knockouts, provide little functional information on essential lipid components, while chemical tools, such as media supplements [3] and lipid chelators [4], provide limited stoichiometric control over lipid composition.

An alternative strategy to chemical manipulation of lipid composition is to engineer cells in which the expression of lipid synthesis pathways is placed under experimental control. It was sought to use this approach to investigate a central chemical parameter in determining the physical state of cell membranes: the proportion of fluidizing double bonds in phospholipid acyl chains (lipid unsaturation). Enzymatic desaturation generates *cis*-double bonds in acyl chains, whose geometry interferes with inter-lipid interactions, thereby reducing lipid packing and fluidizing the bilayer [5]. Membrane fluidity is thought to be maintained by cells in response to changes in temperature [6] or solvents [7] by modulating the fatty acid composition of membrane phospholipids. Changes in fatty acid unsaturation are also associated with human diseases, including the development of type-2 diabetes [8] and tumor proliferation in cancer [9]. However, the functional effects of these physical and chemical parameters on basic cellular physiology are still not fully understood.

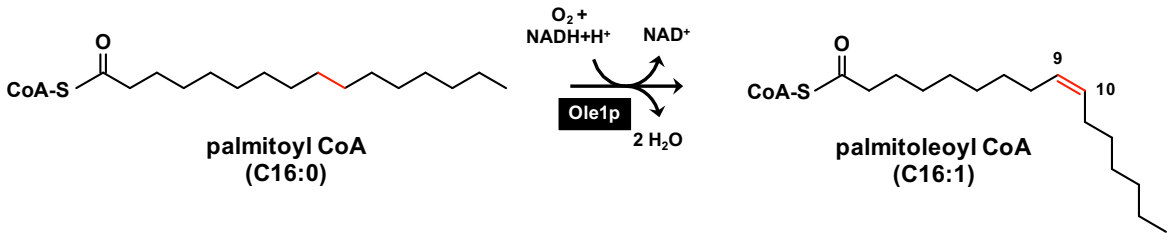

Fig. II-1: Reaction scheme of oxygen- and NADH-dependent desaturation of fatty acid acyl chains catalyzed by Ole1p. Ole1p uses coenzyme A (CoA) bound precursors of fully saturated fatty acids as substrate and introduces a double bond between C9 and C10 yielding the corresponding Δ9-*cis* monounsaturated fatty acid species. The reaction requires NADH as electron donor and molecular oxygen (O_2) as final electron acceptor.

Higher eukaryotes feature a repertoire of desaturases with varying substrates and products [10], including polyunsaturated species whose complex biophysical effects make identifying fluidity-regulated functions a challenge [11]. In contrast, budding yeast features only a single lipid desaturase (Ole1p), which converts a wide range of coenzyme A-bound fatty acids into their corresponding Δ9-*cis* monounsaturated species [12] (Fig. II-1).

Because bilayer fluidity is an important parameter for membrane-associated cellular processes, yeast has evolved mechanisms for modulating the level of *OLE1* in response to metabolic stages during growth [13] and to environmental stimuli, such as the supply of exogenous lipids. In budding yeast, a fatty acid regulatory (FAR) region in the *OLE1* promoter was first identified to be responsive to fatty acid metabolism genes [14]. Later it was found that a pair of ER membrane-bound transcriptional activators – Spt23p and Mga2p [15], which were first identified as regulators of *TY* retrotransposon elements [16] – mediate *OLE1*-specific lipid regulation. Biochemical and genetic experiments have led to a model in which membrane-anchored Spt23p and Mga2p are proteolytically processed in response to changes in fatty acid composition [17]. The resulting active fragments, termed p90 domains, induce *OLE1* expression, though neither protein contains a recognizable DNA binding domain [16, 18, 19]. Recent work has proposed a model in which proteolysis is driven by conformational changes in the transmembrane helices of Spt23p/Mga2p homodimers mediated by the unsaturated lipid content of the ER membrane [20]. Several key aspects of this pathway are still under investigation, including the exact mechanism by which Spt23p/Mga2p or their interacting partners influence gene expression.

In this study it was sought to systematically investigate the physiological effects of changes to lipid unsaturation by bypassing the cell's native lipid regulation pathway. A surprising phenotype was observed resulting from repression of the lipid desaturase-encoding *OLE1*: cell-cell adhesion, termed flocculation, which was found to be a transcriptional response to low membrane fluidity. Flocculation is induced when oxygen availability for lipid desaturation reactions is restricted and is part of a wide-ranging transcriptional response to low membrane fluidity that is activated during microaerobic fermentation.

2.3. Materials and Methods

2.3.1. Yeast strains

Tab. II-1: Yeast strains used in this study. The table lists all strains with corresponding genotypes. Plasmids harbored by respective strains are named as indicated in Tab. II-S2.

strain	genotype	reference
BY4742	*MAT*α; *his3*Δ1; *leu2*Δ0; *lys2*Δ0; *ura3*Δ0	[21]
SII-1	BY4742; *ole1*:: P_{MET3}-*OLE1*	This study
SII-2	BY4742; *spt23*::kanMX (Δ*spt23*)	This study
SII-3	BY4742; *mga2*::*URA3* (Δ*mga2*)	This study
SII-4	BY4742; *flo1*::yECitrine-*URA3* (Δ*flo1*)	This study
SII-5	SII-1; *flo1*::yECitrine-*URA3* (Δ*flo1*)	This study
SII-6	SII-1; *FLO1hd*::T_{CYC1}-kanMX (*FLO1*Δhd)	This study
SII-7	SII-1; *flo8*::yECitrine-*URA3* (Δ*flo8*)	This study
SII-8	SII-1; *flo9*::kanMX (Δ*flo9*)	This study
SII-9	SII-1; *spt23*::kanMX (Δ*spt23*)	This study
SII-10	SII-1; *mga2*::*URA3* (Δ*mga2*)	This study
SII-11	SII-2; pCM188-*SPT23p90*	This study
SII-12	SII-4; pCM188(*LEU2*)-*SPT23p90*	This study
SII-13	SII-3; pCM188(*LEU2*)-*MGA2p90*	This study
SII-14	SII-1; pCM188-*OLE1*	This study
SII-15	SII-1; pGREG523-P_{SPT23}-^{myc}*SPT23*	This study
SII-16	SII-9; pGREG523-P_{SPT23}-^{myc}*SPT23*	This study
SII-17	SII-9; pGREG523-P_{SPT23}-^{myc}*SPT23*$_{W1042L}$	This study
SII-18	SII-9; pGREG523(2μ)-P_{SPT23}-^{myc}*SPT23*	This study
SII-19	SII-9; pGREG523-P_{TEF1}-^{myc}*SPT23*	This study
SII-20	SII-9; pGREG523(2μ)-P_{TEF1}-^{myc}*SPT23*	This study
SII-21	SII-1; pGREG523-P_{MGA2}-^{myc}*MGA2*	This study
SII-22	BY4742; *ura3*::*HAC1*-GFP	This study
SII-23	SII-1; *ura3*::*HAC1*-GFP	This study
SII-24	SII-1; *hac1*::kanMX (Δ*hac1*)	This study
SII-25	SII-1; *ire1*::kanMX (Δ*ire1*)	This study
SII-26	SII-1; pRS416-ER-sfGFP-HDEL	This study

2.3.2. Yeast transformation and strain construction

Genetically modified *S. cerevisiae* strains generated in this study are derived from BY4742 (*MAT*α; *his3*Δ1; *leu2*Δ0; *lys2*Δ0; *ura3*Δ0) obtained from EUROSCARF (Frankfurt, Germany). BY4742 cells were routinely cultured in YPD media (2% glucose; 2% peptone;

1% yeast extract). BY4742 derived strains harboring selectable markers (*URA3*; *LEU2; HIS3*) were grown in appropriate synthetic defined (SD) drop-out media (2% glucose; yeast nitrogen base (YNB); drop-out amino acid supplement). KanMX cassette harboring cells were selected at 200 mg/L G418. Cells were propagated at 30°C. All strains are listed in Tab. II-1.

Transformation of *S. cerevisiae* with previously generated plasmids was routinely performed by using the Frozen-EZ Yeast Transformation II kit (Zymo Research) according to manufacturer's instructions.

S. cerevisiae transformation for genomic integration of integration cassettes (promoter replacement cassette; knockout cassettes) via homologous recombination and plasmid uptake was routinely performed by the standard lithium acetate method [22]. Replacement of endogenous *OLE1* promoter was performed by genomic integration of a P_{MET3} containing promoter replacement cassette (loxP-*LEU2*-loxP-P_{MET3}) amplified by PCR from plasmid p416-*LEU2*-P_{MET3}-yECitrine (OneTaq DNA polymerase; primers P5 & P6). *FLO1* and *FLO8* were knocked-out by replacing the entire ORF, respectively, with the yECitrine-*URA3* cassette from plasmid p416-*LEU2*-P_{TEF1}-yECitrine. *SPT23*, *FLO9*, *HAC1* and *IRE1* were knocked-out by replacing the ORF with the kanMX cassette from plasmid pCM224. *MGA2* was knocked-out by replacing the ORF with the *URA3* cassette from plasmid p416-*LEU2*-P_{TEF1}-yECitrine. The sequence encoding the Flo1p hydrophobic domain (*FLO1hd*) was knocked out by genomically integrating the T_{CYC1}-kanMX cassette from plasmid pGREG506 thereby introducing a premature stop-codon and a terminator sequence to the 3'-end of the *FLO1* ORF. The so modified *FLO1* ORF encodes for a C-terminal shortened protein variant lacking the hydrophobic domain (S1510 – I1537) thus preventing proper Flo1p anchoring at the cell surface. Knockout cassettes (KOCs) were routinely amplified by PCR (OneTaq DNA polymerase) using primers P15 & P16 (*FLO1* KOC); P17 & P18 (*FLO1hd* KOC); P19 & P20 (*FLO8* KOC); P21 & P22 (*FLO9* KOC); P23 & P24 (*SPT23* KOC); P25 & P26 (*MGA2* KOC); P27 & P28 (*HAC1* KOC); P29 & P30 (*IRE1* KOC). A yeast integrative plasmid containing the *HAC1* splicing reporter (pCD256-hac1-gfp; not published; kindly provided by Dr. Itay Budin) was cleaved with PmeI & PacI to generate a linear DNA fragment carrying sequences (718 bp & 586 bp) homologous to the genomic *URA3* ORF flanking regions. The linearized plasmid (1 µg) was applied for transformation to integrate the *HAC1* splicing reporter at the *URA3* locus. Genomic integrations were verified by colony PCR using a respective pair of primers that amplify a DNA fragment containing the artificial integration border resulting from the homologous recombination event.

Confirmation of *flo8-1* allele in the background strain was done by sequencing a portion of the *FLO8* ORF after amplification by PCR (primers P45 & P46) from position -24 to +659 using BY4742 genomic DNA as template.

2.3.3. Plasmid construction

Introduction of selectable loxP-*LEU2*-loxP cassette from plasmid pUG73 [23] in plasmid p416-P_{TEF1}-yECitrine [24] was performed as previously described by Nevoigt *et al.* [25]. The resulting plasmid can be used as a template for amplifying a *TEF1* promoter (P_{TEF1}) containing promoter replacement cassette and was named p416-*LEU2*-P_{TEF1}-yECitrine. To replace the *TEF1* promoter of plasmid p416-*LEU2*-P_{TEF1}-yECitrine with the *MET3* promoter (P_{MET3}), the plasmid was cleaved with SpeI and the amplified P_{MET3}-loxP sequence was inserted via recombination-based cloning. The P_{MET3}-loxP sequence was amplified by PCR (OneTaq DNA polymerase, NEB) from plasmid pUG72-P_{MET3} using primers P3 and P4. pUG72-P_{MET3} was generated by inserting the *MET3* promoter sequence [26] amplified from S288C genomic DNA (OneTaq DNA polymerase; primers P1 & P2) in SpeI cleaved plasmid pUG72 via recombination-based cloning.

The integration of yeast endogenous genes (*OLE1*; *SPT23p90*; *MGA2p90*) in plasmid pCM188 (doxycycline repressible expression, CEN/ARS; *URA3* marker, [27]) was performed by recombination-based cloning. For this, pCM188 was digested with BamHI and NotI and the ORFs were amplified by PCR (Q5 DNA polymerase, NEB) using S228C genomic DNA as template. Plasmids pCM188(*LEU2*)-*SPT23p90* and pCM188(*LEU2*)-*MGA2p90* were generated by inserting an additional loxP-*LEU2*-loxP cassette amplified from plasmid pUG73 [23] (OneTaq DNA polymerase) in HindIII cleaved plasmids pCM188-*SPT23p90* and pCM188-*MGA2p90*. Flanking of PCR products with sequences homologous to the restricted plasmid backbone was achieved by using corresponding overhang primers (primers P7 & P8 *(OLE1);* P9 & P10 (*SPT23p90*); P11 & P12 *(MGA2p90)*; P13 & P14 (loxP-*LEU2*-loxP)).

Plasmids pGREG523-P_{SPT23}-^{myc}*SPT23* and pGREG523-P_{MGA2}-^{myc}*MGA2* (CEN/ARS; *HIS3* marker) for expressing 13xmyc-tagged versions of full length Spt23p or Mga2p from their native promoters P_{SPT23} or P_{MGA2} were generated by replacing the *HIS3* stuffer and *GAL1* promoter (P_{GAL1}) from plasmid pGREG523 [28] with *SPT23* ORF and P_{SPT23} or *MGA2* ORF and P_{MGA2}, respectively. The ORFs and the native promoters (1kb upstream of ORF) were amplified from S288C genomic DNA by using corresponding overhang primers (primers P31 & P32 (*SPT23*); P33 & P34 (P_{SPT23}); P41 & P42 (*MGA2*); P43 & P44 (P_{MGA2})). The PCR amplified ORFs were inserted in the SalI cleaved plasmid pGREG523 by recombination-based cloning, generating plasmids pGREG523-*SPT23* or pGREG523-*MGA2*. P_{GAL1} from

plasmids pGREG523-*SPT23* or pGREG523-*MGA2* were cut out using restriction enzymes AscI and NotI and replaced by PCR amplified P_{SPT23} or P_{MGA2} via *in vivo* recombination cloning. The same way P_{GAL1} was replaced by the *TEF1* promoter (P_{TEF1}) from plasmid p416-P_{TEF1}-yECitrine [24] for generating plasmid pGREG523-P_{TEF1}-^{myc}*SPT23 (*primers P39 & P40 (P_{TEF1})). For generating a high-copy plasmid variants, the CEN/ARS sequence of the pGREG523 backbone was replaced by the 2µ ORI. For that the 2µ ORI of plasmid pRS425 was amplified with overhang primers (P37 & P38) and inserted in PmlI cut plasmids pGREG523-P_{SPT23}-^{myc}*SPT23* and pGREG523-P_{TEF1}-^{myc}*SPT23* via recombination-based cloning resulting in plasmids pGREG523(2µ)-P_{SPT23}-^{myc}*SPT23* and pGREG523(2µ)-P_{TEF1}-^{myc}*SPT23.*

Plasmid pGREG523-P_{SPT23}-^{myc}*SPT23*$_{W1042}$ for expressing a W1042L mutant variant of Spt23p was generated by modifying plasmid pGREG523-P_{SPT23}-^{myc}*SPT23*. For that pGREG523-P_{SPT23}-^{myc}*SPT23* was cut with SpeI and BamHI and the removed sequence part was replaced via recombination-based cloning by the respective PCR amplified sequence part harboring the indicated W1042L mutation. The PCR fragment was amplified from S288C genomic DNA using respective overhang primers (P35 & P36) introducing the new L-Leucine (L) encoding codon (CAA) at the 3' terminal end.

The ER-sfGFP-HDEL encoding cassette of the plasmid pRS415-ER-sfGFP-HDEL (*LEU2* marker; kindly provided by Dr. Eric Snapp; [29]) was amplified with PCR (Q5 DNA polymerase; primers P47 & P48) and cloned into KpnI and SacI cleaved plasmid pRS416 (*URA3* marker).

Co-transformation of linearized plasmid backbone and PCR product for recombination-based cloning *in vivo* were routinely carried out by using the Frozen-EZ Yeast Transformation II kit (Zymo Research) according to manufacturer's instructions. PCR conditions were chosen according to manufacturer's instructions.

Plasmids and primers used in this study are listed in the supporting information (Tab. II-S2 & Tab. II-S3).

2.3.4. Growth and flocculation tests

Aerobic growth of *OLE1*-repressible strains was carried out in 24 well plates (Falcon) with 1 mL media at 30°C using a microplate reader (BioTek Synergy 4; BioTek Instruments) with integrated temperature control and under continuous orbital shaking (slow shaking mode). The plates were sealed with a gas permeable adhesive seal (Thermo Fisher Scientific) to avoid evaporative losses of culture medium. These conditions were chosen to maintain consistent oxygenation of the cultures. Absorbance readings at 600 nm were used to

characterize cell growth and detect flocculation via fluctuations in readings. Flocculation was also detected after 24 hours of growth via 24 well plate imaging (UVP BioSpectrum Multispectral Imaging System) and confocal microscopy of cells in growth media stained with Calcofluor White at 23 °C. Micrographs were acquired on a LSM 710 (Zeiss) scanning confocal microscope with an oil immersion lens (100x magnification, 1.4 numerical aperture) using ZEN 2009 software (Zeiss).

Growth media for flocculation assays without Ca^{2+} were prepared identically to standard synthetic defined (SD) drop-out media but using YNB without calcium (Formedium).

Oxygen-limited fermentation growth of cells was carried out in a home-built apparatus based on 250 mL culture flasks fitted with rubber stopper. Caps were connected with tubing to a water bath, which allowed gas ex-flow via bubbling but restricted gas inflow. Flasks also featured syringe-fitted tubing for culture sampling at time points during growth. Cultures (50 mL) were briefly flushed with nitrogen before sealed after inoculation. Comparative aerobic growth was performed in 250 mL shake flasks with loose-fitting gas-permeable caps. Acute hypoxia was induced by thoroughly flushing aerobically growing cultures with argon and sealing their flasks with a tightly fitting rubber stopper connected to an argon-filled balloon to provide positive pressure.

2.3.5. Fatty acid analysis

Total lipids were routinely extracted from yeast cells harvested from 1 mL liquid culture using a modified Bligh Dyer method [30]. Prior to lipid extraction, yeast cells were pelleted, resuspended in 400 µL 0.9 M Sorbitol/ 0.1 M EDTA (pH 7.0), and treated with 15 units zymolyase (Zymo Research) for 1 h at 35°C. This incubation step had no influence on the lipid composition as confirmed by comparison with the specific lipid composition from cells disrupted by bead beating (Fig. II–S1). Lipids were extracted from the organic phase of a mixture of 1:1:1 chloroform:methanol:water and dried under nitrogen. Lipid incorporated fatty acids were derivatized to their corresponding fatty acid methyl esters (FAMEs) by transesterification using 2% (v/v) sulfuric acid in methanol (90°C; 2 h). FAMEs were subsequently extracted in 400 µL hexane, of which 1 µL was analyzed on an Agilent 5973 – HP6890 GC-MS using a 30 meter DB-5ms capillary column. The oven was held at 40°C for 3 min, followed by a ramp to 300°C at 20°C/min. The MS was operated in selected ion monitoring (SIM) mode using ions of *m/z* 55 and 74, which represent abundant and diagnostic fragment ions of saturated fatty acids (SFAs) and mono-unsaturated fatty acids (MUFAs), respectively. Abundance of fragment ions with *m/z* 55 was used for relative quantification of corresponding fatty acid species.

Analysis of abundance of different lipid classes (GPL; DAG; TAG; EE) were done by Lipotype GmbH, Dresden, Germany. Sample preparation was done according to the instructions provided by the service company. All analyses were done in biological triplicate.

2.3.6. Spectroscopy

Fluorescence anisotropy analysis of membrane fluidity was carried out on 1 mL of cells in stationary phase that were pelleted, resuspended in 400 µL 0.9 M Sorbitol/ 0.1 M EDTA (pH 7.0), and treated with 15 units zymolyase (Zymo Research) for 1 h at 35°C. 1% of a concentrated stock (5 mM) of di-phenyl-hexatriene (Sigma) in ethanol was added and the samples were incubated at room temperature for 30 min. Steady-state anisotropy measurements were made on a Fluorolog spectrofluorometer (Horiba), equipped with automatic polarizers and a temperature controller. Fluorescent protein expression driven by the *FLO1* promoter or the *HAC1* mRNA splicing reporter construct was monitored on a FACSAria II flow cytometer (BD Biosciences).

2.3.7. Spt23p processing

For western blotting, total protein extracts were obtained from strains cultured at specified methionine concentrations using a urea/SDS protein extraction method [31]. Protein extracts were separated by SDS-PAGE (7.5% Mini-PROTEAN-TGX gels; BioRad), blotted onto a PVDF membrane and probed with 9E10 primary antibodies (mouse anti c-MYC; Developmental Studies Hybridoma Bank) and mAbGEa primary antibodies (mouse anti actin; Thermo Fisher Scientific) in 1XPBST. Primary antibodies were detected with a goat anti-mouse IgG secondary antibody conjugated with horseradish peroxidase (Santa Cruz Biotechnology). Horseradish peroxidase activity was detected with SuperSignal™ West Pico Chemiluminescent Substrate (Thermo Fisher Scientific).

2.3.8. Gene expression analysis

To determine the relative expression levels of individual genes (*OLE1*, *FLO1*, *FLO5*, *FLO8*, *FLO9*, *FLO11*, *SPT23*, *MGA2*), total RNA was extracted from cells in stationary phase cultured for flocculation assays using a commercial kit (YeaStar™; Zymo Research) according to manufacturer's instructions. RNA samples were treated with DNaseI (RapidOut DNA Removal Kit; ThermoFisher Scientific) to remove genomic DNA contaminations. One-step qRT-PCR was carried out using a SYBR Green-based kit (Invitrogen) on a StepOnePlus Real-Time PCR System (Applied Biosystems). Primers were previously described by Van Mulders *et al.* [32] and Verbelen *et al.* [33]. Melting curve

analysis was performed according to thermocycler specifications. Relative expression levels were analyzed with the ΔΔct method and normalized to *ACT1* expression.

For global expression analysis, RNA-Seq libraries were prepared from cells at OD_{600} ~ 1 grown in either SD (BY4742, aerobic or hypoxic), SD – uracil (BY4742 expressing plasmid-based p90 constructs), or SD – methionine (P_{MET3}-*OLE1*, with or without addition of 250 µM methionine). In the case of P_{MET3}-*OLE1* strains, growth was carried out in 24 well plates (as described above), with 24x1 mL cultures pooled together per sample. BY4742 cells were grown in 250 mL flasks as described above. After growth, cells were briefly spun down (5000 rpm, 1 minute) and immediately frozen in liquid nitrogen. Total RNA was extracted from frozen pellets via the hot phenol method [34], and mRNA was isolated via poly-A beads (NEB). From these, Illumina RNA-Seq libraries were prepared with the adapter ligation method (NEBNext Ultra RNA Library Prep Kit for Illumina, New England Bio Labs) and barcoded with index oligonucleotides (NEBNext Multiplex Oligos for Illumina, NEB). Samples were pooled, and sequencing was performed on either an Illumina HiSeq 2000 (P_{MET3}-*OLE1* samples, ~2M reads per sample) or MiSeq (p90s and hypoxia samples, ~ 1M reads per sample). HiSeq runs were performed at the Vincent J. Coates Genomics Sequencing Laboratory at UC Berkeley, supported by NIH S10 Instrumentation Grants S10RR029668 and S10RR027303, while MiSeq runs were performed in-house at the Joint BioEnergy Institute. Sequencing reads were aligned to the S288C R64-1-1 reference genome with TopHat 2 (version 2.0.13) with a max intron length of 2500 and differential analysis was performed with Cuffdiff (version 2.2.1) with the –frag-bias-correct and the –multi-read-correct flags. Infinite values for differential expression resulting from assigned reads in one condition were assigned a $\log_2$ value of 10. Statistical analysis and plotting was done in R and GraphPad Prism. Gene Ontology (GO) term mapping was done with PANTHER (version 10.0; http://www.pantherdb.org) according to PANTHER Classification System in terms of “biological processes” in which respective gene products are involved. A processed data file containing all differential expression values and the raw sequencing data are publicly available at the Gene Expression Omnibus (https://www.ncbi.nlm.nih.gov/geo) using the GEO accession number GSE94345.

2.3.9. *HAC1* mRNA splicing

Splicing of *HAC1* mRNA in dependence of lipid unsaturation was investigated by RT-PCR. For that total RNA was extracted from cells in stationary phase cultured for flocculation assays using a commercial kit (YeaStar™; Zymo Research) according to manufacturer’s instructions. RNA samples were treated with DNaseI (RapidOut DNA Removal Kit; ThermoFisher Scientific) to remove genomic DNA contaminations. RT-PCR was performed

using a commercial kit (OneTaq® One-Step RT-PCR kit, NEB) according to manufacturer's instructions (primers P49 & P50 (*HAC1* mRNA)). Reverse transcriptase negative controls (-RT) were performed by using Taq DNA polymerase (OneTaq® 2X Master Mix with Standard Buffer, NEB). PCR samples were analyzed by standard agarose gel electrophoresis (1% agarose in TAE).

2.4. Results

2.4.1. Construction and characterization of a strain featuring a titratable unsaturated lipid content

Different constitutive and repressible promoters were screened (Fig. II-2A) to effectively replace the native *OLE1* promoter, aiming to generate a system that can sample a wide range of phospholipid unsaturation stoichiometry (% of acyl chains with double bonds). One of these was the *MET3* promoter (P_{MET3}), which has previously been characterized as being tightly controlled (repression) by methionine concentrations in the media [26] and has been used to regulate expression of an essential ergosterol synthesis gene in yeast [35, 36]. Substitution of the endogenous *OLE1* promoter with the *MET3* promoter yielded an unsaturated fatty acid auxotroph on agar plates supplemented with methionine (Fig. II-3A). In liquid media, lipid composition of growing cells was dependent on the concentration of methionine in the media, with the proportion of lipid acyl chains with double bonds ranging from 25% to greater than 80% (Fig. II-2C), as measured by gas chromatography – mass spectrometry (GC-MS) of derivatized fatty acids extracted from cell lipids (Fig. II-2B). Variations in lipid unsaturation for the $P_{TEF1\text{-mut}}$ mutant strains (e.g. $P_{TEF1\text{-mut2}}$ vs. $P_{TEF1\text{-mut11}}$) were not large enough to result in wide range of phospholipid unsaturation (Fig. II-2A) as well as in an observable effect on the growth phenotype (data not shown), while the weak expression from the $tetO_7$-P_{CYC1} strain resulted in a substantial drop of fatty acid unsaturation (Fig. II-2A) as well as in a severe growth defect (data not shown) even in the absence of repressor and was therefore also not considered as suitable cellular system. In contrast, the P_{MET3}-*OLE1* system allowed for rapid growth in the absence of the repressor and inhibited growth with increasing methionine concentrations (Fig. II-3B). The effects of methionine on the P_{MET3}-*OLE1* system was further analyzed on the *OLE1* mRNA level. Since P_{MET3} is repressed by methionine, increasing methionine concentrations should result in a decrease of *OLE1* mRNA. *OLE1* mRNA levels were strongly influenced by external methionine and high methionine concentrations (5 mM) caused a substantial decrease of *OLE1* mRNA (Fig. II-2D). Surprisingly, methionine levels of 100 µM to 150 µM resulted in at least an intermediate (at the time point of sample collection) increase of *OLE1* mRNA compared to unmodified BY4741 cells. These results do not entirely match the methionine effects on the level of lipid unsaturation and might be an artifact caused by a direct methionine effect on the cell's overall metabolic state.

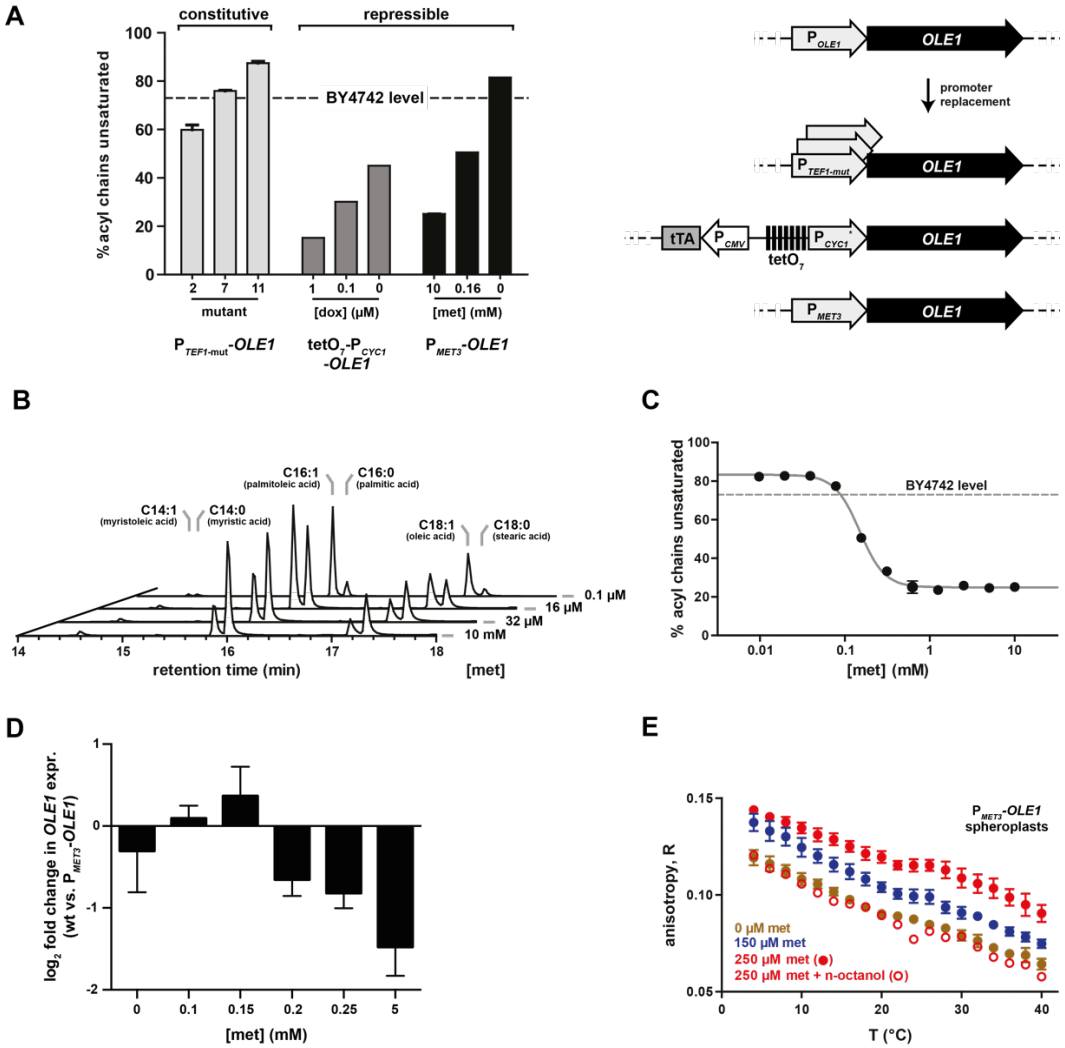

Fig. II-2: Engineering of *OLE1* expression modulates lipid unsaturation. (A) The endogenous *OLE1* promoter (P_{OLE1}) was replaced by 1) a library of *TEF1* promoter mutants ($P_{TEF1\text{-mut}}$) by the strategy described in Nevoigt *et al.* [25], 2) a doxycycline repressible promoter, $tetO_7$-P_{CYC1}, as described by Belli *et al.* [37], or 3) the methionine-repressible *MET3* promoter (P_{MET3}), as described in the text. Fatty acid composition of resulting strains was analyzed as described in Materials and methods. The range of acyl chain unsaturation of P_{MET3}-*OLE1* provided the widest range of manipulation both above and below the level of wild-type cells (BY4742, included for comparison) in these conditions. Promoter replacement of P_{OLE1} was performed with methods analogous to the those described for P_{MET3} insertion. **(B)** GC-MS chromatograms of fatty acid profiles from P_{MET3}-*OLE1* cells at representative external methionine concentrations. **(C)** Percentage of total monounsaturated fatty acid species (% acyl chains unsaturated) at a given methionine concentration was determined from GC-MS data. A sigmoid function (y = a + (b – a)/(1 + 10^((log IC_{50} – x) * m)) was fitted to data points. **(D)** Changes in *OLE1* expression in response to varying external methionine concentrations, as tested by comparing expression in P_{MET3}-*OLE1* vs. unmodified BY4742 cells (wt) grown at respective exogenous methionine. Gene expression was measured by qRT-PCR and shows significant changes of *OLE1* expression. Error bars, SEM (n = 3). **(E)** Spectroscopic measurements of membrane fluidity taken of P_{MET3}-*OLE1* spheroplasts prepared from cells that were grown at different external methionine concentrations. Fluidity was measured at varying temperature by steady state fluorescence anisotropy of di-phenyl-hexatriene (DPH), which was added externally. Anisotropy values are presented as a unit-less ratio: $R = (I_{||} - I_{\perp}) / (I_{||} + 2\, I_{\perp})$, where $I_{||}$ and $I_{\perp}$ are the emission (430 nm) intensities parallel and perpendicular, respectively, to the polarization of the excitation (360 nm). Higher anisotropy values reflect restricted mobility of the DPH probe and thus lower whole-cell membrane fluidity. Membrane fluidity was found to depend on the level of lipid unsaturation content, the presence of the membrane fluidizer n-octanol (0.02% w/v), as well as on the temperature. Values in the presence of n-octanol are shown as an average of two biological replicates. Error bars, SEM (n = 3).

Moderate methionine concentrations might have slightly positive effects on the general fitness of P_{MET3}-*OLE1*, as cells take up methionine from the medium and do not have to synthesize it by themselves, before negative effects resulting from reduced fatty acid unsaturation get eventually dominant. Similar effects were also observed especially for the growth phenotype as intermediate methionine concentrations increased the occurring maximal growth rate (μ_{max}) for P_{MET3}-*OLE1* cells (Fig. II-3D). Nevertheless, methionine effects on total lipid unsaturation were clear and consistent.

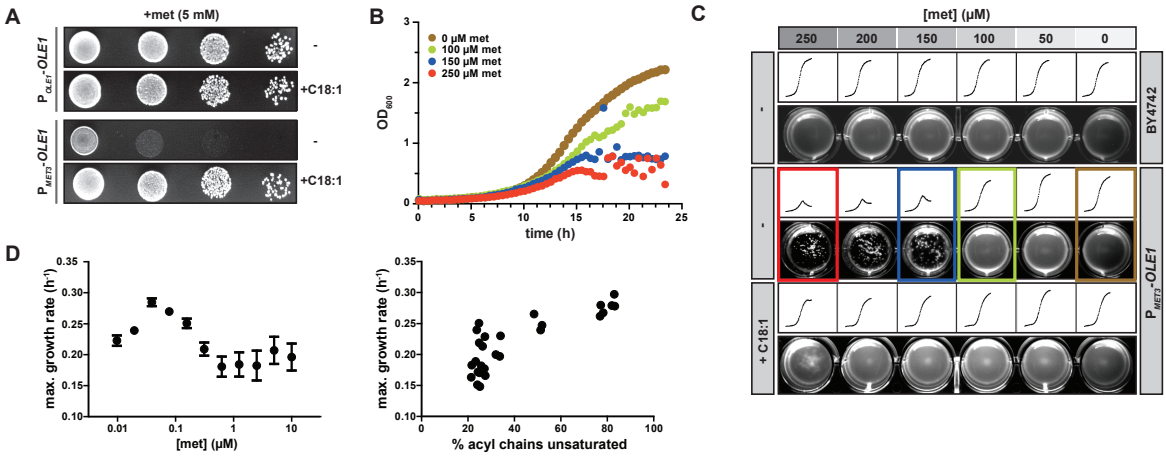

Fig. II-3: Effect of *OLE1* repression on exponential growth and cell-cell adhesion. (A) Replacement of the endogenous *OLE1* promoter (P_{OLE1}) by the methionine repressible *MET3* promoter (P_{MET3}) results in a yeast strain (P_{MET3}-*OLE1*) whose *OLE1* expression is under experimental control. Growth phenotype of P_{MET3}-*OLE1* cells is shown via spotting of a 10-fold dilution series on methionine containing media (5 mM) in the presence and absence of oleic acid. **(B)** Growth curves of P_{MET3}-*OLE1* grown at increasing methionine concentrations show a decrease in growth rate and visible flocculation **(C)**. Flocculation can be prevented by exogenous unsaturated fatty acids. Wild-type cells (BY4742) do not flocculate regardless of external methionine concentrations, in contrast to P_{MET3}-*OLE1* cells grown in the absence of externally supplied oleic acid (C18:1; 0.01% w/v). Top rows, schematic growth curves; bottom rows, photographic documentation of final flocculation phenotype. **(D)** Exponential growth rates as a function of methionine concentrations (Error bars, SEM, n = 3)**.** The relationship between measured unsaturated lipid composition at the end of growth and the max. exponential growth rates of individual cultures grown at varying methionine concentrations. Cells displayed a gradually decreasing growth rate between 30 and 80% unsaturated lipids with a sharp drop below 30%.

To further investigate changes in lipid unsaturation with respect to different lipid classes as well as to verify that specifically the fatty acid unsaturation of membrane-forming glycerophospholipids is altered upon *OLE1* repression, additional GC-MS analyses were performed. The degree of fatty acid unsaturation for glycerophospholipids (GPL) as well as energy storing triacylglycerols (TAG) and diacylglycerols (DAG) (Fig. II-4A) often involved in lipid signaling were all similarly influenced in P_{MET3}-*OLE1* cells when grown at 250 µM methionine compared to when grown in the absence of methionine. The percentage of lipid molecules containing exclusively MUFAs (CXX:2; CXX:3 for TAG) sharply dropped from 50 – 60% down to 10 – 20% for all prominent lipid classes (Fig. II-4B). Accordingly, the

proportion of lipid molecules featuring heterogeneous fatty acid composition (CXX:1; CXX:2 for TAG) or including exclusively fully saturated fatty acids (CXX:0) increased in the same order. Fully saturated lipids were basically not existent in cells with physiological *OLE1* expression and rose up to more than 20% upon *OLE1* repression (Fig. II-4C). The relative abundance of TAG significantly decreased from greater than 50% down to 20% when P_{MET3}-*OLE1* cells were propagated at 250 µM compared to when cells were cultured in corresponding methionine-free medium for an identical time span (Fig. II-4D). A substantial accumulation of TAG is generally observed for yeast in stationary phase [2].

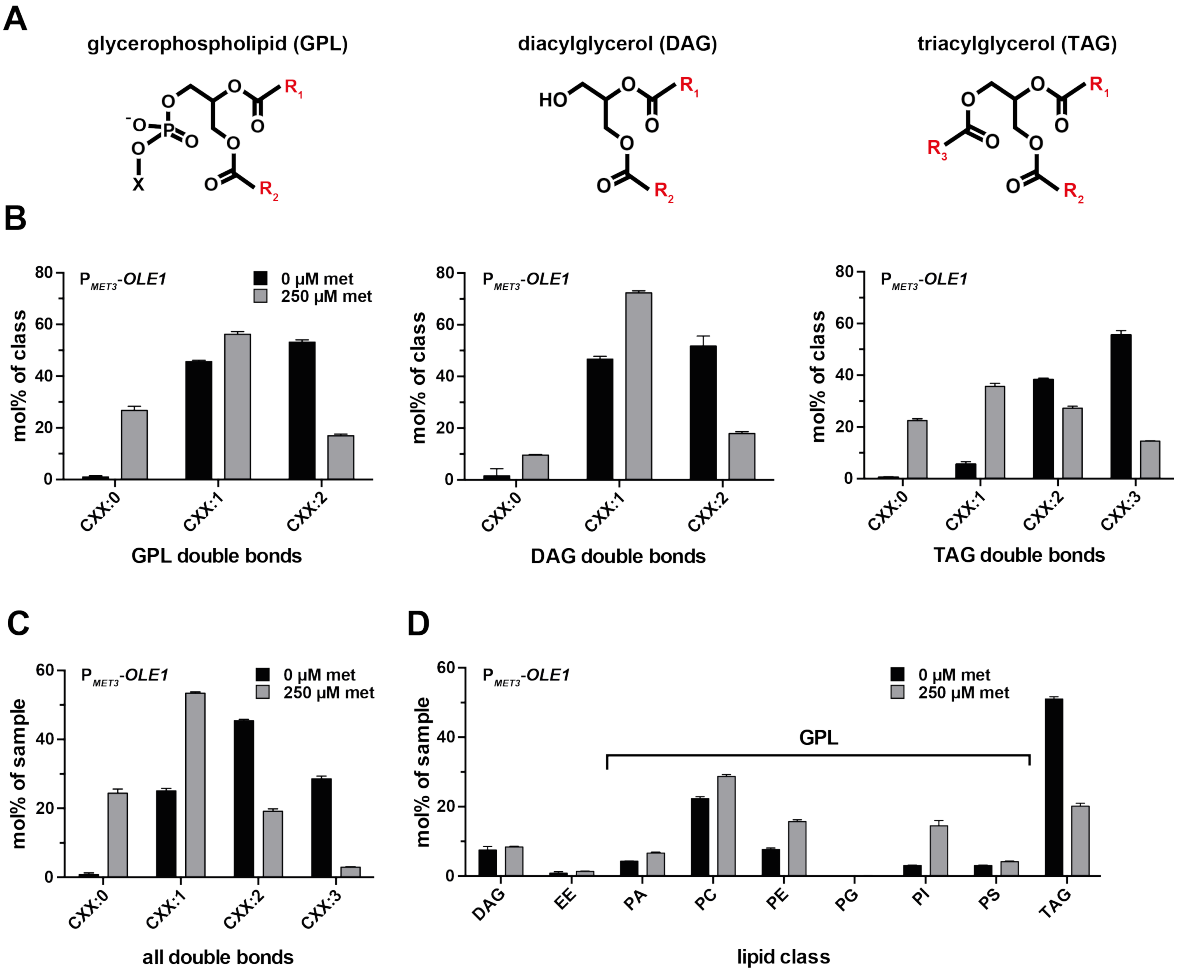

Fig. II-4: Effects of *OLE1* repression on fatty acid unsaturation and relative abundance of different lipid classes. (A) Analyzed lipid classes were membrane-forming glycerophospholipids (GPL), diacylglycerides (DAG), often involved in lipid signaling, as well as energy storing triacylglyerides (TAG) including 3 fatty acid molecules (R_x). **(B)** The percentage (mol%) of molecules including exclusively fully saturated (CXX:0) or monounsaturated fatty acids (CXX:2; CXX:3 for TAG) as well as of molecules featuring heterogeneous fatty acid composition (CXX:1; CXX:1 & CXX:2 for TAG) were determined for indicated lipid classes from P_{MET3}-*OLE1* cells either grown at 250 µM met or in the absence of methionine (0 µM met). **(C)** Compilation of data from (B) showing the average fatty acid composition regardless of lipid classes. **(D)** Changes of relative abundance (mol%) of indicated lipid classes upon *OLE1* repression in P_{MET3}-*OLE1* cells. EE: ergosterol esters; PA: phosphatidic acid; PC: phosphatidylcholine; PE: phosphatidylethanolamine; PG: phosphatidylglycerol; PI: phosphatidylinositol; PS: phosphatidylserine. Error bars, SEM (n = 3).

The accumulation of TAG observed here is therefore not necessarily a direct primary effect of *OLE1* repression but rather a secondary effect that results from a general growth defect upon unnatural fatty acid unsaturation (Fig. II-3B). Absence of methionine benefits growth and thus promotes an earlier transition to stationary phase behavior which is amongst others characterized by the synthesis of energy storing lipids.

Since *OLE1* repression strongly effects fatty unsaturation of membrane-forming GPL, central membrane characteristics such as membrane fluidity should be strongly affected when cells are grown at high methionine concentrations. Fluorescence anisotropy of di-phenyl-hexatriene (DPH) was used to test the effects of lipid unsaturation on membrane fluidity. The emission anisotropy of this probe reflects its thermal motion in the host membrane [38]. Anisotropy measurements on yeast P_{MET3}-*OLE1* spheroplasts incubated with DPH yielded an increasing ordering parameter (R), reflecting lower membrane fluidity, when grown at increasing methionine concentrations (Fig. II-5C). This effect could be partially relieved by the addition of the established membrane fluidizer n-octanol [39] to the spheroplasts (Fig. II-2E). The P_{MET3}-*OLE1* strain characterized here therefore has proven to serve as a suitable cellular model to monitor effects of decreasing membrane fluidity when grown under varying concentrations of methionine.

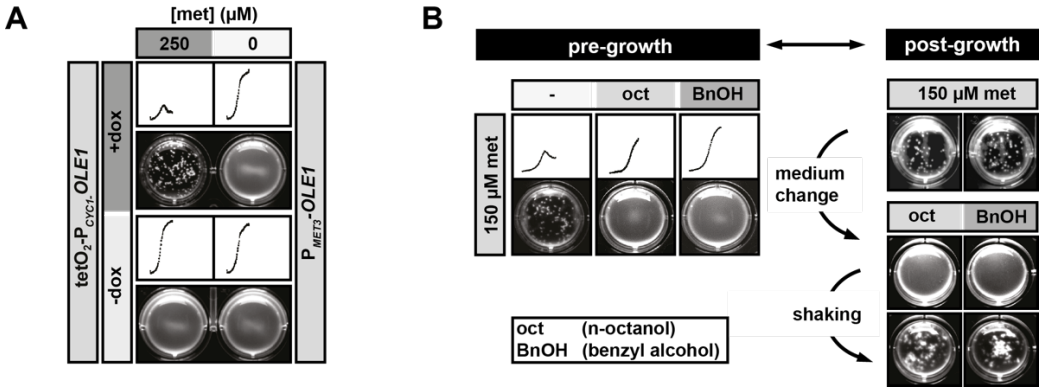

Fig. II-5: Reduced levels of lipid unsaturation and membrane fluidity induce flocculation. (A) Effect of plasmid-based (pCM188-*OLE1*), doxycycline repressible *OLE1* expression on growth and cell aggregation of P_{MET3}-*OLE1* at non-repressed (0 µM met) and repressed (250 µM met) *OLE1* expression. Top rows, schematic growth curves identical to growth curves; bottom rows, photographic documentation of final flocculation phenotype. **(B)** Effect of membrane fluidizers, n-octanol (oct, 0.02% w/v) and benzyl alcohol (BnOH, 10 mM), on flocculation of strain P_{MET3}-*OLE1* when added either during growth or post-growth. For post-growth assays, cells were grown at 150 µM methionine to develop flocculation. Cells were then washed with water, deflocculated by pipetting and tested for reflocculation in the presence of membrane fluidizers.

2.4.2. Membrane fluidity regulates yeast flocculation through Spt23p-mediated activation of *FLO1*

While characterizing the effect of lipid unsaturation on exponential growth rates (Fig. II-3D), an unexpected phenotype was observed: cells with low lipid unsaturation visibly clumped together, forming macroscopic aggregates that precipitated from the medium (Fig. II-3C).

Cell aggregation was blocked when D-mannose was added to the culture medium post-growth, consistent with a role for a class of mannose-binding proteins, termed flocculins, that cause adhesion between the polysaccharide-coated cell walls of neighboring yeast cells [40]. Other monosaccharidic hexoses as well as disaccharidic maltose had no effect on flocculation (Fig. II-6A). Reduced flocculation was also observed when cells were grown in the presence of the established membrane fluidizers n-octanol (oct; 0.02% w/v) and benzyl alcohol [41, 42] (BnOH; 10 mM) (Fig. II-5B), though these did not affect lipid unsaturation (Fig. II-S4B). This indicated that low membrane fluidity, and not lipid composition per se, were responsible for flocculation. Flocculation was unaffected when these additives were introduced post-growth (Fig. II-5B), as was the case for oleic acid (Fig. II-3C), suggesting that flocculation resulted from a transcriptional response to low membrane fluidity.

Expression changes upon *OLE1* repression were screened for a set of flocculation (*FLO*) genes and a significant increase in expression of a single flocculation gene, *FLO1* was identified (Fig. II-S3). Flo1p is a GPI-anchored cell wall mannose binding protein, and thus is functionally consistent with the dispersion of flocs in high concentrations of D-mannose (Fig. II-6A). Deletion of *FLO9*, which was also slightly activated upon *OLE1* repression (Fig. II-S3), had no effect on lipid induced flocculation (Fig. II-6F). In contrast, a partial deletion of the Flo1p hydrophobic domain which impairs the anchorage of the protein to the cell wall [43] resulted in a loss of flocculation (Fig. II-6F) indicating that proper localization and function of *FLO1* and not just the presence of the carbohydrate binding domain is crucial for lipid induced flocculation.

Micrographs (Fig. II–S2) showed that clumping was not due to any sort of defects in cell division (e.g. chain formation [44] or agglomeration [45], but rather resulted from binding of neighboring yeast cells through cell wall interactions. It was possible to restore non-adhesive growth by the addition of exogenous oleic acid to the culture during growth (Fig. II-3C), as well as by plasmid-based expression of *OLE1* (Fig. II-5A, Fig. II-S4A), demonstrating that the flocculation is induced by modified *OLE1* expression levels and altered lipid composition.

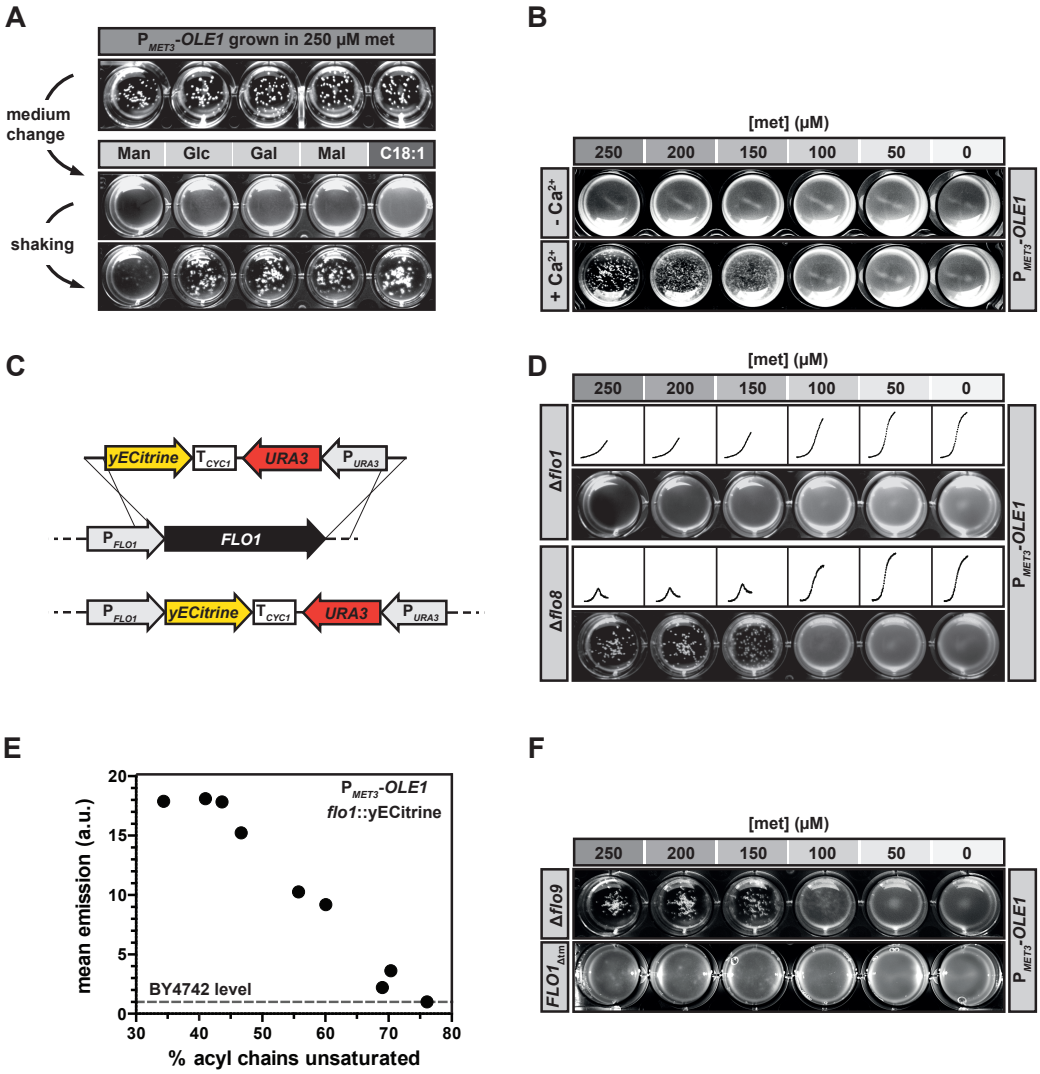

Fig. II-6: Lipid induced flocculation is mediated by Flo1p. (A) The effect of the indicated compounds (sugars & oleic acid) on restoring non-adhesive growth was tested by resuspending adhesive cells (P_{MET3}-*OLE1* grown at 250 µM met) in medium containing D-mannose (Man, 0.5 M), D-glucose (Glc, 0.5 M), D-galactose, (Gal, 0.5 M) D-maltose (Mal, 0.5 M), oleic acid (C18:1, 0.01% w/v). For these post-growth assays, cells were grown at 250 µM methionine to develop flocculation. Cells were then washed with water, deflocculated by pipetting and tested for reflocculation in the presence of indicated compounds. **(B)** The function of flocculins such as *FLO1* strongly depends on the availability of Ca^{2+} which takes part in the binding of the carbohydrate to the protein. In the absence of free Ca^{2+} in the medium, cells do not develop a lipid induced flocculation phenotype. **(C)** To knockout *FLO1* in the P_{MET3}-*OLE1* background, the entire *FLO1* ORF was replaced by a cassette containing the yECitrine ORF as well as an *URA3* selection marker. The resulting genomic construct mediates *FLO1* promoter (P_{FLO1}) driven yECitrine expression. **(D)** Lipid-induced flocculation with *FLO1* (abolishes flocculation) or *FLO8* (no effect) knockouts grown at various external methionine concentrations. **(E)** Fluorescence emission of P_{MET3}-*OLE1* cells with P_{FLO1} driving yECitrine expression grown at different methionine concentrations. Fluorescence emission, measuring P_{FLO1} activity, was correlated with unsaturated lipid stoichiometry. **(F)** Deletion of *FLO9* does not abolish lipid induced flocculation. In contrast, deletion of the hydrophobic domain (Δtm) of *FLO1* strongly impairs flocculation, probably by preventing proper anchorage of Flo1 to the cell surface.

However, the activation of *FLO1* expression was surprising in the S288C strain background, which features an in-frame stop codon in *FLO8*, encoding the major transcription factor activating flocculation. This allele (*flo8-1*, 425 G → A) has been proposed to have been

selected for during strain cultivation due to the difficulty of working with flocculent strains in the lab [46]. It was confirmed that lipid-triggered flocculation was independent of the canonical pathway by knockout of *FLO8*, which did not affect flocculation (Fig. II-6D) nor lipid composition (Fig. II-S4C). In contrast, deletion of *FLO1* completely abolished flocculation (Fig. II-6D) and did not affect lipid unsaturation (Fig. II-S4C). In this deletion strain, *FLO1* was replaced with a fluorescent reporter gene (yECitrine) (Fig. II-6C), which allowed to monitor the increase in P_{FLO1} activity as lipid unsaturation dropped from 80% to 45% (Fig. II-6E).

Induction of the unfolded protein response (UPR) is a known phenotype that is triggered by low lipid unsaturation and thereby increased membrane thickness and lipid packing density [47]. The UPR is a conserved cellular program that is activated by the accumulation of misfolded proteins in the ER lumen and provides multiple strategies to deal with ER stress in order to maintain ER integrity and the proper function of the secretory pathway. Strategies that are provided by the UPR to respond to the accumulation of misfolded proteins include haltering of further protein translation, the synthesis of molecular chaperons that support protein folding and the degradation of harmful protein aggregates [48].

Unfolded proteins are directly sensed by the N-terminal domain of the ER-membrane embedded endoribonuclease Ire1p. Binding of unfolded proteins in the ER lumen to Ire1p induce its oligomerization, thus eventually activating the Ire1p C-terminal RNase domain which is located in the cytosol. Activated Ire1p catalyzes a nonconventional splicing reaction of *HAC1* mRNA that removes an intronic sequence from the *HAC1* mRNA which usually prevents proper mRNA translation due to a physical interaction with the mRNA's 3'UTR, thus producing a translatable *HAC1* mRNA (Fig. II-7A). The Hac1p transcription factor binds the unfolded protein response elements (UPREs) that are found in the promoter of approximately 5% of all genes in yeast [49]. Among them, a large number of ER-resident chaperones were identified as a response to accumulated misfolded proteins [50] as well as genes that are involved in all stages of the secretory pathway [49]. However, in addition to them, components of the phospholipid biosynthetic pathway are targets of Hac1p and the UPR, suggesting a regulatory function of the UPR in the biogenesis of the ER membrane. Indeed, recent work could show that aberrant lipid compositions, or more precisely increased lipid packing within the ER membrane can also directly activate Ire1p and thereby finally inducing UPR [51]. These results suggest two completely distinct types of Ire1p activating stimuli – unfolded proteins and non-physiological lipid bilayer characteristics – although ER membrane-based processes like (co-translational) protein translocation would provide mechanistic explanations how intrinsic membrane properties could influence proper protein folding [52].

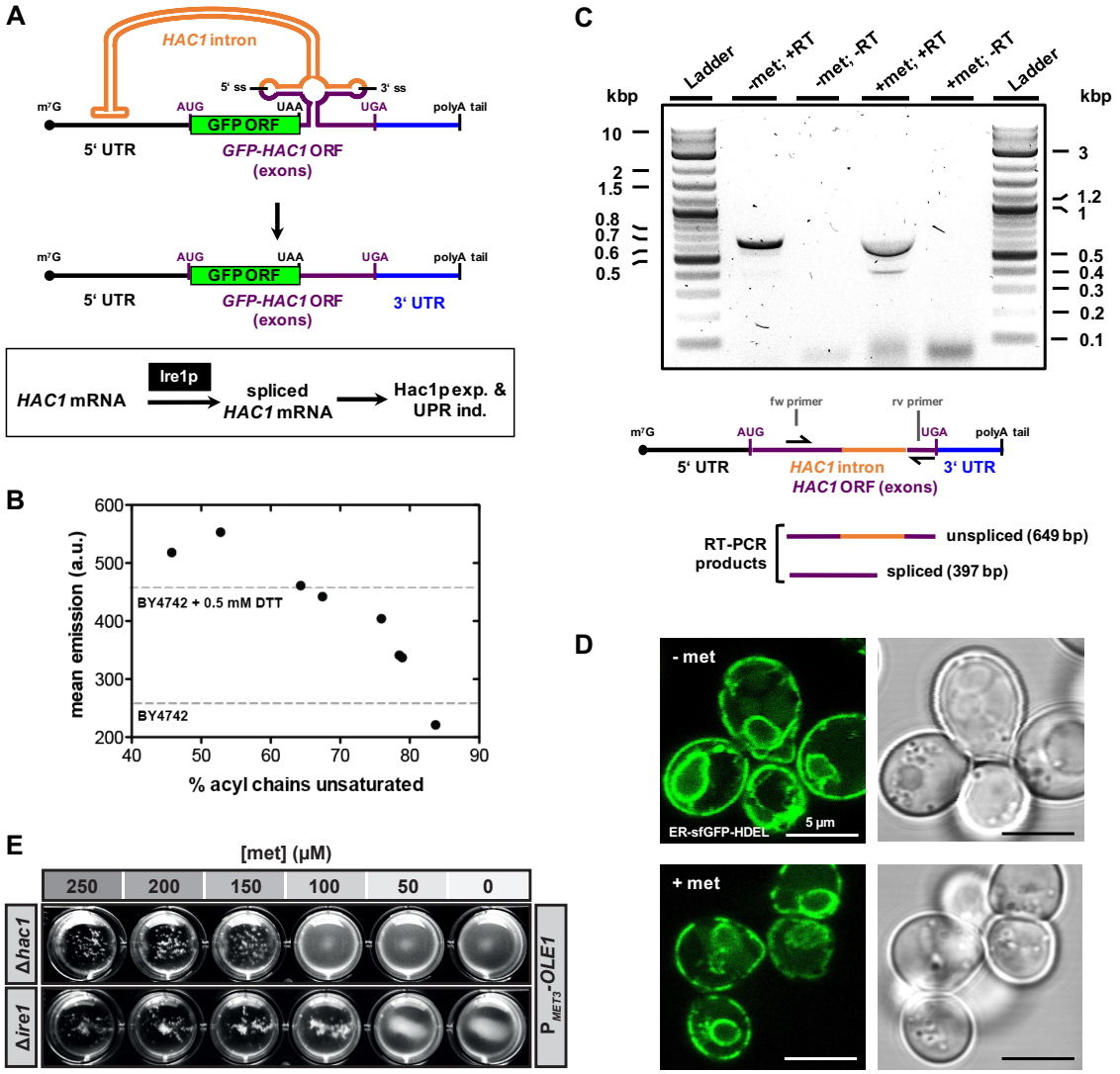

Fig. II-7: Reduced levels of unsaturated lipids induce unfolded protein response (UPR) in budding yeast. (A) *HAC1* mRNA encodes for a transcription activator which serves as a key player of the UPR induction pathway. Natural *HAC1* mRNA owns an intron which prevents its proper translation. Upon ER stress, native *HAC1* mRNA gets processed in a nonconventional splicing reaction catalyzed by the endoribonuclease Ire1p. Splicing removes the 252 bp intron, thus producing a translatable *HAC1* mRNA yielding Hac1p that upregulates UPR genes. A *HAC1* mRNA splicing reporter was used to monitor induction of UPR. The splicing reporter contains the GFP ORF instead of the natural *HAC1* ORF. ER stress-induced mRNA splicing allows for GFP reporter expression. *HAC1* mRNA (splicing reporter) schematics were adopted from Aragon *et al.* [53]. **(B)** GFP expression from the *HAC1* mRNA splicing reporter is induced upon decreased lipid unsaturation in P_{MET3}-*OLE1*. Mean fluorescence emission of cell cultures was measured by flow cytometry. Dotted lines indicate mean fluorescence emission values of untreated wild-type cells (BY4742) and those that were treated with the strong reducing reagent DTT (0.5 mM). **(C)** RT-PCR analysis reveals direct *HAC1* mRNA splicing. Spliced *HAC1* mRNA (397 bp PCR product) can be additionally detected in P_{MET3}-*OLE1* cells grown in 250 µM met whereas cells grown in the absence of methionine yield only unspliced *HAC1* mRNA (649 bp PCR product). Primer binding sites for *HAC1* cDNA are schematically indicated. Note that the length of RT-PCR products does not reflect the length of *HAC1* mRNA. –RT: RT-PCR negative control w/o reverse transcriptase (RT); Ladder: 2-Log DNA ladder (NEB). **(D)** An artificial ER-sfGFP-HDEL fusion protein serves as ER-lumenal marker. P_{MET3}-*OLE1* grown in 250 µM met (+met) show no aberrant ER morphology as compared to cells grown in the absence of methionine (-met). Thus, ER lipid stress is not necessarily accompanied by changes in ER morphology. **(E)** Induction of lipid induced flocculation does not involve the UPR induction pathway. Knockout of either *HAC1* (Δ*hac1*) or *IRE1* (Δ*ire1*) does not abolish methionine-induced development of flocculation in P_{MET3}-*OLE1*.

Since UPR can be directly activated by an unnaturally saturated lipidome and Hac1p activates a large variety of different genes as well as due to the fact that *FLO* gene expression in wild yeasts is inherently induced by various, partially contrary stress stimuli, it should be checked and ruled out that activation of *FLO1* expression is an unspecific result of lipid-mediated UPR induction.

A previously published *HAC1* mRNA splicing reporter [53] was used to monitor UPR induction as the lipidome more and more saturates. Ire1p activation induces *HAC1* mRNA splicing reporter processing, thus leading to induced GFP expression (Fig. II-7A). The P_{MET3}-*OLE1* cellular system proved to functionally activate UPR upon reduction of unsaturated fatty acids. The strongest activation of UPR (measured as GFP fluorescence emission) was detected at unsaturation levels of 55% to 45% (~2.6-fold increase of GFP fluorescence emission) which even exceed the level of induction by the strong reducing reagent DTT (0.5 mM) that breaks disulfide bonds thereby disrupting proper protein folding (Fig. II-7B). Strong UPR induction appeared interestingly exactly in the range of lipid unsaturation which also leads to strong activation of flocculation (Fig. II-2C; Fig. II-3C), thus raising the possibility of an involvement of the UPR in *FLO1* activation. *HAC1* mRNA could be also directly detected by RT-PCR. Only P_{MET3}-*OLE1* cells that were propagated at 250 µM met yielded an additional RT-PCR product that represents a shortened species of the full length *HAC1* mRNA that was in contrast observed for cells either cultured in the presence or absence of external methionine (Fig. II-7C). The lipid composition of the ER membrane is relatively different from that of other membranes such as the plasma membrane – it features almost exclusively glycerophospholipids as well as a high proportion of phosphatidylcholine (PC) [1] which usually contains a high extent of unsaturated fatty acids [54]. Furthermore, the ergosterol content is exceptionally low in that organelle [1], so that taken together, ER membranes feature very high membrane fluidity that might be essential for ER-specialized processes such as protein translocation or even the proper structural organization of the compartment [47]. Therefore, a severe reduction of the overall cellular Ole1p activity might particularly affect ER membranes and strongly disturb organelle morphology, thus, indirectly induce UPR. To check for aberrant ER morphology, a HDEL-sequence tagged GFP variant (sfGFP; superfold) [29] that is targeted to and retained in the ER lumen, was expressed in P_{MET3}-*OLE1* cells with or without altered membrane lipid composition. However, ER morphology was not affected by an overly saturated lipidome, thus indicating that ER lipid stress is not necessarily accompanied by changes in structural ER organization (Fig. II-7D). Knocking out Ire1p and Hac1p eliminates the two key players of UPR induction in budding yeast so that UPR is fully suppressed. Lipid-induced

flocculation was unaffected by both knockouts, definitively ruling out a direct involvement of UPR into the cellular pathway for activating *FLO1* expression (Fig. II-7E).

The observations that membrane-fluidizing additives inhibit flocculation led to the hypothesis that activated forms (cleaved off p90 domains) of known membrane fluidity sensors (Spt23p and Mga2p) can directly initiate *FLO1* transcription, as is the case for *OLE1* in the native feedback loop to maintain physiological membrane fluidity. Previous studies could observe reductions in Spt23p/Mga2p proteolytic processing by the supplementation of the growth media with highly-fluidizing polyunsaturated fatty acids, which are not naturally found in *S. cerevisiae* [15, 55]. Instead it should be tested here, if genetic titration of *OLE1* would modulate Spt23p/Mga2p processing in response to varying levels of unsaturated lipids that are natively found in yeast and thus give stronger evidence of a physiological role for lipid environment-mediated Spt23p/Mga2p proteolytic processing. For that, an N-terminally 13xmyc-tagged Spt23p variant (^{myc}Spt23p) was constructed, whose proteolysis can be monitored by Western blotting (Fig. II-8A) and was expressed from a centromeric plasmid. Spt23p processing and release of p90 domains was induced when *OLE1* was repressed in the presence of methionine, as indicated by a relative enrichment of ^{myc}Spt23p90 over ^{myc}Spt23p (Fig. II-8B). Importantly, ^{myc}*SPT23* was expressed using its endogenous promoter (P_{SPT23}), as overexpression of ^{myc}Spt23p using a strong promoter or a high copy plasmid led to constitutive *FLO1* induction (Fig. II-8E). This was the case not due to an increase of processed ^{myc}Spt23p90 over full-length ^{myc}Spt23p caused by elevated total protein levels (Fig. II-8D) but rather because of an increase in total ^{myc}Spt23p90, which seems to be sufficient to activate *FLO1* expression under wild-type lipid composition (Fig. II-8E). Similar ^{myc}Spt23p processing behavior was observed in an Δ*spt23* background (Fig. II-S5) indicating that additional expression from the endogenous genomic *SPT23* locus as well as potential ^{myc}Spt23p/Spt23p heterodimer formation do not influence protein activation.

In the Δ*spt23* background, proteolytic processing could be completely abolished using a W1042L variant of ^{myc}Spt23p (Fig. II-8B), supporting the importance of this residue in a rotation-based activation mechanism of Spt23p [20].

Lipid dependent processing of the Spt23p paralogue Mga2p was investigated using an equivalent approach. Repression of *OLE1* expression also induced ^{myc}Mga2p proteolytic processing as indicated by a relative enrichment of ^{myc}Mga2p90 over ^{myc}Mga2p. Moreover, *MGA2* expression seems to underlie an additional lipid-dependent control mechanism as increasing protein levels could be observed with a decreasing extent of lipid unsaturation. Even almost no *MGA2* expression was detected at physiological membrane characteristics (0 µM met) which was already slightly increased at 50 µM external methionine (Fig. II-8C).

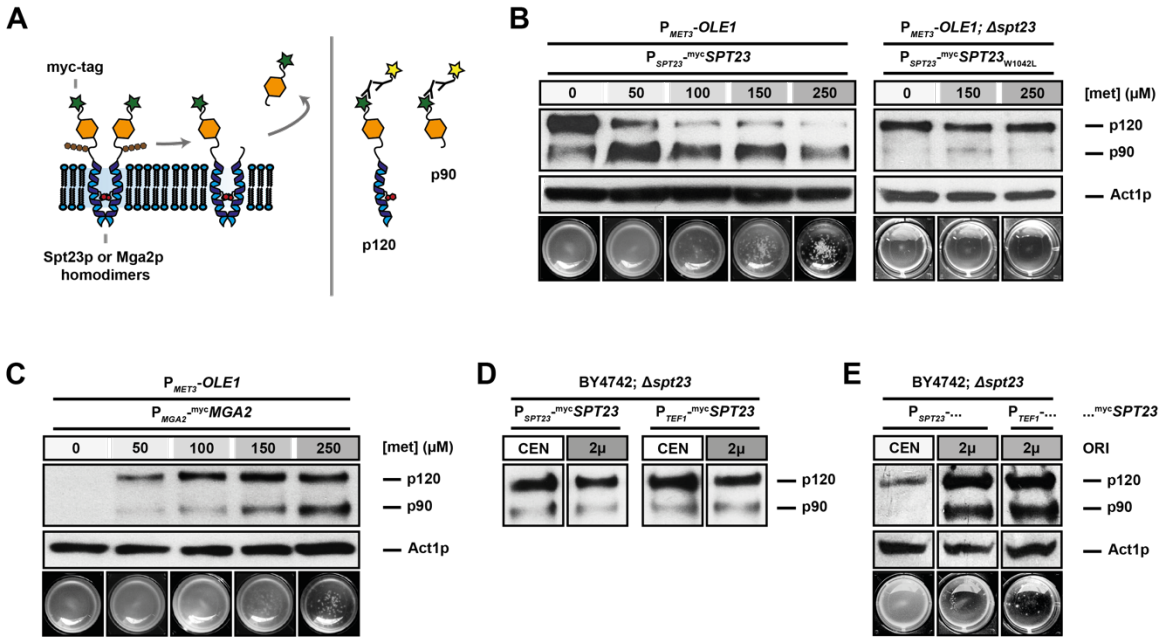

Fig. II-8: Reducing unsaturation of yeast endogenous lipids triggers proteolytic processing of Spt23p and Mga2p. (A) Model of Spt23/Mga2p90 processing upon lowering ER membrane fluidity. Spt23p dimers are proteolytically processed by the 26S proteasome, which releases soluble portions of Spt23p termed Spt23p90 (p90). Shown is a labeled system in which N-terminally 13xmyc-tagged protein variants (^{myc}Spt23p) that can be both detected by Western Blot analysis functionally replaces native proteins. The W1042 residue is indicated in red. **(B)** Western blot analysis showing proteolytic processing of 13xmyc-tagged fluidity sensor Spt23p (^{myc}Spt23p) upon addition of methionine to P_{MET3}-*OLE1* cells. A W1042L ^{myc}Spt23p (^{myc}Spt23p$_{W1042L}$) mutant variant remains largely unprocessed, regardless of methionine addition. Act1p (Actin) was probed as a loading control. **(C)** Western blot analysis showing proteolytic processing of 13xmyc-tagged fluidity sensor Mga2p (^{myc}Mga2p) upon addition of methionine to P_{MET3}-*OLE1* cells. ^{myc}Mga2p was expressed from a centromeric plasmid (pGREG523) under control of its endogenous promoter (P_{MGA2}). The absence of a ^{myc}Mga2p band in the absence of methionine can be explained by transcriptional repression of *MGA2* expression in high lipid unsaturation. **(D)** Different dilutions of total protein extracts form indicated expression variants (from P_{SPT23} or P_{TEF1}; from CEN/ARS ORI or 2μ OR) that contain comparable Spt23p amounts and therefore allow for a comparison of p90 to p120 ratios were analyzed. High Spt23p protein levels do not promote Spt23p proteolytic processing per se. **(E)** High intracellular protein levels of ^{myc}Spt23p caused by expression from a high-copy plasmid variant (2μ ORI) or a strong promoter (P_{TEF1}) led to constitutive induction of *FLO1* expression. This is not a consequence of increased enrichment of ^{myc}Spt23p90 over full-length ^{myc}Spt23p but rather is likely due to an increase in total ^{myc}Spt23p90, which is sufficient to activate *FLO1* expression under wild-type lipid composition.

The Western blot data is supported by *MGA2* expression analysis (RNAseq) showing a strong upregulation of *MGA2* transcription upon *OLE1* repression with a $\log_2$ differential expression value ($\log_2$ DE) of 4.3. FPKM values (fragments of kilobase of transcript per million mapped reads) for *MGA2* in P_{MET3}-*OLE1* grown at 0 μM met of 8.2 (vs. 166.3 when grown at 250 μM met) indicate a generally weak *MGA2* expression level at high lipid unsaturation that might explain low protein levels under these conditions. Gene expression analysis in an *SPT23* knockout strain also suggests a role for Spt23p in the regulation of *MGA2* transcription since upregulation of *MGA2* in the absence of Spt23p was considerably lower ($\log_2$ DE of 4.3 vs. 3.0), however, could not be responsible for the whole effect. Spt23p

might serve only a part of a complex response that acts on *MGA2* expression. Nevertheless, these data provide further evidence that Spt23p and Mga2p act as membrane fluidity sensors that respond to changes in native lipid composition [15, 56].

A following assay addressed genetic roles for *SPT23* and its paralogue, *MGA2*, in *OLE1*-mediated *FLO1* expression and flocculation. Because *OLE1* is freed from its endogenous promoter in the P_{MET3}-*OLE1* background, it was able to delete *SPT23* while maintaining the engineered strain's control of lipid unsaturation with supplemented methionine (Fig. II-S4D). Deletion of *SPT23* strongly reduced flocculation (Fig. II-9A) and *FLO1* expression (Fig. II-9B); flocculation could be fully restored by plasmid-based expression of a *SPT23* variant (^{myc}Spt23p, Fig. II-S5).

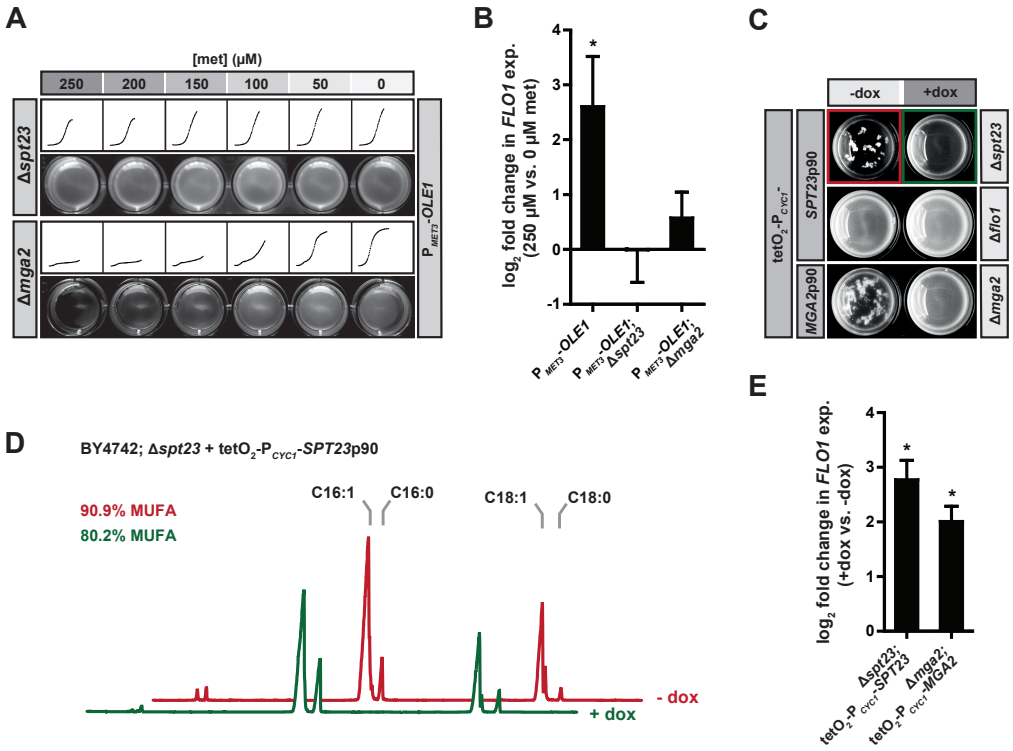

Fig. II-9: Lipid-dependent flocculation is mediated by activated forms of membrane fluidity sensors Spt23p and Mga2p. (A) Effect of *SPT23* or *MGA2* knockout on flocculation phenotype of strain P_{MET3}-*OLE1* grown at various external methionine concentrations. Top rows, schematic growth curves; bottom rows, photographic documentation of final flocculation phenotype. **(B)** Changes in *FLO1* expression upon methionine addition (250 µM vs. 0 µM met) in P_{MET3}-*OLE1*. *FLO1* expression is significantly increased ($p = 0.046$) with functional *SPT23* and *MGA2*, but not in the absence of *SPT23* ($p = 0.99$) or *MGA2* ($p = 0.31$). **(C)** *FLO1*-dependent flocculation can be induced in the wild-type background (BY4742) using repressible (+dox), plasmid-based expression of *SPT23p90* or *MGA2p90* active domains. Flocculation is stronger during expression of *SPT23p90*, indicating the dominant role of this fluidity sensor. Flocculation upon *SPT23p90* expression is abolished in a Δ*flo1* background strain**. (D)** Comparison of fatty acid composition for BY474; Δ*spt23* + $tetO_2$-P_{CYC1}-*SPT23*p90 either in the presence (+dox) or absence (-dox) of the repressor of plasmid-based *SPT23*p90 expression. Exemplary GC-MS chromatograms show that plasmid-based *SPT23*p90 expression slightly increases the content of unsaturated fatty acid species (C14:1, C16:1, C18:1; 90.9%) compared to non-inducing conditions (80.2%). **(E)** Changes in *FLO1* expression upon plasmid-based expression of active variants of membrane fluidity sensors Spt23p90 and Mga2p90, as measured by qRT-PCR. Asterisks designate significant changes in gene expression (*, $p \leq 0.05$). Error bars, SEM ($n = 3$).

MGA2 deletion prevented flocculation as well, but also strongly inhibited cell growth in the presence of external methionine (Fig. II-9A,B), and thus its effects on flocculation could not be fully characterized. This null phenotype could be a result of a potential additional, post-transcriptional role for Mga2p in stabilizing *OLE1* transcripts [57], which would act independently of the applied *OLE1* promoter replacement strategy. To compare the effects of Spt23p and Mga2p on *FLO1* expression, truncated gene products containing only active p90 domains, simulating the proteolysis that activates them endogenously [58], were expressed instead. When these domains were expressed from a repressible promoter ($tetO_2$-P_{CYC1}), flocculation in wild-type cells that was abolished by addition of the repressor (doxycycline) was observed. Flocculation was induced more strongly by Spt23p90 in comparison to Mga2p90, and was abolished completely by deletion of *FLO1* (Fig. II-9C). GC-MS clearly indicated that p90 induced flocculation was no effect of an overly saturated lipidome since plasmid-based p90 expression even increased lipid unsaturation compared to non-inducing conditions (Fig. II-9D). Observed flocculation strengths corresponded to differences in *FLO1* expression upon induction of Spt23p90 and Mga2p90 (Fig. II-9E). Spt23p and Mga2p therefore act upon *FLO1* expression during low lipid unsaturation, with Spt23p serving as the dominant activator.

2.4.3. Lipid-mediated flocculation is triggered by oxygen limitation during fermentation

Next, potential physiological roles for reduced lipid desaturation activating *FLO1* should be identified. For *S. cerevisiae* strains used in brewing, flocculation allows for industrial-scale clarification of the culture (wort) without the use of filtration or centrifugation. Fermentation vessels, unlike laboratory flasks, feature restricted architecture meant to reduce oxygen availability in the culture. While yeast grown anaerobically are strict unsaturated fatty acid auxotrophs [59], it was hypothesized that also a microaerobic environment could restrict Ole1p activity through reduced oxygen binding and availability for the desaturase reaction. To test whether oxygen limitation could drive flocculation, wild-type cells (BY4742) were grown in fermenter like vessels that allow for outflow of gas (e.g. carbon dioxide), but not oxygen uptake (Fig. II-10A).

Growth of cells under these conditions resulted in the increased accumulation of ethanol, i.e. fermentation, compared to well-aerated growth in standard shake flasks (Fig. II-10B and Fig. II-10C) at the expense of biomass (OD_{600} of 2.3 ± 0.06 vs. 2.9 ± 0.06 after 48 hours). As fermentation progressed, triggering of visible flocculation was induced similar to that observed during *OLE1* repression. This did not occur when the culture was well aerated in a standard shake flask, nor in the absence of *FLO1* or *SPT23* (Fig. II-10A).

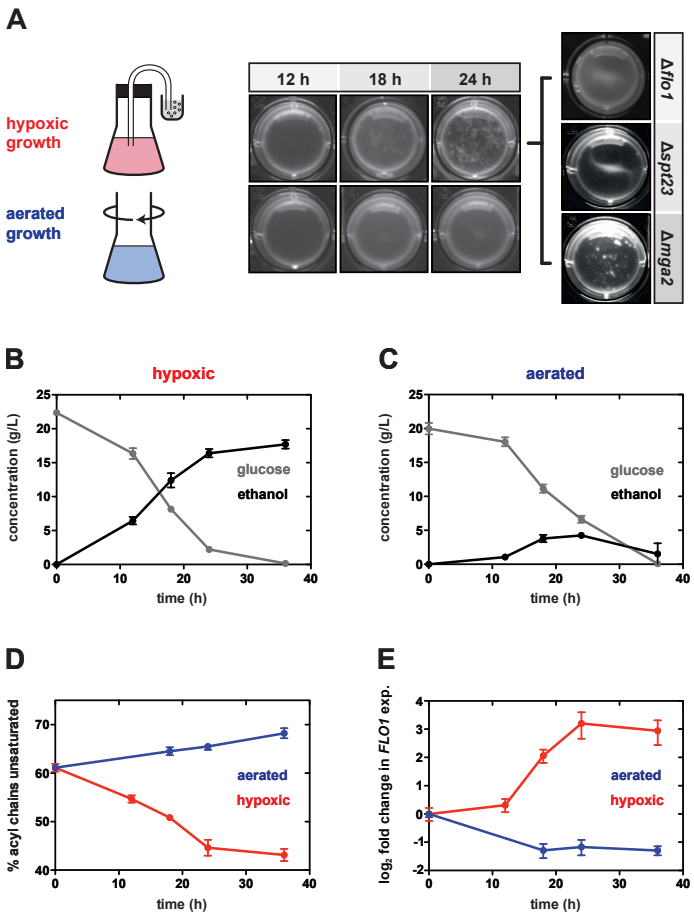

Fig. II-10: Growth under hypoxia induces changes in lipid unsaturation and *FLO1*-dependent flocculation. (A) Wild-type cells (BY4742) were grown either under standard, aerated conditions or in flasks where gas inflow is restricted (see Materials and methods). As growth progresses, visible flocculation occurs only in the oxygen-starved environment. Deletion of either *FLO1* or *SPT23* abolishes hypoxia-induced flocculation, whereas deletion of *MGA2* does not impair flocculation upon growth under limited oxygen availability. **(B)** Oxygen limited conditions correspond to fermentation-style growth, where ethanol accumulates due to the limitation of oxygen for respiration. In contrast, ethanol accumulation is limited during aerated growth **(C)**, where respiration can be active. **(D)** Oxygen restriction leads to a progressive reduction in lipid unsaturation as fermentation progresses, which corresponds to an increase in *FLO1* expression **(E)**, explaining the flocculation phenotype in this environment. Error bars, SEM (n = 3).

The increase in *FLO1* expression under hypoxic growth (Fig. II-10E) mirrored the reduction in lipid unsaturation as fermentation progressed (Fig. II-10D), as monitored by the shift from glucose to ethanol in the culture. Under these conditions, unsaturated lipid stoichiometry was reduced to 45% of all acyl chains, corresponding to the levels where full P_{FLO1} induction and Spt23p processing in P_{MET3}-*OLE1* cells was observed. In contrast to this long-term hypoxia experiment, growth of cells under short-term, strict oxygen starvation, achieved by incubation under argon for 90 minutes, did not lead to increased *FLO1* expression (Fig. II-11A). Because Ole1p acts during *de novo* lipid synthesis, it was hypothesized that only long-term exposure to hypoxic conditions would lead to significant changes in cell lipid composition (Fig. II-11B), and therefore serves as a trigger for flocculation.

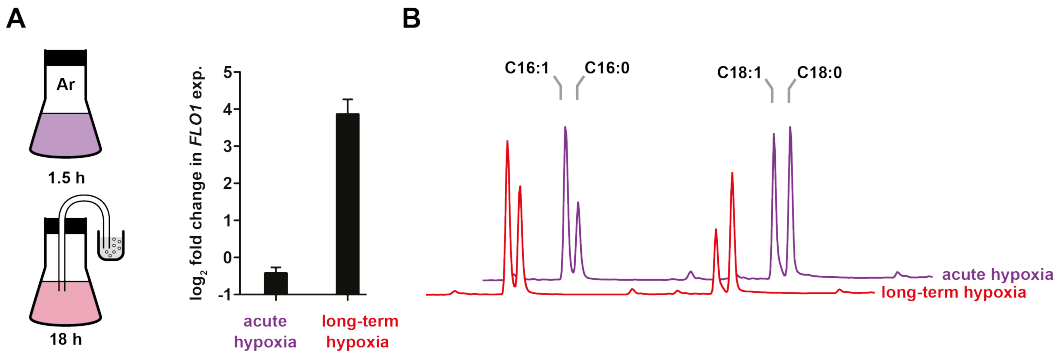

Fig. II-11: Acute hypoxia is not sufficient for changes in lipid unsaturation and *FLO1* expression. (A) Comparison of changes in *FLO1* expression, as compared to aerated growth, for BY4742 either under acute hypoxia (90 minutes under argon) or long-term hypoxia (hypoxic growth; 18 hours in a microaerobic fermenter). Error bars, SEM (n = 3) **(B)** Comparison of fatty acid composition for BY4742 either under acute hypoxia or long-term hypoxic growth. GC-MS chromatograms show that long-term hypoxia leads to a reduction in the major unsaturated species (oleic acid, C18:1) and an increase in major saturated species (palmitic acid, C16:0).

2.4.4. Membrane fluidity-regulated genes are globally activated during microaerobic fermentation

The central and surprising role of lipid composition in regulating a non-membrane process (which is true for flocculation as a cell wall adhesion process) motivated to ask if this was indicative of a larger long-term hypoxic response regulated by membrane fluidity. Deep sequencing of mRNA-derived cDNA (RNA-seq) was used to characterize changes in global gene expression upon *OLE1* repression. Cells (P_{MET3}-*OLE1*) grown in the presence of 250 µM methionine (38.4 ± 2.5 % unsaturated lipids) were sampled after 24 hours of growth and were compared to those with no added methionine (88.3 ± 2.3 % unsaturated lipids). *OLE1* repression led to large-scale gene expression changes, with 1012 genes significantly (q-value ≤ 0.05) upregulated and 882 downregulated (Fig. II-12A).

Systematic GO term mapping of upregulated genes upon *OLE1* repression showed significant enrichment of those involved in lipid and fatty acid metabolism, glycolysis and carbohydrate metabolism, and response to stress stimuli (Fig. II-14A). *FLO1* was one of the strongest overexpressed genes upon *OLE1* repression, with a $\log_2$ differential expression value ($\log_2$ DE) of 5.0. In contrast, downregulated genes include those involved in protein (amino acid) and ribosome synthesis (Fig. II-14B), consistent with non-specific effects of *OLE1* repression in slowing growth and the primary metabolism.

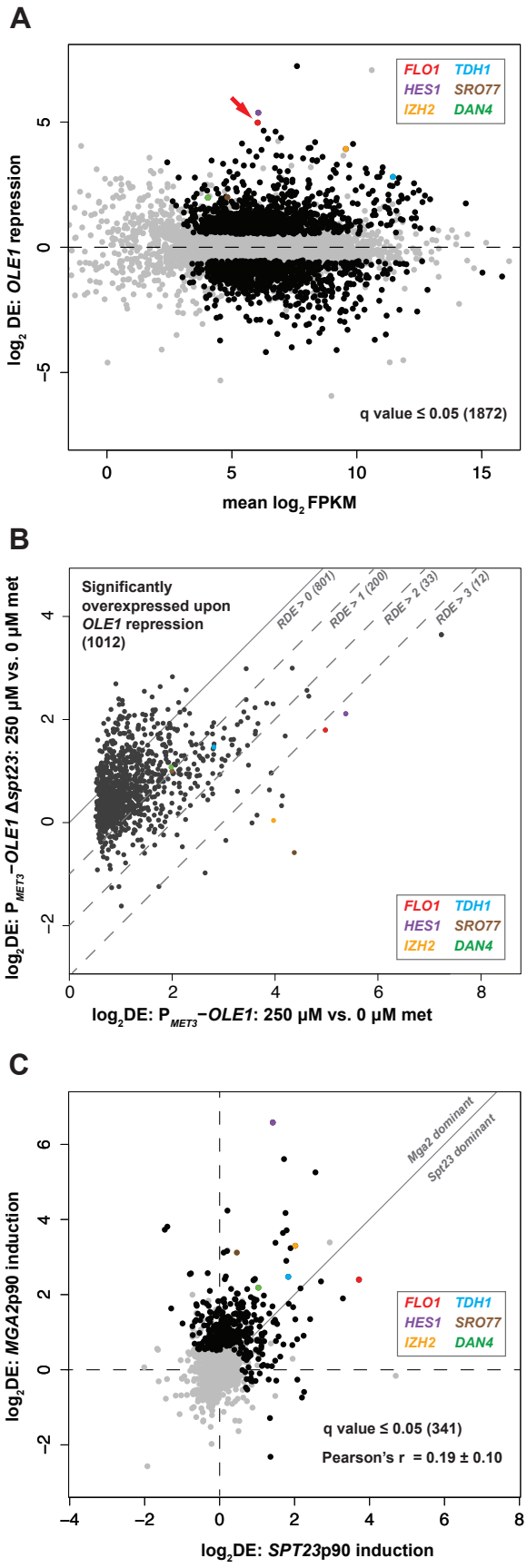

Fig. II-12: Global analysis of membrane fluidity-mediated gene expression. (A) A Bland-Altman plot showing the differential expression (DE) for genes in the P_{MET3}-*OLE1* background grown in the presence of 250 µM (low lipid unsaturation) vs. 0 µM (high lipid unsaturation) methionine, as compared to their mean average normalized expression (FPKM) under these conditions. Genes with significant (q-value ≤ 0.05) differential expression are highlighted in black. Of these 1872 genes, 1012 are upregulated; expression of *FLO1* (in red, arrow) increased more than 30-fold upon *OLE1* repression. **(B)** The effect of Δ*spt23* on the overexpression of *OLE1*-sensitive genes: DE values for P_{MET3}-*OLE1* in 250 µM vs. 0 µM methionine are compared to those for P_{MET3}-*OLE1* Δ*spt23* in 250 µM vs. 0 µM. Of the 1012 upregulated upon *OLE1* repression, 200 feature an at least 2-fold reduction of DE (RDE) in the Δ*spt23* samples. A set of 12 genes including *FLO1* (in red) shows a reduction of gene expression of more than 8-fold upon knocking out *SPT23*. Dashed lines (x – y = 1; 2; 3) visually separate sets of genes with significantly reduced expression and are added for clarity. **(C)** The effect of plasmid-based expression of Spt23p90 and Mga2p90 on the 1012 genes upregulated upon *OLE1* repression (includes gray). Of these, 341 were also significantly induced by either Spt23p90 or Mga2p90 domains (black). This set includes genes involved in a diverse range of cell functions, including metabolism (*TDH1*), lipid synthesis (*HES1*), membrane organization (*SRO77*), metal homoeostasis (*IZH2*), and cell wall structure (*DAN4*). Other examples are listed in Tab. II-S1 by their functional classes. DE values were taken for wild-type cells (BY4742) harboring a plasmid expressing p90 domains of either *SPT23* or *MGA2* grown in either the absence (induced) or presence (repressed) of doxycycline. The vertical line (x – y = 0) separates genes whose expression is dominantly influenced by either Spt23p (below) or Mga2p (above). Dots following the line represent genes that are equally regulated by both transcription activators.

However, these conclusions are based on the assumption that transcriptional changes triggered by *OLE1* repression were largely a result of physiological responses to changes in membrane homeostasis, as opposed to specific activation by lipid-activated transcriptional elements, and could also contain artifacts from reduced growth rates and methionine supplementation. Therefore, expression effects to the induction of active Spt23p90 and Mga2p90 domains were also characterized by RNA-seq. With this approach it should be possible to separate gene regulation effects resulting from specific lipid activation from those that caused by non-specific or secondary effects. These might directly origin from the expose of cells to high external methionine concentrations (e.g. the endogenous *MET3* gene), generally reduced growth rates or cell aggregation and flocculation.

Of the 1012 *OLE1*-sensitive genes (Fig. II-12A), 341 were also significantly activated by either Spt23p90 or Mga2p90 (Fig. II-12C). For *FLO1*, expression was increased by both activators, though more strongly by Spt23p90 (log_2 DE of 3.7 vs. 2.4). Among all genes significantly overexpressed by either p90 domains, there was only a weak correlation between the increase in expression in response to the individual domains (e.g. Mga2p90 vs. Spt23p90, Pearson r = 0.19). Along with the paucity of genes activated by both Mga2p90 and Spt23p90 domains (~15% of the genes activated by either), this indicates a divergent set of targets for these paralogues, despite their presumably similar modes of activation.

Changes in lipid unsaturation have a role in activation of *FLO1* during oxygen limitation (Fig. II-10E; Fig. II-11A). The following experiments should address the question whether and if yes to what extent does this pathway play a role in activation of other Spt23p/Mga2p targets during extended hypoxic growth.

To generate a comparative data set, global expression profiles for wild-type cells (BY4742) grown aerobically compared to those grown under long-term hypoxic conditions (e.g., 18h hours, conditions described above) or under acute hypoxia (90 minutes under argon) were analyzed; first-mentioned conditions mimicked those for *FLO1* expression whereas the latter did not (Fig. II-11). Long-term hypoxia caused widespread changes in gene expression: 1373 upregulated genes with Gene Ontology (GO) terms significantly enriched in the metabolism of coenzymes, vitamins, as well as interestingly fatty acids and lipids (Fig. II-14C), including *OLE1* (log_2 DE of 3.2). In contrast, acute hypoxia induced a significantly smaller transcriptional response (266 upregulated genes), yet still included several canonical hypoxic response elements (e.g. *TIR1* and *ANB1*). These profiles are consistent with previous characterizations of gene-dependent timescales for hypoxia response induction upon oxygen starvation responses in *S. cerevisiae*, which was interpreted as suggesting the activity of multiple oxygen sensors [60]. Of the set of genes identified as

being sensitive to *OLE1* repression and induced by Spt23p90 or Mga2p90 domains (341 genes; Fig. II-12C), 70% were significantly upregulated during long-term hypoxic growth (Fig. II-13A). Differential expression values for long-term hypoxic growth were significantly correlated with differential expression upon *OLE1* repression (Figure S7A, r = 0.38, p = $2x10^{-13}$) and for the additive effects of Spt23p90 and Mga2p90 induction (Fig. II-13B, r = 0.49, p < 10^{-15}), which is consistent with a model in which the two activators have independent effects on transcription (Herschlag and Johnson 1993).

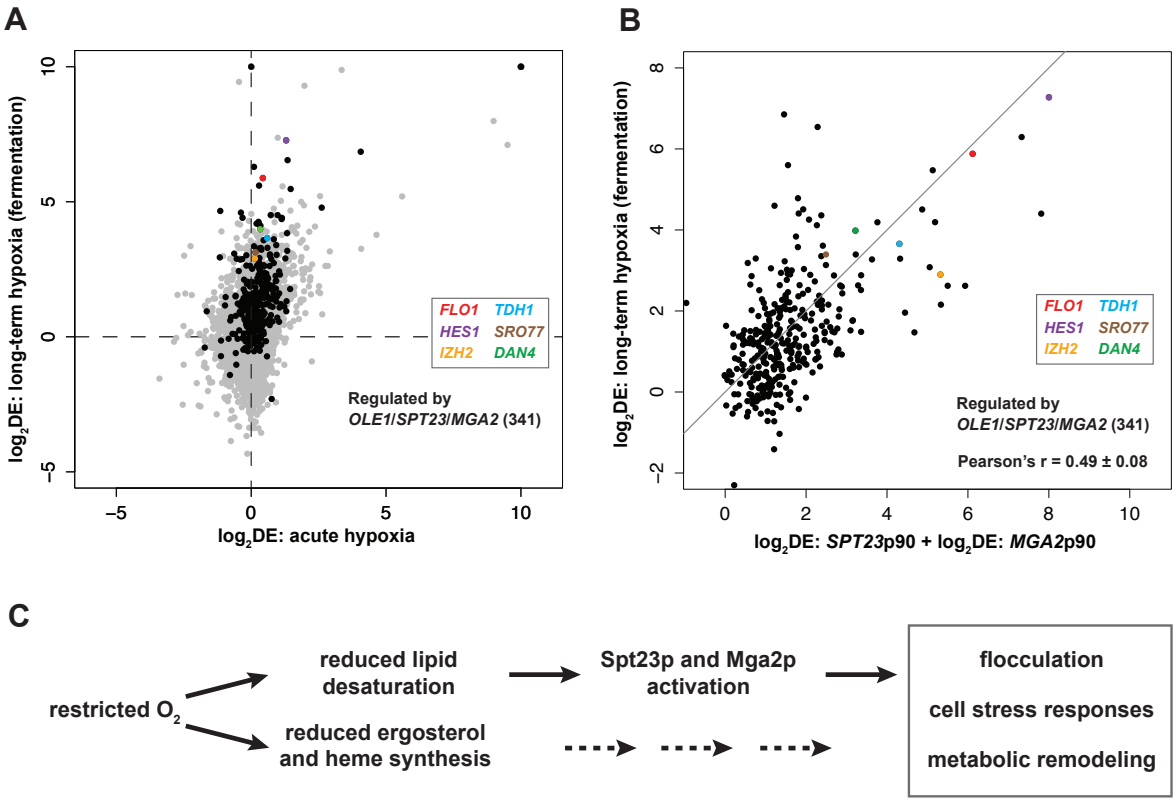

Fig. II-13: Membrane fluidity sensors globally activate gene expression during long-term hypoxic growth. (A) Comparison of differential expression (DE) values upon long-term hypoxia (18 hours) and acute hypoxia (90 minutes) for all genes (gray) and those regulated by membrane fluidity identified in panel B (341 genes; black). Fluidity-regulated genes are induced under long-term hypoxic growth, which correspond to fermentation, but not acute hypoxia. **(B)** Differential expression upon long-term hypoxia is correlated with the combined differential expression due to *SPT23p90* and *MGA2p90* induction (log_2DE *SPT23p90* + log_2DE *MGA2p90*), assuming a model in which the effect of the activators is additive (multiplicative differential expression). Line shows x – y = 0 and is added for clarity. **(C)** Model for the long-term hypoxic response during fermentation. Low oxygen during cell growth reduces lipid unsaturation, activating membrane fluidity sensors (Spt23p and Mga2p), which then induce a wide range of physiological responses to long-term hypoxia (gray box). This pathway acts in parallel with the activity of molecular sensors for sterols and heme, whose synthesis is also oxygen dependent.

These correlations are medium in strength, which likely reflects additional roles for other hypoxic response pathways. In contrast, differential expression values for short-term (90-minute) oxygen starvation were not significantly correlated with either differential expression upon *OLE1* repression (p = 0.07) (Figure S7B) or upon p90 induction (p = 0.5) (Figure S7C).

The ER membrane fluidity regulon is therefore induced by long-term hypoxia in yeast and plays an extensive role in the transcriptional response to fermentation conditions.

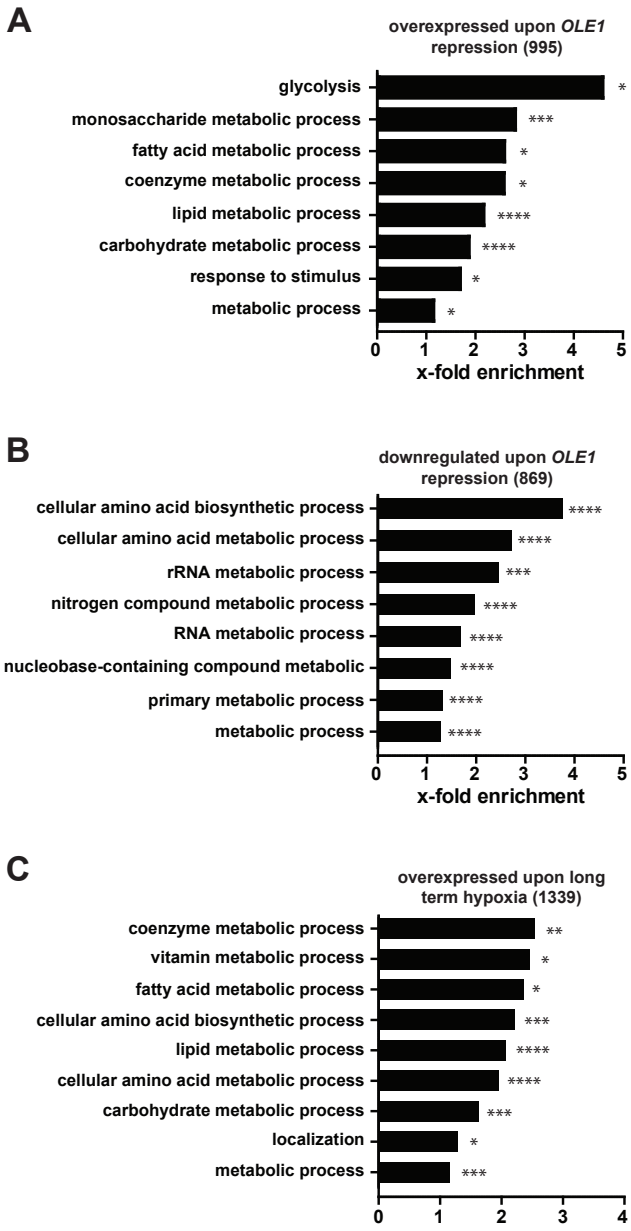

Fig. II-14: Gene Ontology (GO) term mapping of genes overexpressed or downregulated upon stimuli that have proven to alter lipid unsaturation . The analyzed gene sets contain genes that were significantly (q ≤ 0.05) **(A)** overexpressed upon *OLE1* repression, **(B)** that were significantly downregulated upon *OLE1* repression or **(C)** that were significantly overexpressed upon growth under long-term hypoxic conditions. Input gene lists include genes that were identified by RNA-seq analysis and already shown in Fig. II-12A or Fig. II-13A, respectively. GO term mapping was done according to PANTHER Classification System in terms of "biological processes" in which respective gene products are involved. Shown are only those "biological processes" that contain a significant overrepresentation of genes (*, p ≤ 0.05; **, p ≤ 0.01; ***, p ≤ 0.001; ****, p ≤ 0.001). P-values were determined by binomial statistics that were adjusted by Bonferroni correction for multiple testing.

2.5. Discussion

The experiments presented here use rational genetic manipulation of lipid desaturase expression in order to allow for causal study of the roles for lipid unsaturation and membrane fluidity in the physiology of budding yeast. Modulation of *OLE1* promoter activity allowed us to characterize the dependence of yeast physiology on lipid unsaturation. Most strikingly, a role for lipid unsaturation in regulating yeast cell-cell adhesion or flocculation was identified. Flocculation is a well-known aggregation phenotype among different yeast species with a large set of diverse stress conditions, including nutrient limitation and starvation [61-63], temperature and pH stress [62, 64], and cell aging [65-67]. Because native flocculation pathways have generally been studied in yeast species and strains with heterogeneous genetic backgrounds, there has been an assumption that flocculation behavior is a highly strain-specific phenomenon [68]. Due to a nonsense mutation in the *FLO8* gene [46], previous studies showing flocculation in the S288C background relied on restoring Flo8p activity [46, 69], direct expression of different flocculins [32, 70], or overexpression of related factors Gts1p [71] or Mss11p [69]. The work presented here introduces a novel, *FLO8*-independent pathway for inducing flocculation, in which reduction in unsaturated lipid content causes the activation of ER-bound membrane fluidity sensors, primarily Spt23p, that induce *FLO1* expression. This pathway is triggered by genetic repression of *OLE1*, but also by hypoxia (Figure 4), as desaturase activity requires molecular oxygen. It is likely that other stimuli that are expected to reduce membrane fluidity or lipid desaturase activity, e.g. low temperature [56], iron depletion [72], and transition metals [73], can also induce flocculation by increasing Spt23p processing.

It is proposed that the regulation of *FLO1* by lipid composition can account for many of the aggregation features utilized for separating cells from the fermentation broth (or wort) in industrial fermentation. For example, in brewing, initial culture aeration is a long-recognized factor that modulates the extent and timing of flocculation [61] and studies with both beer and wine producing yeast have reported that supplementation of the growth medium with ergosterol and fatty acids counteracts the consequences of anaerobic conditions [61, 74, 75]. This study presents a molecular mechanism that connects oxygen availability and flocculation mediated by the physical state of the ER membrane. In poorly aerated fermenters, oxygen levels are reduced as the culture grows, thereby reducing lipid desaturation reactions and increasing *FLO1* expression. In this context, the late stage switch from glycolytic to respiratory metabolism would especially starve cells and their lipid desaturases from oxygen, thereby providing the trigger for flocculation to increase at the end of fermentation. This work therefore provides a mechanistic understanding of the activation of flocculation due to oxygen restriction and its timing during fermentation - an

important parameter for industrial yeast, as pre-mature flocculation causes incomplete or 'hanging' fermentation and, in the context of brewing, severe off-flavors [64, 68]. Future work will utilize the genetic components and lipid-mediated pathway characterized here to introduce and tailor flocculation behavior in industrial strains.

What physiological benefits for cell aggregation under unsaturated lipid restriction, potentially initiated by oxygen limitation, could lead the evolution of this flocculation pathway? Experiments on laboratory yeast overexpressing *FLO1* show that flocculating cells are physically shielded from harmful effects of the external milieu by diffusion barriers built up within flocs [76]. Flocculation, which is routinely triggered by nutritional starvation in *FLO8* cells, is widely thought of as an adaptive stress response. In the case of oxygen starvation, however, floc formation would appear to be disadvantageous, as aggregates minimize surface area for diffusive uptake of oxygen. On the other hand, such diffusion barriers could generate microenvironments with high local concentrations of limiting nutrients, such as unsaturated fatty acids and sterols, which are released by lysing cells inside of flocs [77, 78]. Alternatively, flocculation could present a strategy for increasing the efficiency of mating, which is itself induced by stress conditions e.g. nitrogen limitation. In this model, flocculation is a prelude to mating by increasing the proximity of neighboring haploid yeast cells [79]. The observations that Spt23p90 and Mga2p90 also activate transcription of a number of meiotic cell cycle and sporulation genes (Tab. II-S1) support such an interplay between unsaturated lipid composition and mating in yeast, which is potentially related to their originally proposed role in mating silencing [19]. In light of the possible commercial origins of laboratory yeast strains [80], the role of saturated lipid and hypoxia-induced flocculation during industrial fermentation is also considered. In brewing, ale strains (*S. cerevisiae*) are known as top-fermenters, as flocs rise to the surface of wort due to association with carbon dioxide bubbles arising from alcohol fermentation. In this context, flocculation could assist in oxygen uptake by bringing the yeast closer to the aerated surface. This would suggest the pathway presented here is a highly strain specific phenomenon. However, a mention that *OLE1* repression also results in cell aggregation in the distantly related, pathogenic fungus *Candida albicans* was noted [81]. Lipid-regulated flocculation pathway could therefore be conserved among non-brewing yeast species, which are similarly equipped with all required components involved in the signal pathway [82].

The central role of Spt23p in regulating *FLO1* expression is in line with a model in which membrane fluidity sensors act not only to maintain unsaturated lipid homeostasis but also as general regulators of cell physiology in response to environmental factors. Several lines of previous evidence support this proposal, including the discovery of *SPT23* and *MGA2* as

silencers of mating genes [19], the finding that Mga2p activates a minimal Low Oxygen Response Element (LORE) promoter [83], and the detection of potentially hundreds of physical interaction sites for active Spt23p/Mga2p fragments using chromatin immunoprecipation DNA microarray (ChIP-chip) [58]. The strains made to analyze *OLE1*-dependent flocculation were used to carry out a genome-wide characterization of genes regulated by membrane fluidity. This effort yielded a large set of genes (~15% of genome) induced by low lipid unsaturation, as well as a subset that are also activated by heterologous expression of pre-processed Spt23p/Mga2p active domains (341 genes). Manual curation of the expression data reveals several functional categories for genes activated by low membrane fluidity, which are summarized in Tab. II-S1. Common targets include synthesis and regulatory genes (involved in the synthesis of fatty acids, phospholipids, sterols, sphingolipids, and lipid droplets) and genes involved in metal homeostasis and tolerance, consistent with the catalytic roles for iron and the inhibitory roles of other metals on lipid metabolism [84, 85]. Repression of *OLE1* or expression of Spt23/Mga2 p90 also induced a number of stress response genes involved in osmotic shock, cold shock, heat stress, and oxidative stress, as well as members of well-characterized cell protein homeostasis pathways: the Heat Shock Response, the Unfolded Protein Response, and ER Associated Degradation. Finally, a prominence of fluidity-regulated genes that encode for catalytic and structural proteins involved in mitochondrial structure and respiratory metabolism was noted, which motivate future experiments on the role of unsaturated lipids in the dynamics and inheritance of these organelles [86].

The global expression analysis supports the hypothesis that the level of unsaturated lipids serves as broad regulator of gene expression during oxygen-limited fermentation. The membrane fluidity regulon (Fig. VI-1) is globally induced upon hypoxic growth (Fig. II-13A, B), and includes classic hypoxia genes (*DAN4*, *TIR* genes), those associated with the diauxic shift (*ISC1*, *SUF1*), and components of both respiratory (*FMP*s) and glycolytic metabolism (*TDH1*, *PCK1*). Specific roles for these proteins in low oxygen responses has long been recognized – *OLE1*, for example, is a canonical hypoxia response gene – but these data confirm that they are a widespread source of transcriptional regulation by oxygen. It is proposed that yeast has evolved lipid homeostasis machinery to adjust enzyme expression levels in accordance to environmental conditions, but has then adapted these sensors to act upon a wide range of molecular functions that are associated with these conditions. For several genes, including *FLO1*, sensing of unsaturated lipids is the dominant pathway for oxygen-induced activation, as transcript levels upon *OLE1* repression or p90 induction closely mimic those upon hypoxia. However, for most targets it is likely that *SPT23*/*MGA2* serve only a part of a complex response from several oxygen sensors in the

cell. Ergosterol synthesis is also oxygen dependent, and Sterol Regulatory Element Binding Proteins (SREBP) have been identified as regulating hypoxia adaptation in fission yeast [87] as well as two families (*DAN* and *TIR*) of hypoxic response genes in *S. cerevisiae* [88]. The emerging roles for different lipid sensors in the yeast hypoxic response can therefore explain the varying timescales and oxygen concentration regimes noted for the induction of different hypoxic response genes, which cannot be explained by the classic yeast oxygen response regulators, Hap1p and Rox1p, as they are singularly activated by heme biosynthesis [60]. In metazoans, hypoxia-inducible factor (HIF-1) acts as a master regulator of hypoxic genes, and along with and its associated hydroxylases is thought to act as a direct sensor to changes in oxygen concentration (Semenza, 2004). In contrast, yeast relies on secondary messengers such as unsaturated fatty acids whose synthesis is intrinsically regulated by environmental oxygen concentration. One limitation of such a sensing mechanism is its temporal response: activation remains until membrane composition is diluted by new lipid synthesis, and is therefore unaffected by acute or short-term changes in the environment. Such kinetics could also be beneficial, however, by allowing the cell to integrate long-term environmental stimuli before committing on major changes to its physiology, such as rewiring basic metabolism or engagement in primitive collective behaviors like flocculation.

2.6. Conclusions

This study introduced a metabolic engineering approach for investigating endogenous lipid synthesis pathways. Transcriptional modulation of the lipid desaturase gene *OLE1* generated a budding yeast strain in which lipid unsaturation and membrane fluidity is under experimental control. Work with this strain led to the unexpected discovery of a non-canonical flocculation pathway, in which ER-localized membrane ordering sensors trigger expression of *FLO1*. This pathway is triggered by low-oxygen conditions in wild-type cells, and provides a mechanistic explanation for sedimentation phenotypes important in industrial yeast. It is shown that the *FLO1* pathway is part of a larger transcriptional response to low oxygen that is mediated by lipid unsaturation and is activated during anaerobic fermentation.

2.7. References

1. **van Meer G, Voelker DR, Feigenson GW**. Membrane lipids: where they are and how they behave. *Nat Rev Mol Cell Biol* 2008;9(2):112-124.
2. **Klose C, Surma MA, Gerl MJ, Meyenhofer F, Shevchenko A et al.** Flexibility of a eukaryotic lipidome--insights from yeast lipidomics. *PLoS One* 2012;7(4):e35063.
3. **Bossie MA, Martin CE**. Nutritional regulation of yeast delta-9 fatty acid desaturase activity. *J Bacteriol* 1989;171(12):6409-6413.
4. **Zidovetzki R, Levitan I**. Use of cyclodextrins to manipulate plasma membrane cholesterol content: evidence, misconceptions and control strategies. *Biochim Biophys Acta* 2007;1768(6):1311-1324.
5. **Spector AA, Yorek MA**. Membrane lipid composition and cellular function. *J Lipid Res* 1985;26(9):1015-1035.
6. **Hazel JR**. Thermal adaptation in biological membranes: is homeoviscous adaptation the explanation? *Annu Rev Physiol* 1995;57:19-42.
7. **Ingram LO**. Adaptation of membrane lipids to alcohols. *J Bacteriol* 1976;125(2):670-678.
8. **Weijers RN**. Lipid composition of cell membranes and its relevance in type 2 diabetes mellitus. *Curr Diabetes Rev* 2012;8(5):390-400.
9. **Igal RA**. Stearoyl-CoA desaturase-1: a novel key player in the mechanisms of cell proliferation, programmed cell death and transformation to cancer. *Carcinogenesis* 2010;31(9):1509-1515.
10. **Hashimoto K, Yoshizawa AC, Okuda S, Kuma K, Goto S et al.** The repertoire of desaturases and elongases reveals fatty acid variations in 56 eukaryotic genomes. *J Lipid Res* 2008;49(1):183-191.
11. **Barelli H, Antonny B**. Lipid unsaturation and organelle dynamics. *Curr Opin Cell Biol* 2016;41:25-32.
12. **Stukey JE, McDonough VM, Martin CE**. Isolation and characterization of OLE1, a gene affecting fatty acid desaturation from Saccharomyces cerevisiae. *J Biol Chem* 1989;264(28):16537-16544.
13. **Casanovas A, Sprenger RR, Tarasov K, Ruckerbauer DE, Hannibal-Bach HK et al.** Quantitative analysis of proteome and lipidome dynamics reveals functional regulation of global lipid metabolism. *Chem Biol* 2015;22(3):412-425.
14. **Choi JY, Stukey J, Hwang SY, Martin CE**. Regulatory elements that control transcription activation and unsaturated fatty acid-mediated repression of the Saccharomyces cerevisiae OLE1 gene. *J Biol Chem* 1996;271(7):3581-3589.
15. **Hoppe T, Matuschewski K, Rape M, Schlenker S, Ulrich HD et al.** Activation of a membrane-bound transcription factor by regulated ubiquitin/proteasome-dependent processing. *Cell* 2000;102(5):577-586.
16. **Zhang S, Burkett TJ, Yamashita I, Garfinkel DJ**. Genetic redundancy between SPT23 and MGA2: regulators of Ty-induced mutations and Ty1 transcription in Saccharomyces cerevisiae. *Mol Cell Biol* 1997;17(8):4718-4729.
17. **Rape M, Hoppe T, Gorr I, Kalocay M, Richly H et al.** Mobilization of processed, membrane-tethered SPT23 transcription factor by CDC48(UFD1/NPL4), a ubiquitin-selective chaperone. *Cell* 2001;107(5):667-677.
18. **Burkett TJ, Garfinkel DJ**. Molecular characterization of the SPT23 gene: a dosage-dependent suppressor of Ty-induced promoter mutations from Saccharomyces cerevisiae. *Yeast* 1994;10(1):81-92.
19. **Dula ML, Holmes SG**. MGA2 and SPT23 are modifiers of transcriptional silencing in yeast. *Genetics* 2000;156(3):933-941.
20. **Covino R, Ballweg S, Stordeur C, Michaelis JB, Puth K et al.** A Eukaryotic Sensor for Membrane Lipid Saturation. *Mol Cell* 2016;63(1):49-59.
21. **Brachmann CB, Davies A, Cost GJ, Caputo E, Li J et al.** Designer deletion strains derived from Saccharomyces cerevisiae S288C: a useful set of strains and plasmids for PCR-mediated gene disruption and other applications. *Yeast* 1998;14(2):115-132.
22. **Gietz RD, Schiestl RH**. High-efficiency yeast transformation using the LiAc/SS carrier DNA/PEG method. *Nat Protoc* 2007;2(1):31-34.
23. **Gueldener U, Heinisch J, Koehler GJ, Voss D, Hegemann JH**. A second set of loxP marker cassettes for Cre-mediated multiple gene knockouts in budding yeast. *Nucleic Acids Res* 2002;30(6):e23.
24. **Alper H, Fischer C, Nevoigt E, Stephanopoulos G**. Tuning genetic control through promoter engineering. *Proc Natl Acad Sci U S A* 2005;102(36):12678-12683.

25. **Nevoigt E, Kohnke J, Fischer CR, Alper H, Stahl U et al.** Engineering of promoter replacement cassettes for fine-tuning of gene expression in Saccharomyces cerevisiae. *Appl Environ Microbiol* 2006;72(8):5266-5273.

26. **Mao X, Hu Y, Liang C, Lu C**. MET3 promoter: a tightly regulated promoter and its application in construction of conditional lethal strain. *Curr Microbiol* 2002;45(1):37-40.

27. **Gari E, Piedrafita L, Aldea M, Herrero E**. A set of vectors with a tetracycline-regulatable promoter system for modulated gene expression in Saccharomyces cerevisiae. *Yeast* 1997;13(9):837-848.

28. **Jansen G, Wu C, Schade B, Thomas DY, Whiteway M**. Drag&Drop cloning in yeast. *Gene* 2005;344:43-51.

29. **Lajoie P, Moir RD, Willis IM, Snapp EL**. Kar2p availability defines distinct forms of endoplasmic reticulum stress in living cells. *Mol Biol Cell* 2012;23(5):955-964.

30. **Bligh EG, Dyer WJ**. A rapid method of total lipid extraction and purification. *Can J Biochem Physiol* 1959;37(8):911-917.

31. **Printen JA, Sprague GF, Jr.** Protein-protein interactions in the yeast pheromone response pathway: Ste5p interacts with all members of the MAP kinase cascade. *Genetics* 1994;138(3):609-619.

32. **Van Mulders SE, Christianen E, Saerens SM, Daenen L, Verbelen PJ et al.** Phenotypic diversity of Flo protein family-mediated adhesion in Saccharomyces cerevisiae. *FEMS Yeast Res* 2009;9(2):178-190.

33. **Verbelen PJ, Depraetere SA, Winderickx J, Delvaux FR, Delvaux F**. The influence of yeast oxygenation prior to brewery fermentation on yeast metabolism and the oxidative stress response. *FEMS Yeast Res* 2009;9(2):226-239.

34. **Collart MA, Oliviero S**. Preparation of yeast RNA. *Curr Protoc Mol Biol* 2001;Chapter 13:Unit13 12.

35. **Asadollahi MA, Maury J, Moller K, Nielsen KF, Schalk M et al.** Production of plant sesquiterpenes in Saccharomyces cerevisiae: effect of ERG9 repression on sesquiterpene biosynthesis. *Biotechnol Bioeng* 2008;99(3):666-677.

36. **Paradise EM, Kirby J, Chan R, Keasling JD**. Redirection of flux through the FPP branch-point in Saccharomyces cerevisiae by down-regulating squalene synthase. *Biotechnol Bioeng* 2008;100(2):371-378.

37. **Belli G, Gari E, Aldea M, Herrero E**. Functional analysis of yeast essential genes using a promoter-substitution cassette and the tetracycline-regulatable dual expression system. *Yeast* 1998;14(12):1127-1138.

38. **Lentz BR**. Membrane “fluidity” as detected by diphenylhexatriene probes. *Chemistry and Physics of Lipids* 1989;50(3):171-190.

39. **Heipieper HJ, Isken S, Saliola M**. Ethanol tolerance and membrane fatty acid adaptation in adh multiple and null mutants of Kluyveromyces lactis. *Res Microbiol* 2000;151(9):777-784.

40. **Stratford M, Assinder S**. Yeast flocculation: Flo1 and NewFlo phenotypes and receptor structure. *Yeast* 1991;7(6):559-574.

41. **Mukhopadhyay K, Kohli A, Prasad R**. Drug susceptibilities of yeast cells are affected by membrane lipid composition. *Antimicrob Agents Chemother* 2002;46(12):3695-3705.

42. **Sinicrope FA, Dudeja PK, Bissonnette BM, Safa AR, Brasitus TA**. Modulation of P-glycoprotein-mediated drug transport by alterations in lipid fluidity of rat liver canalicular membrane vesicles. *J Biol Chem* 1992;267(35):24995-25002.

43. **Bony M, Thines-Sempoux D, Barre P, Blondin B**. Localization and cell surface anchoring of the Saccharomyces cerevisiae flocculation protein Flo1p. *J Bacteriol* 1997;179(15):4929-4936.

44. **Stratford M**. Lectin-mediated aggregation of yeasts--yeast flocculation. *Biotechnol Genet Eng Rev* 1992;10:283-341.

45. **Guinard J, Lewis JM**. STUDY OF THE PHENOMENON OF AGGLOMERATION IN THE YEAST SACCHAROMYCES CEREVISIAE. *Journal of the Institute of Brewing* 1993;99(6):487-503.

46. **Liu H, Styles CA, Fink GR**. Saccharomyces cerevisiae S288C has a mutation in FLO8, a gene required for filamentous growth. *Genetics* 1996;144(3):967-978.

47. **Pineau L, Colas J, Dupont S, Beney L, Fleurat-Lessard P et al.** Lipid-induced ER stress: synergistic effects of sterols and saturated fatty acids. *Traffic* 2009;10(6):673-690.

48. **Gardner BM, Pincus D, Gotthardt K, Gallagher CM, Walter P**. Endoplasmic reticulum stress sensing in the unfolded protein response. *Cold Spring Harb Perspect Biol* 2013;5(3):a013169.

49. **Travers KJ, Patil CK, Wodicka L, Lockhart DJ, Weissman JS et al.** Functional and genomic analyses reveal an essential coordination between the unfolded protein response and ER-associated degradation. *Cell* 2000;101(3):249-258.

50. **Chapman R, Sidrauski C, Walter P**. Intracellular signaling from the endoplasmic reticulum to the nucleus. *Annu Rev Cell Dev Biol* 1998;14:459-485.

51. **Halbleib K, Pesek K, Covino R, Hofbauer HF, Wunnicke D et al.** Activation of the Unfolded Protein Response by Lipid Bilayer Stress. *Mol Cell* 2017;67(4):673-684 e678.

52. **Nilsson I, Ohvo-Rekila H, Slotte JP, Johnson AE, von Heijne G**. Inhibition of protein translocation across the endoplasmic reticulum membrane by sterols. *J Biol Chem* 2001;276(45):41748-41754.

53. **Aragon T, van Anken E, Pincus D, Serafimova IM, Korennykh AV et al.** Messenger RNA targeting to endoplasmic reticulum stress signalling sites. *Nature* 2009;457(7230):736-740.

54. **Pineau L, Bonifait L, Berjeaud JM, Alimardani-Theuil P, Berges T et al.** A lipid-mediated quality control process in the Golgi apparatus in yeast. *Mol Biol Cell* 2008;19(3):807-821.

55. **Jiang Y, Vasconcelles MJ, Wretzel S, Light A, Gilooly L et al.** Mga2p processing by hypoxia and unsaturated fatty acids in Saccharomyces cerevisiae: impact on LORE-dependent gene expression. *Eukaryot Cell* 2002;1(3):481-490.

56. **Nakagawa Y, Sakumoto N, Kaneko Y, Harashima S**. Mga2p is a putative sensor for low temperature and oxygen to induce OLE1 transcription in Saccharomyces cerevisiae. *Biochem Biophys Res Commun* 2002;291(3):707-713.

57. **Kandasamy P, Vemula M, Oh CS, Chellappa R, Martin CE**. Regulation of unsaturated fatty acid biosynthesis in Saccharomyces: the endoplasmic reticulum membrane protein, Mga2p, a transcription activator of the OLE1 gene, regulates the stability of the OLE1 mRNA through exosome-mediated mechanisms. *J Biol Chem* 2004;279(35):36586-36592.

58. **Auld KL, Brown CR, Casolari JM, Komili S, Silver PA**. Genomic association of the proteasome demonstrates overlapping gene regulatory activity with transcription factor substrates. *Mol Cell* 2006;21(6):861-871.

59. **Andreasen AA, Stier TJ**. Anaerobic nutrition of Saccharomyces cerevisiae. I. Ergosterol requirement for growth in a defined medium. *J Cell Comp Physiol* 1953;41(1):23-36.

60. **Kwast KE, Burke PV, Poyton RO**. Oxygen sensing and the transcriptional regulation of oxygen-responsive genes in yeast. *J Exp Biol* 1998;201(Pt 8):1177-1195.

61. **Straver MH, vd Aar PC, Smit G, Kijne JW**. Determinants of flocculence of brewer's yeast during fermentation in wort. *Yeast* 1993;9(5):527-532.

62. **Soares EV, Teixeira JA, Mota M**. Effect of cultural and nutritional conditions on the control of flocculation expression in Saccharomyces cerevisiae. *Can J Microbiol* 1994;40(10):851-857.

63. **Smit G, Straver MH, Lugtenberg BJ, Kijne JW**. Flocculence of Saccharomyces cerevisiae cells is induced by nutrient limitation, with cell surface hydrophobicity as a major determinant. *Appl Environ Microbiol* 1992;58(11):3709-3714.

64. **Stratford M**. Yeast flocculation: a new perspective. *Adv Microb Physiol* 1992;33:2-71.

65. **Soares EV, Mota M**. Flocculation onset, growth phase, and genealogical age in Saccharomyces cerevisiae. *Can J Microbiol* 1996;42(6):539-547.

66. **Powell CD, Quain DE, Smart KA**. The impact of brewing yeast cell age on fermentation performance, attenuation and flocculation. *FEMS Yeast Res* 2003;3(2):149-157.

67. **Barker MG, Smart KA**. Morphological changes associated with the cellular aging of a brewing yeast strain. *J Am Soc Brew Chem* 1996;54(2):121-126.

68. **Verstrepen KJ, Derdelinckx G, Verachtert H, Delvaux FR**. Yeast flocculation: what brewers should know. *Appl Microbiol Biotechnol* 2003;61(3):197-205.

69. **Bester MC, Pretorius IS, Bauer FF**. The regulation of Saccharomyces cerevisiae FLO gene expression and Ca2+ -dependent flocculation by Flo8p and Mss11p. *Curr Genet* 2006;49(6):375-383.

70. **Govender P, Domingo JL, Bester MC, Pretorius IS, Bauer FF**. Controlled expression of the dominant flocculation genes FLO1, FLO5, and FLO11 in Saccharomyces cerevisiae. *Appl Environ Microbiol* 2008;74(19):6041-6052.

71. **Shen H, Iha H, Yaguchi S, Tsurugi K**. The mechanism by which overexpression of Gts1p induces flocculation in a FLO8-inactive strain of the yeast Saccharomyces cerevisiae. *FEMS Yeast Res* 2006;6(6):914-923.

72. **Vasconcelles MJ, Jiang Y, McDaid K, Gilooly L, Wretzel S et al.** Identification and characterization of a low oxygen response element involved in the hypoxic induction of a family of Saccharomyces cerevisiae genes. Implications for the conservation of oxygen sensing in eukaryotes. *J Biol Chem* 2001;276(17):14374-14384.

73. **Kwast KE, Burke PV, Staahl BT, Poyton RO**. Oxygen sensing in yeast: evidence for the involvement of the respiratory chain in regulating the transcription of a subset of hypoxic genes. *Proc Natl Acad Sci U S A* 1999;96(10):5446-5451.

74. **Holmberg SK-B, M. C.** A mutant of Saccharomyces cerevisiae temperature sensitive for flocculation. Influence of oxygen and respiratory deficiency on flocculence. *Carlsberg Research Communications* 1978;43(1):37-47.

75. **Tesniere C, Delobel P, Pradal M, Blondin B**. Impact of nutrient imbalance on wine alcoholic fermentations: nitrogen excess enhances yeast cell death in lipid-limited must. *PLoS One* 2013;8(4):e61645.

76. **Smukalla S, Caldara M, Pochet N, Beauvais A, Guadagnini S et al.** FLO1 is a variable green beard gene that drives biofilm-like cooperation in budding yeast. *Cell* 2008;135(4):726-737.

77. **Iserentant D**. Practical aspects of yeast flocculation. *Cerevisia* 1996;21:30-33.

78. **Steward GG, Russell I**. Yeast flocculation. *Academic Press, New York* 1981.

79. **Goossens KV, Ielasi FS, Nookaew I, Stals I, Alonso-Sarduy L et al.** Molecular mechanism of flocculation self-recognition in yeast and its role in mating and survival. *MBio* 2015;6(2).

80. **Mortimer RK, Johnston JR**. Genealogy of principal strains of the yeast genetic stock center. *Genetics* 1986;113(1):35-43.

81. **Krishnamurthy S, Plaine A, Albert J, Prasad T, Prasad R et al.** Dosage-dependent functions of fatty acid desaturase Ole1p in growth and morphogenesis of Candida albicans. *Microbiology* 2004;150(Pt 6):1991-2003.

82. **Oh CS, Martin CE**. Candida albicans Spt23p controls the expression of the Ole1p Delta9 fatty acid desaturase and regulates unsaturated fatty acid biosynthesis. *J Biol Chem* 2006;281(11):7030-7039.

83. **Jiang Y, Vasconcelles MJ, Wretzel S, Light A, Martin CE et al.** MGA2 is involved in the low-oxygen response element-dependent hypoxic induction of genes in Saccharomyces cerevisiae. *Mol Cell Biol* 2001;21(18):6161-6169.

84. **Pagani MA, Casamayor A, Serrano R, Atrian S, Arino J**. Disruption of iron homeostasis in Saccharomyces cerevisiae by high zinc levels: a genome-wide study. *Mol Microbiol* 2007;65(2):521-537.

85. **Lyons TJ, Villa NY, Regalla LM, Kupchak BR, Vagstad A et al.** Metalloregulation of yeast membrane steroid receptor homologs. *Proc Natl Acad Sci U S A* 2004;101(15):5506-5511.

86. **Stewart LC, Yaffe MP**. A role for unsaturated fatty acids in mitochondrial movement and inheritance. *J Cell Biol* 1991;115(5):1249-1257.

87. **Hughes AL, Todd BL, Espenshade PJ**. SREBP pathway responds to sterols and functions as an oxygen sensor in fission yeast. *Cell* 2005;120(6):831-842.

88. **Davies BS, Rine J**. A role for sterol levels in oxygen sensing in Saccharomyces cerevisiae. *Genetics* 2006;174(1):191-201.

2.8. Supporting information

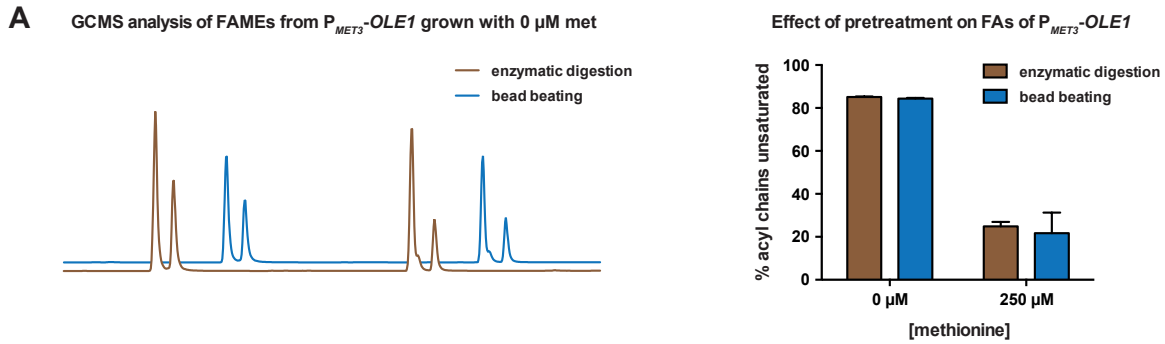

Fig. II–S1: Control measurements of lipid compositions. (A) Lipid extracts from cells either disrupted by enzymatic digestion with zymolyase or mechanical bead beating were analyzed by GC-MS to check for differences in lipid composition in dependence of the method of cell disruption. Fatty acid unsaturation was uninfluenced by the pretreatment of cells. Concerns regarding differences in lipid unsaturation arose due the incubation step (1h, 35°C) involved in the zymolyase treatment of cells for enzymatic disruption of the cell wall since temperature is a critical parameter influencing membrane lipid composition. Left: exemplary GC-MS traces; right: bar diagrams for biological triplicates. Error bars, SEM (n = 3).

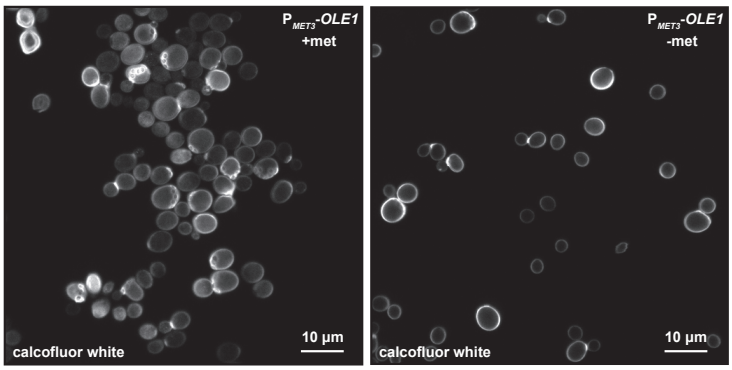

Fig. II–S2: P*MET3*-*OLE1* cells flocculate in methionine, but show no defect in cell division. Confocal fluorescence micrographs of flocculating P*MET3*-*OLE1* cells cultured at 250 µM methionine and freely suspended P*MET3*-*OLE1* cells cultured in methionine-free synthetic dextrose medium. Yeast cell walls were stained with calcofluor white.

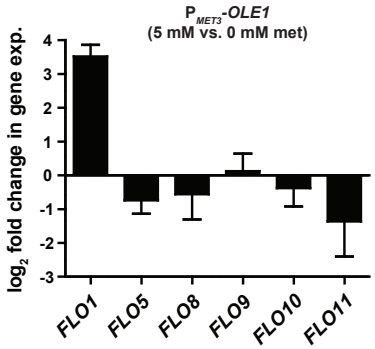

Fig. II-S3: The flocculation gene *FLO1* is uniquely activated upon *OLE1* repression. Changes in expression of different *FLO* genes in response to growth at low lipid unsaturation, as tested by comparing expression in P*MET3*-*OLE1* grown in 5 mM vs. 0 mM exogenous methionine. Gene expression was measured by qRT-PCR and shows significant upregulation only of *FLO1*. Error bars, SEM (n = 3).

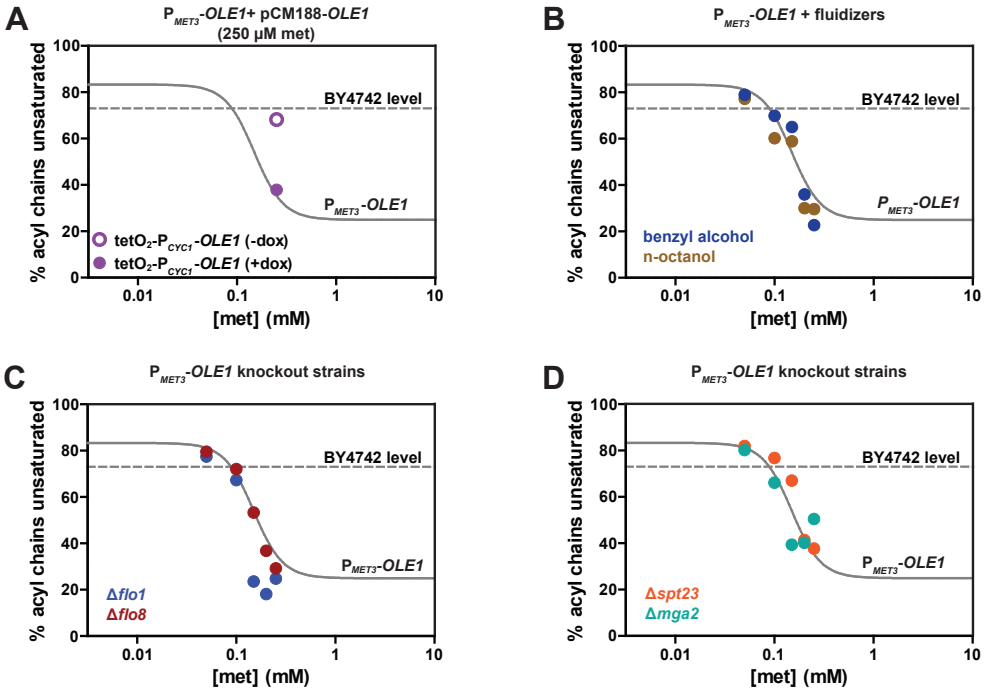

Fig. II-S4: Control measurements of membrane lipid composition upon indicated gene expression, media supplementation and gene knockouts. (A) Lipid unsaturation (% acyl chains unsaturated) of P_{MET3}-*OLE1* cells grown at 250 µM met with (-dox) and without (+dox) additional plasmid-based *OLE1* expression from a $tetO_2$-P_{CYC1} promoter construct. The dependence of lipid unsaturation on methionine without an additional plasmid – from Figure 1D – is included for comparison. **(B)** Lipid unsaturation (% acyl chains unsaturated) of P_{MET3}-*OLE1* cells grown in the presence of membrane fluidizers, n-octanol (0.02% w/v) and benzyl alcohol (10 mM) and various external methionine concentrations (50 µM; 100 µM; 150 µM; 200 µM; 250 µM). The dependence of lipid unsaturation on methionine in the absence of additives – from Figure 1D – is included for comparison. **(C)** Prevention of flocculation in P_{MET3}-*OLE1*; Δ *flo1* does not result from restored lipid unsaturation. Lipid unsaturation upon *OLE1* repression (P_{MET3}-*OLE1* + met) in a *Δflo1* or *Δflo8* background when grown at various methionine concentrations. The dependence of lipid unsaturation on methionine with unaltered *FLO1*/*FLO8* – from Figure 1D – is included for comparison. **(D)** Lipid unsaturation in P_{MET3}-*OLE1* is largely unaffected by *SPT23* and *MGA2*. Lipid unsaturation upon *OLE1* repression (P_{MET3}-*OLE1* + met) in a *Δspt23* or *Δmga2* background when grown at various methionine concentrations. The dependence of lipid unsaturation on methionine with unaltered *SPT23*/*MGA2* – from Figure 1D – is included for comparison.

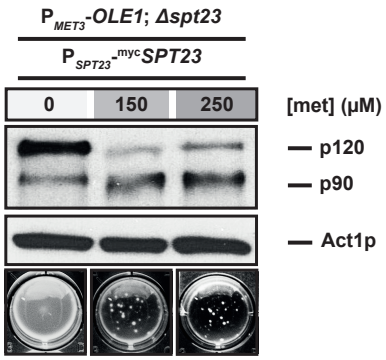

Fig. II-S5: Lipid unsaturation induced proteolytic processing of ^{myc}Spt23p in a *SPT23* knockout background. Expression of ^{myc}Spt23p under control of its endogenous promoter (P_{SPT23}) from a centromeric (CEN) plasmid (pGREG523) in a *SPT23* knockout background (P_{MET3}-*OLE1*; Δ*spt23*) shows a comparable profile of ^{myc}Spt23p proteolytic processing as the background harboring endogenous *SPT23* (Fig. II-8B).

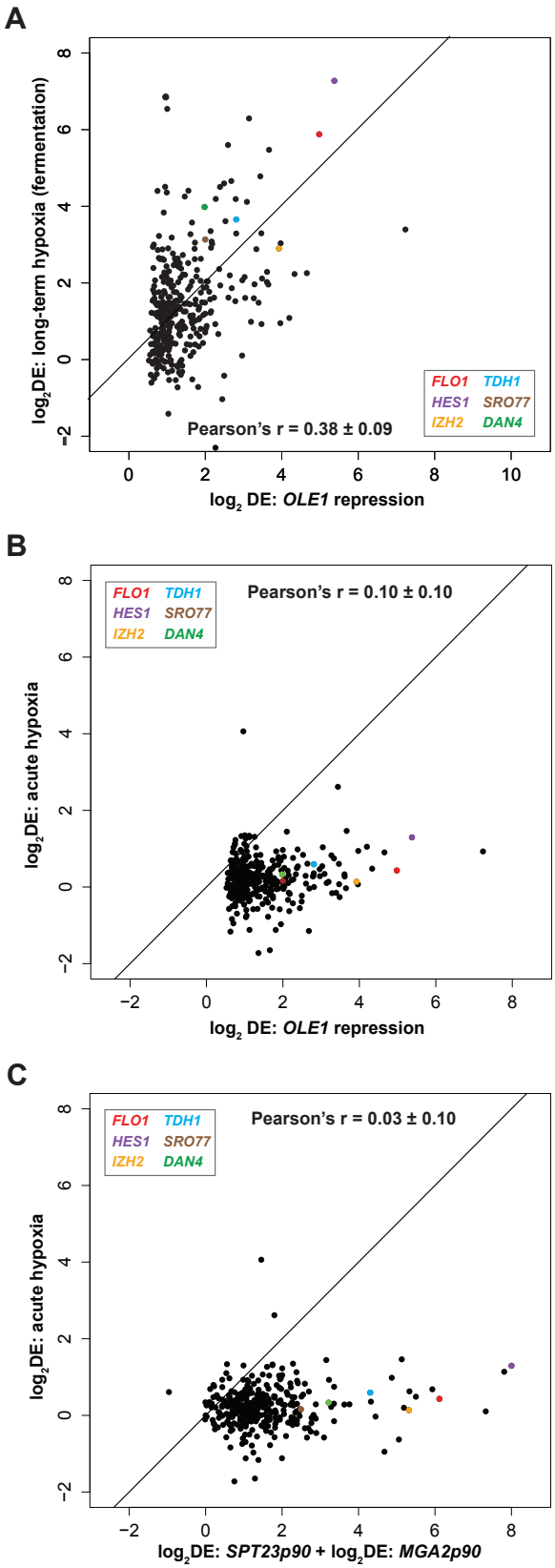

Fig. II-S6: Global expression of membrane fluidity genes under long- and short-term (acute) hypoxia. (A) Differential expression values upon long-term hypoxia are correlated with those upon *OLE1* repression for membrane fluidity genes. Comparison of the changes in differential expression (DE) resulting from low lipid unsaturation (P_{MET3}-*OLE1* in 250 µM vs. 0 µM methionine) with those resulting from long-term hypoxic growth in the background strain (BY4742) for the 341 genes found to be regulated by *OLE1*/*SPT23*/*MGA2* in Figure 5B. These genes feature a medium strength correlation (r = 0.38) between differential expression upon long-term hypoxia and *OLE1* repression. Line shows x – y = 0 and is added for clarity. **(B)** Membrane fluidity-regulated genes are not globally induced under short-term hypoxia. Comparison of the differential expression (DE) resulting from low lipid unsaturation (log_2 DE for P_{MET3}-*OLE1* in 250 µM vs. 0 µM methionine) or **(C)** combined p90 induction (sum of log_2 DE for *SPT23p90* induction and *MGA2p90* induction) with those resulting from acute hypoxia (90 min under argon) in the background strain (BY4742) for the 341 genes found to be regulated by *OLE1*/*SPT23*/*MGA2* in Figure 5B. Differential expression upon acute hypoxia, with few exceptions, is not correlated with activation due to low membrane fluidity, in contrast to long-term hypoxic growth (Figure 5D, S12). Lines show x – y = 0 and are added for clarity.

Tab. II-S1: Functional groups of genes regulated by *SPT23p90* and *MGA2p90*. Genes significantly upregulated (q ≤ 0.05) by *OLE1* repression and significantly upregulated (q ≤ 0.05) by *SPT23p90* or *MGA2p90* expression are listed with their $\log_2$ differential expression values.

	OLE1 repression	*SPT23* activation	*MGA2* activation
metal homeostasis			
ARN1	1,16	0,76	1,48
ARN2	1,05	0,75	0,84
DAP1	1,72	0,63	1,48
FET4	0,76	0,55	1,45
FRE8	1,39	0,45	0,78
HMX1	0,99	0,92	1,46
IZH1	2,03	0,38	1,48
IZH2	3,93	2,02	3,30
IZH4	7,23	0,11	3,12
SIT1	2,60	1,00	0,77
fatty acid synthesis			
ACC1	3,96	0,84	0,98
ELO1	1,35	0,25	1,10
FAS1	3,47	0,55	0,73
FAS2	3,61	0,67	0,94
phospholipid synthesis			
ALE1	2,39	0,51	1,64
APP1	0,84	0,20	0,74
CDS1	0,67	0,20	0,70
CKI1	1,35	-0,26	1,54
CST26	1,05	-0,48	0,67
EKI1	0,69	0,22	0,99
ICT1	3,03	0,14	2,41
INO2	1,30	0,42	1,50
INO4	0,85	-0,10	1,14
OPI3	0,88	0,92	1,77
PGS1	0,98	-0,05	1,13
sterol synthesis			
ARE2	1,99	1,57	0,89
ERG10	1,66	0,15	1,67
ERG13	1,48	-0,27	0,74
MVD1	1,75	-0,26	2,10
SCY1	1,02	-0,67	0,69
SLC1	1,15	-0,47	0,63
sphingolipid synthesis			
LAC1	0,71	0,61	0,60
ORM2	0,92	0,03	1,24
PAH1	1,04	-0,09	1,20
PHS1	0,97	0,38	0,88
PLB2	3,27	0,92	1,68
SUR1	0,62	0,75	0,31
lipid droplet synthesis			
ATG15	1,37	0,56	1,76
OSH6	1,20	-0,35	1,76
UPC2	1,73	0,22	0,91
YSR3	2,49	0,71	0,51
peroxisomal			
ECI1	1,05	0,24	1,25
FOX2	1,29	-0,01	0,67
LPX1	0,75	0,61	-0,01
LPX1	0,75	0,61	-0,01
PEX31	2,01	0,72	1,53
POT1	2,64	1,36	-2,32
POX1	1,46	1,12	0,95
SPS19	2,69	1,48	1,33
cell wall			
FIT2	2,18	1,05	0,47
FIT3	2,07	0,73	0,77
FLO1	4,98	3,72	2,40
FLO9	0,92	2,07	0,81
sporulation			
GSC2	1,17	0,66	0,89
OSW2	3,33	0,94	2,42
SPO1	1,61	1,11	0,58
SPO73	0,67	0,48	2,02
SPS100	3,65	0,21	4,24
SPS19	2,69	1,48	1,33

	OLE1 repression	*SPT23* activation	*MGA2* activation
hypoxic response			
DAN4	1,98	1,03	2,19
RIM8	0,91	0,07	1,84
TIR1	0,96	2,20	-0,74
TIR2	1,00	0,41	1,88
oxidative stress			
ALD6	2,97	0,49	0,80
GRE3	1,03	-0,49	0,59
HMX1	0,99	0,92	1,46
PST2	0,63	0,77	1,05
TSA1	1,36	-0,15	0,90
TSA2	1,56	0,73	1,09
protein folding			
ADD37	1,74	0,27	1,25
EMC10	0,51	-0,33	-0,32
ERO1	0,76	-0,20	0,77
GET3	1,23	-0,17	1,05
HRD1	1,69	0,36	0,71
HSP26	2,27	3,29	1,90
JEM1	0,64	0,27	0,81
KAR2	1,66	0,07	1,11
LHS1	1,31	-0,20	0,54
MIA40	0,65	-0,58	0,57
PDI1	1,73	0,13	0,89
SSA4	1,43	-0,24	0,92
SSE2	1,05	0,49	0,75
TSA1	1,36	-0,15	0,90
UBX2	1,05	0,02	0,93
thermal stress response			
FUN19	1,44	0,11	0,70
TIP1	2,10	1,18	1,97
TIR1	0,96	2,20	-0,74
osmotic shock response			
ALD6	2,97	0,49	0,80
GRE3	1,03	-0,49	0,59
HSP12	1,81	1,31	-0,26
RVS161	0,52	0,52	0,43
SMP1	0,64	1,40	0,09
meiotic cell cycle			
CDC4	1,38	-0,42	0,76
DMC1	2,81	2,16	2,17
GAC1	1,83	0,91	1,89
IML3	0,85	0,63	1,76
IML3	0,85	0,63	1,76
ZIP1	1,84	-1,29	1,63
diauxic shift			
CAT8	0,74	0,74	-0,53
ICL1	1,06	0,50	1,07
ISC1	1,34	0,05	1,33
NQM1	1,92	0,17	2,48
SUF1	1,07	-0,30	1,84
glycolytic metabolism			
ENO1	2,96	0,97	0,53
PCK1	3,97	1,19	0,76
TDH1	2,81	1,83	2,47
mitochondrial			
AIM2	0,57	-0,32	0,58
FMP25	1,26	-0,11	1,44
FMP40	1,22	1,41	1,69
FMP46	1,61	0,69	1,26
FUN14	1,67	0,69	0,99
MDM10	0,95	1,11	1,35
OM45	1,34	0,08	0,75
TIM23	1,77	-0,20	0,63

Tab. II-S2: Plasmids used in this study. The table summarizes basic characteristics and properties of indicated plasmids.

Plasmid	description	reference
p416-P_{TEF1}-yECitrine	-	[24]
p416-*LEU2*-P_{TEF1}-yECitrine	-	[25]
p416-*LEU2*-P_{MET3}-yECitrine	CEN/ARS; *URA3*; *LEU2*; amp^R; methionine repressible expression of yECitrine	This study
pCM188	-	[27]
pCM224	-	[37]
pCM188-*OLE1*	CEN/ARS; *URA3*; amp^R; doxycycline repressible expression of Ole1p	This study
pCM188-*SPT23p90*	CEN/ARS; *URA3*; amp^R; doxycycline repressible expression of Spt23p90	This study
pCM188(*LEU2*)-*SPT23p90*	CEN/ARS; *URA3*; *LEU2*; amp^R; doxycycline repressible expression of Spt23p90	This study
pCM188(*LEU2*)-*MGA2p90*	CEN/ARS; *URA3*; *LEU2*; amp^R; doxycycline repressible expression of Mga2p90	This study
pUG72	-	[23]
pUG72-P_{MET3}	PCR template for P_{MET3}-loxP	This study
pUG73	-	[23]
pGREG506	-	[28]
pGREG523	-	[28]
pGREG523-P_{SPT23}-^{myc}*SPT23*	CEN/ARS; *HIS3*; kanMX; amp^R; expression of an N-terminally 13xmyc-tagged Spt23p variant (^{myc}Spt23p) from native *SPT23* promoter	This study
pGREG523-P_{SPT23}-^{myc}*SPT23*$_{W1042L}$	CEN/ARS; *HIS3*; kanMX; amp^R; expression of an N-terminally 13xmyc-tagged Spt23p W1042L mutant variant (^{myc}Spt23p$_{W1042L}$) from native *SPT23* promoter	This study

plasmid	description	reference
pGREG523(2µ) –P_{SPT23}-^{myc}*SPT23*	2µ ORI; *HIS3*; kanMX; amp^R; expression of an N-terminally 13xmyc-tagged Spt23p variant (^{myc}Spt23p) from native *SPT23* promoter	This study
pGREG523–P_{TEF1}-^{myc}*SPT23*	CEN/ARS; *HIS3*; kanMX; amp^R; expression of an N-terminally 13xmyc-tagged Spt23p variant (^{myc}Spt23p) from strong *TEF1* promoter	This study
pGREG523(2µ) –P_{TEF1}-^{myc}*SPT23*	2µ ORI; *HIS3*; kanMX; amp^R; expression of an N-terminally 13xmyc-tagged Spt23p variant (^{myc}Spt23p) from strong *TEF1* promoter	This study
pGREG523-P_{MGA2}-^{myc}*MGA2*	CEN/ARS; *HIS3*; kanMX; amp^R; expression of an N-terminally 13xmyc-tagged Mga2p variant (^{myc}Mga2p) from native *MGA2* promoter	This study
pRS415-ER-sfGFP-HDEL	-	[29]
pRS416-ER-sfGFP-HDEL	CEN/ARS; *URA3*; amp^R; expression of an ER guided GFP variant (sfGFP, superfold) that retains in the ER lumen because of an C-terminally attached HDEL sequence	This study

Tab. II-S3: Primers used in this study. Underlined sequence parts represent homology regions of overhang primers used recombination-based cloning approaches.

primer	sequence (5' → 3')	amplicon
P1 (fw)	GCTATACGAAGTTATTAGGTGATATCAGATCCACTAGTATCGTTTAATTTAGTACTAACAGAGACTTTTGTCACAAC	P_{MET3}
P2 (rv)	GGGAGACCGGCAGATCCGCGGCCGCATAGGCCACTAGTGTTAATTATACTTTATTCTTGTTATTATTATACTTTCTTAGTTCCTTTTC	P_{MET3}
P3 (fw)	GATAACACTTTGTAAGCCTTTGCTGGGATCTTCACAGCGAGCTCTCGAGAACCCTTAAT	P_{MET3}-loxP
P4 (rv)	TACGCCAAGCGCGCAATTAACCCTCACTAAAGGGAACAAAAGCTGCCAGCTGAAGCTTCGTACGC	P_{MET3}-loxP
P5 (fw)	GGCGCTTATCTGGTGGGCTTCCGTAGAAGAAAAAAAGCTGTTGACAGCTGAAGCTTCGTACGC	P_{MET3}-PRC
P6 (rv)	ATTGGTCGTCAATCAATTCAATAGTAGTTCCAGAAGTTGGCATGTTAATTATACTTTATTCTTG	P_{MET3}-PRC
P7 (fw)	CACAAATACACACACTAAATTACCGGATCAATTCGGGGGATCCATGCCAACTTCTGGAACTACTATTGAATTG	*OLE1*
P8 (rv)	TTACATGATGCGGCCCTCCTGCAGGGCCCTAGCGGCCGCTTTAAAAGAACTTACCAGTTTCGTAGATTTCACC	*OLE1*
P9 (fw)	ACTAAATTACCGGATCAATTCGGGGGATCCATGATGAGTGGCACAGGAAAC	*SPT23p90*
P10 (rv)	TGCGGCCCTCCTGCAGGGCCCTAGCGGCCGCTTTAACCCCTAACGTCACACATGG	*SPT23p90*
P11 (fw)	ACTAAATTACCGGATCAATTCGGGGGATCCATGCAGCAGAACAGTGAG	*MGA2p90*
P12 (rv)	TGCGGCCCTCCTGCAGGGCCCTAGCGGCCGCTCTATTCATCCCCGTCTTCTTC	*MGA2p90*
P13 (fw)	GGTTTTGGGACGCTCGAAGGCTTTAATTTGCGGCCCTGAAGCTTCGTACGCTGCAG	loxP-*LEU2*-loxP
P14 (rv)	TTCACACAGGAAACAGCTATGACCATGATTACGCCCGCATAGGCCACTAGTGGATCTG	loxP-*LEU2*-loxP
P15 (fw)	TAAGCTCTCTTCCGGGTTCTTATTTTTAATTCTTGTCACCAGTAAACAGAACATCCAAAAATGTCTAAAGGTGAAGAATTATTCACTGG	*FLO1* KOC
P16 (rv)	CATGTCAGCGTATAATTAGCAAAGAAAAGATACACAGATACGTAAAAAGAACGCGAATTTTAGCAGATTGTACTGAGAGTGCAC	*FLO1* KOC
P17 (fw)	CAGCCTCGTAGCACACCAGCAAGCAGCATGGTAGGATATAGTACAGCTTCTTTAGAAATTTAACACCGATTATTTAAAGCTGCAGG	*FLO1hd* KOC
P 18(rv)	TGTCAGCGTATAATTAGCAAAGAAAAGATACACAGATACGTAAAAAGAACGCGAATTTTAGGGTACCCTTAATTAAGACAACCC	*FLO1hd* KOC
P19 (fw)	AAAAATAAACACGAAGACGTTTATAGACATAAATAAAGAGGAAACGCATTCCGTGGTAGAATGTCTAAAGGTGAAGAATTATTCACTGG	*FLO8* KOC
P20 (rv)	GCTTTTTATTATGTTTCCTGTCATTAAGAGTTTTTATTTTTTATTATAATACTCAACACGTGACTGCAGATTGTACTGAGAGTGCAC	*FLO8* KOC
P21 (fw)	ACAGGTACGCTCTTTAAATTGCAATTTAAAAAGAACAATTGTACAATAAAAGCCCCAAAACGTACGCTGCAGGTCGAC	*FLO9* KOC
P22 (rv)	TGTCAGCGTATATTTAGCAAAGAAAAGATACACAGATACGTAAAAAGAACGCGAATTTTAGCGGCGTTAGTATCGAATCG	*FLO9* KOC
P23 (fw)	TTATACTCTAGATATCCTCTAAACGACTAATCACAACAGTAGTACACCACTGAAACGTACGCTGCAGGTCGAC	*SPT23* KOC
P24 (rv)	GCAAAATAATAAAAAATGAATCTATATAGTGTAAGGATTATGTAGCTAGAAAAATGTCTGCGGCGTTAGTATCGAATCG	*SPT23* KOC

primer	sequence (5' → 3')	amplicon
P25 (fw)	CCTTATTGTGCATTTAAAGGCACTTATTGAAGGTCATTTTGGCGAACAGAACATTTCGTTGGTATTTCACACCGCATAGGG	*MGA2* KOC
P26 (rv)	TAAGTGTACTGTCTTTTCATTATACACACATATATATATATATATACGTAAAAAAGCAGAGCAGATTGTACTGAGAGTGCAC	*MGA2* KOC
P27 (fw)	TTAACTCAGTGTCAAACATAACAACCTCCTCCTCCCCCACCTACGACAACAACCGCCACTCGTACGCTGCAGGTCGAC	*HAC1* KOC
P28 (rv)	AAAACCCACCAACAGCGATAATAACGAGAAAAAAAAAATTATACCCTCTTGCGATTGTCTGCGGCGTTAGTATCGAATCG	*HAC1* KOC
P29 (fw)	CCTTCATACACATTAAAAAAACAGCATATCTGAGGAATTAATATTTTAGCACTTTGAAAACGTACGCTGCAGGTCGAC	*IRE1* KOC
P30 (rv)	ATGATCAAAGTAACATTAATGCAATAATCAACCAAGAAGAAGCAGAGGGGCATGAACATGGCGGCGTTAGTATCGAATCG	*IRE1* KOC
P31 (fw)	GAATTCGATATCAAGCTTATCGATACCGTCGACAATGAGTGGCACAGGAAACGT	*SPT23* ORF
P32 (rv)	GCGTGACATAACTAATTACATGACTCGAGGTCGACTTAATTGACTCGCATGTCGTTTAGAAT	*SPT23* ORF
P33 (fw)	AACAAAAGCTGGAGCTCGTTTAAACGGCGCGCCGATGAGGTCGCTGGCGTAG	P_{SPT23}
P34 (rv)	GCTTTTGTTCACCGTTAATTAACCCGGGGATCATTTTCAGTGGTGTACTACTGTTGTG	P_{SPT23}
P35 (fw)	TGGTCGTCCACAGGTTTTAATAG	$SPT23_{W1042L}$
P36 (rv)	CAAATTCGATAATGTGAAACATAATAAGAGTACTAAAGTTAAGGGGATCAAAAAGAATAGGAGCATCTTATCA	$SPT23_{W1042L}$
P37 (fw)	GGTTAATGTCATGATAATAATGGTTTCTTAGGACGCCTGAACGAAGCATCTGTG	2µ ORI
P38 (rv)	GCACATTTCCCCGAAAAGTGCCACCTGGGTCCTTTTCATGATCCAATATCAAAGGAAATGATAGC	2µ ORI
P39 (fw)	AACAAAAGCTGGAGCTCGTTTAAACGGCGCGCCATAGCTTCAAAATGTTTCTACTCCTT	P_{TEF1}
P40 (rv)	GCTTTTGTTCACCGTTAATTAACCCGGGGATCATAAACTTAGATTAGATTGCTATGCTTTCT	P_{TEF1}
P41 (fw)	GAATTCGATATCAAGCTTATCGATACCGTCGACAATGCAGCAGAACAGTGAGTTC	*MGA2* ORF
P42 (rv)	GCGTGACATAACTAATTACATGACTCGAGGTCGACCTAACTGACAATTAAATCGTTCAACATTC	*MGA2* ORF
P43 (fw)	AACAAAAGCTGGAGCTCGTTTAAACGGCGCGCCGAAAAATCCAAATGTTCTTCCTTGC	P_{MGA2}
P44 (rv)	GCTTTTGTTCACCGTTAATTAACCCGGGGATCATAACGAAATGTTCTGTTCGCC	P_{MGA2}
P45 (fw)	AGAGGAAACGCATTCCGTG	*FLO8* ORF (-24 to +659)
P46 (rv)	GCAGGTGCCATAGGATTTCC	*FLO8* ORF (-24 to +659)
P47 (fw)	GCGCGCGTAATACGACTCACTATAGGGCGAATTGCTGCAGCCCGGGGGATC	ER-sfGFP-HDEL
P48 (rv)	GCGCGCAATTAACCCTCACTAAAGGGAACAAAAGCTGCAAAAGCTGGAGCTCAGTTTATCA	ER-sfGFP-HDEL
P49 (fw)	CAGGGATTTCCAGAGCACG	*HAC1* mRNA
P50 (rv)	TCATGAAGTGATGAAGAAATCATTC	*HAC1* mRNA

Chapter III

Heterologous expression of stearoyl-CoA desaturases from trypanosomes

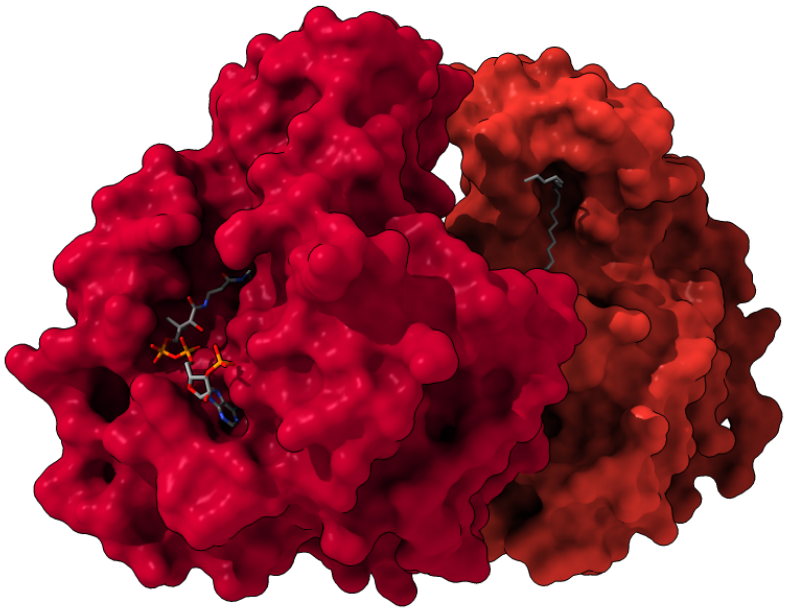

3. Chapter III: Heterologous expression of stearoyl-CoA desaturases from trypanosomes

3.1. Abstract

A yeast strain in which expression of *OLE1*, encoding for the sole fatty acid desaturase found in *S. cerevisiae,* is under experimental control serves as a cellular platform to assay the activity of heterologously expressed stearoyl-CoA desaturases (SCDs). Functional expression of SCDs complements for repressed endogenous *OLE1*, thus providing for an easy, fast and affordable assay read-out that is based on simply restoring growth or preventing a prominent flocculation phenotype. Based on this assay, putative SCDs from human pathogens *T. brucei* and *T. cruzi* were functionally expressed in *S. cerevisiae*, thereby confirming their SCD activity. The assay presented here might also provide a tool to screen for inhibitors of SCDs, which are interesting drug targets in the treatment of a variety of disease states as well as bacterial and parasitic infections in humans.

3.2. Introduction

Members of the genus *Trypanosoma* such as *Trypanosoma brucei* and *Trypanosoma cruzi* belong to the world's most prevalent human pathogens with millions of people infected, even more being at risk of infection, causing thousands of fatalities per year [1, 2]. *T. brucei* is the infective agent of the sleeping sickness (African Trypanosomiasis) whereas *T. cruzi* is endemic to South Africa and causes the so-called Chargas' disease (American Trypanosomiasis). Persons affected suffer from serious health problems without good chances of recovery due to a limited number of drugs for chemotherapy that also feature little efficiency, severe side effects and high costs [1]. Moreover, available drugs lose efficiency as parasites can acquire drug resistances [3]. These facts emphasize that the development of more efficient drugs with higher potency and specificity is highly urgent. Screenings to identify new anti-trypanosomal drugs can either test natural substances, synthetic compounds or novel agents that were rationally designed. Even the screening of compounds already used for treating other human diseases can identify potent anti-trypanosomal drugs, also taking advantage that these agents have passed a multitude of clinical trials and are already approved [4]. Independent from the agent source, reliable drug screens are required to evaluate the efficiency of promising candidates. The yeast *Saccharomyces cerevisiae* has been successfully used as a heterologous expression system to study the effect of drugs on defined protein targets [5]. Several protein encoding sequences of trypanosomal origin were already successfully expressed in *S. cerevisiae* and complemented for the loss-of-function of homologous endogenous genes [6-12]. Thus, yeast as heterologous expression system provides a well-characterized platform that can be exploited to identify novel anti-parasitic drugs [13]. The power of yeast cell-based assays are founded on the easy and versatile genetic accessibility of yeast and the high degree of conservation of cellular processes among eukaryotic cells in combination with technical advantages of yeast cell cultures. Moreover, *in vivo* drug screens in a suitable eukaryotic environment provide advantages over classical biochemical *in vitro* assays as they already select for essential drug intrinsic properties such as the ability to permeate biological membranes as well as intracellular stability [14]. This way, yeast cell-based assays are also attractive for anti-cancer drug research [15] or the identification of potential drugs to treat other diseases that rely on human endogenous gene products [16]. High-throughput drug screens for anti-parasitic agents against heterologously expressed drug target proteins were also successfully developed and pioneered in yeast [13, 17].

Fatty acid desaturases were identified as promising drug targets in the human pathogen trypanosomes *T. brucei* and *T. cruzi*. These pathogens feature a normal set of lipids common to eukaryotic organisms including phospholipids [18], sphingolipids [19, 20], sterols [21] and tri- and diacylglycerols [22] containing saturated as well as mono- and

polyunsaturated fatty acids [4]. However, the ratio of saturated to mono- and polyunsaturated fatty acids can vary tremendously between the different life cycles of the pathogens: Trypanosomes as insect-resident epimastigotes are exposed to environmental temperatures of 28°C and feature are high degree of (poly)unsaturated fatty acids that can make up to 60% of total fatty acids whereas fatty acid unsaturation of metacyclic trypomastigotes in the human/mammalian host at 37°C is significantly reduced [23]. These findings suggest that the ability to modify membrane fluidity is a critical parameter of trypanosomes to adapt to dramatic changes in their environmental temperature exposed to during their typical life cycles and imply homeoviscous adaption as a prominent virulence factor. In the recent years, biosynthesis pathways of unsaturated fatty acids in trypanosomes have been studied and principle mechanisms and key players were identified [24-26]. Desaturases for the synthesis of highly prevalent polyunsaturated fatty acids use monounsaturated fatty acids as substrate which are synthesized by a Δ9 stearoyl-CoA desaturase (SCD) [25, 27]. This relationship emphasizes SCDs as key determinants in the synthesis of polyunsaturated fatty acids and homeoviscous adaption of trypanosomes, thus indicating that fatty acid desaturases might be good targets for anti-trypanosomal drugs. The *T. brucei* and *T. cruzi* SCDs were shown to be specifically inhibited by the thiourea drug isoxyl which is already used to treat infections with *Mycobacterium tuberculosis* [28, 29]. Experiments that showed an inhibitory effect of isoxyl on trypanosomal SCD were principally based on the exposure of trypanosomes to the active agent in combination with GC-MS analysis of the lipid composition [4, 30] and did not use heterologous expression systems, thus rendering the analysis time consuming, little affordable and complex in application. The study presented here, was aimed to provide the basis for investigating the potency of fatty acid desaturase inhibitors towards trypanosomal SCDs using the power of a cost-effective yeast-based assay that is easy in use and does not require large technical efforts.

3.3. Materials and Methods

3.3.1. Yeast strains

Tab. III-1: Yeast strains used in this study. The table lists all strains with corresponding genotypes. Plasmids harbored by respective strains are named as indicated in Tab. III-S1.

strain	genotype	reference
BY4742	*MAT*α; *his3*Δ1; *leu2*Δ0; *lys2*Δ0; *ura3*Δ0	[31]
SII-1	BY4742; *ole1*:: P_{MET3}-*OLE1*	This study; section 2.3.1
SIII-1	SII-1; pCM188	This study
SIII-2	SIII-1; pGREG523-P_{SPT23}-^{myc}*SPT23*	This study
SII-14	SII-1; pCM188-*OLE1*	This study; section 2.3.1
SIII-3	SII-14; pGREG523-P_{SPT23}-^{myc}*SPT23*	This study
SIII-4	SII-1; pCM188-*OLE1*-yEGFP	This study
SIII-5	SII-1; pCM188-*K.l.OLE1*	This study
SIII-6	SIII-5; pGREG523-P_{SPT23}-^{myc}*SPT23*	This study
SIII-7	SII-1; pCM188-*K.l.OLE1*-yEGFP	This study
SIII-8	SII-1; pCM188-*T.b.*SCD	This study
SIII-9	SIII-8; pGREG523-P_{SPT23}-^{myc}*SPT23*	This study
SIII-10	SII-1; pCM188-*T.b.*SCD-yEGFP	This study
SIII-11	SII-1; pCM188-*T.c.*SCD	This study
SIII-12	SIII-11; pGREG523-P_{SPT23}-^{myc}*SPT23*	This study
SIII-13	SII-1; pCM188-*T.c.*SCD-yEGFP	This study

3.3.2. Yeast transformation and strain construction

Genetically modified *S. cerevisiae* strains generated in this study are derived from BY4742 (*MAT*α; *his3*Δ1; *leu2*Δ0; *lys2*Δ0; *ura3*Δ0) obtained from EUROSCARF (Frankfurt, Germany). BY4742 cells were routinely cultured in YPD media (2% glucose; 2% peptone; 1% yeast extract). BY4742 derived strains harboring selectable markers (*URA3*; *HIS3*) were grown in appropriate synthetic defined (SD) drop-out media (2% glucose; yeast nitrogen base (YNB); drop-out amino acid supplement). Cells were propagated at 30°C. All strains are listed in Tab. III-1.

Transformation of *S. cerevisiae* with previously generated plasmids was routinely performed by using the Frozen-EZ Yeast Transformation II kit (Zymo Research) according to manufacturer's instructions.

3.3.3. Plasmid construction

The introduction of stearoyl-CoA desaturase (SCD) encoding sequences (*OLE1*; *K.l.OLE1*; *T.b.*SCD; *T.c.*SCD) into plasmid pCM188 was done by recombination-based cloning *in vivo*. For that, plasmid pCM188 [32] was cleaved with BamHI and NotI and the respective ORFs were amplified by PCR (Q5 DNA polymerase, NEB). *OLE1* was amplified from S288C genomic DNA. *K.l.OLE1* was amplified from *K. lactis* genomic DNA isolated by a modified alkaline lysis from zymolyase treated *K. lactis* MWL9S1 cells (kind gift of Prof. Dr. Michele M. Bianchi; Sapienza University of Rome) and subsequent column purification of DNA by using a commercial kit (ZR Plasmid Miniprep – Classic Kit, Zymo Research). *Trypanosoma brucei* (*T.b.*) and *Trypanosoma cruzi* (*T.c.*) genomic DNA (kind gift of Prof. Dr. Nestor Luis Uzcategui Araujo; Universidad Central de Venezuela) served as a template for amplifying the respective ORFs (*T.b.*: Tb427.08.6000-t26; *T.c.*: Tc00.1047053509239.10). Flanking of PCR products with sequences homologous to the restricted plasmid backbone was achieved by using corresponding overhang primers (primers P1 & P2 (*OLE1*), P3 & P4 (*K.l.OLE1*); P5 & P6 (*T.b.*SCD); P7 & P8 (*T.c.*SCD)).

For C-terminal GFP-tagging of SCDs, the yEGFP encoding sequence was inserted downstream of the respective SCD ORF that were cloned into plasmid pCM188 beforehand via homologous recombination-based cloning *in vivo*. The yEGFP sequence was amplified from plasmid pKT103 [33] with primers P13 and P9 (for *OLE1*), P10 (for *K.l.OLE1*), P11 (for *T.b.*SCD) or P12 (for *T.c.*SCD).

Co-transformation of linearized plasmid backbone and PCR product for recombination-based *in vivo* cloning was routinely carried out by using Frozen-EZ Yeast Transformation II kit (Zymo Research) according to manufacturer's instructions. PCR conditions were chosen according to manufacturer's instructions.

Plasmids and primers used in this study are listed in the supporting information (Tab. III-S1 & Tab. III-S2).

3.3.4. Sequence analysis

Alignment of protein sequences and determination of protein identity was performed online with the Clustal Omega Multiple Sequence Alignment Program (EMBL-EBI).

3.3.5. Microscopy

Cells expressing C-terminally GFP-tagged SCDs were analyzed using a microscopy setup consisting of a Leica TCS SP5 II spectral confocal laser scanning microscope (Leica Microsystems, CLSM) equipped with a 100-x oil objective (HCX PL APO CS 100x/1.44).

GFP was excited at 488 nm and emission was detected between 510 – 585 nm. Prior to microscopy analysis, cells were grown to exponential phase (OD_{600} = 1.0) in appropriate synthetic defined drop out medium.

For DNA staining with DAPI, 1 mL of a cell culture grown to exponential phase was mixed with 2.5 µL of a DAPI (Sigma Aldrich) stock solution (1 $mg \cdot mL^{-1}$) to a final concentration of 2.5 $\mu g \cdot mL^{-1}$. Cells were then incubated for 30 min at 30°C, harvested by centrifugation, washed 2 times with 1XPBS und used for microscopy analysis. DAPI was excited at 405 nm and emission was detected between 435 – 485 nm.

3.3.6. Growth assays on agar medium

Growth assays were performed for characterizing the growth phenotype of (genetically modified) strains under defined growth conditions. Cells used for growth assays were grown overnight in appropriate synthetic defined media or YPD (where applicable) at 30°C in a rotary shaker at 200 rpm. Cells from overnight cultures were harvested by centrifugation and washed 2 times with sterile water (ddH_2O) to remove any remaining residuals from the culture medium. For each preparation, fresh suspensions were adjusted to OD_{600} = 1.0 ± 0.05 using H_2O and from these 10-fold serial dilutions were set up (1:10 - OD_{600} = 0.1; 1:100 - OD_{600} = 0.01; 1:1000 - OD_{600} = 0.001). 7 µL from each dilution and all strains to be compared were spotted in a row on indicated agar medium. Plates were incubated at 30°C for 3 days. The growth phenotype was evaluated by comparing the size of colonies from sample strains and positive/negative controls by eye.

These growth assays were applied to evaluate the growth phenotype and cell viability upon doxycycline-mediated repression of plasmid-based heterologous SCD expression in the genomic P_{MET3}-*OLE1* background.

3.3.7. Growth and flocculation tests

Growth assays in liquid media and flocculation tests were performed as previously described (section 2.3.4).

3.3.8. Fatty acid analysis

The GC-MS analysis of fatty acids was performed as previously described (section 2.3.5).

3.3.9. Spt23p processing

Proteolytic processing of myc-tagged Spt23p was monitored as previously described (section 2.3.7).

3.4. Results and Discussion

3.4.1. Assay design

A lipid engineering approach revealed physiological roles of membrane fluidity and packing of glycerophospholipids in cellular membranes for yeast flocculation (section 2.4.2) [34]. Flocculation is induced upon decreased membrane fluidity resulting either from repression of genomic *OLE1*, encoding for the sole fatty acid desaturase in yeast, or from growth under hypoxic conditions which reduces the overall cellular Ole1p activity due to limited dissolved oxygen (serves as a co-factor of the Ole1p catalyzed desaturation reaction) availability. Membrane fluidity and flocculation inducing Flo1p expression are linked by ER membrane-resident membrane fluidity sensors, Spt23p and Mga2p, which are activated upon decreased membrane rigidity and lipid packing by proteasome-mediated proteolytic processing. The resulting soluble activated fragments (p90 domains) translocate to the nucleus where they induce gene expression. Prominent targets of p90 transcription activators are *OLE1*, thereby constituting a feedback loop to maintain physiological membrane fluidity, and, among others, *FLO1* encoding for a cell wall protein that binds sugar moieties of adjacent cells, thus mediating cell-cell interactions termed flocculation. Upon formation of flocs consisting of thousands of cells, these flocs rapidly separate from the medium by sedimentation [35], thereby leading to a clear, prominent and easily detectable phenotype. Such strong phenotypes are e.g. required for phenotypic drug screening approaches and can serve as assay readouts for screenings, aimed to identifying particular enzyme functions.

The *OLE1*-mediated flocculation phenotype can be exploited to assay for e.g. stearoyl-CoA desaturase (SCD) activity of enzymes that complement for repressed Ole1p activity, thus inhibiting flocculation as well as for drugs or conditions that negatively affect SCD activity, thus leading to flocculation. A potential assay construct to screen for enzymatic SCD activity was already introduced in Fig. II-5A.

This assay system (Fig. III-1) consists of a yeast strain background that allows for methionine-mediated repression of genomically encoded *OLE1* (induces flocculation) and a vector (pCM188-*OLE1*) allowing for orthogonally controlled expression of *OLE1* (orthogonal control of gene expression by using the *MET3* promoter and an artificial $tetO_2$-*CYC1* promoter construct is also demonstrated in Fig. IV-3). Plasmid-based expression of a functional stearoyl-CoA desaturase prevents flocculation (positive result), whereas repressed plasmid-based expression (control) or non-functional enzymes do not prevent flocculation (negative result) (Fig. III-1).

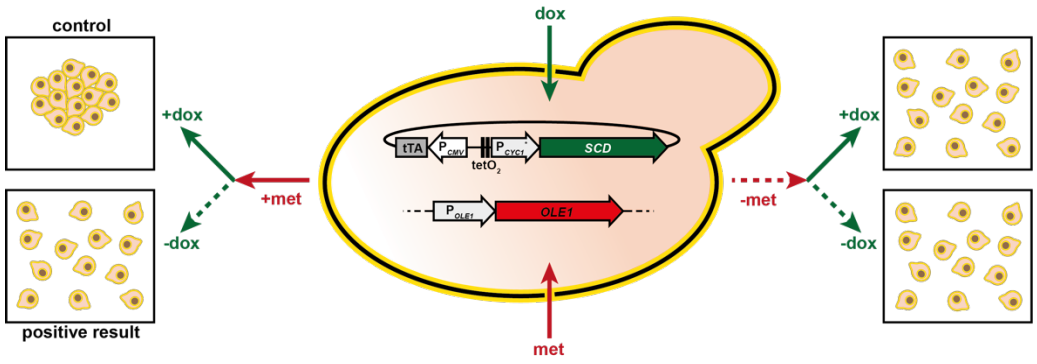

Fig. III-1: Schematic representation of the assay system. Cells of the P_{MET3}-*OLE1* strain harbor a plasmid that allows for doxycycline-repressible expression of SCD candidates. Methionine-repressed (250 µM met) *OLE1* expression from the genome induces flocculation, which can be prevented by plasmid-based expression of a functional SCD that complements for repressed Ole1p expression (positive result).

3.4.2. Defining protein targets

The described assay should be suitable to identify putative stearoyl-CoA desaturase activity of two uncharacterized proteins of *Trypanosoma brucei* (*T.b*) and *Trypanosoma cruzi* (*T.c.*) that share intermediate identity (*T.b.*: 39.4% and *T.c.*: 38.7%) to *S. cerevisiae* Ole1p and feature a homologous protein architecture, therefore identifying these proteins as potential SCD candidates (Fig. III-2). Unlike mammalian Δ9 fatty acid desaturases, yeast Ole1p is a chimeric protein, consisting of a N-terminal fatty acid desaturase domain that is linked to a C-terminal cytochrome b_5-like domain [36]. This protein intrinsic cytochrome b_5 is reduced by a NADH cytochrome b_5 reductase and provides reducing equivalents required for the desaturation reaction [37]. In contrast, mammalian fatty acid desaturases interact with free cytochrome b_5 that is anchored in the ER membrane by a hydrophobic 19 residues long C-terminal region [38]. The desaturase domain of yeast Ole1p harbors two ~50 amino acids long hydrophobic sequences, which are divided into one 9 residues long cluster of charged, helix-breaking amino acids and two (20 – 23 amino acid) hydrophobic clusters that might span the ER membrane and anchor the protein within the bilayer as well as positioning the active site of the desaturase domain on the cytosolic surface of the ER [39]. Furthermore, the protein contains three histidine clusters (HX_4H and HX_2HH) that are highly conserved among fatty acid desaturases as they coordinate elemental iron and are therefore essential for the catalytic activity of the enzymes [40]. Putative SCDs from *T. brucei* and *T. cruzi* share all described features of *S.c.*Ole1p (Fig. III-2), rendering these promising SCD candidates to exhibit enzymatic function when expressed in yeast.

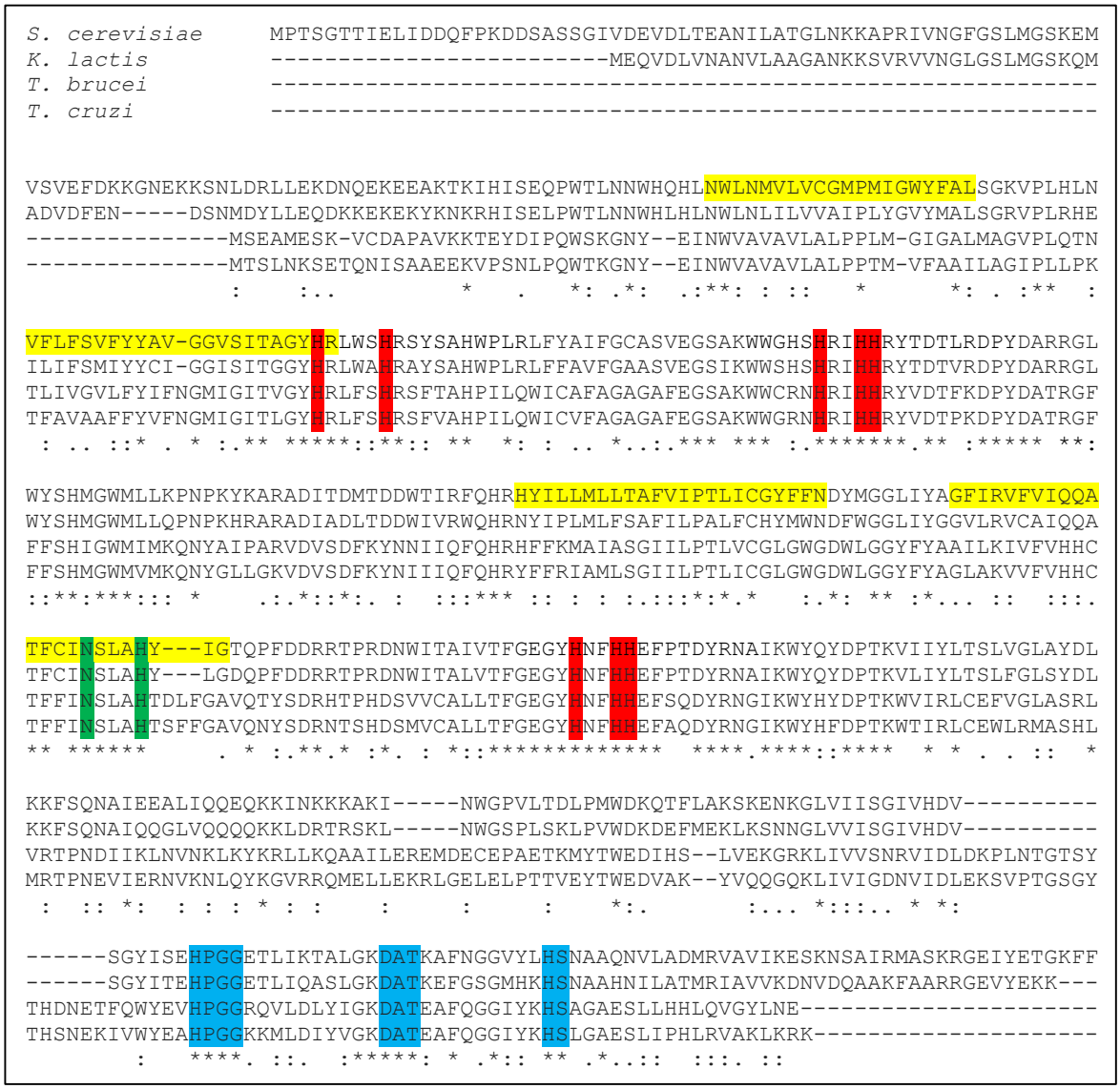

Fig. III-2: Multiple protein sequence alignment of stearoyl-CoA desaturases from yeasts and from trypanosomes. Sequences from verified stearoyl-CoA desaturases (SCDs) from the yeast *S. cerevisiae* and *K. lactis*, as well as putative SCDs from *T. brucei* and *T. cruzi* were aligned. Consensus symbols denote the degree of conservation observed in each column: (*) residues in the column are identical in all sequences; (:) conserved substitutions with residues having highly similar properties; (.) semi-conserved substitutions with residues having weakly similar properties. Yellow sequence parts of *S.c.*Ole1p mark predicted alpha-helical transmembrane domains. Conserved histidine clusters (HX_4H; HX_2HH) required to coordinate catalytic iron ions are shown in red. A conserved NX_3H cluster that is required to coordinate a water molecule is shown in green. Conserved amino acids of the cytochrome b5 domain corresponding to a heme binding pocket are highlighted in blue.

Furthermore, both enzymes meet criteria that propose them as useful targets for anti-parasitic drugs [11]: (i) stearoyl-CoA desaturases were found to be essential enzymes for the parasites *T. brucei* and *T. cruzi* as assessed by gene knock-down experiments [30] and chemical evaluation [4]. The latter was performed by the treatment of *T. cruzi* infected mice with the thiourea drug isoxyl (thiocarlide; 4,4'-diisoamyloxydi-phenylthiourea) which is known to be an effective anti-tuberculosis drug and was identified as an inhibitor of the Δ9-stearoyl desaturase of *Mycobacterium tuberculosis* [29]. (ii) Moreover, the putative *T.c.*SCD

was suggested by the TDR targets database (http://tdrtargets.org) as potential drug target against major tropical disease pathogens. (iii) The protein targets have homologues in human, sharing low similarity (T.b.: 29.6% and *T.c.*: 27.6%) and feature a significantly different architecture especially regarding the missing cytochrome b_5 domain. (iv) The heterologously expressed proteins are essential for the used expression strain (BY472; P_{MET3}-*OLE1* grown in 5 mM met) or cause a prominent (flocculation) phenotype.

3.4.3. Functional SCD expression

A series of pCM188-based plasmids containing the stearoyl-CoA desaturase (SCD) ORFs of (i) *S. cerevisiae*, *S.c.OLE1*; (ii) of the closely related yeast *Kluyveromyces lactis*, *K.l.OLE1* or the ORFs of the putative SCDs from (iii) *T. brucei*, *T.b.*SCD or (iv) *T. cruzi*, *T.c.*SCD were constructed. The plasmid contains the constitutive $tetO_2$-P_{CYC1} promoter driving the SCD expression, which can be repressed by the addition of e.g. the tetracycline analogue doxycycline. The yeast strain BY4742-P_{MET3}-*OLE1* having its endogenous *OLE1* under control of the methionine repressible *MET3* promoter was transformed with these plasmids and resulting strains were used for initial growth assays, testing for functional complementation of repressed genomic *S.c.OLE1*. For that, serial dilutions of the respective strains were dropped on methionine-containing (5 mM) and methionine-free agar either supplemented with doxycycline (40 $\mu g \cdot mL^{-1}$) or free of doxycycline. All strains grew unimpaired on methionine-free (-met; -dox) medium as genomic *OLE1* was fully expressed and addition of doxycycline (-met; +dox) did also not affect growth. In contrast, growth was almost fully repressed in methionine and doxycycline containing medium (+met; +dox) since both, plasmid-based SCD expression as well as genomic *OLE1* expression was fully repressed. However, growth was restored in the absence of doxycycline (+met; -dox), thus verifying that the putative SCDs from *T. brucei* and *T. cruzi* possess the predicted enzymatic activity and can complement for the loss of *OLE1* function (Fig. III-3). *T.c.*SCD expression was found to rescue growth more effectively, as compared to *T.b.*SCD expression which might suggest slightly higher stearoyl-CoA activity of *T.c.*SCD when expressed in yeast. This conclusion was also consistent with GC-MS control measurements of total fatty acid unsaturation (Fig. III-S2). Growth of liquid cultures was similarly rescued upon heterologous expression of both SCD from *T. brucei* and *T. cruzi* (Fig. III-S1). The SCD from *K. lactis* complemented reduced *OLE1* activity very effectively as one could predict from the high identity (70.4%) of both primary protein structures. *K.l.*Ole1p was therefore considered as the heterologous positive control since proteins from *K. lactis* are known to complement well for *S. cerevisiae* endogenous proteins and are therefore often used as selection markers, e.g. *K.l.URA3* [41].

To test for the development of the flocculation phenotype upon heterologous expression of SCDs, growth assays in 1 mL liquid cultures were performed. Previous experiments revealed a reliable development of flocculation of strain SII-1 in 250 µM external methionine (Fig. II-3). Respective strains harboring SCD plasmids as well as empty vector control (e.v.) were grown in the presence or absence of methionine and doxycycline in all 4 possible permutations as illustrated in Fig. III-1. The predicted characteristic flocculation profile at the indicated conditions clearly illustrates enzymatic SCD activity. SCD expression from plasmids (-dox) resulted in suppression of the flocculation behavior when cells were grown in the presence of methionine. Repression of plasmid-based expression traced restoration of flocculation unambiguously to enzymatic SCD activity. In the negative control with an empty vector, flocculation was not suppressed in the presence of methionine, independent external doxycycline. Thus, the flocculation-based assay has proven to clearly indicate enzymatic SCD activity.

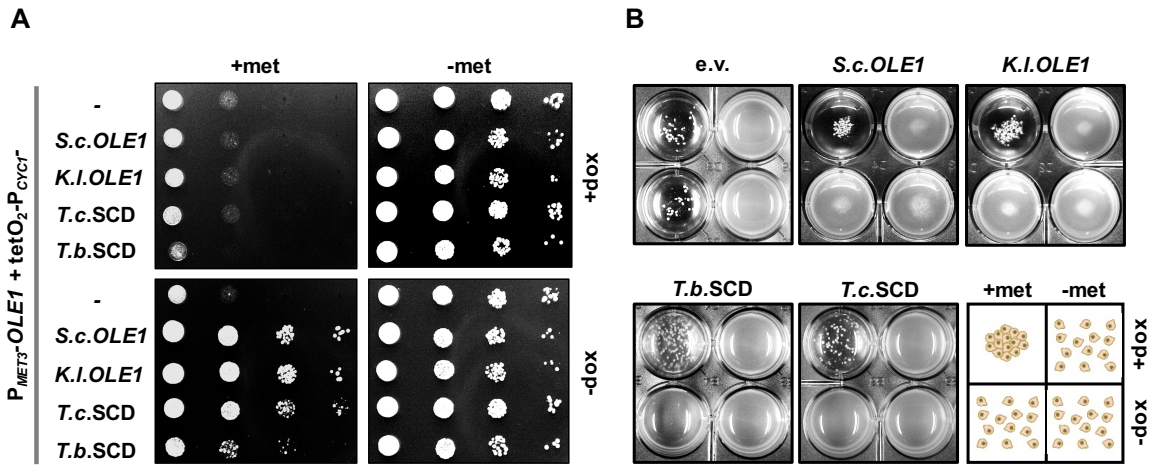

Fig. III-3: Putative stearoyl-CoA desaturases from *T. brucei* and *T. cruzi* functionally complement for the yeast endogenous Ole1p. (A) Growth assay on agar plates to test for functional complementation of repressed genomic *S.c.OLE1*. The growth phenotype of P_{MET3}-*OLE1* cells is shown via spotting a 10-fold dilution series on methionine containing medium (+met; 5 mM) in the presence or absence of doxycycline (+dox; 40 µg·mL^{-1}). The growth defect upon repression (+met; +dox) of genomically encoded *S.c.OLE1* is rescued by plasmid-based expression (+met; -dox) of SCDs from *K. lactis*, *T. brucei* and *T. cruzi* as well as by the endogenous enzyme from *S. cerevisiae* (*S.c.OLE1*, positive control). Growth on methionine free medium (-met) was unimpaired as expected and was tested to verify the functionality of the genomically encoded Ole1p. **(B)** Suppression of flocculation upon plasmid-based SCD expression tested in 1 mL liquid cultures. Cells strongly flocculated in the presence of methionine (250 µM) when plasmid-based SCD expression was repressed (+dox; 40 µg·mL^{-1}). SCD expression (-dox) prevented flocculation and clearly demonstrated stearoyl-CoA desaturase activity of heterologously expressed enzymes. The empty vector (e.v.) did not prevent flocculation.

3.4.4. Control experiments to verify SCD activity

Ole1p is anchored to the ER membrane where it interacts with cytochrome b_5 reductases and fatty acid CoA substrates deriving from fatty acid synthase reaction to generate CoA-bound precursors of monounsaturated fatty acids (MUFA). These are further utilized by e.g.

ER localized Gat1p, Gat2p and Slc1p to generate diacylglycerols (DAGs) by stepwise acylation of glycerol-3-phosphate [42, 43]. DAGs are further converted to glycerophospholipids or triacylglycerols. The ER localization of the glycerophospholipid biosynthesis machinery emphasizes the requirement of correct ER residency of SCD to allow for MUFA delivery in the place of demand. The check whether heterologously expressed SCDs from *K. lactis* and trypanosomes behave like the yeast endogenous SCD and are correctly localized to the ER membranes, SCDs were C-terminally tagged with GFP and subcellular localization was determined by confocal fluorescence microscopy (Fig. III-4A). GFP-fused yeast endogenous Ole1p was localized in the cortical ER membranes tethered to the plasma membrane as well as in the ER membranes attached to the nuclear envelop as visualized by DAPI co-staining of nuclear DNA [44]. GFP-fusions of heterologously expressed SCDs exhibited the same subcellular distribution pattern. Thus, previously detected SCD activity is supported by the closely interlinked localization-function relationship.

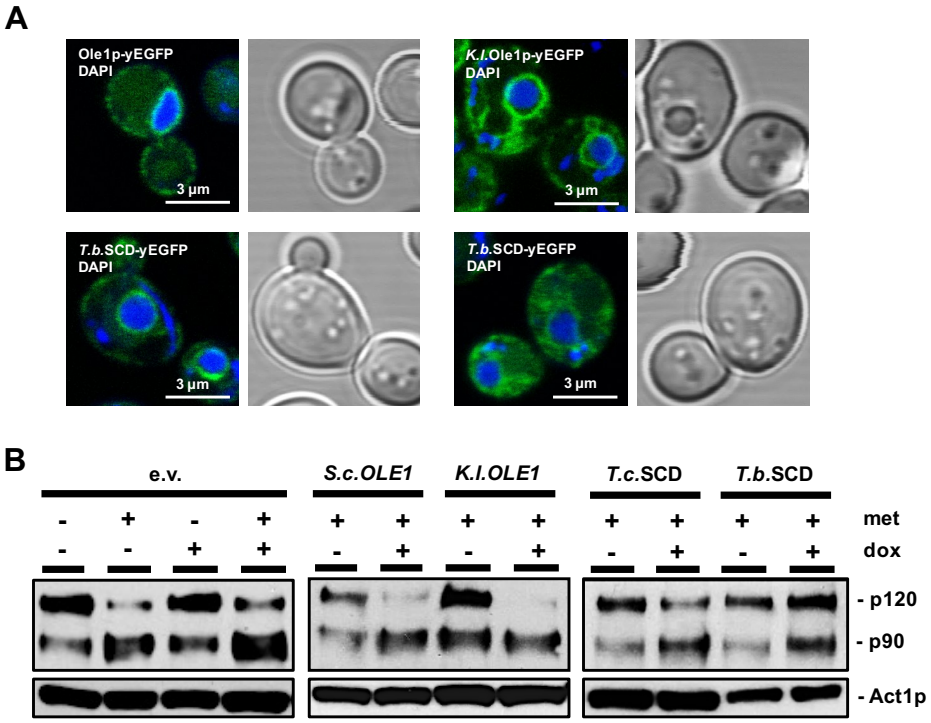

Fig. III-4: Foreign SCDs are correctly localized in ER membranes and influence proteolytic processing of Spt23p similar to Ole1p. (A) Yeast endogenous SCD, Ole1p, as well as foreign SCDs from *K. lactis* (*K.l.*), *T. brucei* (*T.b.*) and *T. cruzi* (*T.c.*) were fused to yEGFP (green) and subcellular localization was determined by confocal fluorescence microscopy. Co-straining of DNA with DAPI (blue) revealed that foreign SCDs localized to the ER membranes attached to the nuclear membrane as well as to the cortical ER membranes tethered to the plasma membrane, also true for native *S.c.*Ole1p. **(B)** Western Blot analysis to monitor proteolytic processing of Stp23p in dependence of heterologous SCD expression. The ratio of acitivated Spt23p (p90) over the full length protein (p120) increased upon repression of *OLE1* in the empty vector control (e.v.). Spt23p90 accumulation could be abolished by plasmid-based expression of foreign SCDs from *K. lactis*, *T. brucei* and *T. cruzi*.

Spt23p proteolytic processing upon *S.c.OLE1* repression and simultaneous heterologous SCD expression was monitored by Western blot analyses to link *FLO1* upregulation to Spt23p activation triggered by changes in membrane fluidity. In the empty vector control (e.v.), a characteristic accumulation of the activated Spt23p fragment (p90) was observed upon methionine-mediated *S.c.OLE1* repression and this was independent of external doxycycline. Accumulation of Spt23p90 was strongly reduced upon plasmid-based heterologous SCD expression (+met; -dox) in comparison to the empty vector control at equivalent conditions (+met; -dox) as well as to repressed plasmid-based SCD expression (+met; +dox) (Fig. III-4B). Thus, enzymatic activity of foreign SCDs from *T. brucei*, *T. cruzi* but also from *K. lactis* is able to reduce yeast ER membrane fluidity below the threshold level that prevents sufficient Spt23p proteolytic processing to induce flocculation. Furthermore, it is shown that foreign SCDs interact with the OLE pathway [45] in an identical manner as the native yeast stearoyl-CoA desaturase, Ole1p. GC-MS analyses also demonstrated that foreign SCDs effectively reduced the amount of fully saturated fatty acid species, although, *K. lactis* Ole1p and yeast endogenous *S.c.*Ole1p (Fig. II-S4A) had a stronger effect on lipid unsaturation. Expression of trypanosomal SCDs had a major effect on C18 fatty acid unsaturation and caused a slight decrease of C16 (~76% to ~63%) and a shift towards C18 fatty acid species (Fig. III-S2).

3.5. Conclusions

Yeast has proven to be a suitable host for the heterologous expression of stearoyl-CoA desaturases (SCDs) from *T. brucei* and *T. cruzi*. These enzymes were previously identified as putative SCDs based on sequence homology to enzymes with verified SCD activity. Gene knockdown experiments in the donor organism [30] and chemical evaluation [4] suggested that both enzymes indeed possess enzymatic SCD activity. The study presented here, describes for the first time the heterologous expression of putative *T.b*.SCD and *T.c*.SCD in budding yeast and clearly verified their stearoyl-CoA activity using different approaches (e.g. *OLE1* complementation, GC-MS analysis). By using a strain background that has its endogenous stearoyl-CoA desaturase gene under control the repressible *MET3* promoter as expression system, it was possible to set up a simple and affordable SCD activity screen. Growth or flocculation served as assay read-out that can even be easily detected by eye. This assay might be useful for *in vivo* drug screenings as *Trypanosoma* SCDs have proven to be promising drug targets for the treatment of parasitic infections in humans [30]. Growth and flocculation assays were performed in 24-well plates but could be easily transferred to 384-well microtiter trays thereby allowing for a higher throughput, maybe also in combination with robotic assistance. Moreover, yeast-based assays allow to screen for drugs against enzymes of human infecting parasites without necessarily coming in contact with the pathogen itself, which would require special laboratory equipment.

However, the functionality of this assay for successful identification of SCD inhibitors has not been confirmed, yet. Yeast cells might be resistant against actually potent SCD inhibitors due to their thick cell wall or due to the presence of effective drug efflux pumps in their plasma membrane [46]. These factors might decrease the sensibility of the assay to an unfavorably low level. However, the assay system offers multiple ways to adjust and fine-tune the sensibility of a potential screen. Growth of the platform strain as well as development of flocculation is determined by the ratio of *OLE1* to heterologous SCD expression. Since expression of both genes can be orthogonally controlled, expression of *Trypanosoma* SCDs could be downregulated to an absolute minimum that just supports growth. The decreased amount of target protein as well as the fine-tuned critical ratio of *OLE1* to SCD expression might increase the sensitivity of the screen as it was previously demonstrated [11]. Furthermore, yeast is readily accessible to genetic modifications by e.g. using the straightforward CRISPR/Cas9 technology (chapter V) thereby easily allowing for knocking-out genes that encode for drug efflux pumps or other genes that impair the sensitivity of the system. Deletion of *PDR5* that encodes for the yeast major ABC multidrug transporter [47] was previously shown to increase the sensitivity of a similar drug screen [11].

3.6. References

1. **Barrett MP, Burchmore RJ, Stich A, Lazzari JO, Frasch AC et al.** The trypanosomiases. *Lancet* 2003;362(9394):1469-1480.
2. **Odiit M, Kansiime F, Enyaru JC**. Duration of symptoms and case fatality of sleeping sickness caused by Trypanosoma brucei rhodesiense in Tororo, Uganda. *East Afr Med J* 1997;74(12):792-795.
3. **Barrett MP, Vincent IM, Burchmore RJ, Kazibwe AJ, Matovu E**. Drug resistance in human African trypanosomiasis. *Future Microbiol* 2011;6(9):1037-1047.
4. **Alloatti A, Testero SA, Uttaro AD**. Chemical evaluation of fatty acid desaturases as drug targets in Trypanosoma cruzi. *Int J Parasitol* 2009;39(9):985-993.
5. **Zhang N, Bilsland E**. Contributions of Saccharomyces cerevisiae to understanding mammalian gene function and therapy. *Methods Mol Biol* 2011;759:501-523.
6. **Balliano G, Dehmlow H, Oliaro-Bosso S, Scaldaferri M, Taramino S et al.** Oxidosqualene cyclase from Saccharomyces cerevisiae, Trypanosoma cruzi, Pneumocystis carinii and Arabidopsis thaliana expressed in yeast: a model for the development of novel antiparasitic agents. *Bioorg Med Chem Lett* 2009;19(3):718-723.
7. **Carrillo C, Canepa GE, Giacometti A, Bouvier LA, Miranda MR et al.** Trypanosoma cruzi amino acid transporter TcAAAP411 mediates arginine uptake in yeasts. *FEMS Microbiol Lett* 2010;306(2):97-102.
8. **Erben ED, Daum S, Tellez-Inon MT**. The Trypanosoma cruzi PIN1 gene encodes a parvulin peptidyl-prolyl cis/trans isomerase able to replace the essential ESS1 in Saccharomyces cerevisiae. *Mol Biochem Parasitol* 2007;153(2):186-193.
9. **Mokry DZ, Manandhar SP, Chicola KA, Santangelo GM, Schmidt WK**. Heterologous expression studies of Saccharomyces cerevisiae reveal two distinct trypanosomatid CaaX protease activities and identify their potential targets. *Eukaryot Cell* 2009;8(12):1891-1900.
10. **Cortes LK, Scarcelli JJ, Taron CH**. Complementation of essential yeast GPI mannosyltransferase mutations suggests a novel specificity for certain Trypanosoma and Plasmodium PigB proteins. *PLoS One* 2014;9(1):e87673.
11. **Bilsland E, Pir P, Gutteridge A, Johns A, King RD et al.** Functional expression of parasite drug targets and their human orthologs in yeast. *PLoS Negl Trop Dis* 2011;5(10):e1320.
12. **Saye M, Miranda MR, di Girolamo F, de los Milagros Camara M, Pereira CA**. Proline modulates the Trypanosoma cruzi resistance to reactive oxygen species and drugs through a novel D, L-proline transporter. *PLoS One* 2014;9(3):e92028.
13. **Bilsland E, Sparkes A, Williams K, Moss HJ, de Clare M et al.** Yeast-based automated high-throughput screens to identify anti-parasitic lead compounds. *Open Biol* 2013;3(2):120158.
14. **Barberis A, Gunde T, Berset C, Audetat S, Luthi U**. Yeast as a screening tool. *Drug Discov Today Technol* 2005;2(2):187-192.
15. **Menacho-Marquez M, Murguia JR**. Yeast on drugs: Saccharomyces cerevisiae as a tool for anticancer drug research. *Clin Transl Oncol* 2007;9(4):221-228.
16. **Marjanovic J, Chalupska D, Patenode C, Coster A, Arnold E et al.** Recombinant yeast screen for new inhibitors of human acetyl-CoA carboxylase 2 identifies potential drugs to treat obesity. *Proc Natl Acad Sci U S A* 2010;107(20):9093-9098.
17. **Klein RD, Favreau MA, Alexander-Bowman SJ, Nulf SC, Vanover L et al.** Haemonchus contortus: cloning and functional expression of a cDNA encoding ornithine decarboxylase and development of a screen for inhibitors. *Exp Parasitol* 1997;87(3):171-184.
18. **Serricchio M, Butikofer P**. Trypanosoma brucei: a model micro-organism to study eukaryotic phospholipid biosynthesis. *FEBS J* 2011;278(7):1035-1046.
19. **Mina JG, Pan SY, Wansadhipathi NK, Bruce CR, Shams-Eldin H et al.** The Trypanosoma brucei sphingolipid synthase, an essential enzyme and drug target. *Mol Biochem Parasitol* 2009;168(1):16-23.
20. **Fridberg A, Olson CL, Nakayasu ES, Tyler KM, Almeida IC et al.** Sphingolipid synthesis is necessary for kinetoplast segregation and cytokinesis in Trypanosoma brucei. *J Cell Sci* 2008;121(Pt 4):522-535.
21. **Kessler RL, Soares MJ, Probst CM, Krieger MA**. Trypanosoma cruzi response to sterol biosynthesis inhibitors: morphophysiological alterations leading to cell death. *PLoS One* 2013;8(1):e55497.
22. **Allmann S, Mazet M, Ziebart N, Bouyssou G, Fouillen L et al.** Triacylglycerol Storage in Lipid Droplets in Procyclic Trypanosoma brucei. *PLoS One* 2014;9(12):e114628.

23. **Florin-Christensen M, Florin-Christensen J, de Isola ED, Lammel E, Meinardi E et al.** Temperature acclimation of Trypanosoma cruzi epimastigote and metacyclic trypomastigote lipids. *Mol Biochem Parasitol* 1997;88(1-2):25-33.

24. **Alloatti A, Uttaro AD**. Highly specific methyl-end fatty-acid desaturases of trypanosomatids. *Mol Biochem Parasitol* 2011;175(2):126-132.

25. **Tripodi KE, Buttigliero LV, Altabe SG, Uttaro AD**. Functional characterization of front-end desaturases from trypanosomatids depicts the first polyunsaturated fatty acid biosynthetic pathway from a parasitic protozoan. *FEBS J* 2006;273(2):271-280.

26. **Livore VI, Tripodi KE, Uttaro AD**. Elongation of polyunsaturated fatty acids in trypanosomatids. *FEBS J* 2007;274(1):264-274.

27. **Petrini GA, Altabe SG, Uttaro AD**. Trypanosoma brucei oleate desaturase may use a cytochrome b5-like domain in another desaturase as an electron donor. *Eur J Biochem* 2004;271(6):1079-1086.

28. **Grzegorzewicz AE, Kordulakova J, Jones V, Born SE, Belardinelli JM et al.** A common mechanism of inhibition of the Mycobacterium tuberculosis mycolic acid biosynthetic pathway by isoxyl and thiacetazone. *J Biol Chem* 2012;287(46):38434-38441.

29. **Phetsuksiri B, Jackson M, Scherman H, McNeil M, Besra GS et al.** Unique mechanism of action of the thiourea drug isoxyl on Mycobacterium tuberculosis. *J Biol Chem* 2003;278(52):53123-53130.

30. **Alloatti A, Gupta S, Gualdron-Lopez M, Nguewa PA, Altabe SG et al.** Stearoyl-CoA desaturase is an essential enzyme for the parasitic protist Trypanosoma brucei. *Biochem Biophys Res Commun* 2011;412(2):286-290.

31. **Brachmann CB, Davies A, Cost GJ, Caputo E, Li J et al.** Designer deletion strains derived from Saccharomyces cerevisiae S288C: a useful set of strains and plasmids for PCR-mediated gene disruption and other applications. *Yeast* 1998;14(2):115-132.

32. **Gari E, Piedrafita L, Aldea M, Herrero E**. A set of vectors with a tetracycline-regulatable promoter system for modulated gene expression in Saccharomyces cerevisiae. *Yeast* 1997;13(9):837-848.

33. **Sheff MA, Thorn KS**. Optimized cassettes for fluorescent protein tagging in Saccharomyces cerevisiae. *Yeast* 2004;21(8):661-670.

34. **Degreif D, de Rond T, Bertl A, Keasling JD, Budin I**. Lipid engineering reveals regulatory roles for membrane fluidity in yeast flocculation and oxygen-limited growth. *Metab Eng* 2017;41:46-56.

35. **Verstrepen KJ, Derdelinckx G, Verachtert H, Delvaux FR**. Yeast flocculation: what brewers should know. *Appl Microbiol Biotechnol* 2003;61(3):197-205.

36. **Mitchell AG, Martin CE**. A novel cytochrome b5-like domain is linked to the carboxyl terminus of the Saccharomyces cerevisiae delta-9 fatty acid desaturase. *J Biol Chem* 1995;270(50):29766-29772.

37. **Martin CE, Oh CS, Jiang Y**. Regulation of long chain unsaturated fatty acid synthesis in yeast. *Biochim Biophys Acta* 2007;1771(3):271-285.

38. **Guiles RD, Altman J, Kuntz ID, Waskell L, Lipka JJ**. Structural studies of cytochrome b5: complete sequence-specific resonance assignments for the trypsin-solubilized microsomal ferrocytochrome b5 obtained from pig and calf. *Biochemistry* 1990;29(5):1276-1289.

39. **Stukey JE, McDonough VM, Martin CE**. The OLE1 gene of Saccharomyces cerevisiae encodes the delta 9 fatty acid desaturase and can be functionally replaced by the rat stearoyl-CoA desaturase gene. *J Biol Chem* 1990;265(33):20144-20149.

40. **Shanklin J, Whittle E, Fox BG**. Eight histidine residues are catalytically essential in a membrane-associated iron enzyme, stearoyl-CoA desaturase, and are conserved in alkane hydroxylase and xylene monooxygenase. *Biochemistry* 1994;33(43):12787-12794.

41. **Gueldener U, Heinisch J, Koehler GJ, Voss D, Hegemann JH**. A second set of loxP marker cassettes for Cre-mediated multiple gene knockouts in budding yeast. *Nucleic Acids Res* 2002;30(6):e23.

42. **Pagac M, de la Mora HV, Duperrex C, Roubaty C, Vionnet C et al.** Topology of 1-acyl-sn-glycerol-3-phosphate acyltransferases SLC1 and ALE1 and related membrane-bound O-acyltransferases (MBOATs) of Saccharomyces cerevisiae. *J Biol Chem* 2011;286(42):36438-36447.

43. **Bratschi MW, Burrowes DP, Kulaga A, Cheung JF, Alvarez AL et al.** Glycerol-3-phosphate acyltransferases gat1p and gat2p are microsomal phosphoproteins with differential contributions to polarized cell growth. *Eukaryot Cell* 2009;8(8):1184-1196.

44. **Tatzer V, Zellnig G, Kohlwein SD, Schneiter R**. Lipid-dependent subcellular relocalization of the acyl chain desaturase in yeast. *Mol Biol Cell* 2002;13(12):4429-4442.

45. **Ballweg S, Ernst R**. Control of membrane fluidity: the OLE pathway in focus. *Biol Chem* 2017;398(2):215-228.

46. **Cannon RD, Lamping E, Holmes AR, Niimi K, Baret PV et al.** Efflux-mediated antifungal drug resistance. *Clin Microbiol Rev* 2009;22(2):291-321, Table of Contents.

47. **Mamnun YM, Schuller C, Kuchler K**. Expression regulation of the yeast PDR5 ATP-binding cassette (ABC) transporter suggests a role in cellular detoxification during the exponential growth phase. *FEBS Lett* 2004;559(1-3):111-117.

3.7. Supporting information

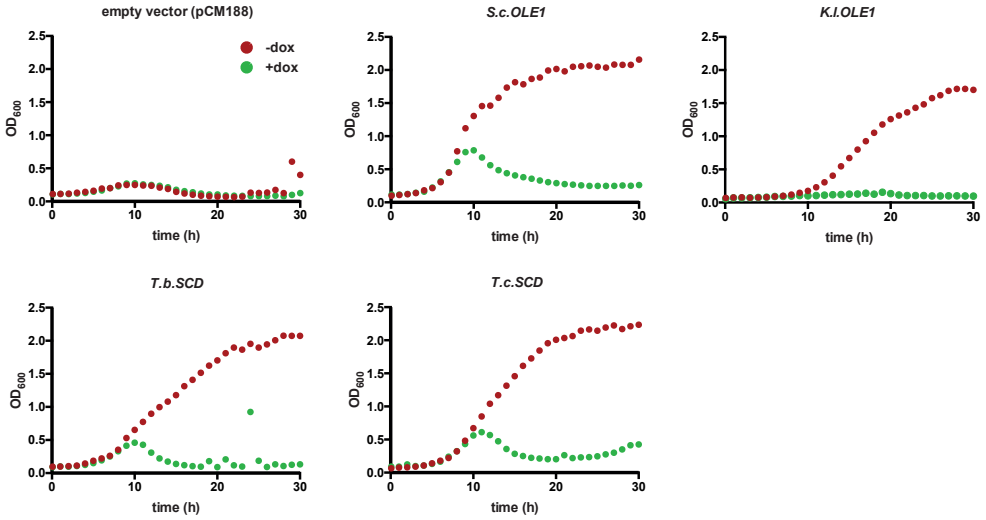

Fig. III-S1: Effect of heterologous SCD expression on growth in liquid media. Growth curves of P$_{MET3}$-*OLE1* cells harboring plasmids that encode for indicated SCDs from *S. cerevisiae* (*S.c.*), *K. lactis* (*K.l.*), *T. brucei* (*T.b.*) and *T. cruzi* (*T.c.*) in the presence (40 µg·mL^{-1}) or absence of doxycycline (repressor). Experiments were performed in a repressed P$_{MET3}$-*OLE1* background (150 µM met). Heterologous expression of SCDs rescued the growth defect upon repressed genomically encoded *OLE1*. A strain harboring an empty vector served as negative control.

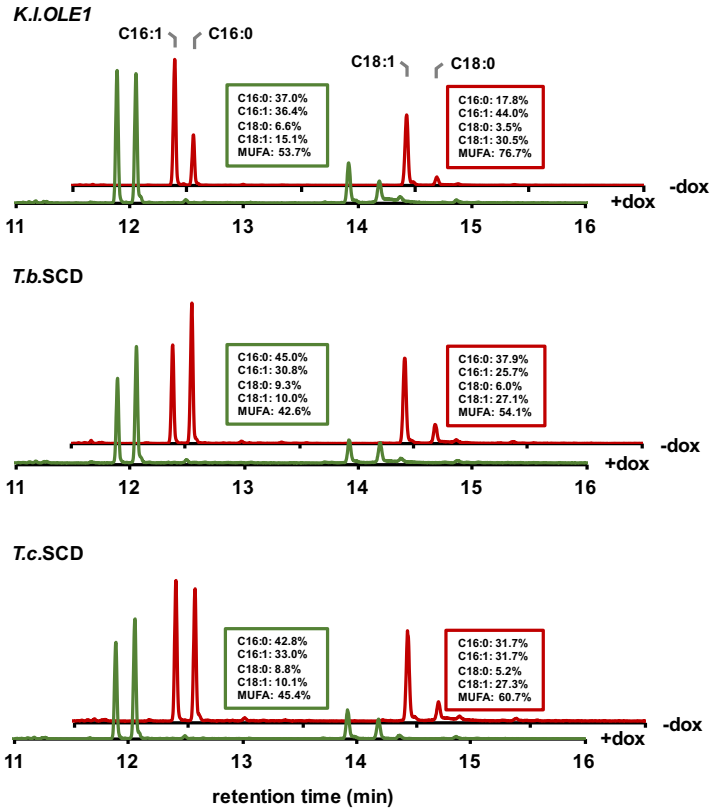

Fig. III-S2: Fatty acid composition of P$_{MET3}$-*OLE1* cells expressing indicated foreign SCDs as measured by GC-MS analysis. Chromatograms of GC-MS analysis show an increasing level of monounsaturated fatty acid (MUFA) species upon heterologous expression (-dox) of SCDs from *K. lactis*, *T. brucei* and *T. cruzi* compared to repressed expression (+dox). GC-MS analyses were performed in a repressed P$_{MET3}$-*OLE1* background (250 µM met). Indicated percentage values focus on major fatty acid classes (C16 and C18), C14 species are not indicated.

Tab. III-S1: Plasmids used in this study. The table summarizes basic characteristics and properties of indicated plasmids.

Plasmid	description	reference
pCM188	-	[32]
pKT103	-	[33]
pCM188-*OLE1*	CEN/ARS; *URA3*; amp^R; doxycycline repressible expression of Ole1p	This study; section 2.3.1
pCM188-*OLE1*-yEGFP	CEN/ARS; *URA3*; amp^R; doxycycline repressible expression of C-terminally yEGFP-tagged Ole1p	This study
pCM188-*K.l.OLE1*	CEN/ARS; *URA3*; amp^R; doxycycline repressible expression of *Kluyveromyces lactis* Ole1p	This study
pCM188-*K.l.OLE1*-yEGFP	CEN/ARS; *URA3*; amp^R; doxycycline repressible expression of C-terminally yEGFP-tagged *Kluyveromyces lactis* Ole1p	This study
pCM188-*T.b.*SCD	CEN/ARS; *URA3*; amp^R; doxycycline repressible expression of *Trypanosoma brucei* SCD	This study
pCM188-*T.b.*SCD-yEGFP	CEN/ARS; *URA3*; amp^R; doxycycline repressible expression of C-terminally yEGFP-tagged *Trypanosoma brucei* SCD	This study
pCM188-*T.c.*SCD	CEN/ARS; *URA3*; amp^R; doxycycline repressible expression of *Trypanosoma cruzi* Ole1p	This study
pCM188-*T.c.*SCD-yEGFP	CEN/ARS; *URA3*; amp^R; doxycycline repressible expression of C-terminally yEGFP-tagged *Trypanosoma cruzi* Ole1p	This study
pGREG523-P$_{SPT23}$-^{myc}*SPT23*	CEN/ARS; *HIS3*; kanMX; amp^R; expression of an N-terminally 13xmyc-tagged Spt23p variant (^{myc}Spt23p) from native *SPT23* promoter	This study; section 2.3.1

Tab. III-S2: Primers used in this study. Underlined sequence parts represent homology regions of overhang primers used recombination-based cloning approaches.

Primer	sequence (5' → 3')	amplicon
P1 (fw)	CACAAATACACACACTAAATTACCGGATCAATTCGGGGGATCCATGCCAACTTC TGGAACTACTATTGAATTG	*OLE1*
P2 (rv)	TTACATGATGCGGCCCTCCTGCAGGGCCCTAGCGGCCGCTTTAAAAGAACTTAC CAGTTTCGTAGATTTCACC	*OLE1*
P3 (fw)	CACAAATACACACACTAAATTACCGGATCAATTCGGGGGATCCATGGAGCAAGT GGATTTAGTGA	*K.l.OLE1*
P4 (rv)	TTACATGATGCGGCCCTCCTGCAGGGCCCTAGCGGCCGCTCTACTTCTTTTCGT AAACTTCACCTC	*K.l.OLE1*
P5 (fw)	CACAAATACACACACTAAATTACCGGATCAATTCGGGGGATCCATGAGCGAAGC AATGGAAAG	*T.b.SCD*
P6 (rv)	TTACATGATGCGGCCCTCCTGCAGGGCCCTAGCGGCCGCTTCACTCATTCAAGT AGCCCAC	*T.b.SCD*
P7 (fw)	CACAAATACACACACTAAATTACCGGATCAATTCGGGGGATCCATGACGAGTTT AAACAAAAGCGAG	*T.c.SCD*
P8 (rv)	TTACATGATGCGGCCCTCCTGCAGGGCCCTAGCGGCCGCTTCACTTACGCTTCA ATTTGGC	*T.c.SCD*
P9 (fw)	TAGTAAGAGAGGTGAAATCTACGAAACTGGTAAGTTCTTTATGTCTAAAGGTGA AGAATTATTCACT	yEGFP (*OLE1*)
P10 (fw)	CTAAGTTCGCCGCAAGAAGAGGTGAAGTTTACGAAAAGAAGATGTCTAAAGGTG AAGAATTATTCACT	yEGFP (*K.l.OLE1*)
P11 (fw)	GAGCCTTCTCCATCACCTACAAGTGGGCTACTTGAATGAGATGTCTAAAGGTGA AGAATTATTCACT	yEGFP (*T.b.SCD*)
P12 (fw)	CCTGATTCCTCACCTGCGTGTCGCCAAATTGAAGCGTAAGATGTCTAAAGGTGA AGAATTATTCACT	yEGFP (*T.c.SCD*)
P13 (rv)	TTACATGATGCGGCCCTCCTGCAGGGCCCTAGCGGCCGCTTTATTTGTACAATT CATCCATACCATGG	yEGFP

Chapter IV

Ergosterol is essential for protein sorting, endocytosis and protein compartmentation within the plasma membrane of yeast cells

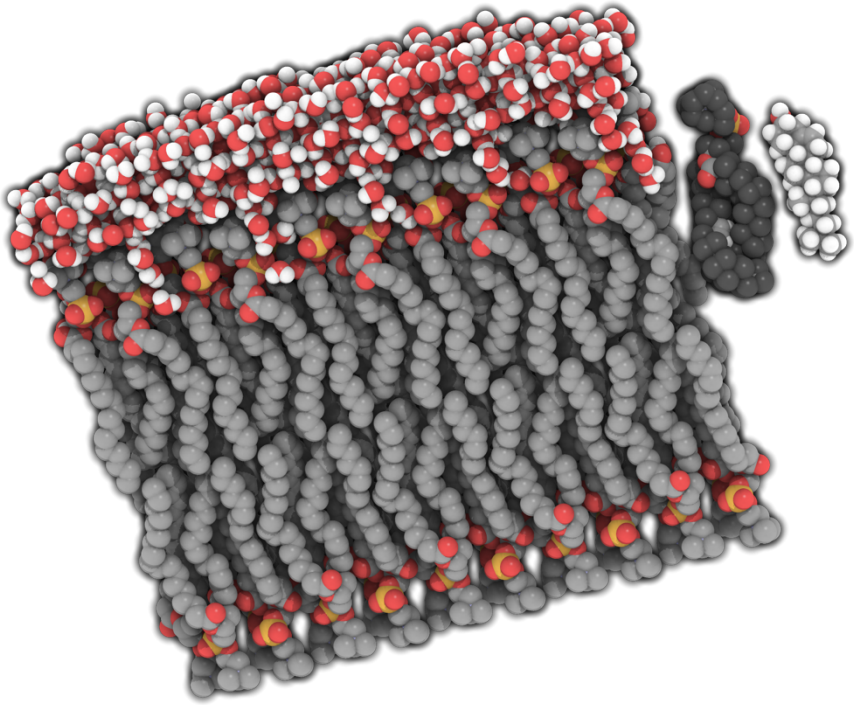

4. Chapter IV: Ergosterol is essential for protein sorting, endocytosis and protein compartmentation within the plasma membrane of yeast cells

4.1. Abstract

Ergosterol and sphingolipids form spatially discrete membrane patches with liquid-ordered phase behavior within the plasma membrane of yeast that feature a special protein equipment. These membrane areas referred to as lipid rafts are suggested to be implicated in lateral compartmentation of the plasma membrane as well as in fundamental biological processes such as endo- and exocytosis. Ergosterol was furthermore shown to be essential for proper protein sorting and intracellular protein delivery. Studies on the physiological roles of ergosterol for yeast and on the physiological effects of ergosterol depletion used viable yeast knock-out strains that are defective in late steps of the ergosterol biosynthetic pathway thereby accumulating different sterol species without necessarily altering the cell's total sterol content. The study presented here addresses *ERG9*, an essential gene involved in the ergosterol biosynthetic pathway and uses a metabolic engineering approach to achieve control over the total sterol biosynthetic activity of the cell. Cells that allow for manipulating the native sterol homeostasis were employed to unveil physiological effects of ergosterol and total sterol depletion on fundamental membrane associated processes such as protein sorting and endo- and exocytosis as well as on the cell's general viability. Furthermore, it is shown that ergosterol and sterols in general are essential for native lateral compartmentation of the plasma membrane of yeast.

4.2. Introduction

Sterols are essential membrane components of organisms from various domains and kingdoms. Although the chemical structures of the respectively prevalent sterol classes differ from each other in detail, all of them share identical physicochemical properties being responsible for a conserved function of sterols for the organization of biological membranes. The major sterol of higher eukaryotes and vertebrates is cholesterol, while ergosterol is dominant in fungi. Plants feature a diverse and complex set of sterols with stigmasterol and sitosterol as major components of plant sterol profiles (reviewed in [1]). Membranes of some extremophilic bacteria feature a sterol-like class of membrane molecules, hopanoids, suggested to be required for stress tolerance under extreme conditions [2]. Other bacterial representatives such as proteobacteria and mycoplasma species even contain eukaryotic sterols instead of hopanoids, although they are not synthesized by these organisms themselves but taken up from the environment [3]. In contrast to that, archaea are not known to synthesize sterols, however, these organisms have evolved other strategies and use different membrane molecules such as glycerol-ether lipids to ensure the stability and robustness of their plasma membrane [4].

Plasma membranes feature the highest fraction of sterols and sphingolipids (besides glycerophospholipids) from all eukaryotic membranes, which is about 30 to 40% for sterols and 10 to 20% for sphingolipids [5]. Because of their chemical structures, sterols and fully saturated sphingolipids interact in a special manner, thereby clustering into spatially discrete membrane patches with liquid-ordered phase behavior instead of homogenously mixing with glycerophospholipids which, in turn, form liquid-crystalline (liquid-disordered) membrane areas [6]. According to the umbrella model [7], sterols are shielded by head-groups of sphingolipids from the aqueous phase on both side of the bilayer, thereby forming tightly packed and stable sterol-lipid complexes [8]. The typical yeast sterol, ergosterol, was shown to form the most stable microdomains of all sterol derivatives tested [9].

The first notion of lipid-determined plasma membrane compartmentation is related of the observation that mammalian plasma membrane proteins show different abilities to accumulate in or associate with detergent-resistant membrane (DRM) areas [10]. Subsequently it was shown that DRMs of the yeast plasma membrane feature a high content of ergosterol and sphingolipids [11, 12]. This observation joined the concepts of liquid-ordered membrane areas and DRM-mediated lateral plasma membrane compartmentation and gave rise to the concept of protein-lipid domains forming lipid rafts in the plasma membrane [13] although these termini should not be seen as being fully equivalent [14]. Besides the partitioning effect of sterols in eukaryotic membranes, it was

shown that lipid rafts are implicated in protein sorting [12], protein secretion, endocytosis [15] and establishing cell polarity [16], although little is known about how ergosterol and sphingolipids are involved in detail [17].

The biosynthesis of sterols takes place in the ER. From there, sterols are subsequently transported to the plasma membrane using the conventional secretory pathway [18] but is not restricted to this as yeast *sec* mutants that are defective in exocytosis also feature a natural ergosterol content in the plasma membrane [19]. Sterols are also internalized by endocytosis and are therefore present in endocytic vesicles but are subsequently recycled back to the plasma membrane [20]. Assembly of lipid rafts and DRMs in yeast as well as corresponding protein-lipid interactions seems to begin already in the ER and progresses along the secretory pathway [11, 21] whereas in mammalian cells lipid raft formation seems to take place in the Golgi [10, 22]. Sterols and fungal ergosterol are chemical derivatives of isoprene which is synthesized from acetyl-CoA [23]. The conversion of acetyl-CoA to ergosterol represents a multistep biosynthetic pathway that shares intermediates with overlapping pathways, finally leading to ubiquinone, heme A, dolichols and others [24]. The first step of the, from then on, linear sterol biosynthetic pathway is carried out by Erg9p, the squalene synthase, that catalyzes the condensation of two farnesyl pyrophosphate molecules to form squalene [25] (Fig. IV-1).

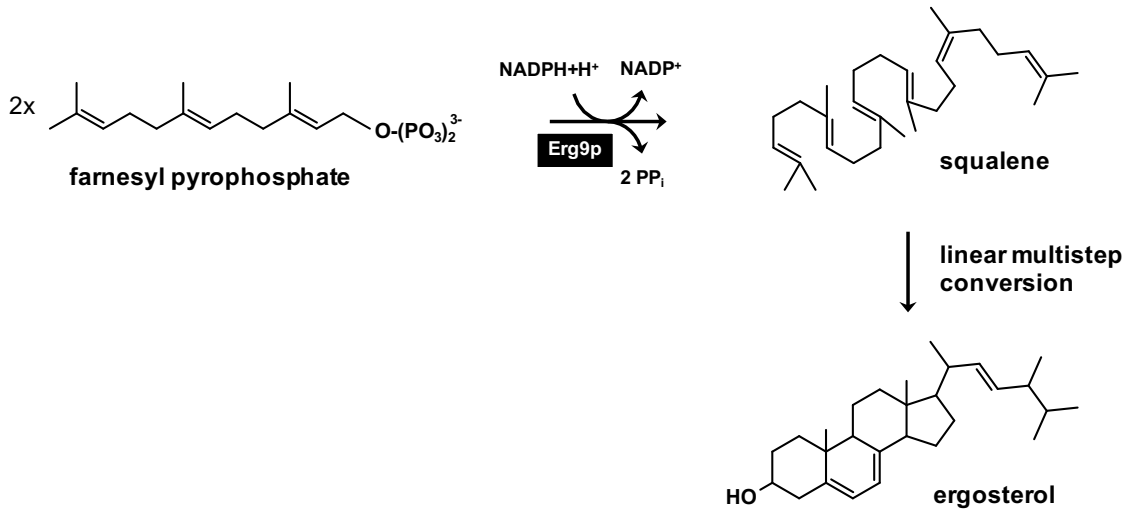

Fig. IV-1: Reaction scheme of Erg9p catalyzed condensation of farnesyl pyrophosphate yielding squalene. Erg9p joins two farnesyl pyrophosphate moieties to form squalene in an NADPH-requiring reaction. The squalene synthase regulates the flux of intermediates through the FPP branch point towards the linear biosynthetic pathway thus regulating the total sterol biosynthetic activity of the cell.

Erg9p is considered a gate keeper enzyme as it determines the flux of intermediates through the FPP branch point towards the ergosterol biosynthetic pathway. Thus, by regulating the expression of *ERG9* it is possible to achieve control over the total sterol

biosynthetic activity of the cell [24]. The study presented here uses this approach to genetically control the total ergosterol/ sterol content of yeast cells thus generating a cellular model to unveil physiological roles of ergosterol for yeast and to explore physiological effects of ergosterol/ sterol depletion. It is shown that depletion of ergosterol and sterols in total affect fundamental membrane associated processes suggested to be closely affiliated with biological functions such as endo- and exocytosis, intracellular protein sorting and trafficking as well as plasma membrane compartmentation.

4.3. Materials and Methods

4.3.1. Yeast strains

Tab. IV-1: Yeast strains used in this study. The table lists all strains with corresponding genotypes. Plasmids harbored by the respective strains are named as indicated in Tab. IV-S1. * The doxycycline repressible promoter construct contains a *CYC1* minimal promoter mediating no/ strongly reduced transcription in the absence of a functional tetracycline transactivator (tTA).

strain	genotype	reference
BY4742	*MAT*α; *his3*Δ1; *leu2*Δ0; *lys2*Δ0; *ura3*Δ0	[26]
BMA64-1A	*MAT*a*; his3-11,15; leu2-3,112; ura3-1; trp1*Δ2; *ade2-1*; *can1-100*	[27]
SIV-1	BY4742; *erg9*::tetO$_2$-P$_{CYC1}$-*ERG9* *	This study
SIV-2	SIV-1; *ole1*::P$_{MET3}$-*OLE1*	This study
SIV-3	SIV-1; pGREG576-*UPC2*	This study
SIV-4	SIV-1; pGREG600-*UPC2*	This study
SIV-5	BY4742; *trp1*::loxP-*URA3*-*loxP* (Δ*trp1*)	This study
SIV-6	SIV-1; *trp1*::loxP-*URA3*-loxP (Δ*trp1*)	This study
SIV-7	SIV-5; pGREG503	This study
SIV-8	SIV-6; pGREG503	This study
SIV-9	SIV-5; pGREG503-*TAT2*	This study
SIV-10	SIV-6; pGREG503-*TAT2*	This study
SIV-11	BY4742; *ole1*::P$_{MET3}$-*OLE1*; pCM188-*OLE1*	This study
SIV-12	SIV-1; pGREG600-*TAT2*	This study
SIV-13	SIV-1; pGREG600-P$_{TAT2}$-*TAT2*	This study
SIV-14	BY4742; pGREG600-*CAN1*	This study
SIV-15	SIV-14; pGREG505-*PIL1*-RedStar	This study
SIV-16	BY4742; *can1*::*CAN1*-yEGFP	This study
SIV-17	SIV-1; *can1*::*CAN1*-yEGFP	This study
SIV-18	SIV-16; *erg6*::loxP-*LEU2*-loxP (Δ*erg6*)	This study
SIV-19	BY4742; *pma1*::*PMA1*-yEGFP	This study
SIV-20	SIV-1; *pma1*::*PMA1*-yEGFP	This study
SIV-21	SIV-19; *erg6*::loxP-*LEU2*-loxP (Δ*erg6*)	This study
SIV-22	BY4742; pGREG600-*TOK1*	This study

4.3.2. Yeast transformation and strain construction

Genetically modified *S. cerevisiae* strains generated in this study are derived from BY4742 (*MAT*α; *his3*Δ1; *leu2*Δ0; *lys2*Δ0; *ura3*Δ0) obtained from EUROSCARF (Frankfurt, Germany). BY4742 cells were routinely cultured in YPD media (2% glucose; 2% peptone; 1% yeast extract). BY4742 derived strains harboring selectable markers (*URA3*; *LEU2;*

HIS3) were grown in appropriate synthetic defined (SD) drop-out media (2% glucose; yeast nitrogen base (YNB); drop-out amino acid supplement). KanMX cassette harboring cells were selected at 200 mg/L G418. Cells were propagated at 30°C. All strains are listed in Tab. IV-1.

Transformation of *S. cerevisiae* with previously generated plasmids was routinely performed by using the Frozen-EZ Yeast Transformation II kit (Zymo Research) according to manufacturer's instructions.

S. cerevisiae transformation for genomic integration of integration cassettes (promoter replacement cassette; knockout cassettes; GFP tag) via homologous recombination and plasmid uptake was routinely performed by the standard lithium acetate method [28]. For genomic integrations of PCR derived DNA fragments, PCR products from a reaction sample (400 µL) were concentrated by ethanol precipitation [29], dissolved in 20 µL sterile H_2O and used for transformation. Replacement of the endogenous *ERG9* promoter was performed by genomic integration of the doxycycline repressible promoter construct (kanMX-tTA-$tetO_2$-P_{CYC1}), which was amplified by PCR from plasmid pCM224 (OneTaq DNA polymerase, NEB) with primers P1 and P2. Replacement of the endogenous *OLE1* promoter was previously described (section 2.3.2). *TRP1* was knocked-out by replacing part of the ORF with the loxP-*URA3*-loxP marker cassette from plasmid pUG72 [30]. *ERG6* was knocked out by replacing the entire ORF with the loxP-*LEU2*-loxP cassette from plasmid pUG73 [30]. Knockout cassettes (KOCs) were routinely amplified by PCR (OneTaq DNA polymerase) using primers P3 & P4 (*TRP1* KOC); P5 & P6 (*ERG6* KOC). For GFP-tagging of Can1p and Pma1p, the yEGFP-T_{ADH1} cassette of plasmid pKT209 [31] was amplified by PCR (OneTaq DNA polymerase) using overhang primers (primers P7 & P8 for *CAN1*; P9 & P10 for *PMA1*) and was genomically integrated at the 3'-terminus of the *CAN1* ORF or *PMA1* ORF, respectively, with simultaneous removal of the endogenous stop codons in order to allow for the expression of the fusion protein. Marker-free genomic integration of the yEGFP-T_{ADH1} cassette was facilitated by the use of an all-in-one plasmid-based CRISPR/Cas9 system using manually designed 20 bp protospacer sequences (TGGCGTGGAAATGTGATCAA for the *CAN1* locus; TGATTAAATGCTACTTCAAC for the *PMA1* locus). Successful genomic integrations were verified by colony PCR using a respective pair of primers suitable to amplify a DNA fragment containing the artificial integration border resulting from the homologous recombination event. Correct integration of the yEGFP encoding sequence into the *CAN1* or *PMA1* locus could also be monitored by fluorescence microscopy.

4.3.3. Plasmid construction

Integration of yeast endogenous genes (*UPC2*; *TAT2*; *CAN1*; *TOK1*) in plasmid pGREG600 [32] was done by recombination-based cloning. For that, plasmid pGREG600 was digested with SalI and the ORFs were amplified by PCR (Q5 DNA polymerase, NEB) using S228C genomic DNA as template. Flanking of PCR products with sequences homologous to the restricted plasmid backbone was achieved by using corresponding overhang primers (primers P11 & P12 for *UPC2;* P13 & P14 for *CAN1*; P15 & P16 for *TAT2*; P17 & P18 for *TOK1*; P19 & P20 for *PIL1*). Plasmid pGREG600 contains a GFP sequence downstream of the cloning site so that resulting plasmids encode for C-terminally GFP fused proteins, respectively. For generating plasmid pGREG505-*PIL1*-RedStar, the RedStar encoding sequence amplified (primer P21 & P22) from plasmid pYM38 [33] was inserted beforehand into XhoI-cleaved plasmid pGREG505 (*LEU2* marker) by recombination-based cloning yielding a plasmid that can be analogously treated like pGREG600 for subsequent *PIL1* ORF integration. Integration of the *UPC2* ORF into plasmid pGREG576 was done in an analogous manner using primers P11 and P23. Plasmid pGREG576 [32] contains a GFP sequence upstream of the cloning site so that the generated plasmid pGREG576-*UPC2* mediates the expression of an N-terminal GFP-Upc2p fusion protein. The *TAT2* ORF (primers P24 & P25) was integrated into plasmid pGREG503 as previously described for drag-and-drop-cloning [32] with plasmids of the pGREG series. Plasmid pGREG600-P_{TAT2}-*TAT2* for expressing a C-terminally GFP tagged Tat2p variant from the native *TAT2* promoter (P_{TAT2}) was generated by replacing the *GAL1* promoter (P_{GAL1}) from plasmid pGREG600-*TAT2*. The yeast endogenous *TAT2* promoter (P_{TAT2}) was amplified from S228C genomic DNA by using appropriate overhang primers P26 and P27. P_{GAL1} from plasmid pGREG600-*TAT2* was cut out using the restriction enzymes AscI and NotI and replaced by PCR amplified P_{TAT2} via *in vivo* recombination cloning.

The construction of plasmid pCM188-*OLE1* was previously described (section 2.3.3).

Co-transformation of BY4742 and generated derivatives with linearized plasmid backbone and PCR product for recombination-based cloning *in vivo* were routinely carried out by using the Frozen-EZ Yeast Transformation II kit (Zymo Research) according to manufacturer's instructions. PCR conditions were chosen according to manufacturer's instructions. Plasmids and primers used in this study are listed in Tab. IV-S1 and Tab. IV-S2.

4.3.4. Ergosterol analysis

Total ergosterol was routinely extracted from yeast cells as described by Rodriguez *et al.* [34]. The amount of ergosterol (as µg·(mg cells, dry weight)$^{-1}$) was determined by GC-MS

analysis using a defined amount of cholesterol (10 µg·mL^{-1}) as internal sample standard. The measured amount of ergosterol was normalized to the detected cholesterol content presuming that the extraction efficiencies for both sterol species is highly similar. 1 µL of the extracts was analyzed on an Agilent 5973 – HP6890 GC-MS using a 30 m DB-5ms capillary column. The GC oven temperature was held at 80°C for 1 min, followed by a ramp of 20°C·min^{-1} to 280°C with a subsequent 20 min hold time at 280°C. A second temperature ramp of 20°C·min^{-1} to 300°C was applied with a following final hold time for 2 min [24]. The MS was operated in selected ion monitoring (SIM) mode using ions of *m/z* 386 and 396 which represent the molecular ions of cholesterol and ergosterol, respectively. Abundance of molecular ions with *m/z* 386 and 396 were used for relative quantification of corresponding sterol species.

4.3.5. Preparation of yeast spheroplasts and growth experiments

Spheroplasts were generally prepared as described by Bertl *et al.* [35, 36]. For that, yeast cells were grown overnight in appropriate synthetic defined media or YPD (where applicable) at 30°C on a rotary shaker at 200 rpm. Cells from overnight cultures were harvested by centrifugation and resuspended in 3 mL incubation buffer (50 mM KH_2PO_4; 40 mM beta-mercaptoethanol; pH7.2 with KOH) and incubated for 15 min at room temperature under continuous shaking (200 rpm). 3 mL of the spheroplasting buffer (50 mM KH_2PO_4; 2.4 M sorbitol; 40 mM beta-mercaptoethanol; 150 mg BSA; 1 mg zymolyase 20-T (nacalai tesque); pH7.2 with KOH) were added to the previously prepared cell suspension, gently vortexed and incubated at room temperature for at least 45 min. Spheroplasts were harvested by gentle centrifugation (500 x g), resuspended in 10 mL stabilizing buffer (230 mM KCl, 10 mM $CaCl_2$; 5 mM $MgCl_2$; 5 mM TRIS/MES at pH7.2) and supplemented with 1% glucose.

In order to examine the growth of $tetO_2$-P_{CYC}-*ERG9* spheroplasts, freshly isolated spheroplasts from cells grown in the presence (40 µg·mL^{-1}) or absence of doxycycline were incubated for 5 days at 30°C in stabilizing buffer supplemented with 1% glucose as well as with doxycycline (40 µg·mL^{-1}) when corresponding to respective pre-culture conditions. Microscopy images of the spheroplast cultures were taken every 24 h using a Canon EOS450D digital camera (Canon Inc., Tokyo, Japan) connected to a Zeiss IM100 inverted microscope (Carl Zeiss Microscopy, Göttingen, Germany). The diameter (d) of 100 representative spheroplasts was determined using the line selection and analyzing tool of the ImageJ software (written by Wayne Rasband, NIH, Bethesda, Maryland) and the spheroplast surface area was calculated by using the formula for spherical geometrical objects ($A = \pi \cdot d^2$).

4.3.6. Microscopy

Cells expressing N-terminal (GFP-Upc2p), C-terminal GFP-fusion proteins (Upc2p-GFP; Tat2p-GFP; Can1p-GFP; Pma1p-GFP; Tok1p-GFP) or Pil1p-RedStar were analyzed using a microscopy setup consisting of a Leica TCS SP5 II spectral confocal laser scanning microscope (Leica Microsystems, CLSM) equipped with a 100-x oil objective (HCX PL APO CS 100x/1.44). GFP was excited at 488 nm and emission was detected between 510 – 585 nm. RedStar was excited at 561 nm and emission was detected between 580 – 700 nm. Prior to microscopy analysis, cells were grown to exponential phase (OD_{600} = 1.0) in appropriate synthetic defined drop out medium. Expression from *GAL1* promoter was guaranteed in glucose-free galactose containing medium (2%). For DNA staining with DAPI, 1 mL of a cell culture grown to exponential phase was mixed with 2.5 µL of a DAPI (Sigma Aldrich) stock solution (1 mg·mL^{-1}) to a final concentration of 2.5 µg·mL^{-1}. Afterwards, cells were incubated for 30 min at 30°C, harvested by centrifugation, washed 2 times with 1XPBS und used for microscopy analysis. DAPI was excited at 405 nm and emission was detected between 435 – 485 nm. To evaluate the pattern of protein distribution within the plasma membrane, cells were scanned along the z-axis (z-stack) by collecting sets of multiple optical sections ~300 nm apart from each other and single images were merged into a 2D stack for maximum intensity projections (MIP) with the Leica “LAS AF Lite” software. Single images of the z-stacks showing the tangential confocal section (TCS) as well as the equatorial confocal section (ECS) of the cell were also used to evaluate the protein distribution within the plasma membrane (Fig. IV-11).

4.3.7. Growth assays on agar medium

Growth assays were performed as previously described (section 3.3.6).

These growth assays were applied to evaluate physiological effects of doxycycline-mediated repression of *ERG9* expression and to verify proper biological function of GFP-tagged Can1p by uptake of the toxic L-arginine analogue L-canavanine. Defined volumes of sterile filtered doxycycline (4 mg·mL^{-1} in H_2O) or L-canavanine (4 mg·mL^{-1} in H_2O) stock solutions were added to already autoclaved agar (~50°C) to adjust final concentrations as respectively indicated.

4.3.8. Electrophysiological measurements of plasma membrane capacitance

Electrophysiological measurements were performed with freshly isolated spheroplasts of BY4742; tetO2-P_{CYC1}-*ERG9* cells previously grown in the presence (40 µg·mL^{-1}) or absence of doxycycline to feature an altered membrane lipid composition. Endo- and exocytosis in these yeast spheroplasts were analyzed by patch-clamp techniques as described elsewhere [37].

4.4. Results and Discussion

4.4.1. Construction and characterization of a strain featuring a controllable ergosterol content

To gain experimental control of the transcription level of *ERG9* which has proven to be an essential ergosterol synthesis gene in yeast [24, 38], a strategy that includes the exchange of the native *ERG9* promoter (P_{ERG9}) was followed. For that, a promoter system mediating tetracycline-controlled transcriptional activation, that was adopted for yeast [39, 40], was tested. The tetracycline responsive promoter system used in this study represents a tet-off system, meaning that the presence of the effector molecule tetracycline or synthetic derivatives such as doxycycline prevent transcription (turn-off). In the absence of the effector, transcription is mediated by the transcription activating effect of the artificial tTA (tetracycline transactivator). tTA is an artificial fusion protein that binds the TRE (tetracycline response element) upstream of the *CYC1* minimal (*) promoter (P_{CYC1}*; includes the TATA region) that has lost its native transcription mediating function and just provides essential sequences required for binding of the RNA polymerase II containing transcription machinery [41] and determines the starting point of transcription. The tTA fusion protein comprises the *E. coli* TetR (Tet repressor) and VP16, a transcription activator in eukaryotes that origins from the herpes simplex virus. The TetR domain of tTA recognizes and binds 19 bp sequences (2 repeats in the $tetO_2$ construct) adopted from the *E. coli* endogenous tetracycline operon (tetO) within the TRE, thereby fixing the VP16 domain in close proximity of P_{CYC1}*. VP16 recruits the yeast endogenous transcription machinery and mediates transcription. Doxycycline in the medium is taken up by cells and gets intracellularly bound by TetR which subsequently undergoes a conformational change, thus preventing proper binding to the TRE. This way, the transcription activating effect of VP16 to *ERG9* is omitted [42] and *ERG9* expression is strongly decreased. Potential remaining *ERG9* expression may arise from residual basal transcription activing properties of P_{CYC1}* or leakiness of repression.

The promoter substitution strategy should result in a strain that features a wide range of its ergosterol as well as of its total sterol content. A complete knockout of *ERG9* which worked for other genes (e.g. *ERG2* [43]; *ERG6* [44] and *ERG24* [45]) whose gene products are involved in later steps of the ergosterol biosynthetic pathway could not be exploited to monitor effects of an altered total sterol content as *ERG9* is an essential gene and conditional mutation leads to strict ergosterol auxotrophy.

Substitution of the endogenous *ERG9* promoter (P_{ERG9}) by the artificial doxycycline repressible promoter system (Fig. IV-2A) resulted in a strain whose total ergosterol content

could be varied in a range from ~80 to ~20 µg·(mg cells, dw)$^{-1}$ depending on the external doxycycline concentration (Fig. IV-2B). Growth of this strain was strongly reduced on agar plates as well as in liquid media supplemented with doxycycline (Fig. IV-2C,D). A slight reduction of growth in liquid media was observed even in the absence of the repressor (Fig. IV-2D). A similar study that put *ERG9* transcription under control of the methionine repressible *MET3* promoter also showed that repression of *ERG9* resulted in drastically lowered specific growth rates and also reduced the final biomass concentration [38].

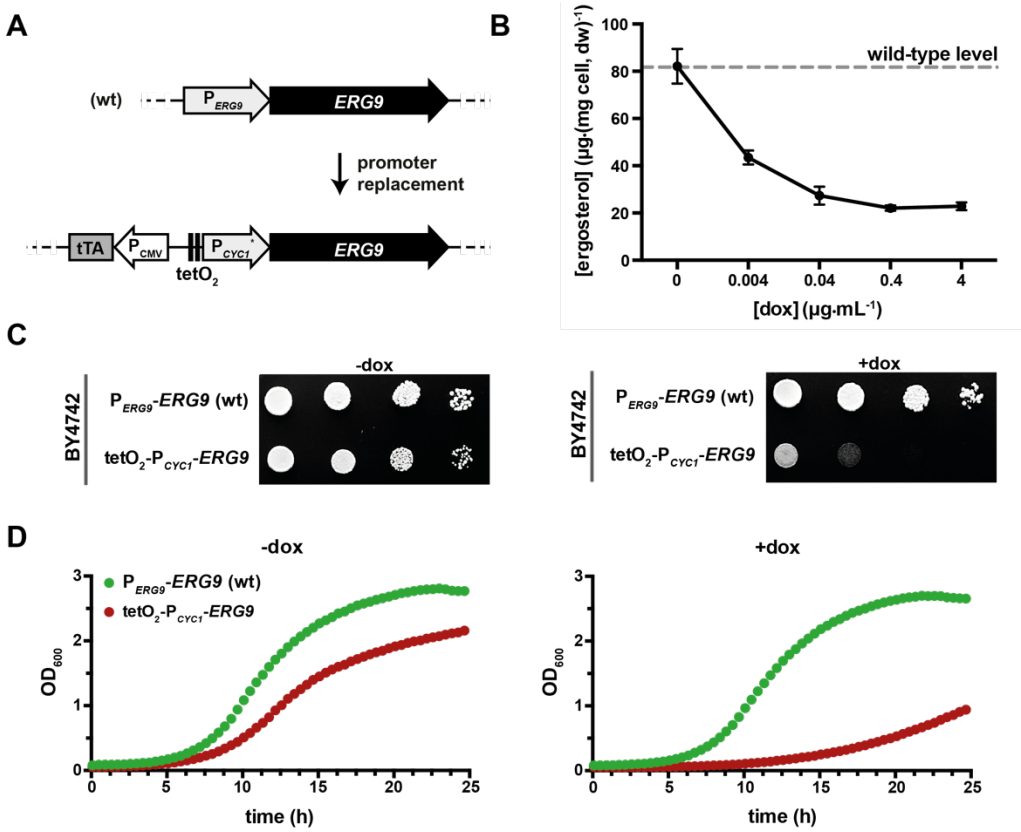

Fig. IV-2: Effect of *ERG9* repression on exponential growth. (A) The native *ERG9* promoter was replaced by a tetracycline/doxycycline repressible promoter system. The promoter replacement cassette encodes for the tetracycline transactivator (tTA), an artificial fusion protein that binds the tet operator sequences (tetO; 2x) and recruits the endogenous transcription machinery to the *CYC1* minimal (*) promoter via its C-terminal viral transcription activation domain (VP16) thereby mediating *ERG9* transcription. Binding of tTA to tetO is prevented in the presence of tetracycline or synthetic analogues such as doxycycline. This way, the transcription activating effect of VP16 is inhibited. **(B)** Ergosterol content of $tetO_2$-P_{CYC1}-*ERG9* cells (W303 background) at given doxycycline concentrations as determined from GC-MS data. The ergosterol level of wild-type cells is indicated as a dashed line for comparison. The bars represent the range of two measured values displayed as arithmetic mean. n = 2 **(C)** The growth phenotype of $tetO_2$-P_{CYC1}-*ERG9* cells is shown via spotting of a 10-fold dilution series in the presence (40 µg·mL^{-1}) or absence of doxycycline in the medium. Growth of $tetO_2$-P_{CYC1}-*ERG9* cells was strongly impaired in the presence of doxycycline whereas growth of the wild-type background (BY4742; P_{ERG9}-*ERG9*) was unimpaired by doxycycline. **(D)** Growth of the $tetO_2$-P_{CYC1}-*ERG9* strain was also strongly reduced in liquid media supplemented with doxycycline (40 µg·mL^{-1}). However, a slight reduction of growth was observed even in the absence of the repressor.

The regulatory effects of the artificial $tetO_2$-P_{CYC1} promoter system on transcription do not depend on any yeast endogenous regulatory proteins and do not involve effector molecules that can be metabolized by yeast. By this way, basic conditions that allow for a fully independent, orthogonal control of transcription of two independent genes by both promoter systems are fulfilled. To test whether both promoter systems can be used to orthogonally control gene expression, a strain combining the P_{MET3}-*OLE1* and $tetO_2$-P_{CYC}-*ERG9* genetic modifications was constructed. Both modifications were already analyzed individually and featured an obvious phenotypic output (Fig. II-3A; Fig. IV-2). Upon methionine or doxycycline supplementation of the medium, the double-modified strain behaved exactly as the respective strain featuring the single promoter substitution (Fig. IV-3). Since both effectors and especially methionine had already strong growth repressing effects under the tested conditions, potential additive effects of simultaneous repression of *OLE1* and *ERG9* could not be revealed. However, both promoter systems have proven to be controlled independently and allow for an orthogonal control of genes important in lipid biosynthesis.

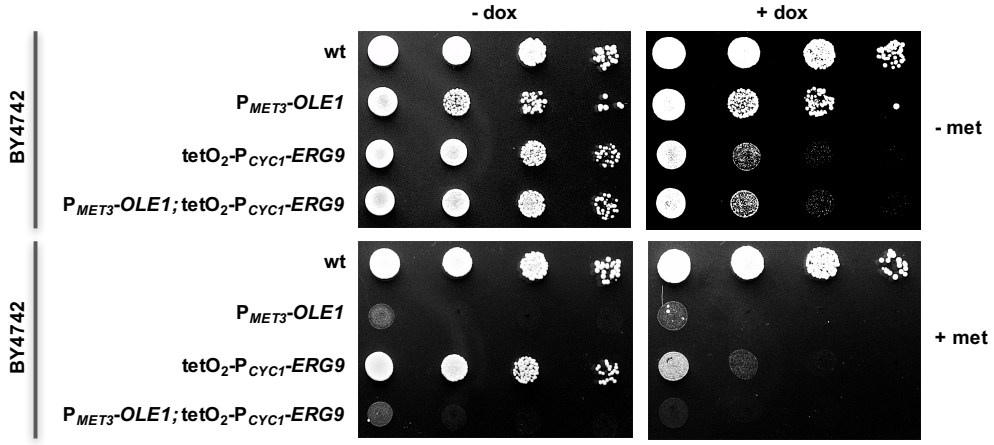

Fig. IV-3: Individual control of *OLE1* and *ERG9* expression in the same cell by employing orthogonal gene expression tools. Growth of a BY4742 background (wt) and strains featuring an individual and a double *OLE1*- and *ERG9*-promoter substitution, respectively, under control conditions (-met, -dox) was compared to growth in media supplemented with methionine (5 mM), doxycycline (40 µg·mL^{-1}) or both. The native *OLE1* promoter was replaced by the methionine-repressible *MET3* promoter (P_{MET3}), whereas the *ERG9* promoter was replaced by the doxycycline repressible $tetO_2$-P_{CYC1}* promoter construct.

The strong growth defect upon sterol depletion shown here, emphasizes that yeast cells must have evolved regulatory systems to maintain sterol/ergosterol homeostasis. This regulatory system controls the ergosterol biosynthesis on the level of transcription as a response to reduced ergosterol synthesis caused by environmental stimuli such as hypoxia [46] or antimycotic agents impairing the synthesis of ergosterol. This regulatory system involves ergosterol sensing proteins, Upc2p and its paralogue Emc22p, that recognize ergosterol as the final product of the ergosterol biosynthetic pathway and subsequently extract single ergosterol molecules from the lipid bilayers, mainly the plasma membrane.

Upc2p and Emc22p are zinc finger motif containing transcription factors that have been suggested to bind and activate genes involved in ergosterol biosynthesis and sterol uptake upon intracellular sterol depletion. Ergosterol associated Upc2p features a characteristic conformation that hides and masks the intrinsic N-terminal NLS of the protein's DNA binding domain. Dissociation of ergosterol from the lipid binding domain (LBD) of Upc2p results in a conformational change thereby unmasking the NLS, eventually leading to nuclear localization of Upc2p. In the nucleus, Upc2p shows its transcription activating properties and upregulates the ergosterol biosynthetic pathway and sterol uptake. The exact mechanism of Upc2p-mediated transcription activation as well as potential coactivators are still under investigation. The reversible shuttling of Upc2p between cytosol and nucleus is used in this study to monitor ergosterol depletion upon *ERG9* repression on a cell biological level. For that GFP-tagged versions of Upc2p were expressed form a plasmid. This way, it should be possible to easily monitor subcellular localization of Upc2p by confocal fluorescence microscopy. N-terminal tagging of Upc2p was considered to have a lesser influence on the subcellular protein localization patterns since C-terminal tagging could mask the NLS, thereby impairing nuclear targeting. However, N-terminal GFP-Upc2p fusion proteins located exclusively in the nucleus of $tetO_2$-P_{CYC1} cells even in the absence of the repressor (Fig. IV-4A), thus not allowing to monitor changes in of Upc2p localization upon ergosterol depletion.

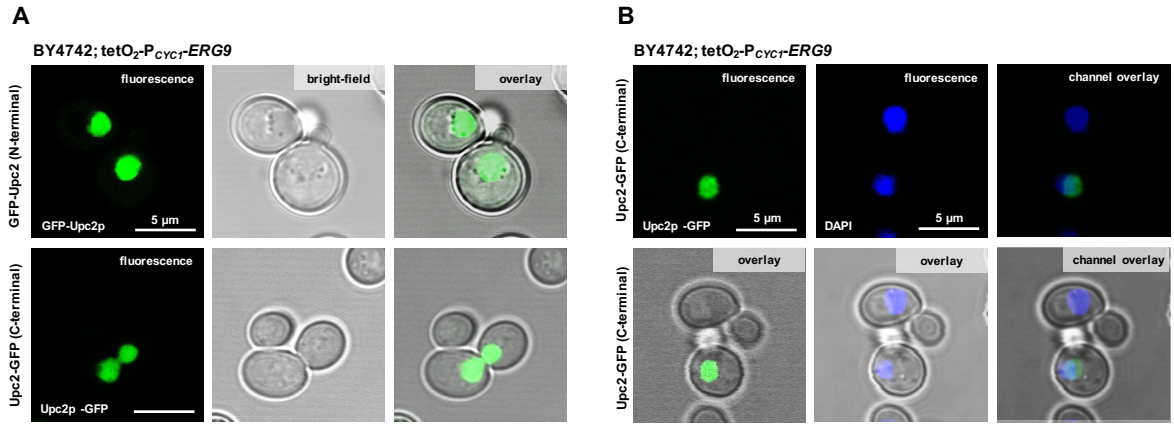

Fig. IV-4: Subcellular localization of GFP-UPC2p and Upc2p-GFP in a $tetO_2$-P_{CYC1}-*ERG9* background. (A) Images show representative yeast cells expressing GFP-tagged variants of Upc2p (top: N-terminal GFP-fusion; bottom: C-terminal GFP-fusion). **(B)** Nuclear localization of Upc2p-GFP was confirmed by co-localization studies with DAPI stained nuclear chromatin. The channel overlay image of fluorescence channels shows subcellular co-localization of both fluorophores.

Although N-terminally GFP-tagged Upc2p was used for similar studies [47], it was tested whether C-terminal tagging could prevent potential LBD impairment resulting from GFP-tagging and could restore expected cytosolic protein residency. Deletion of the LBD was previously shown to lead to strong nuclear localization, independent from the ergosterol

status of the cell [47]. Surprisingly, C-terminal Upc2p-GFP fusion proteins located exclusively in the nucleus as well (Fig. IV-4A), as confirmed by co-localization studies with DAPI stained nuclear chromatin (Fig. IV-4B), even though it was shown elsewhere that C-terminal tagging of Upc2p does not impair its proper biological function [48]. Identical nuclear protein localization was also overserved in the genetic background of BY4742 (data not shown) thus ruling out that manipulation of *ERG9* expression is somehow involved in the unusual subcellular protein distribution. Single point mutations that have shown to cause strong nuclear targeting of Upc2p [47] were also ruled out, since plasmid incorporated ORF did not feature any mutations as confirmed by sequencing. Thus, an Upc2p localization assay could not be used to monitor ergosterol depletion on a cell biological level.

4.4.2. Tryptophan permease Tat2p is mistargeted in ergosterol depleted yeast cells

Modifications of the physicochemical properties and lipid composition of biological membranes can severely influence the integrity of membrane associated processes such as proper protein sorting and protein delivery via the secretory pathway. A number of studies identified lipid rafts and incorporated ergosterol as being involved in and important for membrane trafficking and correct intracellular delivery of raft-associated plasma membrane proteins thereby also ensuring their proper biological function [11, 21, 49-51]. A well-studied example for controlling the overall protein activity by regulated sorting of membrane traffic rather than by *de novo* protein synthesis is the delivery of the tryptophan permease Tat2p to the plasma membrane in response to environmental factors. In wild-type cells grown at low tryptophan, Tat2p is targeted to the plasma membrane via the secretory pathway [52] or via an exocytic pathway including the *trans*-Golgi and early endosomes [53] whereas at high tryptophan, Tat2p goes directly to the vacuole via an unconventional route leading from the *trans*-Golgi to early endosomes to late endosomes and is not recycled from the plasma membrane via endocytosis [51]. In a *ERG6* knockout mutant (Δ*erg6*) that is defective in producing ergosterol but instead accumulates other sterols up to the stage of zymosterol [54], Tat2p is not properly delivered to the plasma membrane anymore. In this case, Tat2p is targeted to the vacuole instead or even accumulates in late endosomes [51]. The missorting in Δ*erg6* cells is moreover accompanied by an inability to take up tryptophan efficiently. Knockout of *ERG2* whose gene product accepts the sterol intermediate synthesized by Erg6p as substrate, also results in missorting of Tat2p and subsequent vacuolar degradation [43]. Depletion of total sterols by using a mevalonate auxotrophic Δ*erg13* strain disrupted detergent-insoluble membrane domains (lipid rafts) and prevented proper Tat2p targeting to the plasma membrane. These finding are in line with missorting of Tat2p in cells treated with the Erg9p-

inhibitor zaragozic acid (ZA) [55], in which the metabolite flux towards the ergosterol biosynthetic pathway and the total sterol synthesis gets limited. All these observations support a model in which Tat2p is missorted to the vacuole in the absence of (Δ*erg13*) or mal-organized (unusual sterol composition in Δ*erg6* and Δ*erg2*) lipid rafts. Interestingly, Tat2p was found to be not sorted to the vacuole anymore in strains defective in Rsp5p complex-mediated ubiquitination (Δ*bul1*) even upon altered sterol composition [51]. Therefore, it seems likely that Rsp5p-mediated ubiquitination (which is also involved in Spt23p proteolytic processing (section 1.5)) directs Tat2p towards the vacuole instead of to the plasma membrane. Although Rsp5p seems to be resident in lipid rafts as well as in non-lipid raft membrane compartments, there is evidence that protein ubiquitination by Rsp5p occurs predominantly in phospholipid-enriched non-raft membrane areas. Taking together, a model is supported in which Tat2p resident in the bulk lipid fraction is ubiquitinated and directed the late endosomes and to the vacuole, whereas Tat2p escapes from ubiquitination when located in a lipid-raft environment. Since lipid raft forming ergosterol and sphingolipids are progressively enriched along the secretory pathway and reach their highest level within the plasma membrane so that raft-associated Tat2p is practically dragged along to the cell surface. This model therefore assumes that intracellular Tat2p sorting is regulated in the *trans*-Golgi (where ubiquitination takes place) and thus late within the secretory pathway [56]. Factors that may be responsible for the lipid-raft association of Tat2p might be related to the chemical structure of sterols incorporated in lipid rafts. Sterols that accumulate in Δ*erg6*- (zymosterol) and Δ*erg2*-cells (fecosterol) differ from ergosterol regarding the main alkyl chain as well as regarding the main sterol scaffold.

The $tetO_2$-P_{CYC1}-*ERG9* strain which features controllable expression of *ERG9* and thus a reduced total sterol biosynthesis is distinctively different from Δ*erg6* and Δ*erg2* strains used for Tat2p localization studies as these are defective in late steps of the ergosterol biosynthetic pathway. Reduction of overall cellular *ERG9* activity rather resembles the ZA-mediated Erg9p inhibition or the controlled feeding of mevalonate to an Δ*erg13* strain for which Tat2p missorting was also observed. To test the effects of genetically reduced *ERG9* expression on the subcellular localization of Tat2p and the Tat2p-mediated tryptophan uptake related thereto, a strict tryptophan auxotrophic strain was constructed in the genetic background of $tetO_2$-P_{CYC1}-*ERG9*.

For that, *TRP1* was knocked-out and the requirement of tryptophan uptake from the medium for growth of this strain was confirmed. Growth of the resulting $tetO_2$-P_{CYC1}-*ERG9; Δtrp1* strictly relied on the availability and uptake of external tryptophan at high concentrations (200 $\mu g \cdot mL^{-1}$) (Fig. IV-5).

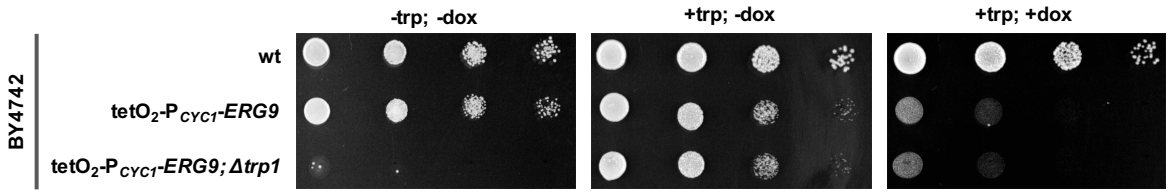

Fig. IV-5: Knocking-out *TRP1* yields a strict tryptophan auxotrophic strain whose growth depends on externally available tryptophan. Growth of a wild-type background (BY4742), the $tetO_2$-P_{CYC1}-*ERG9* mutant and a strain featuring an additional *TRP1* knockout ($tetO_2$-P_{CYC1}-*ERG9*; Δ*trp1*) was compared in the presence or absence of doxycycline (dox; 40 µg·mL^{-1}) and tryptophan (trp; 200 µg·mL^{-1}). Only growth of the Δ*trp1* strain was inhibited in the absence of tryptophan, whereas both other strain grew unimpaired (left). Growth of the Δ*trp1* strain was restored by tryptophan supplementation of the medium (middle). Upon repression of *ERG9*, both strain with $tetO_2$-P_{CYC1}-*ERG9* genetic background grew poorly even in the presence of tryptophan (right).

In contrast, growth of the Δ*trp1* cells could not be restored at low external tryptophan concentrations (Fig. IV-6B) being two orders of magnitude lower (2 µg·mL^{-1}) than the concentrations used for strain characterization (Fig. IV-5). However, intermediate tryptophan concentrations (20 µg·mL^{-1}) were sufficient to allow for growth of an comparable strain ($tetO_2$-P_{CYC1}-*ERG9*; Δ*trp1* (e.v.)) under equivalent growth conditions (0 µg·mL^{-1} dox) (Fig. IV-6A; bottom).

Increasing doxycycline concentrations (0.4 and 4 µg·mL^{-1}) which reduced *ERG9* expression, successively impaired growth on intermediate tryptophan medium (Fig. IV-6A; left column), though growth on high tryptophan was completely unaffected by repressed *ERG9* expression (Fig. IV-6A; right column). Growth inhibition was comparable to that observed in previous growth assays, which used 40 µg·mL^{-1} doxycycline (Fig. IV-S1). These findings suggest a Tat2p loss-of-function effect that might be caused by altered ergosterol/sterol biosynthesis upon *ERG9* repression, as was previously observed for similar cellular systems using zaragozic acid treated cells or an Δ*erg13* background. Intermediate tryptophan concentrations (20 µg·mL^{-1}) revealed this loss-of-function effect, whereas high tryptophan masked detrimental effects of potential Tat2p mislocalization. This is likely due to compensation of Tat2p malfunction by unspecific amino acid permeases (e.g. Gap1p [57]) or by other uptake systems that are able to deliver tryptophan intracellularly only when large chemical gradients are present. In contrast, growth at intermediate tryptophan seems to be dependent on sufficient overall cellular activity of Tat2p. To trace the doxycycline-mediated growth effect specifically back to reduced cellular Tat2p activity, it was tested whether additional plasmid-based *TAT2* expression could restore growth at intermediate tryptophan and simultaneous *ERG9* repression.

Indeed, growth of cells under these conditions was restored when cells were enabled for additional strong *TAT2* expression from the *GAL1* promoter, while cells that contained an empty vector (e.v.) grew still impaired (Fig. IV-6C). This experiment indicates clearly Tat2p

loss-of-function upon *ERG9* repression. These findings further suggest that growth defects upon *ERG9* repression, as shown in Fig. IV-2C and Fig. IV-3 are also caused (at least to a great extent) by the Tat2p loss-of-function, since standard tryptophan concentrations in synthetic medium are in the same concentration range as those used for growth assays with intermediate tryptophan (20 vs. 50 µg·mL^{-1}).

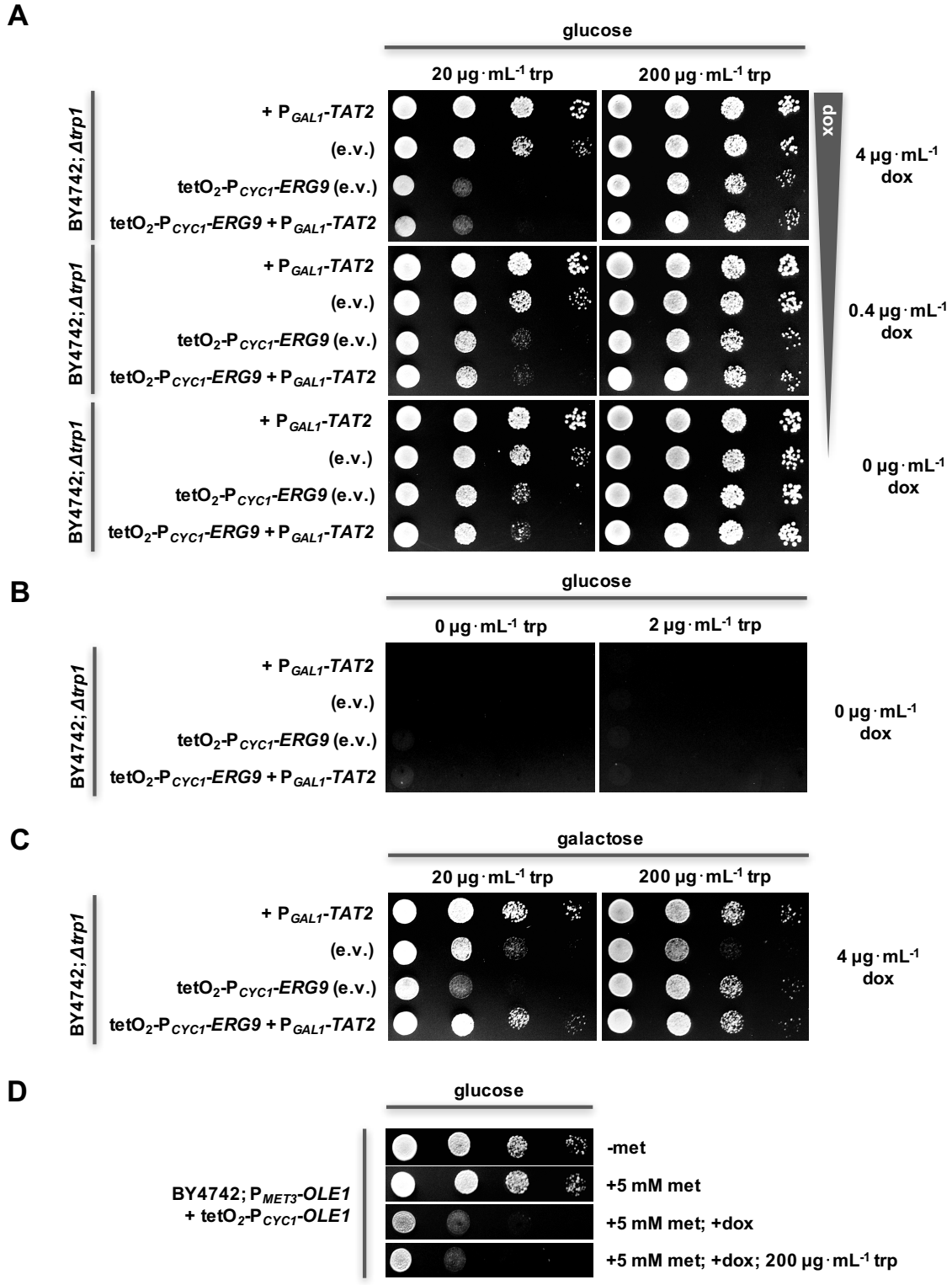

Fig. IV-6: Repression of *ERG9* expression converts Δ*trp1* cells to tryptophan auxotrophs in the presence of intermediate external tryptophan concentrations. (A) Growth of plasmid harboring (empty pGREG503 (e.v.) or pGREG503-*TAT2*) Δ*trp1* cells in wild-type (BY4742) and $tetO_2$-P_{CYC1}-*ERG9* genetic background was compared at intermediate (20 µg·mL^{-1}) and high (200 µg·mL^{-1}) tryptophan concentrations as well as in the additional presence (0.4 or 4 µg·mL^{-1}) or absence of doxycycline (dox). Since *TAT2* in pGREG503-*TAT2* is expressed under control of the *GAL1* promoter (P_{GAL1}-*TAT2*), growth on glucose medium is not affected by the respectively harbored plasmid, since plasmid-based expression is only activated on galactose medium as shown in (C). Growth of $tetO_2$-P_{CYC1}-*ERG9*; Δ*trp1* strains was severely impaired at intermediate tryptophan concentrations when *ERG9* expression was repressed (+dox) whereas cells grew unimpaired on high tryptophan medium even with repressed *ERG9* expression. **(B)** Growth of strains introduced in (A) was compared on low tryptophan (2 µg·mL^{-1}) as well as on tryptophan-free medium. Low tryptophan medium did not allow for growth of Δ*trp1* strains. **(C)** Influence of additional plasmid-based expression of *TAT2* on impaired growth of $tetO_2$-P_{CYC1}-*ERG9*; Δ*trp1* cells on intermediate tryptophan medium and upon simultaneous *ERG9* expression was tested. Plasmid-based *TAT2* expression was able to restore growth of $tetO_2$-P_{CYC1}-*ERG9*; Δ*trp1* under the conditions indicated. **(D)** Controls to rule out, that high tryptophan conditions directly influence doxycycline-regulated gene expression using the artificial $tetO_2$-P_{CYC1} promoter construct. High external tryptophan levels did not reduce growth inhibiting effects of doxycycline repressed *OLE1* expression (from a plasmid) in a strain background with repressed *OLE1* expression from the genomic gene copy (P_{MET3}-*OLE1* at 5 mM met; see Fig. II-3A).

The range of doxycycline concentrations used for the experiment shown in Fig. IV-6 did not correspond to the range for which a notable change of the ergosterol content could be measured (Fig. IV-2B). These observations indicate that cells grown in liquid media are more sensitive to external doxycycline probably due to a more efficient uptake of the repressor from the surrounding milieu.

Potential concerns that high tryptophan conditions could directly weaken the repressing effect of doxycycline were ruled out by using an equivalent cellular system whose growth performance does not rely on the intracellular delivery of tryptophan. For that, plasmid-based *OLE1* expression was placed under control of the $tetO_2$-P_{CYC1} promoter construct. Cells were only able to grow when plasmid-based expression was active in the P_{MET3}-*OLE1* background with *OLE1* expression repressed in the presence of 5 mM methionine. The presence of high tryptophan (200 µg·mL^{-1}) did not influence the doxycycline-mediated repression of *OLE1* expression and growth was prevented (repression of genomic *OLE1* at 5 mM met) to the same extent as in the absence of tryptophan (Fig. IV-6D).

To investigate the subcellular localization of Tat2p upon normal and decreased *ERG9* expression, plasmids were constructed that mediate expression of a C-terminally GFP-tagged Tat2p variant whose localization can be monitored by confocal fluorescence microscopy.

The expression was placed under control of the native *TAT2* promoter (P_{TAT2}) to circumvent artifacts that may result from unnaturally high expression levels. Higher expression levels mediated by the strong *GAL1* promoter lead to a less contrasted protein distribution pattern than observed at lower expression from P_{TAT2} as Tat2p was still located to a large extend in

the plasma membrane even under high tryptophan conditions (Fig. IV-S2). When grown under low tryptophan conditions, Tat2p was located to a large extent in the plasma membrane in BY4742; $tetO_2$-P_{CYC1}-*ERG9* in the absence of doxycycline (resembles wild-type conditions regarding *ERG9* expression levels) as it is also usual for wild-type cells (data not shown) [51]. In contrast, high external tryptophan concentrations targeted Tat2p mostly to the vacuole and hardly any Tat2p remained in the plasma membrane (Fig. IV-7; left). Under conditions that resemble those that caused a severe growth defect in Δ*trp1* cells (-trp; 40 µg·mL^{-1} dox), Tat2p was not detected in the plasma membrane but accumulated in internal vacuolar structures when *ERG9* was repressed.

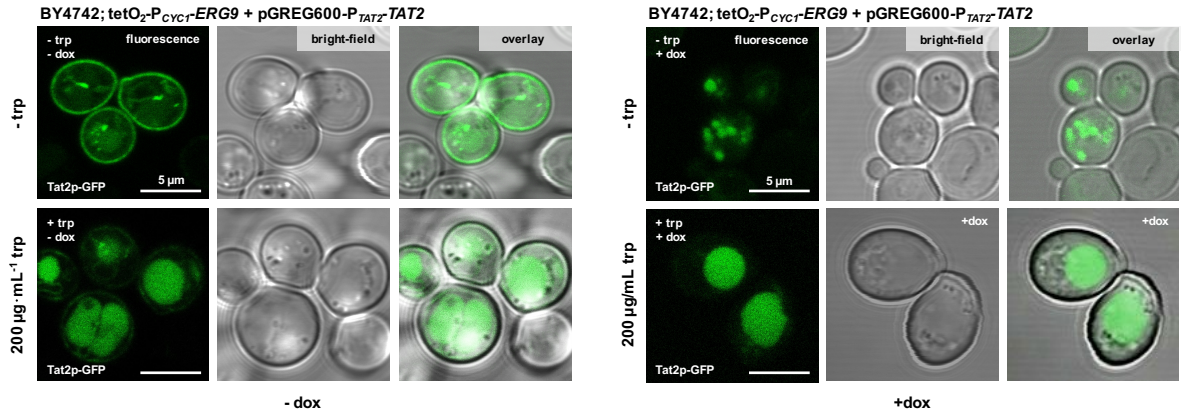

Fig. IV-7: Subcellular localization of the tryptophan permease Tat2p in dependence of tryptophan concentration and *ERG9* expression. Tat2p localization was examined in the presence (200 µg·mL^{-1}) and absence of external tryptophan as well as in the presence (40 µg·mL^{-1}) and absence of doxycycline that represses the expression of *ERG9* in the $tetO_2$-P_{CYC1}-*ERG9* background. Tat2p located to a large extend in the plasma membrane under wild-type conditions (-dox) in tryptophan-free medium whereas Tat2p-GFP did not stain the plasma membrane in the presence of doxycycline. High tryptophan medium caused predominant delivery of Tat2p to the vacuole. Representative images are shown.

These results support the observed growth defect in intermediate tryptophan conditions in combination with *ERG9* repression (Fig. IV-6) and identify protein mislocalization as the cause for a loss of Tat2p-mediated tryptophan uptake activity as it was previously reported for other mutant strains also defective in the ergosterol biosynthesis [51].

4.4.3. Sterols are required for proper endocytic activity in yeast

Because ergosterol was identified to be required for proper endocytic function in yeast [15, 54], it was reasoned elsewhere [55] that an involvement of endocytosis in the extensive delivery of Tat2p to the vacuole observed upon ergosterol depletion is unlikely and protein missorting in the secretory pathway is rather responsible for vacuolar Tat2p localization. Studies evaluating the effect of ergosterol on endocytosis used double deletion strains featuring various combinations of knockouts of non-essential genes *ERG2*, *ERG3*, *ERG4*,

ERG5 and *ERG6* [15, 54]. Although these *erg* mutants are just defective in late parts of the ergosterol biosynthesis, severe impairment of endocytosis was observed partially leading to internalization defects, where especially the initial internalization step was affected and further downstream trafficking remained nearly uninfluenced [58]. These findings suggest that ergosterol is required for the internalization step in yeast. Identification of genes that were previously identified as *END* genes (ENDocytosis defective) being the same as *ERG* genes (ERGosterol biosynthesis), e.g. *END11* corresponds to *ERG2*, further emphasized a crucial role of ergosterol for endocytosis. Endocytosis defects arising in viable *erg* mutants indicate that impairment of internalization may correlate with changes in the sterol structure rather than with the total sterol content of the membranes. However, studies in animal cells using drugs that block cholesterol biosynthesis or chelating agents that sequester and thus reduce the total cholesterol amount, also detected defects in endocytosis and geometry of clathrin coated vesicles [59, 60] as well as a loss of invaginated caveolae [61, 62] for which a role in endocytosis is also discussed. These findings, in turn, also suggest a model in which the total sterol content plays a critical role for the full integrity of the endocytic process.

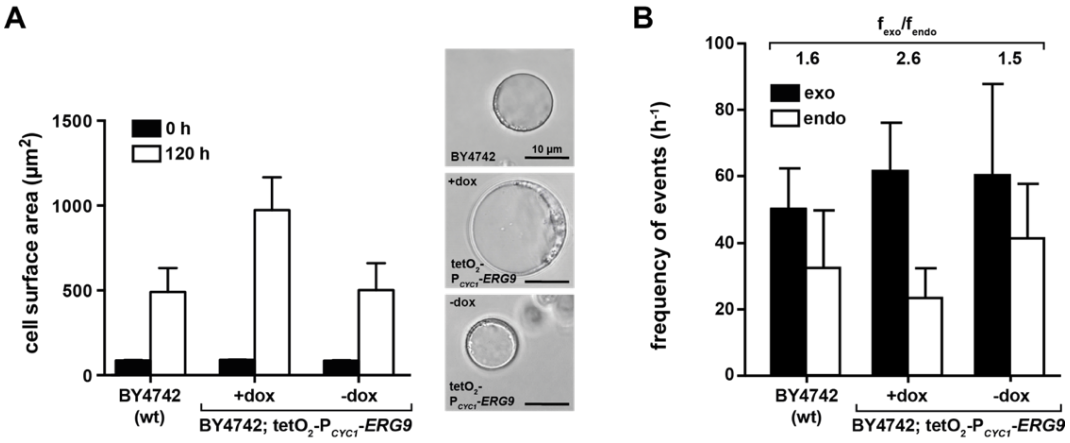

Fig. IV-8: Endocytosis in yeast is severely impaired upon *ERG9* repression. (A) Spheroplasts of BY4742 and of its derivative strain with controllable *ERG9* expression ($tetO_2$-P_{CYC1}-*ERG9*) were grown for 120 h in saline buffer supplemented with glucose (1%). Cells of $tetO_2$-P_{CYC1}-*ERG9* used for zymolyase treatment where grown in the presence (40 µg·mL^{-1}) or absence of doxycycline and spheroplasts were subsequently incubated under identical conditions. Diameters of ~100 spheroplasts for each strain and each condition were measured and the mean cells surface area was calculated. Black bars represent the mean cell surface area at t = 0 whereas white bars show the mean cell surface area after t = 120 h. Spheroplasts with repressed *ERG9* expression (+dox) increased much stronger in cell surface area (~900 µm^2) than spheroplasts with normal *ERG9* expression levels (BY4742; $tetO_2$-P_{CYC1}-*ERG9*, -dox) (~400 µm^2) as also indicated by representative microscopy images. **(B)** An altered ergosterol content affects endocytosis in yeast. Repression of *ERG9* expression shifted the ratio of exo- to endocytic events from ~1.5 (observed for BY4742 and $tetO_2$-P_{CYC1}-*ERG9*, -dox) to ~2.6. Black bars represent the frequency of exocytic events whereas white bars indicate the frequency of endocytic events.

The $tetO_2$-P_{CYC1}-*ERG9* system allows to reduce the total sterol/ergosterol content *in vivo* by genetic control and thereby to examine the *in vivo* requirement of a natural total sterol content for endo- and exocytosis without the use of externally supplemented drugs. In an

equivalent approach as previously described for *OLE1* repression [63], the effect of *ERG9* repression on endo- and exocytic activity was examined by electrophysiological capacity measurements and determination of changes in cell size using spheroplasts which have lost the ability for cell division due to the lack of their cell wall [64].

Depletion of the total sterol/ergosterol content, resulting from inhibition of *ERG9* expression, stimulated cell expansion (measured as increase of cell diameter and calculated cell surface area) of spheroplasts after 120 h incubation in glucose-containing medium much stronger than observed for $tetO_2$-P_{CYC1}-*ERG9* with unrepressed *ERG9* (-dox) or the wild-type background (BY4742) (Fig. IV-8A). A continuous increase of spheroplast size in the presence of glucose was previously described. In this study, enlargement of the cell surface area was traced back on energy dependent endo- and exocytic activity taking place even in spheroplasts when glucose is available (not in the absence of glucose) with a nearly balanced however slightly higher frequency of exocytic over endocytic events. This imbalance with an excess of exocytic activity results in a net delivery of new membrane material realized by fusion of secretory vesicles with the plasma membrane, finally leading to a slight cell expansion [37]. A slight excess of exocytic events was also detected for the BY4742 wild-type background used for this study as well as for the $tetO_2$-P_{CYC1}-*ERG9* strain, when cultured in the absence of doxycycline (-dox; unrepressed *ERG9* expression). A similar ratio of exo- to endocytic frequencies (f_{exo}/f_{endo} of 1.6 and 1.5) was observed for both strains and conditions (Fig. IV-8B), accounting for the similar increase of respective spheroplasts sizes. However, this balance was strongly disturbed by repressing the expression of *ERG9* ($tetO_2$-P_{CYC1}-*ERG9*; +dox) leading to an exo- to endocytosis ratio of 2.6 (Fig. IV-8B) which is exclusively caused by a significant reduction of endocytic activity (42 vs. 24 events/ h and membrane patch). This strong inhibition of endocytosis caused, in turn, the much stronger growth of spheroplasts upon *ERG9* repression with an increase of membrane surface area of ~900 μm^2 compared to ~400 μm^2 observed for spheroplasts with natural *ERG9* expression (Fig. IV-8A).

The significant decrease of endocytic activity upon sterol/ergosterol depletion in yeast observed here, is in line with effects upon sterol/cholesterol depletion described for animal cells and further highlights the requirement of sterols for proper endocytosis. Even though a crucial role for sterols in endocytosis is apparent, little is known on how sterols participate in endocytosis in general or in its initial internalization step in particular. However, several different scenarios can be discussed. Ergosterol or ergosterol-enriched membrane microdomains (lipid rafts) could serve as anchor-points and interaction sites for the endocytosis machinery with the plasma membrane (e.g. eisosomes). In this model, lipid rafts recruit specific membrane-resident or membrane-associated proteins (probably due to

beneficial thermodynamic protein-lipid interactions or direct interaction of ergosterol and proteins via a sterol-binding domain [65, 66]) that are involved in endocytosis themselves, recruit further proteins that promote endocytosis or even serve as receptors of receptor-mediated endocytosis. However, *erg* mutants (Δ*erg2*; Δ*erg6*) also showed severe impairment of fluid phase endocytosis (pinocytosis) [54], suggesting a more fundamental role for sterols in endocytosis. This role might comprise basic physicochemical membrane parameters such as membrane fluidity or membrane curvature that have to fulfill certain criteria and have to lie within a certain physiological range to support proper function. It is well known that strains defective in sterol/ergosterol biosynthesis feature unnaturally low membrane fluidity (high rigidity) [67] and an increase in membrane rigidity was reported to be correlated with the severity of internalization defects [54]. These findings are perfectly in line with a study showing that an unnaturally saturated lipidome, resulting from *OLE1* repression, strongly decreased membrane fluidity and thereby severely impaired endocytosis and shifted the ratio of exo- to endocytosis from 1.6 to 3.6 [63]. Furthermore, it was shown that depletion of cholesterol in membranes of animal cells causes flattening of clathrin-coated pits [59, 60] whose formation is an essential step of the initial internalization during endocytosis and present in both, receptor-mediated and fluid-phase endocytosis. Assuming that ergosterol features a similar function in yeast membranes as cholesterol in animal bilayers, it could be suggested that the amount of sterols within biological membranes or membrane fluidity in general affect the morphology and curvature of the plasma membrane. Unnatural membrane lipid composition and non-physiologically high membrane rigidity could then directly counteract and impede the specific curvature of membranes inherent for coated-pits and vesicles whose three-dimensional geometry is generally determined by the architecture of the clathrin coat [68]. That is why only relatively small deviations from the ideal membrane curvature can be tolerated. However, the role of ergosterol for endocytosis might be also a combination of discussed functions.

4.4.4. Membrane compartmentation is disturbed upon ergosterol depletion as detected by membrane localization of marker proteins Can1p and Pma1p

The plasma membrane of *S. cerevisiae* is laterally compartmented, consisting of distinct domains hosting different proteins and membrane lipids. GFP-staining of marker proteins occupying these plasma membrane compartments revealed at least three different modes of distinctive protein distribution patterns. A patchy compartment containing the arginine permease Can1p (membrane compartment of Can1p; MCC) concentrates proteins in discrete patches estimated to be ~300 nm in diameter, whereas a mesh-shaped compartment accommodates one of the most abundant proteins within the plasma

membrane, the H^+-ATPase Pma1p and is therefore called MCP (membrane compartment of Pma1p). Colocalization studies using marker proteins Can1p and Pma1p could show that both compartments, MCC and MCP, are non-overlapping, exclude each other and cover together the whole plasma membrane surface [50]. A third protein distribution mode is characterized by an even and homogenous dispersion of proteins through the cell surface which is e.g. occupied by the glucose transporter Hxt1p and the general amino acid permease Gap1p. The phenomenon of lateral protein compartmentation within the plasma membrane was identified as being associated with the inhomogeneous distribution of membrane lipids and the formation of membrane microdomains enriched in ergosterol and sphingolipids (lipid rafts) as the ergosterol binding agent filipin stained preferentially MCC domains [69]. Lipid rafts feature a dense lipid packing as well as a high order parameter which makes them resistant to detergents, but still allow for free diffusion of membrane proteins and support their proper function. The resistance towards membrane disrupting detergents was exploited to isolate intact lipid rafts thereby also pulling out membrane proteins that are stably associated with or even embedded within them. This way it could be shown that Can1p [50] is associated with lipid rafts and that the lateral membrane protein compartmentation is connected to an uneven lipid distribution. Additionally, it was found that the knockout of genes whose gene products are involved in lipid biogenesis, e.g. *ERG2*, *ERG5*, *ERG6* and *ERG24*, strongly affected the wild-type pattern of protein segregation [69]. However, it is still unclear, whether the separation of membrane lipids creates distinct lipid environments that are preferentially occupied by certain proteins or alternatively, if protein-protein interactions are the primary determinant of lateral membrane lipid compartmentation [69].

The previously characterized strain BY4742; $tetO_2$-P_{CYC1}-*ERG9* that has proven to allow for a considerable reduction of the ergosterol/sterol content upon *ERG9* repression with striking impairment of proper protein sorting and delivery as well as endocytosis, was used as a model to monitor ergosterol (lipid raft) dependent lateral protein segregation within the plasma membrane.

For that, marker proteins of both prominent membrane compartments, MCC and MCP, were C-terminally tagged with GFP to allow for visualizing protein compartmentation *in vivo* by fluorescence microscopy. C-terminal fusion proteins proved to be fully functional. Strains expressing Can1p-GFP (from a plasmid) are sensitive to the toxic L-arginine analogue L-canavanine just like the wild-type background (BY4742) whereas a strain expressing a non-functional Can1p mutant version (BMA64-1A) grew unimpaired on L-canavanine containing medium (Fig. IV-9A). Moreover, Can1p-GFP was properly endocytosed and subsequently delivered to the vacuole at high extracellular arginine concentrations as is was also reported

for the wild-type protein [70] (Fig. IV-9B). This experiment illustrates that the lateral Can1p distribution within the plasma membrane should ideally be examined in cells grown in arginine-free medium that allows for extensive plasma membrane staining. The proper functionality of Pma1p-GFP was obvious from the pure viability of transformants since loss of Pma1p function is lethal [71]. The typical patchy distribution of Can1p was maintained within the plasma membrane even in spheroplasts (Fig. IV-9C), indicating that lateral protein compartmentation is not stabilized by the cell wall but is a pure membrane associated effect or if at all, is supported by internal structures such as the cortical actin network which, however, couldn't be confirmed by experimental data shown elsewhere [72].

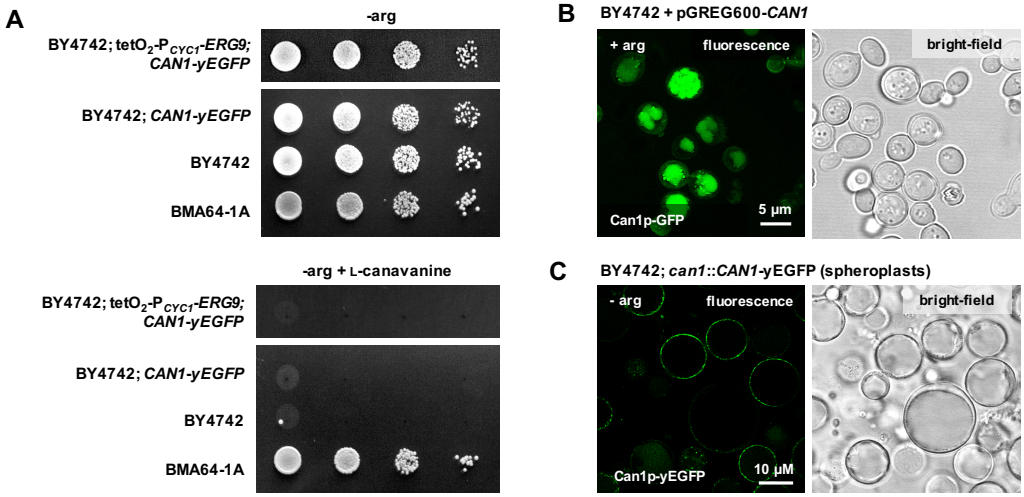

Fig. IV-9: C-terminal GFP-tagging of Can1p does not impair protein functionality. (A) Growth assays to examine Can1p transport activity by sensitivity to the toxic L-arginine analogue L-canavanine. Growth of strains (wild-type BY4742 and $tetO_2$-P_{CYC1}-*ERG9*) expressing Can1p-GFP was inhibited on L-arginine-free medium in the presence of L-canavanine (60 µg·mL^{-1}) as it was also true for BY4742 expression the wild-type protein (positive control) whereas growth was unimpaired on L-canavanine-free medium. A strain (BMA64-1A) expressing no functional Can1p grew unimpaired on both media (negative control). **(B)** Fluorescence image showing the subcellular localization of Can1p-GFP within cells grown in the presence of high arginine concentrations (60 µg·mL^{-1}) and corresponding bright-field image. In the presence of high external arginine concentrations, Can1p is targeted to the vacuole and plasma membrane staining disappears, which is present when grown in arginine-free medium **(C)**. The patchy distribution of Can1p is retained even in spheroplasts lacking their cell wall.

The membrane compartment MCC is not exclusively occupied by the introduced marker protein Can1p. In addition, integral membrane proteins such as Fur4p and Sur7p, among others, also serve as established marker proteins for MCC. Also cytosolic proteins Pil1p and Lsp1p that are components of the so called eisosome, a multiprotein complex hypothesized to be involved in endocytosis, colocalize with Can1p and MCC [73]. To test whether the C-terminal Can1p-GFP variant is distributed within the plasma membrane in its natural way and allows for native intermolecular interactions suggested to be involved in the formation of eisosomes, colocalization studies of Can1p-GFP and Pil1p-RedStar were performed.

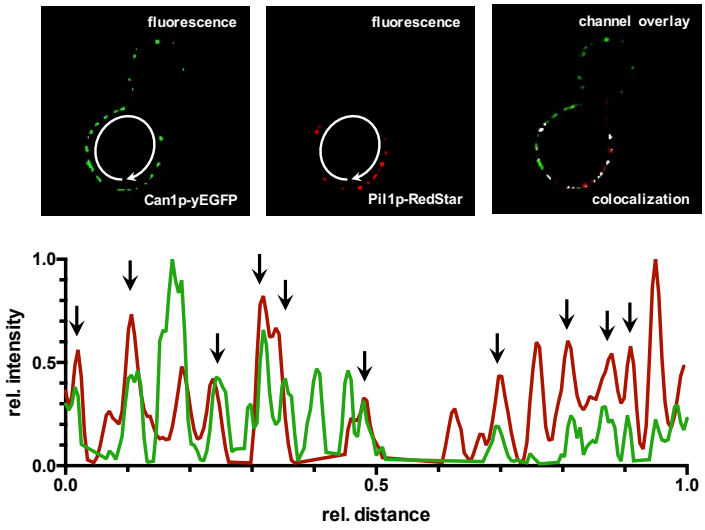

Fig. IV-10: Colocalization of Can1p-GFP and Pil1p-RedStar. Representative images of BY4742 cells expressing Can1p-GFP and Pil1-RedStar (from a plasmid, pGREG600) under control of P_{GAL1} are shown. White color in the overlay image of fluorescence channels display subcellular co-localization of both fluorophores. Fluorescence intensity profiles along the plasma membrane (see white arrows) for both proteins were tracked. Traces were normalized to the same maximal intensity. The overlay of both traces shows that places of accumulation for both proteins correspond to each other as indicated (see black arrows).

Both proteins colocalized (at least partially) - several local maxima of fluorescence intensity profiles along the plasma membrane of both proteins matched well (Fig. IV-10) and clearly indicated the occupation of identical membrane compartments in general. However, a few patches with only GFP fluorescence and some with only RedStar fluorescence could be identified. Based on all these results, it was concluded that Can1p-GFP featured wild-type protein behavior and could be used to study changes in protein distribution upon ergosterol depletion.

To prevent effects that might result from unnatural expression characteristics (e.g. expression level or timing of expression) a chromosomal C-terminal Can1p-GFP fusion was constructed. This allows for expression of the fusion protein from the natural genetic context. Protein distribution patterns within the plasma membrane of yeast were examined by confocal fluorescence microscopy. For that, yeast cells were scanned along the z-axis by collecting single images of multiple optical sections (Fig. IV-11A).

Single images of the z-stack were merged into a 2D stack by maximum intensity projection (MIP) reflecting the protein distribution over the entire membrane (Fig. IV-11B). Single images such as the tangential confocal section (TCS) representing the top/bottom of the cell as well as the equatorial confocal section (ECS) were also used to evaluate the pattern of protein compartmentation and potential changes upon ergosterol depletion.

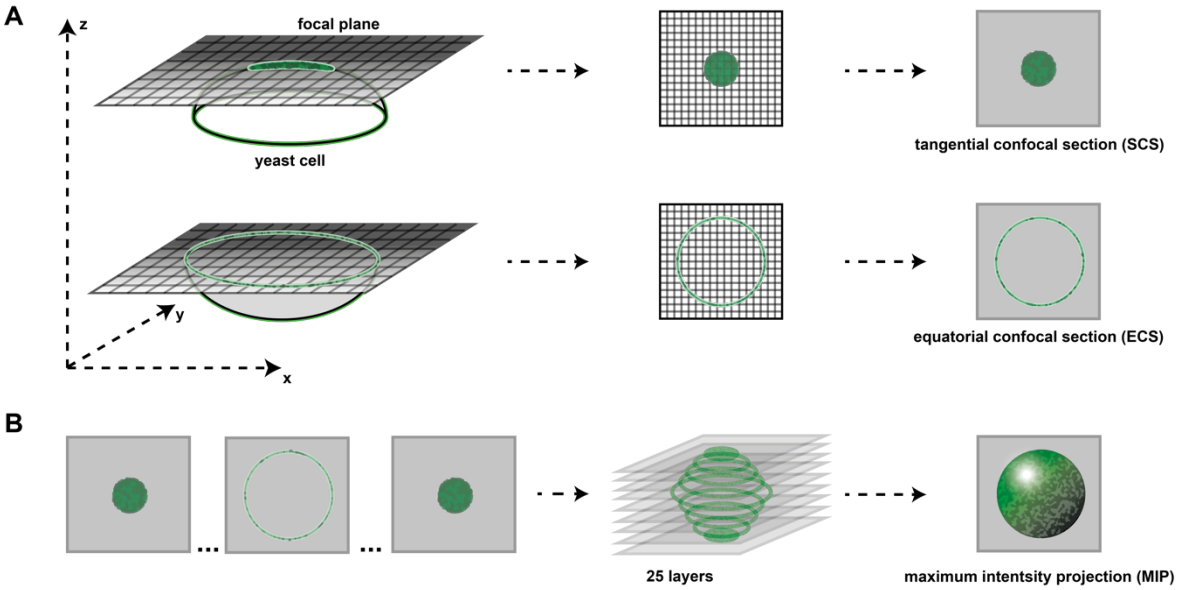

Fig. IV-11: Confocal fluorescence microscopy used for evaluating the distribution patter of proteins within the plasma membrane of yeast. (A) Yeast cells were scanned along the z-axis by vertically moving the focal plane thereby imaging multiple confocal section of the cell. The tangential confocal section (TCS) as well as the equatorial confocal section (ECS) were used to evaluate the protein distribution pattern. **(B)** Single images (~25) were merged into a 2D-stack by maximum intensity projection (MIP) to illustrate the protein distribution over the entire cell surface.

Can1p-GFP expressed from the genome in the wild-type background (BY4742) localized well to the plasma membrane and displayed the characteristic clustered pattern all over the cell surface. The same was true for $tetO_2$-P_{CYC1}-*ERG9* cells when grown in the absence of doxycycline thus allowing for expressing *ERG9* in a physiological range (Fig. IV-12; top & middle). Can1p-GFP fluorescence bleached rapidly, indicating relatively small protein-fluorophore levels within the plasma membrane as also briefly mentioned elsewhere [50]. In contrast to the observed characteristic protein distribution pattern of Can1p-GFP, imaging of the GFP-tagged potassium channel Tok1p revealed a homogenous signal within the plasma membrane (Fig. IV-S3A) as also observed for the previously mentioned proteins Hxt1p and Gap1p [50]. The characteristic distribution pattern of Tok1p-GFP was considered as being stereotypical for non-laterally segregated proteins and further used for comparison.

The characteristic pattern of Can1p-GFP accumulating in MCC patches within the plasma membrane serves as a sensitive marker for MCC integrity. To check for MCC integrity upon ergosterol depletion, $tetO_2$-P_{CYC1}-*ERG9*; *can1*::*CAN1*-GFP cells were grown in the presence of doxycycline, thus repressing *ERG9* expression, and confocal fluorescence microscopy analysis was performed as previously described (Fig. IV-11) to evaluate changes of protein distribution.

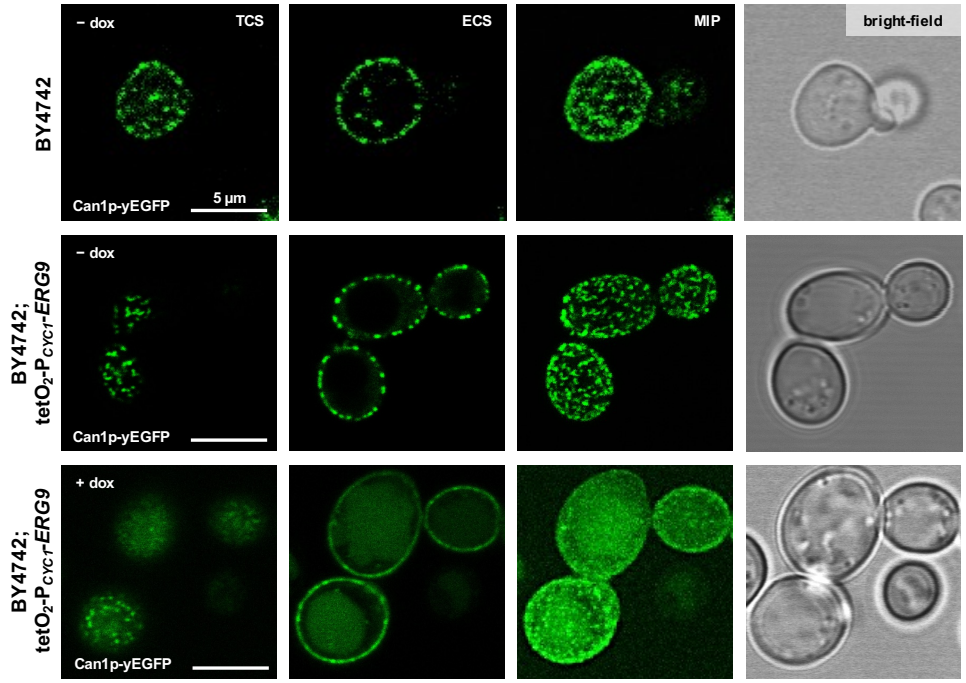

Fig. IV-12: Patterns of Can1p distribution within the plasma membrane of cells with natural or decreased *ERG9* expression. Fluorescence microscopy images of the tangential (TCS) equatorial (ECS) confocal sections as well as corresponding maximum intensity projections (MIP) and bright-field images are shown. The characteristic patchy pattern of Can1p-GFP distribution observed in the wild-type background (BY4742; top) and $tetO_2$-P_{CYC1}-*ERG9* cells grown in the absence of doxycycline (middle) changed to a more homogenous protein distribution in the plasma membrane upon doxycycline-mediated (40 µg·mL^{-1}) repression of *ERG9* in the $tetO_2$-P_{CYC1}-*ERG9* background (bottom).

The distribution of Can1p-GFP was affected in cells grown in the presence of doxycycline manifested in such that protein accumulation was less discrete and fluorescence foci were less separated from the neighboring membrane sections (Fig. IV-12; bottom). For semi-quantitative analysis, fluorescence intensity along the membrane was tracked, normalized to the same maximal intensity, and compared for representative $tetO_2$-P_{CYC1}-*ERG9* cells grown in the presence or absence of doxycycline. Cells that were grown in the absence of doxycycline and showed the wild-type pattern of Can1p distribution in MCC patches yielded a fluorescence intensity plot characterized by sharp peaks ranging from minimal to maximal relative fluorescence intensities. Due to this distribution, the set of fluorescence intensity values is characterized by a relatively low mean fluorescence intensity and a large deviation. In contrast to that, proteins that are homogeneously distributed within the membrane yield a pattern of fluorescence intensity exhibiting a relatively high mean fluorescence intensity and a decreased deviation as shown for Tok1p (Fig. IV-S3B).

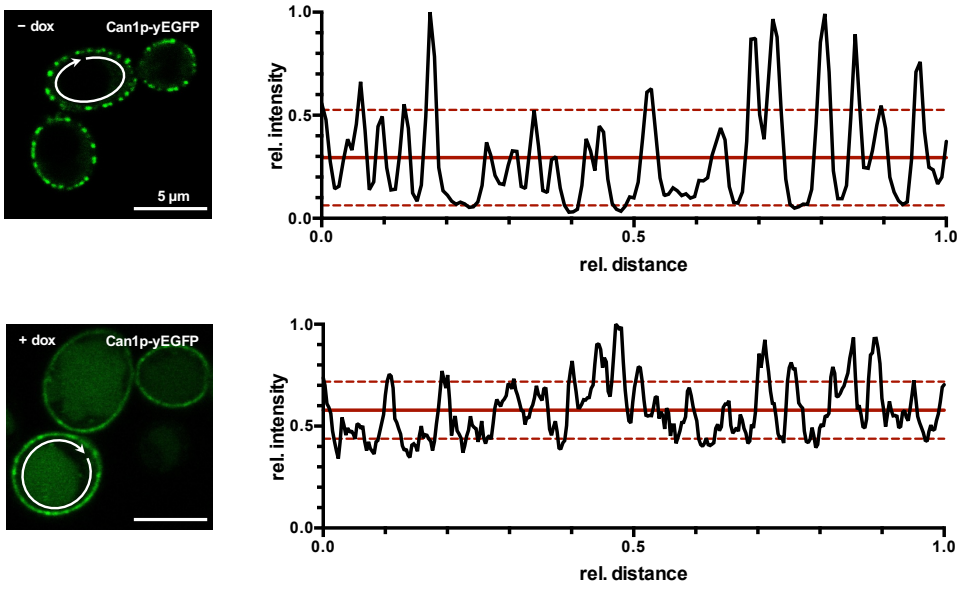

Fig. IV-13: Characteristic intensity profiles of Can1p-GFP fluorescence along the plasma membrane of cells with natural or disturbed *ERG9* expression. The fluorescence intensity profiles were tracked from the corresponding ECS images (left) and normalized to the same maximal fluorescence intensity and track length. The mean fluorescence intensity (continuous red line) as well as standard deviations (dashed red line) were calculated for each total set of fluorescence intensity values and are indicated for comparison. Can1p-GFP intensity profile patterns changed upon *ERG9* repression showing an elevated mean fluorescence intensity and a decreased standard deviation.

For $tetO_2$-P_{CYC1}-*ERG9* cells grown in the presence of doxycycline, properties of the Can1p-GFP fluorescence intensity profile were shifted towards an elevated mean fluorescence and a decreased deviation, which is characteristic for evenly distributed proteins. The altered distribution pattern upon *ERG9* repression strongly suggests that lipids and the lipid composition, particularly ergosterol and sterols, play a crucial role in the lateral segregation of the plasma membrane and are inseparably linked to each other.

Representative images (Fig. IV-12; bottom) show a vacuolar GFP straining in cells with disturbed MCC localization of Can1p that was not observed for cells with a regular Can1p pattern in the plasma membrane. This observation supports the assumption that protein compartmentation is linked to protein stability and protein turnover and that the basal Can1p turnover is faster when the protein is not localized in MCC patches. Experiments presented elsewhere [69] could show that Can1p was more accessible to liberation from the membrane by mild detergents when the wild-type pattern of protein distribution was disturbed. Moreover, Can1p internalization in arginine-rich medium occurred much faster upon knockout of *NCE102* which also strongly disturbs proper membrane compartmentation and MCC formation. Since Can1p delivery to the vacuole induced by an excess of external arginine is mediated by classical endocytosis, one could argue that MCC localization protects Can1p from initialization by endocytosis. However, this hypothesis is

in conflict with the observed colocalization of Can1p and Pil1p, a component of the eisosome which is believed to be involved in the initialization of endocytosis [74], unless coating of MCCs by cytosolic Pil1p inhibits endocytosis and directs the endocytic activity to neighboring membrane areas. In this model, eisosomes would mark membrane sites with silenced endocytic activity [73].

The equatorial confocal section (ECS) of BY4742 wild-type cells also showed an inhomogeneous distribution for Pma1p-GFP within the plasma membrane. However, the extension of areas occupied by Pma1p was much larger and the pattern was significantly different from that housed by Can1p-GFP. This became especially evident from the tangential confocal section (TCS) as well as from the maximal intensity projection (MIP) (Fig. IV-14; top). The observed pattern corresponds well to the previously described mesh-shaped pattern of Pma1p in the plasma membrane of yeast. The characteristic Pma1p pattern shown here also supports the previously reported non-overlapping of both membrane compartments [50], MCC and MCP, as the distribution of dark holes within the mesh of Pma1p fits well to the general distribution of membrane spots occupied by Can1p. Moreover, the fluorescence of Pma1p-GFP was much stronger compared to the one observed for Can1p-GFP which is consistent with the high abundance of Pma1p in the plasma membrane [75]. This ratio also emphasizes that expression rates for both GFP-tagged proteins were at natural levels. The general Pma1p distribution pattern in $tetO_2$-P_{CYC1}-*ERG9* cells grown in the absence of doxycycline was equivalent to the one observed for the wild-type background showing the characteristic dark patches missing the protein (Fig. IV-14; middle). The observation that membrane compartments covered by Can1p and Pma1p exclude each other [50] compared with the fact that Can1p is associated with ergosterol-rich lipid rafts indicates that Pma1p just occupies the membrane areas (MCP) that are mainly composed of bulk lipids (glycerophospholipids) and that surround MCCs. This way, the rigorous exclusion of Pma1p from MCCs shows how the non-homogenous membrane lipid composition and ergosterol/sphingolipid patches provide a mechanism for negatively controlling the membrane protein segregation. This functional exclusion must, however, include a controlling mechanism that is based e.g. on protein properties itself or the mechanism that delivers proteins to the plasma membrane, since not all membrane proteins such as Tok1p (Fig. IV-S3), Hxt1p and Gap1p are either excluded from or accumulated in lipid-raft structures.

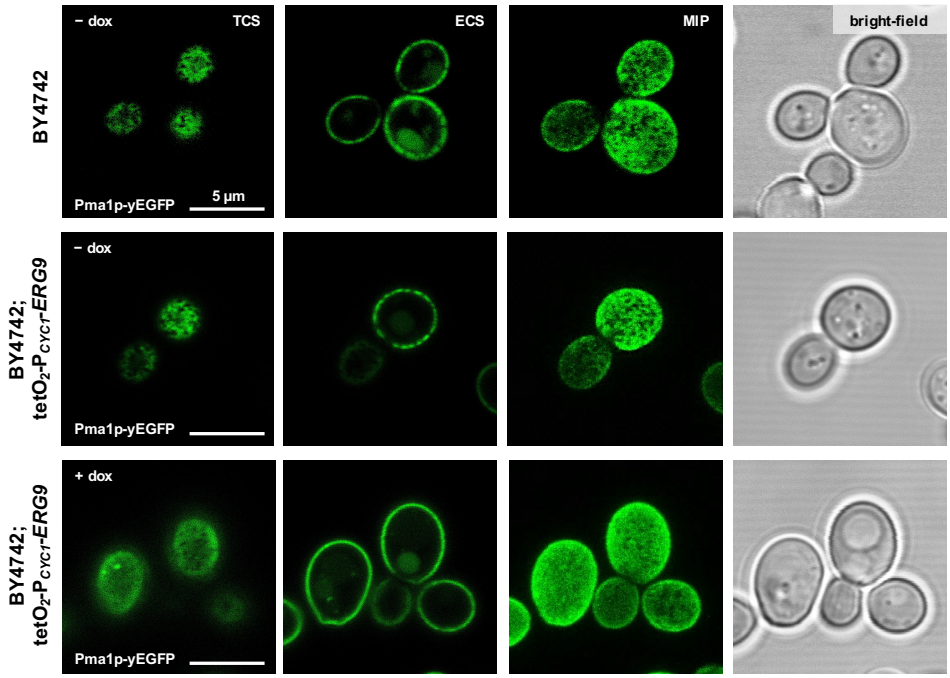

Fig. IV-14: Patterns of Pma1p distribution within the plasma membrane of cells with natural or decreased *ERG9* expression. Fluorescence microscopy images of the tangential (TCS) equatorial (ECS) confocal sections as well as corresponding maximum intensity projections (MIP) and bright-field images are shown. The characteristic mesh-shaped pattern of Pma1p-GFP distribution leading to dark holes within the cell surface was observed in the wild-type background (BY4742; top) and $tetO_2$-P_{CYC1}-*ERG9* cells grown in the absence of doxycycline (middle). This pattern changed to a more homogenous Pma1p distribution in the plasma membrane upon doxycycline-mediated (40 µg·mL^{-1}) repression of *ERG9* in the $tetO_2$-P_{CYC1}-*ERG9* background (bottom).

Disruption of MCCs, resulting from *ERG9* repression, as previously shown by an altered Can1p-GFP distribution (Fig. IV-12) should consequently also modify Pma1p distribution, if Pma1p is actively excluded from ergosterol/sphingolipid patches. Changes in lateral Pma1p segregation would be evident from a decrease of Pma1p-free membrane spots by infiltration of Pma1p as well as by a more homogenous protein distribution within the plasma membrane. Indeed, when Pma1p-GFP expressing $tetO_2$-P_{CYC1}-*ERG9* cells were grown in the presence of doxycycline, Pma1p distribution became much more homogenous as evident from TCS, ECS and MIP images (Fig. IV-14; bottom). These results strongly support the hypothesis of plasma membrane segregation by active exclusion as well as the involvement of ergosterol-rich membrane microdomains in this mechanism. Control experiments showing that the patchy distribution of Can1p as well as the complementary network-like Pma1p distribution are also strongly affected in the ergosterol biosynthesis mutant Δ*erg6* (Fig. IV-S4) further support this hypothesis and suggest that not just the total ergosterol/sterol content but also the chemical sterol structure play a crucial role for lateral membrane segregation [73].

However, basic question of lateral membrane compartmentation such as the mechanism how proteins are directed to specific membrane compartments as well as the functional significance of plasma membrane compartmentation could not be answered so far. To target the first mentioned question, different mechanisms including the protein structure itself can be discussed. Membrane compartments rich in ergosterol and sphingolipids are significantly thicker than membrane areas with a high glycerophospholipid content [76] as it is also generally true for highly ordered membranes compared to bilayers featuring a low ordering parameter [1]. Studies on the prokaryotic membrane fluidity sensor DesK from *Bacillus subtilis* clearly show that membrane proteins are able to sense the thickness of lipid bilayers in which they are embedded in [77] and change/lose their structure and function [78] in dependence of their lipid environment. In this scenario, the overall length of transmembrane domains would be the crucial factor that directs proteins to membrane partitions of different thickness [79]. This way, the driving force of lateral protein segregation would be of thermodynamic nature with the goal of maximizing beneficial hydrophobic protein-bilayer interactions and preventing hydrophobic mismatches that would be e.g. assured for longer transmembrane helices only in thicker membrane areas. On a second level, protein-protein interactions might direct further proteins to these membrane compartments. On the functional level, protein segregation within the plasma membrane might be relevant for clustering of proteins whose functions are coupled or at least beneficial for each other. This way membrane microdomains would form microenvironments with particular biological functions. On the other hand, proteins whose functions negatively affect each other or even work in the opposite direction could be functionally separated by membrane microdomains. The two proteins, Can1p and Pma1p, shown here might even serve as an example for that model: The plasma membrane H^+-ATPase pumps protons out from the cells thereby generating a proton gradient that can drive the uptake of nutrients against the corresponding (electro)chemical gradient mediated by proton symporters like Can1p in a secondary-active transport process [80, 81]. This way, proton gradient generating and consuming processes would be spatially separated by membrane microdomains.

4.5. Conclusions

This study introduces a metabolic engineering approach for regulating the yeast endogenous sterol biosynthetic activity by controlling the expression of *ERG9*, the gate keeper enzyme determining the flux of intermediates towards the ergosterol biosynthetic pathway. This cellular model was used to monitor physiological effects of ergosterol and total sterol depletion. Besides a general impairment of the cell's general viability, it was shown that sterol depletion causes cellular mislocalization of Tat2p, a plasma membrane-resident tryptophan permease, to the vacuole thereby severely impairing the ability of tryptophan uptake from the extracellular environment. Furthermore, it was shown that sterol depletion significantly decreases the general endocytic activity of yeast as evaluated by electrophysiological capacity measurements. Plasma membrane compartmentation characterized by the inhomogeneous distribution of marker proteins Can1p and Pma1p was affected upon *ERG9* repression and down-regulation the cell's ergosterol biosynthetic activity. The cellular system allowing for genetically controlling the ergosterol biosynthesis has proven to be a suitable model to monitor physiological effects of sterol depletion and was used to emphasize essential roles of sterols for fundamental cellular processes and properties.

4.6. References

1. **Dufourc EJ**. Sterols and membrane dynamics. *J Chem Biol* 2008;1(1-4):63-77.
2. **Ricci JN, Morton R, Kulkarni G, Summers ML, Newman DK**. Hopanoids play a role in stress tolerance and nutrient storage in the cyanobacterium Nostoc punctiforme. *Geobiology* 2017;15(1):173-183.
3. **Dahl J**. The role of cholesterol in mycoplasma membranes. *Subcell Biochem* 1993;20:167-188.
4. **Jain S, Caforio A, Driessen AJ**. Biosynthesis of archaeal membrane ether lipids. *Front Microbiol* 2014;5:641.
5. **van Meer G, Voelker DR, Feigenson GW**. Membrane lipids: where they are and how they behave. *Nat Rev Mol Cell Biol* 2008;9(2):112-124.
6. **Mouritsen OG, Jorgensen K**. Small-scale lipid-membrane structure: simulation versus experiment. *Curr Opin Struct Biol* 1997;7(4):518-527.
7. **Huang J, Feigenson GW**. A microscopic interaction model of maximum solubility of cholesterol in lipid bilayers. *Biophys J* 1999;76(4):2142-2157.
8. **Mesmin B, Maxfield FR**. Intracellular sterol dynamics. *Biochim Biophys Acta* 2009;1791(7):636-645.
9. **Xu X, Bittman R, Duportail G, Heissler D, Vilcheze C et al.** Effect of the structure of natural sterols and sphingolipids on the formation of ordered sphingolipid/sterol domains (rafts). Comparison of cholesterol to plant, fungal, and disease-associated sterols and comparison of sphingomyelin, cerebrosides, and ceramide. *J Biol Chem* 2001;276(36):33540-33546.
10. **Brown DA, Rose JK**. Sorting of GPI-anchored proteins to glycolipid-enriched membrane subdomains during transport to the apical cell surface. *Cell* 1992;68(3):533-544.
11. **Bagnat M, Keranen S, Shevchenko A, Shevchenko A, Simons K**. Lipid rafts function in biosynthetic delivery of proteins to the cell surface in yeast. *Proc Natl Acad Sci U S A* 2000;97(7):3254-3259.
12. **Bagnat M, Simons K**. Cell surface polarization during yeast mating. *Proc Natl Acad Sci U S A* 2002;99(22):14183-14188.
13. **Rajendran L, Simons K**. Lipid rafts and membrane dynamics. *J Cell Sci* 2005;118(Pt 6):1099-1102.
14. **Lichtenberg D, Goni FM, Heerklotz H**. Detergent-resistant membranes should not be identified with membrane rafts. *Trends Biochem Sci* 2005;30(8):430-436.
15. **Heese-Peck A, Pichler H, Zanolari B, Watanabe R, Daum G et al.** Multiple functions of sterols in yeast endocytosis. *Mol Biol Cell* 2002;13(8):2664-2680.
16. **Wachtler V, Balasubramanian MK**. Yeast lipid rafts?--an emerging view. *Trends Cell Biol* 2006;16(1):1-4.
17. **Alvarez FJ, Douglas LM, Konopka JB**. Sterol-rich plasma membrane domains in fungi. *Eukaryot Cell* 2007;6(5):755-763.
18. **Zinser E, Paltauf F, Daum G**. Sterol composition of yeast organelle membranes and subcellular distribution of enzymes involved in sterol metabolism. *J Bacteriol* 1993;175(10):2853-2858.
19. **Maxfield FR, Menon AK**. Intracellular sterol transport and distribution. *Curr Opin Cell Biol* 2006;18(4):379-385.
20. **Pichler H, Riezman H**. Where sterols are required for endocytosis. *Biochim Biophys Acta* 2004;1666(1-2):51-61.
21. **Lauwers E, Andre B**. Association of yeast transporters with detergent-resistant membranes correlates with their cell-surface location. *Traffic* 2006;7(8):1045-1059.
22. **Brown DA, London E**. Structure and function of sphingolipid- and cholesterol-rich membrane rafts. *J Biol Chem* 2000;275(23):17221-17224.
23. **Dupont S, Lemetais G, Ferreira T, Cayot P, Gervais P et al.** Ergosterol biosynthesis: a fungal pathway for life on land? *Evolution* 2012;66(9):2961-2968.
24. **Paradise EM, Kirby J, Chan R, Keasling JD**. Redirection of flux through the FPP branch-point in Saccharomyces cerevisiae by down-regulating squalene synthase. *Biotechnol Bioeng* 2008;100(2):371-378.
25. **Fegueur M, Richard L, Charles AD, Karst F**. Isolation and primary structure of the ERG9 gene of Saccharomyces cerevisiae encoding squalene synthetase. *Curr Genet* 1991;20(5):365-372.

26. **Brachmann CB, Davies A, Cost GJ, Caputo E, Li J et al.** Designer deletion strains derived from Saccharomyces cerevisiae S288C: a useful set of strains and plasmids for PCR-mediated gene disruption and other applications. *Yeast* 1998;14(2):115-132.

27. **Entian K-D, Kötter P**. 25 Yeast Genetic Strain and Plasmid Collections. *Methods in Microbiology* 2007;36:629-666.

28. **Gietz RD, Schiestl RH**. High-efficiency yeast transformation using the LiAc/SS carrier DNA/PEG method. *Nat Protoc* 2007;2(1):31-34.

29. **Green MR, Sambrook J**. *Molecular Cloning: A Laboratory Manual*: Cold Spring Harbor Laboratory Press; 2012.

30. **Gueldener U, Heinisch J, Koehler GJ, Voss D, Hegemann JH**. A second set of loxP marker cassettes for Cre-mediated multiple gene knockouts in budding yeast. *Nucleic Acids Res* 2002;30(6):e23.

31. **Sheff MA, Thorn KS**. Optimized cassettes for fluorescent protein tagging in Saccharomyces cerevisiae. *Yeast* 2004;21(8):661-670.

32. **Jansen G, Wu C, Schade B, Thomas DY, Whiteway M**. Drag&Drop cloning in yeast. *Gene* 2005;344:43-51.

33. **Janke C, Magiera MM, Rathfelder N, Taxis C, Reber S et al.** A versatile toolbox for PCR-based tagging of yeast genes: new fluorescent proteins, more markers and promoter substitution cassettes. *Yeast* 2004;21(11):947-962.

34. **Rodriguez S, Kirby J, Denby CM, Keasling JD**. Production and quantification of sesquiterpenes in Saccharomyces cerevisiae, including extraction, detection and quantification of terpene products and key related metabolites. *Nat Protoc* 2014;9(8):1980-1996.

35. **Bertl A, Bihler H, Reid JD, Kettner C, Slayman CL**. Physiological characterization of the yeast plasma membrane outward rectifying K+ channel, DUK1 (TOK1), in situ. *J Membr Biol* 1998;162(1):67-80.

36. **Bertl A, Slayman CL**. Cation-selective channels in the vacuolar membrane of Saccharomyces: dependence on calcium, redox state, and voltage. *Proc Natl Acad Sci U S A* 1990;87(20):7824-7828.

37. **Carrillo L, Cucu B, Bandmann V, Homann U, Hertel B et al.** High-resolution membrane capacitance measurements for studying endocytosis and exocytosis in yeast. *Traffic* 2015;16(7):760-772.

38. **Asadollahi MA, Maury J, Moller K, Nielsen KF, Schalk M et al.** Production of plant sesquiterpenes in Saccharomyces cerevisiae: effect of ERG9 repression on sesquiterpene biosynthesis. *Biotechnol Bioeng* 2008;99(3):666-677.

39. **Belli G, Gari E, Aldea M, Herrero E**. Functional analysis of yeast essential genes using a promoter-substitution cassette and the tetracycline-regulatable dual expression system. *Yeast* 1998;14(12):1127-1138.

40. **Gari E, Piedrafita L, Aldea M, Herrero E**. A set of vectors with a tetracycline-regulatable promoter system for modulated gene expression in Saccharomyces cerevisiae. *Yeast* 1997;13(9):837-848.

41. **Kamakaka RT, Bulger M, Kadonaga JT**. Potentiation of RNA polymerase II transcription by Gal4-VP16 during but not after DNA replication and chromatin assembly. *Genes Dev* 1993;7(9):1779-1795.

42. **Zhu Z, Zheng T, Lee CG, Homer RJ, Elias JA**. Tetracycline-controlled transcriptional regulation systems: advances and application in transgenic animal modeling. *Semin Cell Dev Biol* 2002;13(2):121-128.

43. **Daicho K, Makino N, Hiraki T, Ueno M, Uritani M et al.** Sorting defects of the tryptophan permease Tat2 in an erg2 yeast mutant. *FEMS Microbiol Lett* 2009;298(2):218-227.

44. **Gaber RF, Copple DM, Kennedy BK, Vidal M, Bard M**. The yeast gene ERG6 is required for normal membrane function but is not essential for biosynthesis of the cell-cycle-sparking sterol. *Mol Cell Biol* 1989;9(8):3447-3456.

45. **Lorenz RT, Parks LW**. Cloning, sequencing, and disruption of the gene encoding sterol C-14 reductase in Saccharomyces cerevisiae. *DNA Cell Biol* 1992;11(9):685-692.

46. **Davies BS, Rine J**. A role for sterol levels in oxygen sensing in Saccharomyces cerevisiae. *Genetics* 2006;174(1):191-201.

47. **Yang H, Tong J, Lee CW, Ha S, Eom SH et al.** Structural mechanism of ergosterol regulation by fungal sterol transcription factor Upc2. *Nat Commun* 2015;6:6129.

48. **Marie C, Leyde S, White TC**. Cytoplasmic localization of sterol transcription factors Upc2p and Ecm22p in S. cerevisiae. *Fungal Genet Biol* 2008;45(10):1430-1438.

49. **Abe F, Iida H**. Pressure-induced differential regulation of the two tryptophan permeases Tat1 and Tat2 by ubiquitin ligase Rsp5 and its binding proteins, Bul1 and Bul2. *Mol Cell Biol* 2003;23(21):7566-7584.

50. **Malinska K, Malinsky J, Opekarova M, Tanner W**. Visualization of protein compartmentation within the plasma membrane of living yeast cells. *Mol Biol Cell* 2003;14(11):4427-4436.

51. **Umebayashi K, Nakano A**. Ergosterol is required for targeting of tryptophan permease to the yeast plasma membrane. *J Cell Biol* 2003;161(6):1117-1131.

52. **Beck T, Schmidt A, Hall MN**. Starvation induces vacuolar targeting and degradation of the tryptophan permease in yeast. *J Cell Biol* 1999;146(6):1227-1238.

53. **Harsay E, Schekman R**. A subset of yeast vacuolar protein sorting mutants is blocked in one branch of the exocytic pathway. *J Cell Biol* 2002;156(2):271-285.

54. **Munn AL, Heese-Peck A, Stevenson BJ, Pichler H, Riezman H**. Specific sterols required for the internalization step of endocytosis in yeast. *Mol Biol Cell* 1999;10(11):3943-3957.

55. **Daicho K, Maruyama H, Suzuki A, Ueno M, Uritani M et al.** The ergosterol biosynthesis inhibitor zaragozic acid promotes vacuolar degradation of the tryptophan permease Tat2p in yeast. *Biochim Biophys Acta* 2007;1768(7):1681-1690.

56. **Delic M, Valli M, Graf AB, Pfeffer M, Mattanovich D et al.** The secretory pathway: exploring yeast diversity. *FEMS Microbiol Rev* 2013;37(6):872-914.

57. **Van Zeebroeck G, Rubio-Texeira M, Schothorst J, Thevelein JM**. Specific analogues uncouple transport, signalling, oligo-ubiquitination and endocytosis in the yeast Gap1 amino acid transceptor. *Mol Microbiol* 2014;93(2):213-233.

58. **Munn AL, Riezman H**. Endocytosis is required for the growth of vacuolar H(+)-ATPase-defective yeast: identification of six new END genes. *J Cell Biol* 1994;127(2):373-386.

59. **Rodal SK, Skretting G, Garred O, Vilhardt F, van Deurs B et al.** Extraction of cholesterol with methyl-beta-cyclodextrin perturbs formation of clathrin-coated endocytic vesicles. *Mol Biol Cell* 1999;10(4):961-974.

60. **Subtil A, Gaidarov I, Kobylarz K, Lampson MA, Keen JH et al.** Acute cholesterol depletion inhibits clathrin-coated pit budding. *Proc Natl Acad Sci U S A* 1999;96(12):6775-6780.

61. **Hailstones D, Sleer LS, Parton RG, Stanley KK**. Regulation of caveolin and caveolae by cholesterol in MDCK cells. *J Lipid Res* 1998;39(2):369-379.

62. **Schnitzer JE, Oh P, Pinney E, Allard J**. Filipin-sensitive caveolae-mediated transport in endothelium: reduced transcytosis, scavenger endocytosis, and capillary permeability of select macromolecules. *J Cell Biol* 1994;127(5):1217-1232.

63. **Cucu B, Degreif D, Bertl A, Thiel G**. Vesicle fusion and fission in plants and yeast. *Cell Calcium* 2017;67:40-45.

64. **Fukudomi T, Kotani T, Miyakawa I**. A simple method for culture and stable maintenance of giant spheroplasts from the yeast Saccharomyces cerevisiae. *J Gen Appl Microbiol* 2011;57(4):177-182.

65. **Epand RM, Thomas A, Brasseur R, Epand RF**. Cholesterol interaction with proteins that partition into membrane domains: an overview. *Subcell Biochem* 2010;51:253-278.

66. **Epand RM**. Cholesterol and the interaction of proteins with membrane domains. *Prog Lipid Res* 2006;45(4):279-294.

67. **Lees ND, Bard M, Kemple MD, Haak RA, Kleinhans FW**. ESR determination of membrane order parameter in yeast sterol mutants. *Biochim Biophys Acta* 1979;553(3):469-475.

68. **Pearse BM, Smith CJ, Owen DJ**. Clathrin coat construction in endocytosis. *Curr Opin Struct Biol* 2000;10(2):220-228.

69. **Grossmann G, Opekarova M, Malinsky J, Weig-Meckl I, Tanner W**. Membrane potential governs lateral segregation of plasma membrane proteins and lipids in yeast. *EMBO J* 2007;26(1):1-8.

70. **Opekarova M, Caspari T, Pinson B, Brethes D, Tanner W**. Post-translational fate of CAN1 permease of Saccharomyces cerevisiae. *Yeast* 1998;14(3):215-224.

71. **Serrano R, Kielland-Brandt MC, Fink GR**. Yeast plasma membrane ATPase is essential for growth and has homology with (Na+ + K+), K+- and Ca2+-ATPases. *Nature* 1986;319(6055):689-693.

72. **Malinska K, Malinsky J, Opekarova M, Tanner W**. Distribution of Can1p into stable domains reflects lateral protein segregation within the plasma membrane of living S. cerevisiae cells. *J Cell Sci* 2004;117(Pt 25):6031-6041.

73. **Grossmann G, Malinsky J, Stahlschmidt W, Loibl M, Weig-Meckl I et al.** Plasma membrane microdomains regulate turnover of transport proteins in yeast. *J Cell Biol* 2008;183(6):1075-1088.

74. **Walther TC, Brickner JH, Aguilar PS, Bernales S, Pantoja C et al.** Eisosomes mark static sites of endocytosis. *Nature* 2006;439(7079):998-1003.

75. **Ferreira T, Mason AB, Slayman CW**. The yeast Pma1 proton pump: a model for understanding the biogenesis of plasma membrane proteins. *J Biol Chem* 2001;276(32):29613-29616.

76. **Pencer J, Nieh MP, Harroun TA, Krueger S, Adams C et al.** Bilayer thickness and thermal response of dimyristoylphosphatidylcholine unilamellar vesicles containing cholesterol, ergosterol and lanosterol: a small-angle neutron scattering study. *Biochim Biophys Acta* 2005;1720(1-2):84-91.

77. **Inda ME, Vandenbranden M, Fernandez A, de Mendoza D, Ruysschaert JM et al.** A lipid-mediated conformational switch modulates the thermosensing activity of DesK. *Proc Natl Acad Sci U S A* 2014;111(9):3579-3584.

78. **Johannsson A, Smith GA, Metcalfe JC**. The effect of bilayer thickness on the activity of (Na+ + K+)-ATPase. *Biochim Biophys Acta* 1981;641(2):416-421.

79. **Munro S**. An investigation of the role of transmembrane domains in Golgi protein retention. *EMBO J* 1995;14(19):4695-4704.

80. **Morsomme P, Slayman CW, Goffeau A**. Mutagenic study of the structure, function and biogenesis of the yeast plasma membrane H(+)-ATPase. *Biochim Biophys Acta* 2000;1469(3):133-157.

81. **Goffeau A, Slayman CW**. The proton-translocating ATPase of the fungal plasma membrane. *Biochim Biophys Acta* 1981;639(3-4):197-223.

4.7. Supporting information

Tab. IV-S1: Plasmids used in this study. The table summarizes basic characteristics and properties of indicated plasmids.

Plasmid	description	reference
pUG72	-	[30]
pUG73	-	[30]
pKT203	-	[31]
pGREG503	-	[32]
pGREG600	-	[32]
pCM224	-	[39]
pCM188-*OLE1*	CEN/ARS; *URA3*; amp^R; doxycycline repressible expression of Ole1p	This study
pGREG576-*UPC2*	CEN/ARS; *URA3*; kanMX; amp^R; expression of N-terminally GFP-tagged Upc2p from galactose inducible *GAL1* promoter	This study
pGREG600-*UPC2*	CEN/ARS; *URA3*; kanMX; amp^R; expression of C-terminally GFP-tagged Upc2p from galactose inducible *GAL1* promoter	This study
pGREG503-*TAT2*	CEN/ARS; *HIS3*; kanMX; amp^R; expression of Tat2p from galactose inducible *GAL1* promoter	This study
pGRE600-*TAT2*	CEN/ARS; *URA3*; kanMX; amp^R; expression of C-terminally GFP-tagged Tat2p from galactose inducible *GAL1* promoter	This study
pGREG600-P$_{TAT2}$-*TAT2*	CEN/ARS; *URA3*; kanMX; amp^R; expression of C-terminally GFP-tagged Tat2p from native *TAT2* promoter	This study
pGREG600-*CAN1*	CEN/ARS; *URA3*; kanMX; amp^R; expression of C-terminally GFP-tagged Can1p from galactose inducible *GAL1* promoter	This study
pGREG600-*TOK1*	CEN/ARS; *URA3*; kanMX; amp^R; expression of C-terminally GFP-tagged Tok1p from galactose inducible *GAL1* promoter	This study
pGREG505-*PIL1*-RedStar	CEN/ARS; *URA3*; kanMX; amp^R; expression of C-terminally RedStar-tagged Pil1p from galactose inducible *GAL1* promoter	This study

Tab. IV-S2: Primers used in this study. Underlined sequence parts represent homology regions of overhang primers used in recombination-based cloning approaches.

Primer	sequence (5' → 3')	amplicon
P1 (fw)	GCCTAAACGAGCAGCGAGAACACGACCACGGGCTATATAAATGGAAAGTTAGGACAGGGGCCAGCTGAAGCTTCGTACGC	$tetO_2$-P_{CYC1} PRC
P2 (rv)	CAGCTTCAAAGCTGCCTTCATCTCGACCGGATGCAATGCCAATTGTAATAGCTTTCCCATCGCATAGGCCACTAGTGGATCTG	$tetO_2$-P_{CYC1} PRC
P3 (fw)	GCATTGGTGACTATTGAGCACGTGAGTATACGTGATTAAGCACACAAAGGCAGCTTGGAGTCTGAAGCTTCGTACGCTGCAG	*TRP1* KOC
P4 (rv)	CCAATCCAAAAGTTCACCTGTCCCACCTGCTTCTGGGTAATCAAACAAGGGAATAAACGAATGAGCATAGGCCACTAGTGGATCTG	*TRP1* KOC
P5 (fw)	CGATTTAAGTTTTACATAATTTAAAAAAACAAGAATAAAATAATAATATAGTAGGCAGCATAAGCTGAAGCTTCGTACGCTGCAG	*ERG6* KOC
P6 (rv)	CTGCATATATAGGAAAATAGGTATATATCGTGCGCTTTATTTGAATCTTATTGATCTAGTGAATGCATAGGCCACTAGTGGATCTG	*ERG6* KOC
P7 (fw)	GGGAAGATCATGAACCAAAGACTTTTTGGGACAAATTTTGGAATGTTGTAGCAGGTGACGGTGCTGGTTTA	yEGFP (*CAN1*)
P8 (rv)	GATCCCTTAAACTTTCTTTTCGGTGTATGACTTATGAGGGTGAGAATGCGAAACGAGGCAAGCTAAACAGATC	yEGFP (*CAN1*)
P9 (fw)	AAGACTTCATGGCTGCTATGCAAAGAGTCTCTACTCAACACGAAAAGGAAACCGGTGACGGTGCTGGTTTA	yEGFP (*PMA1*)
P10 (rv)	GCGGCTTATTCTTGTTGGCTCCTAATTCTTTTTAGTGTATCAGTTCCCATTGATCGAGGCAAGCTAAACAGATC	yEGFP (*PMA1*)
P11 (fw)	GAATTCGATATCAAGCTTATCGATACCGTCGACAATGAGCGAAGTCGGTATACAG	*UPC2* ORF
P12 (rv)	GTTCTTCTCCTTTACTCATTCTCGAGTCGACTAACGAAAAATCAGAGAAATTTGTTGTTG	*UPC2* ORF
P13 (fw)	GAATTCGATATCAAGCTTATCGATACCGTCGACAATGACCGAAGACTTTATTTCTTCTGTC	*TAT2* ORF
P14 (rv)	GTTCTTCTCCTTTACTCATTCTCGAGGTCGACAAACACCAGAAATGGAACTGTCTC	*TAT2* ORF
P15 (fw)	GAATTCGATATCAAGCTTATCGATACCGTCGACAATGACAAATTCAAAAGAAGACG	*CAN1* ORF
P16 (rv)	GTTCTTCTCCTTTACTCATTCTCGAGGTCGACGCTGCTACAACATTCCAAAATTTG	*CAN1* ORF
P17 (fw)	GAATTCGATATCAAGCTTATCGATACCGTCGACAATGACAAGGTTCATGAACAGC	*TOK1* ORF
P18 (rv)	GTTCTTCTCCTTTACTCATTCTCGAGGTCGAAAGTGTCTTTCTATGCTCAC	*TOK1* ORF
P19 (rv)	GAATTCGATATCAAGCTTATCGATACCGTCGACAATGCACAGAACTTACTCTTTAAGAAATT	*PIL1* ORF
P20 (fw)	GCTCCAGCACCAGCACCAGCACCTGCTCCCATCTCGAGAGCTGTTGTTTGTTGGGGAAG	*PIL1* ORF
P21 (rv)	GTTCTTATGTAGTGACACCGATTATTTAAAGCTGCAGGTCGACCTCGAGATGGGAGCAGGTGCTGGTGC	RedStar ORF
P22 (fw)	GTGGGGGGAGGGCGTGAATGTAAGCGTGACATAACTAATTACATGACTCGAGTTACAAGAACAAGTGGTGTCTAC	RedStar ORF
P23 (rv)	GCGTGACATAACTAATTACATGACTCGAGGTCGACTCATAACGAAAAATCAGAGAAATTTGTTGTTG	*UPC2* ORF

Primer	sequence (5' → 3')	amplicon
P24 (fw)	GAATTCGATATCAAGCTTATCGATACCGTCGACAATGACCGAAGACTTTATTTC	*TAT2* ORF
P25 (rv)	GCGTGACATAACTAATTACATGACTCGAGGTCGACTTAACACCAGAAATGGAACTG	*TAT2* ORF
P26 (fw)	AACAAAAGCTGGAGCTCGTTTAAACGGCGCGCCCTTACCAATGGGTGCGCTTA	P_{TAT2}
P27 (rv)	CTTGACAGAAGAAATAAAGTCTTCGGTCATATGAGAGTGTGTTGCGTAATTTG	P_{TAT2}

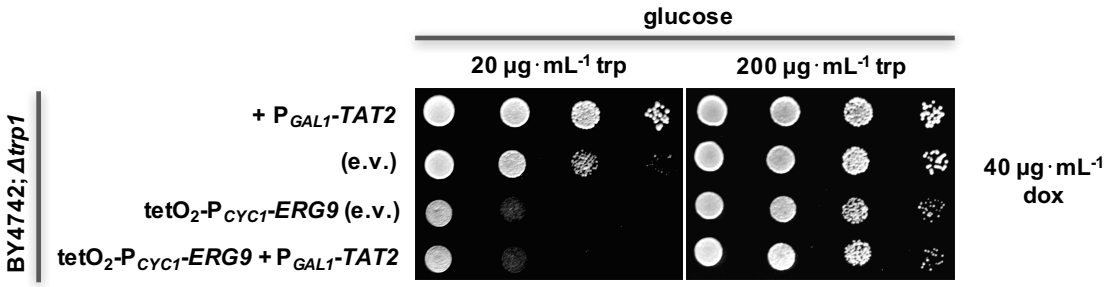

Fig. IV-S1: Growth of Δ*trp1* at intermediate and high tryptophan and strong doxycycline-mediated *ERG9* repression. Growth of plasmid harboring (empty pGREG503 (e.v.) or pGREG503-*TAT2*) Δ*trp1* cells in wild-type (BY4742) and $tetO_2$-P_{CYC1}-*ERG9* genetic background was compared at intermediate (20 µg·mL^{-1}) and high (200 µg·mL^{-1}) tryptophan concentrations as well as in the additional presence of 40 µg·mL^{-1} doxycycline (dox). Since *TAT2* in pGREG503-*TAT2* is expressed under control of the *GAL1* promoter (P_{GAL1}-*TAT2*), growth on glucose medium is not affected by the respectively harbored plasmid, since plasmid-based expression is only activated on galactose medium as shown in (Fig. IV-6C). Growth of the $tetO_2$-P_{CYC1}-*ERG9*; Δ*trp1* strains was severely impaired at intermediate tryptophan concentrations when *ERG9* expression was repressed (+dox) whereas cells grew unimpaired on high tryptophan medium even with repressed *ERG9* expression.

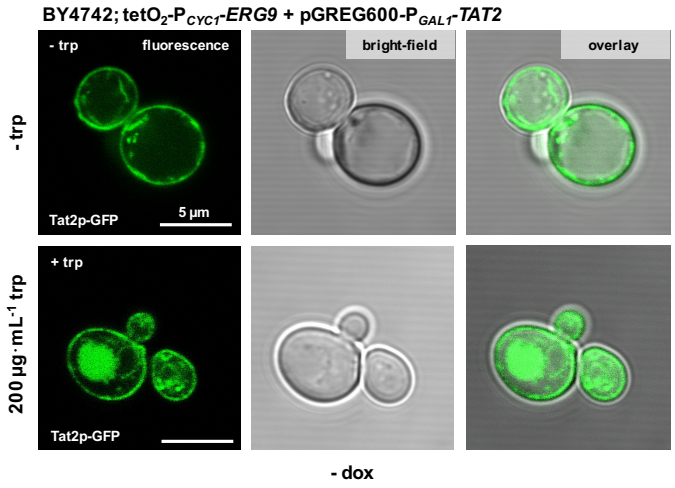

Fig. IV-S2: Tat2p is targeted to a great extent to the plasma membrane at high expression levels even under high tryptophan conditions. C-terminally GFP-tagged Tat2p was expressed from the strong *GAL1* promoter and subcellular localization was investigated in the presence (200 µg·mL^{-1}) and absence of tryptophan. Besides vacuolar delivery, Tat2p localized to the plasma membrane when expressed from the P_{GAL1} even at high external tryptophan concentrations.

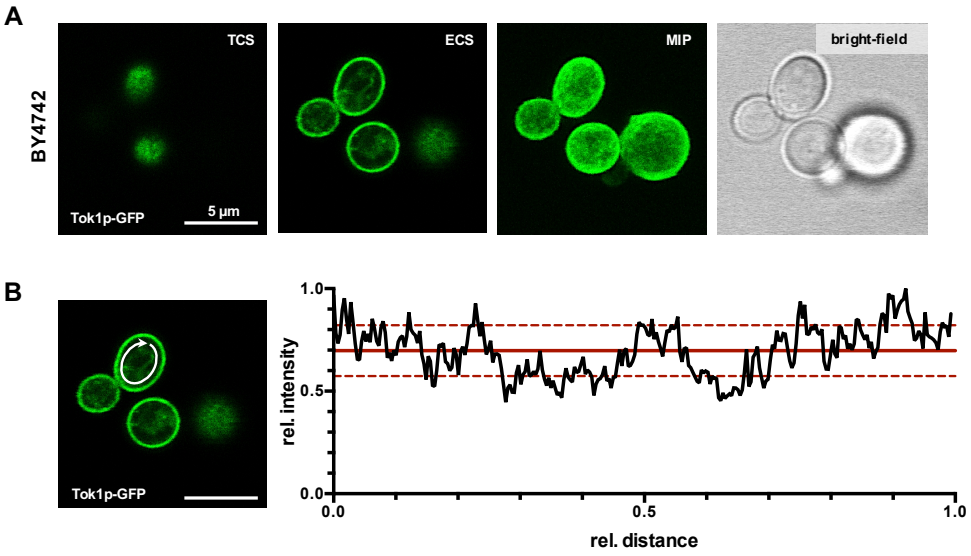

Fig. IV-S3: Tok1p-GFP is homogeneously distributed within the plasma membrane of yeast cells. (A) Fluorescence microscopy images of the tangential (TCS) equatorial (ECS) confocal sections as well as corresponding maximum intensity projections (MIP) and bright-filed images are shown. All images clearly show a homogeneous distribution of Tok1p-GFP within the plasma membrane of yeast. **(B)** Characteristic intensity profile of Tok1p-GFP fluorescence along the plasma membrane. The fluorescence intensity profile was tracked from the indicated ECS image and normalized to the maximal fluorescence intensity and track length. The mean fluorescence intensity (continuous red line) as well as standard deviations (dashed red line) were calculated for the total set of fluorescence intensity values and is indicated for comparison.

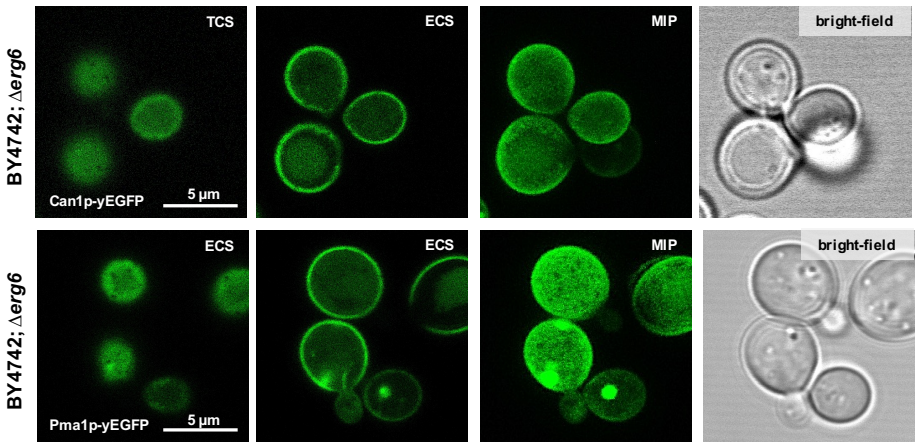

Fig. IV-S4: Lateral protein segregation within the plasma membrane as well as MCC and MCP integrity are disturbed upon knockout of *ERG6*. Fluorescence microscopy images of the tangential (TCS) equatorial (ECS) confocal sections as well as corresponding maximum intensity projections (MIP) and bright-field images are shown. BY4742 cells lacking Erg6p lose their characteristic punctuate pattern of Can1p-GFP distribution as well as the mesh-shaped pattern of Pma1p-GFP distribution within their plasma membrane.

Chapter V

Preloading budding yeast with all-in-one CRISPR/Cas9 vectors for easy and high-efficient genome editing

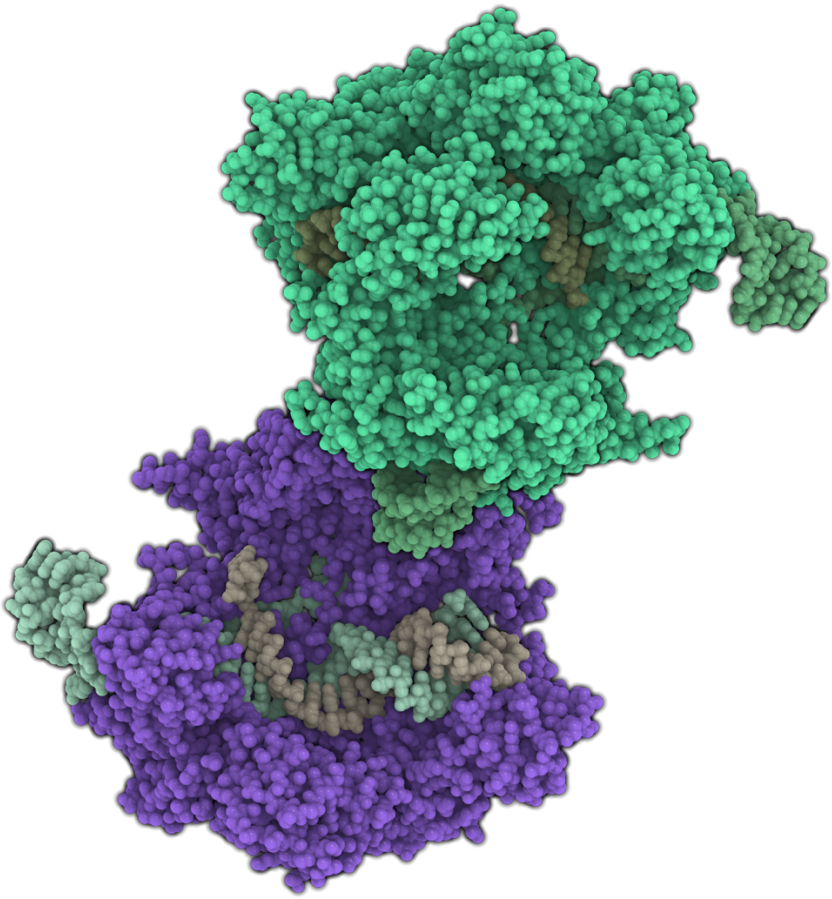

5. Chapter V: Preloading budding yeast with all-in-one CRISPR/Cas9 vectors for easy and high-efficient genome editing

5.1. Abstract

Previous chapters included many experiments using genetically modified yeast strains featuring gene knockouts, promoter replacements and genomically integrated gene expression cassettes. Generation of those strains is time consuming and even often fails when applying established genetic engineering techniques due to the limited efficiency of homologous recombination-based genomic manipulations in *S. cerevisiae*. The CRISPR/Cas9 technology has greatly improved genome editing in *S. cerevisiae* over recent years. However, current CRISPR/Cas9 systems also suffer from work-intensive cloning procedures and the requirement of co-transforming target cells with multiple system components at once which can reduce the effectivity of such applications. To overcome previously described limitations, a new set of all-in-one CRISPR/Cas9 vectors that mediate constitutive gRNA expression whereas Cas9 expression can be either driven from a constitutive or an inducible promoter was constructed. The introduction of desired gRNA targeting sequences into the here introduced inducible single gRNA vector relies simply on homologous recombination-mediated one-step assembly of overlapping single-stranded oligonucleotides, thus reducing efforts of plasmid cloning to an absolute minimum. By employing the inducible system, yeast cells can be easily preloaded with plasmids encoding for a functional CRISPR/Cas9 system, thereby chronologically separating the cloning procedure from the genome editing step. The CRISPR/Cas9 vectors were tested for conventional marker-based genome editing applications. Gene knockouts could be achieved with high efficiency and effectivity by simply transforming preloaded cells with a selectable disruption cassette without the need of co-introducing any CRISPR/Cas9 system component. Furthermore, the feasibility of efficient gene knockouts even when multiple gene copies were present such as in industrial (non-haploid) strain backgrounds is demonstrated. Simultaneous deletion of two different genes in a haploid genetic background was also possible by using a multiplex variant of the inducible all-in-one vector.

5.2. Introduction

The CRISPR/Cas9 technology has become an important and powerful tool in yeast genome editing and is by now a routinely used biomolecular technique in yeast laboratories all over the world. Daily routine benefits from a fast and affordable technique that is additionally easy in application. Thus, the „yeast community" has developed a number of variants of the CRISPR/Cas9 technology that allow for a convenient application of the system [1].
A functional CRISPR/Cas9 system consists of two components – the Cas9 endonuclease and a guide RNA (gRNA). The Cas9 protein binds the gRNA, which contains a 5'-terminal 20 bp targeting sequence, to form a functional protein-RNA complex. By this means, Cas9 is enabled to scan DNA targets such as genomic DNA in an gRNA-guided manner for sequences (so-called protospacer sequences) that are identical to the specific gRNA-targeting sequence. Identified target sequences are cleaved by the Cas9 endonuclease if a protospacer adjacent motif (PAM) follows the protospacer sequence within the genome. Early plasmid-based approaches employed separate vectors for expressing Cas9 and the gRNA. Thereby, gRNA cassette-encoding plasmids had to be cloned every time from scratch to target a new gene locus, resulting in an inconvenient overall procedure. Consecutive transformations of the Cas9 expression plasmid and the gRNA-encoding plasmid (plus donor DNA where applicable) were necessary to yield efficient gene disruption or genomic integration of the donor DNA since the overall efficiency suffers from the multiplicative linking of the efficiency of the individual transformation events. These restrictions could be avoided by stably integrating a Cas9 expression cassette into the genome so that only the gRNA has to be expressed from an episomal plasmid [2]. This way, genetic modifications can be performed efficiently by just co-transforming a respective gRNA-encoding plasmid together with the donor DNA. Nevertheless, this approach requires previous time-consuming genetic modifications of the desired background strain which also limits its simple use.

Recently, various approaches were published that allow for a simultaneous expression of Cas9 and the gRNA from a single plasmid as well as convenient introduction of the 20 bp gRNA protospacer sequence. This were either introduced by restriction free cloning [3], PCR-based amplification of the whole vector backbone combined with Gibson Assembly [4], Gibson Assembly-mediated introduction of oligonucleotides [5], Golden Gate Assembly with protospacer sequence containing gBlocks [6] or by classical restriction ligation-based cloning using hybridized oligonucleotides as an insert [7]. One-step transformation of all CRISPR/Cas9 system components together with the donor DNA yielded genomic editing in all cases. Although these approaches already allow for an easy application of the CRISPR/Cas9 technology additional improvements can help for further streamlining the

workflow by simultaneously further increasing the effectivity of CRISPR/Cas9-mediated genomic editing in *S. cerevisiae*. One improvement was inspired by the “synthesis of DNA fragments in yeast by one-step assembly of overlapping oligonucleotides” [8] which should be an appropriate method for a straightforward introduction of the 20 bp protospacer sequence into the expression vector. By using this method, plasmid cloning relies solely on the robust yeast-endogenous homologous recombination (HR) machinery without the need for any PCR applications or any other conventional *in vitro* cloning method. A second improvement should help to overcome limitations of transformation efficiency that result from co-transforming of multiple system components (donor DNA and gRNA/Cas9 encoding elements) which is an essential step of all so far published CRISPR/Cas9 technology variants. In the system presented here, the gRNA protospacer sequence is introduced into the plasmid by *in vivo* recombination-based cloning and subsequently uses yeast cells derived from a single clone for a second transformation with the respective donor DNA. Thus, every single yeast cell used for this second transformation should be already preloaded with all essential CRISPR/Cas9 components and the overall efficiency relies solely on the transformation efficiency regarding the donor DNA and is not a multiplicative product of single transformation efficiencies of different system components. By exploiting the tightly controllable yeast endogenous *GAL1* promoter for expression of the Cas9 endonuclease, the CRISPR/Cas9 system is kept inactive until donor DNA is delivered and intracellularly available, thus preventing induction of DSBs without proper repair using donor DNA as a template for homology directed repair.

5.3. Materials and Methods

5.3.1. Yeast strains

Experiments were performed with the haploid yeast strain CEN.PK2-1C [9], its diploid derivative CEN.PK2 [9] and the tetraploid yeast strain YCC78 (Y558) [10]. CEN.PK2 strains were obtained from EUROSCARF. Detailed information on the respective genotypes are available in Tab. V-1.

Wild-type strains were routinely cultured in YPD media (2% glucose, 2% peptone, 1% yeast extract). Strains harboring plasmids with the *URA3* marker were grown in appropriate synthetic defined drop-out media (2% glucose or 2% galactose, yeast nitrogen base (YNB), amino acid supplement without uracil). Cells were routinely propagated at 30°C.

Tab. V-1: Yeast strains used in this study. The table lists all strains with corresponding genotypes. Plasmids harbored by respective strains are named as indicated in Tab. V-S1.

strain	genotype	reference
CEN.PK2-1C	*MATa*; *his3Δ1*; *leu2-3,112*; *ura3-52*; *trp1-289*; *MAL2-8c*; *SUC2*	[9]
CEN.PK2-1D	*MATα*; *his3Δ1*; *leu2-3,112*; *ura3-52*; *trp1-289*; *MAL2-8c*; *SUC2*	[9]
CEN.PK2	*MATa/ MATα*; *his3Δ1/ his3Δ1*; *leu2-3,112/ leu2-3,112*; *ura3-52/ ura3-52; trp1-289/ trp1-289*; *MAL2-8c/ MAL2-8c*; *SUC2/ SUC2*	[9]
YCC78 (Y558)	*MATa/ MATa/ MATα/ MATα;* *ura3-52/ ura3-52/ ura3-52/ ura3-52;* *LYS2/ lys2-801/ LYS2/ lys2-801;* *ade2-101/ ade2-101/ ade2-101/ ade2-101;* *HIS3/ his3Δ200/ his3Δ200/ his3Δ200;* *trp1Δ1/ trp1Δ1/ trp1Δ1/ trp1Δ1;* *TYR1/ tyr1/ TYR1/ TYR1*	[10]
BY4741	*MATα*; *his3Δ*1; *leu2Δ*0; *met15Δ*0; *ura3Δ*0	[11]
SV-1	CEN.PK2-1C; pCAS9i-anti*ADE2*	This study
SV-2	CEN.PK2-1C; ade2::loxP-*LEU2*-loxP; pCAS9i-anti*ADE2*	This study
SV-3	CEN.PK2-1C; pCAS9i (empty)	This study
SV-4	CEN.PK2-1C; pCAS9id-anti*ADE2/CAN1*	This study
SV-5	CEN.PK2; pCAS9i-anti*ADE2*	This study
SV-6	YCC78; pCAS9i-anti*ADE2*	This study
SV-7	CEN.PK2-1C; pCAS9id-anit*MAT*x/*MAT*z	This study
SV-8	BY4741; pCAS9id-anit*MAT*x/*MAT*z	This study
SV-9	CEN.PK2-1C; pGREG506	This study
SV-10	BY4741; pGREG506	This study
SV-11	CEN.PK2-1D; pGREG506	This study

5.3.2. Plasmid construction and yeast transformation

The 2-micron (2µ) sequence of plasmid pRS425 was amplified with the primers P1 and P2 and used to replace the CEN/ARS sequence of the BglII/NheI (NEB) cleaved plasmid pCM188 [12] via recombination-based cloning resulting in plasmid pCM188(2µ). The gRNA expression cassette from plasmid p425-SNR52p-gRNA.HIS3-SUP4t (is equivalent to p426-SNR52p-gRNA.CAN1.Y-SUP4t [13] but with pRS426 backbone and anti*HIS3*-gRNA; kindly provided by Dr. Christopher Schneider; Technische Universität Darmstadt) was amplified with two individual PCRs (Q5 DNA polymerase, NEB) using overhang primers P3 & P4 (for P_{SNR52}) and P5 & P6 (for gRNA scaffold sequence - T_{SUP4}). The overhang primers were designed in a way that introduces a gRNA stuffer sequence (contains unique KpnI & MssI restriction sites) between P_{SNR52} and the gRNA scaffold sequence and allows for integrating the gRNA expression cassette into AvrI (NEB) cleaved vector pCM188(2µ). Assembly of the universal gRNA cassette and simultaneous integration into pCM188(2µ) were performed by *in vivo* recombination-based cloning. The *URA3* marker-2µ-universal gRNA cassette from the yielded plasmid was amplified (Q5 DNA polymerase, NEB) with the primers P7 & P8 and introduced into the KpnI & SnaBI cleaved plasmid p414-TEF1p-Cas9-CYC1t [13] by recombination-based cloning with simultaneous removal of the *TRP1* marker and the CEN/ARS sequence. The resulting plasmid was called pCAS9c (constitutive). To generate pCAS9i (inducible), P_{TEF1} from plasmid pCAS9c was replaced by P_{GAL1}. For that, pCAS9c was linearized with SpeI (NEB) and P_{GAL1} amplified (Q5 DNA polymerase, NEB) from plasmid pGREG504 [14] with primers P9 & P10 was introduced by recombination-based cloning. Multiplex plasmids pCAS9cd und pCAS9id (duplex) were generated by introducing a second gRNA expression cassette into NotI-cleaved plasmids pCAS9c and pCAS9i. The gRNA expression cassette was PCR-amplified (Q5 DNA polymerase, NEB) with primers P34 and P35 from plasmid pCAS9c or pCAS9i, respectively. All cloning products were checked by PCRs using pairs of primers that amplify a DNA fragment containing the artificial integration border that results from the HR event.

Transformation of CEN.PK2-1C for recombination-based cloning *in vivo* was routinely carried out by using the Frozen-EZ Yeast Transformation II kit (Zymo Research) according to the manufacturer's instructions. PCRs were performed according to the manufacturer's instructions. Primers and oligonucleotides used in this study are listed in Tab. V-1.

5.3.3. gRNA protospacer sequences

The anti-*ADE2* protospacer sequence (AATTGTAGAGACTATCCACA) was taken from the previously described CasEMBLR approach [15]. The anti-*CAN1* protospacer sequence

(GATACGTTCTCTATGGAGGA) was adopted from DiCarlo *et al.* [13]. The protospacer sequences anti-*ADE8* (GAGAACAAGCCTCTGACGGC), anti-*MAT*x (TCTTCTGTTGTTAC ACTCTC) and anti-*MAT*z (CACTCTACAAAACCAAAACC) were designed by using the ATUM gRNA Design Tool (https://www.atum.bio/eCommerce/cas9/input).

5.3.4. Assembly PCR

A full-length gRNA expression cassette that contains an *ADE2* targeting protospacer sequence was constructed via assembly PCR. First, two individual fragments were amplified (Q5 DNA polymerase): P11 & P12 were used to amplify P_{SNR52} (F1; 311 bp) and P13 & P14 were used to amplify the gRNA scaffold - T_{SUP4} sequence (F2; 211 bp) from vector pCAS9c, respectively. P12 & P13 are overhang primers that introduce the 20 bp *ADE2* targeting protospacer sequence to one end of both fragments, respectively, that also functions as overlapping regions for the assembly reaction. F1 and F2 were gel purified (Zymoclean Gel DNA Recovery Kit, Zymo Research) and 3 µL of each gel purified fragment were used as a template for a second PCR (assembly reaction; Q5 DNA polymerase, NEB) employing primers P11 & P14. The resulting assembly product (AP; 502 bp) was checked via gel electrophoretic analysis (Fig. V-S1).

5.3.5. Introduction of gRNA protospacer sequences into plasmids pCAS9c(d) and pCAS9i(d)

Different methods (A; B; C) were used to introduce the respective gRNA protospacer sequence into plasmids pCAS9c(d) and pCAS9i(d):

Method A: Co-transformation of KpnI & PmeI (NEB) cleaved plasmid pCAS9c/pCAS9i (250 ng) with oligonucleotides (500 pmol each; P12 & P13 for *ADE2;* P28 & P29 for *ADE8*) carrying the protospacer sequence or the complementary sequence, respectively, at their 5' ends.

Method B: Co-transformation of KpnI & PmeI (NEB) cleaved plasmid pCAS9c/pCAS9i (250 ng) with the anti-*ADE2* gRNA expression cassette (10 µL) generated via assembly PCR.

Method C: The entire vector backbone was amplified (Q5 DNA polymerase, NEB) with primers carrying the protospacer sequence or the complementary sequence, respectively, at their 5' ends (P12 & P13 for *ADE2;* P28 & P29 for *ADE8*) using KpnI & PmeI cleaved pCAS9c/pCAS9i as the template. 20 µL of the unpurified PCR product were directly used for transformation. In case of pCAS9cd/pCAS9id, the plasmids were amplified by two individual PCRs with overhang primers adding different gRNA protospacer sequences to the ends of each plasmid fragment (pCAS9id-anti*ADE2*/*CAN1*: P12 & P36 for the large

fragment, P13 & P37 for the short fragment; pCAS9id-anti*MAT*x/*MAT*z: P41 & P42 for the large fragment, P40 & P43 for the short fragment). The large fragments are amplified from NotI-cleaved template plasmids whereas StuI & SalI cleaved plasmids serve as templates for amplifying the short fragments. 10 µL of each PCR product were used for transformation. Circularization of the plasmids should be achieved for all methods via homologous recombination in yeast without requiring any other *in vitro* cloning method. This keeps the systems as simple as possible.

As a proof of principle, successful introduction of the *ADE2* targeting protospacer sequence into plasmid pCAS9i with methods A, B or C was proved with colony PCR. A pair of primers was used with one primer (P25) binding within the protospacer sequence and the other one (P26) within the plasmid backbone.

5.3.6. Assays for testing functionality and efficiency of pCAS9c- and pCAS9i-based approaches

For testing plasmid pCAS9c, yeast cells were inoculated at OD_{600} = 0.2 – 0.3 in YPD and grown to OD_{600} = 0.9 – 1.0 at 30°C with continuous shaking (200 rpm). Cells from 4 mL of this suspension were used for transformation using a commercial kit (Frozen-EZ Yeast Transformation II kit; Zymo Research). Depending on the method (A; B; C) employed for introducing the gRNA protospacer sequence, cells were transformed with the respective DNA components and PCR-amplified donor DNA (loxP-*LEU2*-loxP for *ADE2* locus: 1 µg (20 µL); loxP-*LEU2*-loxP as 500 bp fragments for *ADE2* locus: 0.5 µg (10 µL) each; loxP-kanMX-loxP for *ADE8* locus: 1 µg (20 µL); *HIS3* for *CAN1*: 1µg (20µL)).

The respective gRNA targeting sequence was introduced in plasmid pCAS9i using method A (for pCAS9id with method C) and cells harboring pCAS9i with introduced gRNA targeting sequence were selected on SD-ura agar plates. Single colonies were inoculated in SD-ura and grown over night at 30°C. From the overnight cultures, fresh cultures were set up at OD_{600} = 0.2 – 0.3 in SD-ura and grown to OD_{600} = 0.9 – 1.0 at 30°C with continuous shaking (200 rpm). Cells from 4 mL suspension were washed once with sterile water, transferred to 4 mL SGal-ura medium and incubated for 1 h at 30°C. These cells were transformed with PCR-amplified donor DNA (see above) using the Frozen-EZ Yeast Transformation II kit (Zymo Research).

To enhance transformation efficiency, cells were resuspended in 1 mL YPD (pCAS9c) or YPGal (pCAS9i) after incubation in EZ3 solution (1 h) and incubated at 30°C for 2 h for recovery. After the recovery period, cells transformed with loxP-*LEU2*-loxP donor DNA were spread on SD-ura-leu or SGal-ura-leu agar plates, respectively. YCC78 cells that were transformed with loxP-kanMX-loxP donor DNA were plated on YPD+G418 (200 $\mu g \cdot mL^{-1}$) or

YPGal+G418, respectively, to select for positive transformants. G418 resistant transformants were replica plated on SD-ura plates to screen for the presence of pCAS9 plasmids. Cells that were disrupted in the *CAN1* locus were selected in arginine-free (-arg) canavanine-containing (60 µg/L) medium.

For gRNA negative control experiments (-gRNA), unmodified plasmids pCAS9c or pCAS9i (250 ng) harboring no proper gRNA targeting sequence were employed for previously described approaches.

loxP-*LEU2*-loxP donor DNA for integration into the *ADE2* locus was amplified from plasmid pUG73 [16] by PCR (OneTaq DNA polymerase, NEB) using primers P15 and P24. Fragmented loxP-*LEU2*-loxP donor DNA was PCR-amplified as five separate 500 bp fragments (F1: P15 & P16; F2: P17 & P18; F3: P19 & P20; F4: P21 & P22; F5: P23 & P24). loxP-kanMX-loxP donor DNA for integration into the *ADE8* locus was amplified from plasmid pUG6 [17] by PCR (OneTaq DNA polymerase, NEB) using primers P30 and P31. *HIS3* donor DNA for integration into the *CAN1* locus was amplified from plasmid pGREG504 [14] by PCR (OneTaq DNA polymerase, NEB) using primers P38 and P39. PCR-amplified donor DNA had approx. concentrations of 50 ng·µL^{-1} as determined by comparison to DNA marker ladder so that 1 µg of donor DNA in total (20 µL) was typically employed for each transformation.

Assays to determine plasmid functionality and efficiency were performed as at least biological triplicates. The arithmetic mean was calculated to determine the average number of positive transformants.

5.3.7. Colony PCR

Colony PCRs were performed in order to confirm the integration of donor DNA into the respective locus. A pair of primers was used with one primer binding within the genomic locus and the other one within the integrated donor DNA cassette so that a PCR product (loxP-*LEU2*-loxP in *ADE2*: P27 & P16; loxP-kanMX-loxP in *ADE8*: P32 & P33) only appears when the right cassette was integrated into the right locus. For preparing the PCR template, yeast cells were suspended in 30 µL of 0.2% SDS and incubated for 10 min at 95°C. 0.5 µL of the cell suspension was used as template for a 25 µL PCR mix. Colony PCRs were conducted with the Taq polymerase (OneTaq 2X Master Mix with Standard Buffer; NEB).

5.4. Results and Discussion

5.4.1. General design of the system

The aim was to develop a CRISPR/Cas9 system for application in *S. cerevisiae* that is based on a single plasmid and especially allows for a simple introduction of a gRNA protospacer sequence for targeting any desired gene or locus of the yeast (nuclear) genome. For that, plasmid pCAS9c was constructed that harbors a 38 bp stuffer within its gRNA expression cassette which serves as a placeholder for the protospacer sequence to be introduced. The stuffer can be easily removed by simply double-cleaving pCAS9c with KpnI and PmeI (Fig. V-1A). The "synthesis of DNA fragments in yeast by one-step assembly of overlapping oligonucleotides" [8] was considered to be appropriate as a fast, easy and low-cost method for introducing a desired 20 bp gRNA protospacer sequence into the double-cleaved plasmid. By using this method, protospacer introduction and plasmid recircularization would rely solely on the robust yeast-endogenous homologous recombination (HR) machinery without the need for any PCR applications or any other conventional *in vitro* cloning method. Just commercially available short oligonucleotides that not even need to be hybridized beforehand would be required to introduce and determine any desired protospacer sequence.

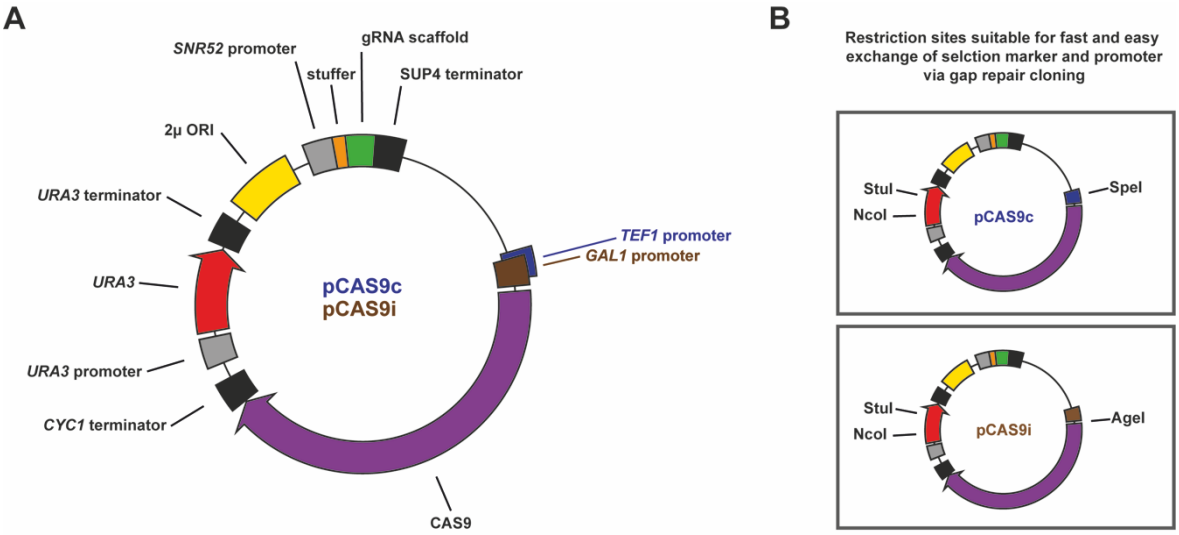

Fig. V-1: Schematic representation of the all-in-one gRNA-Cas9 expression vectors pCAS9c and pCAS9i. (A) Both plasmids contain identical backbone elements such as an *URA3* selection marker, a 2-micron (2 µ) sequence and an ampR bacterial selection marker (not shown) as well as a universal gRNA expression cassette consisting of the yeast-endogenous *SNR52* promoter, the constant guide RNA scaffold sequence and the *SUP4* terminator sequence. A stuffer sequence serves as a placeholder for the respective gRNA targeting (protospacer) sequence. Both plasmids differ in the promoter that is driving the expression of the Cas9 gene. Cas9 is either expressed from the constitutive *TEF1* promoter (pCAS9c) or from the inducible *GAL1* promoter (pCAS9i). **(B)** Both plasmids harbor specific restriction sites that allow for an easy exchange of the *URA3* selection marker (StuI, NcoI) and the respective promoter sequences (P_{TEF1}: SpeI; P_{GAL1}: AgeI) via gap repair cloning.

Plasmid pCAS9c was furthermore designed to support its convenient application: Plasmid pCAS9c harbors a 2µ ORI (Fig. V-1A) that allows for a high copy number and promotes high expression levels of gRNA and Cas9. Additionally, 2µ plasmids show decreased segregational stability as compared to centromeric plasmids [18] which benefits the loss of pCAS9c after genome editing operations. The *URA3* selection marker allows for positive selection of cells, that have lost pCAS9c plasmids, on 5-FOA containing media [19]. However, the application of pCAS9c is not limited to the use of *URA3* as selection marker since pCAS9 plasmids contain unique restriction sites (Fig. V-1B) that allow for a fast and easy exchange of boths, the selection marker as well as the *TEF1* promoter via gap repair cloning. This way, these plasmids provide a good basis for generating derivative plasmids harboring dominant antibiotic resistance markers (kanMX, natMX) that are useful to maintain pCAS9 plasmids in wild yeasts and industrial strains that do not support the use of standard selection markers. Promoter exchange might be desired if high Cas9 expression levels from pCAS9c severely impair growth of the background strain, as it was described elsewhere [4].

5.4.2. Single plasmid-mediated CRISPR/Cas9 genome editing

The *ADE2* locus was selected as target for site-specific cleavage and for subsequent integration of a donor DNA cassette (loxP-*LEU2*-loxP) that serves as a template for homologous recombination-based repair of gRNA-Cas9 induced DNA double-strand breaks (DSBs). The *ADE2* locus was chosen since interruption of the adenine biosynthetic pathway at the stage of Ade2p leads to the intracellular accumulation of a red pigment (AIR) and accordingly to the formation of red colonies [20] which serves as an easy assay read-out. Red colony color in combination with a Leu^+ phenotype indicates that the desired donor DNA was integrated in the right locus and therefore clearly characterizes positive transformants.

To functionally test the pCAS9c plasmid construct, cells of the haploid laboratory strain CEN.PK2-1C were co-transformed with KpnI & PmeI cleaved pCAS9c, oligonucleotides carrying the *ADE2* targeting protospacer sequence or the complementary sequence, respectively, at their 5’ ends (method A) as well as PCR-amplified loxP-*LEU2*-loxP donor DNA. Method A would serve as an extraordinarily straightforward approach if protospacer introduction into plasmid pCAS9c by assembling overlapping oligonucleotides would be efficient enough to allow for a single transformation to deliver all the required CRISPR/Cas9 components (Cas9, gRNA, donor DNA) into a cell. However, no transformants could be obtained by using this approach (Fig. V-3A) which might be due to a low efficiency of

recombination between two individual ss-oligonucleotides and the linearized plasmid compared to when a single dsDNA fragment derived from two annealed ss-oligos is employed as protospacer insert that worked for other approaches [2]. To test the general functionality of plasmid pCAS9c, the previous transformation was repeated, but both ss-oligonucleotides were replaced by a pre-assembled gRNA expression cassette (10 µL) (method B) constructed by assembly PCR (Fig. V-S1). This approach gave approximately 30 positive transformants, whereas a control experiment without gRNA in which only uncleaved and unmodified pCAS9c was used (-gRNA control) yielded no transformants (Fig. V-3A;B). This demonstrates that anti-*ADE2* gRNA and Cas9 were successfully expressed from pCAS9c and CRISPR/Cas9-mediated cleavage of *ADE2* efficiently promoted genomic integration of the loxP-*LEU2*-loxP donor DNA. It was tested further, whether plasmid pCAS9c is also suitable for an approach where the gRNA protospacer sequence is introduced by amplifying the whole vector backbone with overhang primers carrying the anti-*ADE2* protospacer sequence at their 5' ends, respectively (method C). Circularization of the plasmid and thereby reconstitution of the functional gRNA expression cassette are obtained by *in vivo* homologous recombination. CEN.PK2-1C was co-transformed with the PCR-amplified pCAS9c backbone and loxP-*LEU2*-loxP donor DNA. This approach yielded a similar number of transformants as the previously described approach that used a pre-assembled gRNA expression cassette (Fig. V-3A;B).

5.4.3. High-efficient genome editing by preloading yeast with all-in-one CRISPR/Cas9 vectors

To follow up on a straightforward approach that utilizes one-step assembly of overlapping single-stranded oligonucleotides for introducing the protospacer sequence, plasmid pCAS9c was further modified. For this, the constitutive *TEF1* promoter of pCAS9c was replaced with the tightly controllable and inducible yeast endogenous *GAL1* promoter, yielding plasmid pCAS9i (Fig. V-1A). A desired protospacer sequence can be introduced into pCAS9i via *in vivo* homologous recombination-based cloning by either using cloning method A, B or C without being at risk to generate lethal gRNA-Cas9 induced DNA DSBs. This way, plasmid assembly and CRISPR/Cas9-mediated genome editing (e.g. donor DNA integration) can be chronologically separated into two individual sequential steps.

Cloning methods A, B and C (Fig. V-2) were proved to be suitable to introduce the *ADE2* gRNA targeting sequence into plasmid pCAS9i as confirmed by colony PCR (Fig. V-S2). Since cloning method A is the least labor-intensive and therefore most interesting approach, three randomly selected transformants generated with this method were used for further proceeding. All cells derived from a single transformant harbor plasmid pCAS9i that

encodes for the Cas9 endonuclease as well as the anti-*ADE2* gRNA. By switching cells to galactose medium (SGal-ura) for 1 h prior to transformation with donor DNA (Fig. V-2), every single cell that is used for transformation should be already pre-loaded with anti-*ADE2* gRNA and Cas9, so that a functional CRISPR/Cas9 system is constituted, enabling introduction of DSBs in the *ADE2* locus. Only those cells in which DSBs were repaired by correct integration of the loxP-*LEU2*-loxP cassette were selected on appropriate medium (SGal-leu-ura).

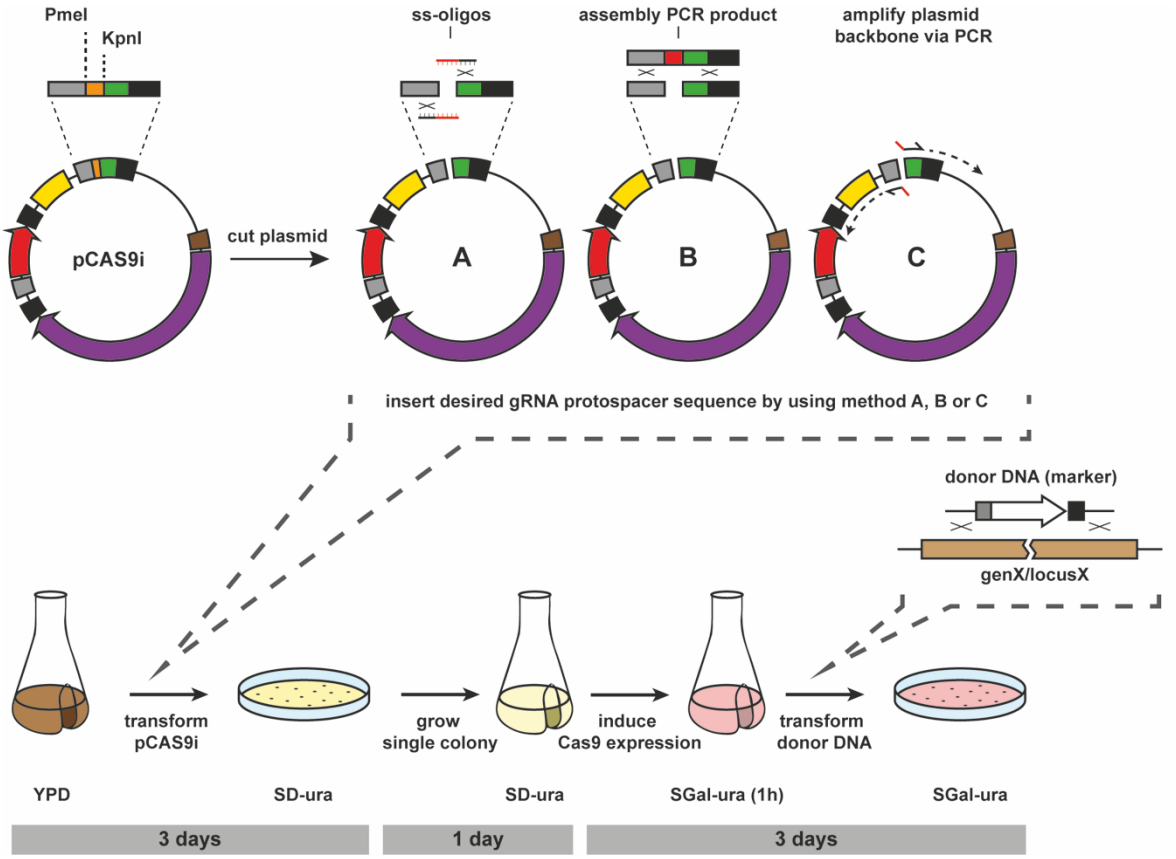

Fig. V-2: General experimental procedure of pCAS9i-supported CRISPR/Cas9 genome editing in *S. cerevisiae*. The stuffer sequence of plasmid pCAS9i is removed by double-cleaving the vector with KpnI and PmeI (top left). A desired protospacer sequence can be introduced into the linearized vector pCAS9i by method A (one-step assembly of overlapping single-stranded oligonucleotides), method B (introduction of a gRNA expression cassette previously generated with assembly PCR) or method C (PCR amplification of pCAS9i backbone with overhang primers that add the protospacer sequence to both ends of the PCR product) (top row). The target strain is (co-)transformed with all plasmid components so that plasmid assembly and recircularization occurs *in vivo* by recombination-based cloning. Positive transformants are selected on SD-ura agar plates (bottom left). Proper introduction of the desired gRNA protospacer sequence into plasmid pCAS9i can be checked optionally by colony PCR. A single transformant harboring the protospacer containing plasmid (pCAS9i-anti*X*) is grown overnight in SD-ura liquid medium and used for a second transformation with the respective donor DNA to be genomically integrated. Prior to this second transformation pCAS9-anti*X* harboring cells are shifted to SGal-ura medium for 1 h in order to introduce Cas9 expression from the *GAL1* promoter and preloading cells with gRNA and the Cas9 endonuclease. Transformed cells can be selected on appropriate SGal agar medium. If a donor DNA contains a selection marker, cells may be spread on SGal-ura medium that is lacking for a second nutrient (bottom row).

The pCAS9i-based approach was expected to be much more efficient than the one that uses pCAS9c, since negative effects resulting from the inevitable requirement of co-transforming more than one system component, as well as of temporal timing of gRNA/Cas9 expression and donor DNA delivery/ availability are not prejudicial to the overall efficiency anymore. Indeed, with an identical number of cells employed for transformation, obtained some 20-fold more positive transformants were obtained with the pCAS9i-based approach, as compared to the afore described approaches (Fig. V-3A,B). Obtained transformation efficiencies (Tab. V-2) were in the same range as for previously reported CRISPR/Cas9 applications [13]. Identical results can be expected when strains are used that were derived from cloning methods B and C since both of them yield exactly the same plasmid pCAS9i-anti*ADE2*. A control strain harboring unmodified pCAS9i (without the anti-*ADE2* protospacer sequence) yielded no positive transformants after transformation with donor DNA (Fig. V-3A).

Disruption of *ADE2* by genomic integration of the loxP-*LEU2*-loxP cassette was confirmed by colony PCR with five randomly selected transformants obtained by using plasmids pCAS9c and pCAS9i-based approaches. All tested transformants were confirmed to be positive with no exception (Fig. V-S3).

To characterize the efficiency of plasmid loss after genome editing, positive transformants were cultured for a single round in non-selective medium (YPD) overnight. Subsequently, cells were spread on YPD to obtain single colonies and colonies were picked and streaked on YPD and SD-ura agar plates. 94% (47 from 50) of the cells did not grow on uracil-free medium anymore which indicates a high frequency of plasmid loss. In daily lab applications, *URA3* would also allow for a positive selection of plasmid-freed cells on 5-FOA containing medium.

5.4.4. pCAS9i-mediated toxicity

Unrepaired DNA DSBs are lethal in *S. cerevisiae* [21, 22] leading to a beneficial reduction of false positive clones in CRSIPR/Cas9 applications. Therefore, the degree of toxicity caused by the expression of a functional CRISPR/Cas9 system from plasmid pCAS9i-anti*ADE2* should be determined. For that, plasmid pCAS9i-anti*ADE2* harboring cells were spotted in 10-fold serial dilutions on uracil-free glucose (SD-ura) or galactose (SGal-ura) containing medium that only selects for plasmid-carrying cells. On glucose containing medium, cells grew unaffected as Cas9 expression is repressed, whereas galactose containing medium, i.e. expression of a functional Cas9-gRNA complex, strongly impaired growth (Fig. V-3C). Cells that were either expressing a functional *ADE2*-targeting CRISPR/Cas9 system but provided no proper genomic target sequence that could be

addressed by the Cas9-gRNA complex (a strain that was already disrupted in *ADE2* by previously CRISPR/Cas9-supported donor DNA integration) or that contained the native *ADE2* locus but expressed no *ADE2*-targeting gRNA (empty pCAS9i harboring the protospacer stuffer sequence) served as controls that were expected to grow unaffected.

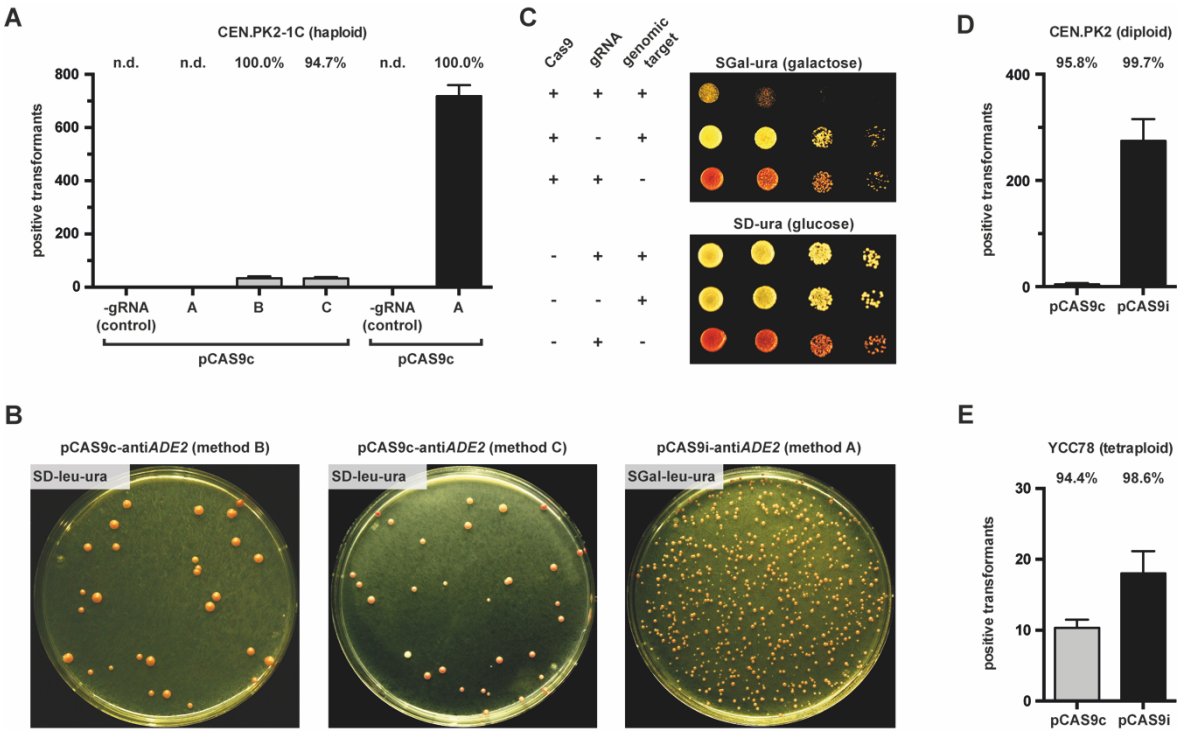

Fig. V-3: Application of Cas9- and gRNA-encoding plasmids pCAS9c- and pCAS9i for CRISPR/Cas9-supported genome editing of yeast cells with different ploidy levels. (A) An *ADE2* disruption (*ade2*::loxP-*LEU2*-loxP) was introduced in the haploid strain CEN.PK2-1C by pCAS9c- (grey bars) or pCAS9i- (black bars) based approaches and the number of positive (knockout) transformants was determined. gRNA negative controls (-gRNA; used unmodified plasmids pCAS9c or pCAS9i that do not encode for a functional anti-*ADE2* gRNA) yielded no positive transformants. Mean values and standard deviations from at least triplicate experiments are indicated. The identical number of cells was employed for each transformation and approach. Efficiencies are indicated above the bars and represent the percentage of positive transformants of all cells that survived after transformation on the SGal-leu-ura selection media. n.d. = not detected **(B)** Representative agar plates showing the number of positive *ADE2* knockout transformants of the haploid strain CEN.PK2-1C (see A) that were yielded with approaches that used pCAS9c (method B or method C) or pCAS9i (method A). Cells were selected on indicated media, respectively. **(C)** pCAS9i-mediated toxicity was investigated by spotting plasmid pCAS9i-anti*ADE2* harboring cells in 10-fold serial dilutions on glucose and galactose containing media, respectively. Growth on galactose containing media was severely impaired as Cas9 expression is activated. Control strains that do not express a functional gRNA (empty pCAS9i without anti-*ADE2* protospacer sequence) or that do not provide a proper genomic protospacer sequence (cells are already disrupted in *ADE2* by previously CRISPR/Cas9-supported donor DNA integration) grew unimpaired on galactose containing medium. **(D)** Number of diploid CEN.PK2 cells with successfully disrupted *ADE2* by pCAS9c- (grey bars) or pCAS9i- (black bars) based approaches. **(E)** For the tetraploid strain YCC78, CRISPR/Cas9-supported disruption of *ADE8* (*ade8*::loxP-kanMX-loxP) was performed with a pCAS9c- or a pCAS9i-based approach and the number of positive transformants was determined. Unless specified differently (as for CEN.PK2-1C), anti-*ADE2*/*ADE8* protospacer sequence was introduced into pCAS9c by method C and into pCAS9i by method A. For further explanations of the graphs see (A).

Both control strains grew unimpaired on galactose containing media (Fig. V-3C). These results indicate a high degree of CRISPR/Cas9-induced toxicity when no donor DNA for HR-mediated repair of DSBs is available and helps to select for positive transformants in the pCAS9i-based CRISPR/Cas9 approach.

For a similar test, highly diluted suspensions of pCAS9i-anti*ADE2* harboring CEN.PK2-1C cells as well as of the previously described control strains were plated on glucose- (SD-ura) and galactose containing (SGal-ura) media to obtain single colonies. On glucose containing medium, colonies recovered from all plated cells for all tested strains (Fig. V-S4), whereas galactose strongly impaired the appearance of colonies when pCAS9i-anti*ADE2* was present in an unmodified CEN.PK2-1C genetic background (Fig. V-S4A). Only a small percentage of cells (2.7 ± 0.5%; n = 3) formed colonies with the same size as cells did on the reference media (SD-ura) (Fig. V-S4A). The vast majority (93.3 ± 2.5%; n = 3) of these cells that survived and grew unaffected on the SGal-ura medium turned out to be *ade2* knockout mutants as evaluated from their phenotype (red colony color; Ade^- as confirmed by replica plating on SGal-ura-ade medium). *ADE2* knockouts most probably resulted from NHEJ-mediated imperfect DNA repair and accompanying indel errors. Those errors additionally destroy the proper genomic gRNA-Cas9 targeting sequence thus protecting cells from further toxic DNA DSBs and simultaneously selecting for cells with imprecisely repaired DNA. This way, the pCAS9i-based approach provides an efficient tool to introduce gene knockouts that is extremely simple in application, just requires two approximately 50 bp oligonucleotides and not even involves a single PCR step.

5.4.5. Editing the genome of diploid and tetraploid yeast strains

Unlike most laboratory strains, wild yeasts and industrial strains do not harbor a single set of chromosomes, but they are rather diploid [23-25] or even feature higher ploidy levels that can e.g. derive from allo- or autopolyploidization [26]. Since metabolic engineering approaches to improve fermentation performance or product yield of industrial strains often require the knockout of genes that are e.g. involved in competing metabolic pathways [27], highly efficient CRISPR/Cas9 systems are crucial as multiple copies of the same gene have to be addressed at once. Wild yeasts are usually not accessible to metabolic engineering approaches since they do not feature any auxotrophies [23] and therefore e.g. do not support plasmid maintenance. In this case, the deletion of all copies of a marker gene is required to generate auxotrophic mutants [28]. To test the plasmid-based systems for such purposes, the diploid (2n) strain CEN.PK2 as well as the tetraploid (4n) strain YCC78 were employed instead of the haploid strain CEN.PK2-1C. For diploid CEN.PK2, *ADE2* was targeted the same way as previously described for its haploid strain derivative with the

difference that red coloring of colonies this time indicates the knockout of both *ADE2* copies. However, the *ADE2*-based assay could not be applied for the tetraploid strain YCC78 since its four *ADE2* copies already encode for a dysfunctional protein variant (Tab. V-1). Here, *ADE8* was targeted instead, which encodes for a protein that acts upstream of Ade2p in the adenine biosynthetic pathway and exploited the epistatic relationship of *ade8* over *ade2* to select for white colonies [20]. White coloring of colonies indicates a knockout of all four *ADE8* gene copies.

For application in strain backgrounds with higher ploidy levels, the respective protospacer sequences was introduced into plasmid pCAS9c with method C and into plasmid pCAS9i with method A (Fig. V-2). By employing plasmid pCAS9c for disrupting *ADE2* in diploid CEN.PK2 cells, only a few positive transformants were obtained, whereas the pCAS9i-based approach yielded hundreds of transformants (Fig. V-3D) that could be evaluated as being positive based on their phenotype (red colony color; Leu^+). Also for the tetraploid background strain, both plasmid-based approaches yielded quadruple *ade8* knockout mutants, as clearly evident from the white appearance of the obtained colonies. Moreover, successful genomic integration of the loxP-kanMX-loxP donor DNA into the *ADE8* locus was confirmed by colony PCR (Fig S5). The pCAS9i-approach yielded twice as much positive transformants of YCC78 as compared to the pCAS9c use, even though the absolute number of positive transformants was generally lower than for haploid or diploid strain backgrounds (Fig. V-3D). Measured transformation efficiencies emphasize highly efficient genome editing (Tab. V-2). A few single di- and tetraploid transformants appeared to feature the respective positive growth phenotype (Leu^+ or G418 resistant), suggesting the integration of the marker cassette, but seem not to have all gene copies deleted as indicated by their colony coloring, e.g. white diploids or red tetraploids. Such false transformants arose at lower rate for pCAS9i- (2n: < 1%; 4n: < 2%) than for pCAS9c-based (2n: < 5% & 4n: < 6%) approaches.

5.4.6. Multiplex genome editing

To test the plasmid systems for multiplex genome editing applications a second gRNA expression cassette was inserted into plasmids pCAS9c and pCAS9i yielding plasmids pCAS9cd and pCAS9id (duplex) that allow for expression of two different gRNAs. Each plasmid can be amplified by two individual PCRs that add different protospacer sequences to one end of each fragment, respectively (similar to method C). These protospacer sequences function additionally as homology sequences for correct plasmid circularization by homologous recombination *in vivo*. Since both pairs of primers feature identical annealing sequences, NotI-digested (Primers PW & PZ; for large fragment) or StuI/SalI-

cleaved (Primers PX & PY; for short fragment) plasmids have to be employed as PCR templates to prevent the amplification of the corresponding undesired part of the plasmid (Fig. V-4A). The *CAN1* locus was chosen as second genomic target since its disruption allows for positive selection and therefore provides the possibility to select for the correct integration of the right donor DNA into the right locus as it is also true for the previously used *ADE2*-based assay.

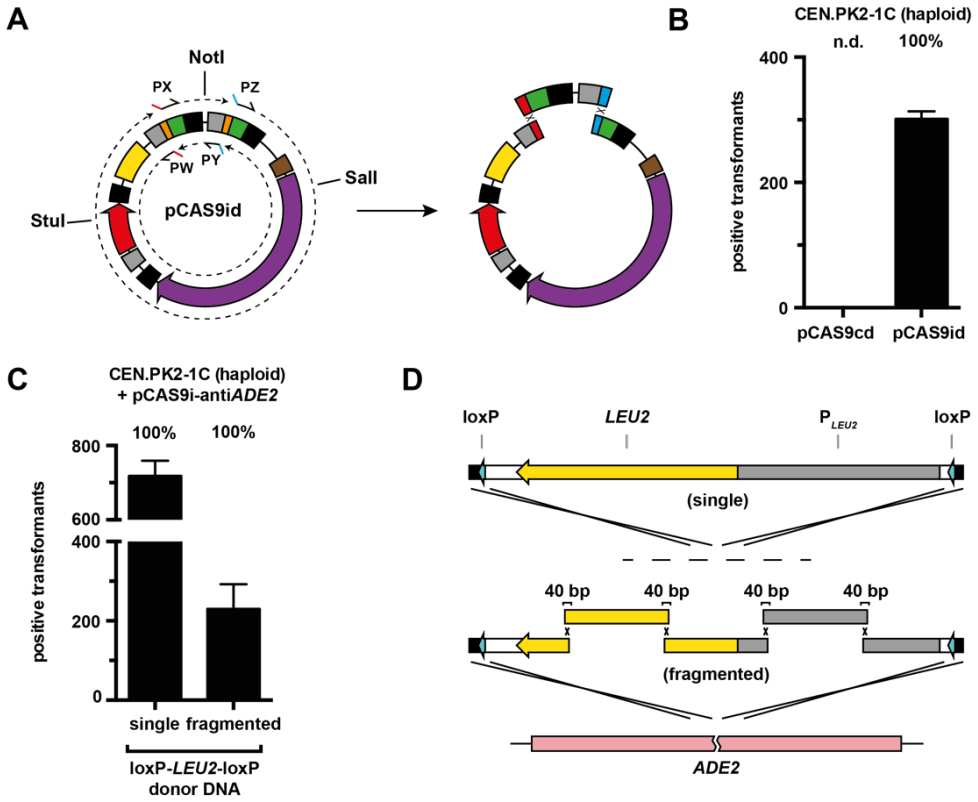

Fig. V-4: Multiplex genome editing and simultaneous assembly and CRISPR/Cas9-mediated integration of a fragmented donor DNA. (A) Plasmid pCAS9id is amplified by two individual PCRs to add both different protospacer sequences to one end of both fragments, respectively. Linearized plasmids are employed as PCR template to avoid the amplification of the undesired plasmid fragment (NotI-cleaved plasmid for use with primers PW & PZ; StuI/SalI-cleaved plasmid for use with primers PX & PY). Note: Primers PX & PZ and PW & PY, respectively, contain identical annealing sequences which would result in four different PCR products if uncut plasmid is employed as PCR template. The gRNA protospacer containing plasmid is subsequently circularized by homologous recombination-based cloning *in vivo*. **(B)** Simultaneous disruption of *ADE2* (*ade2*::loxP-*LEU2*-loxP) and *CAN1* (*can1*::*HIS3*) in the haploid strain CEN.PK2-1C was successfully achieved by using an pCAS9id-based approach. The efficiency is indicated above the bar and represents the percentage of positive transformants of all cells that survived after transformation on the SGal-leu-ura-his-arg + canavanine (60 mg/L) selection media. **(C)** The pCAS9i-based approach was tested to support the *in vivo* assembly and simultaneous integration of multiple DNA fragments. The number of positive transformants was compared when the loxP-*LEU2*-loxP donor DNA was genomically integrated as a single fragment (single; data taken from Fig. 1A) or as five individual fragments (fragmented) that have to be assembled additionally. Efficiencies are indicated above the bars and represent the percentage of positive transformants of all cells that survived after transformation on the SGal-leu-ura selection media. **(D)** The fragmented loxP-*LEU2*-loxP donor DNA (2.5 kbp) was split up into five 500 bp fragments that share 40 bp of homology to each other, respectively (bottom).

Haploid CEN.PK2-1C cells were co-transformed with both pCAS9cd-anti*ADE2*/*CAN1* PCR fragments as well as with both donor DNA cassettes (loxP-*LEU2*-loxP for *ADE2* and *HIS3* for *CAN1*) and plated cells on SD-ura-leu-his-arg + canavanine medium, however, yielding no transformants. In contrast, cells that were preloaded with pCAS9id-anti*ADE2*/*CAN1* and subsequently transformed with both donor DNA fragments were successfully deleted in both genes simultaneously with high efficiency (Fig. V-4B). Approximately 300 positive transformants were obtained as one could evaluate from their phenotype (red colony color; canavanine resistant; Leu^+; His^+). Due to its low-labor intensive workflow the all-in-one plasmid-based approach is considered as advantageous to previously described multiplex genome editing applications. For these, successful genome engineering was only possible when double gRNA expression vectors were assembled beforehand by standard cloning methods and employed for co-transformation together with donor DNA [2, 4].

Tab. V-2: Transformation efficiencies obtained for pCAS9i(d)-supported gene editing. Transformation efficiency values were defined as the ratio of positive transformants to all viable cells that were initially employed for transformation. (n = 3)

strain	ploidy	plasmid	transformation efficiency
CEN.PK2-1C	1n	pCAS9i-anti*ADE2*	$2.8 \pm 0.6 \times 10^{-5}$
CEN.PK2-1C	1n	pCAS9i-anti*ADE2*/*CAN1*	$1.2 \pm 0.2 \times 10^{-5}$
CEN-PK2	2n	pCAS9i-anti*ADE2*	$2.1 \pm 0.5 \times 10^{-5}$
YCC78	4n	pCAS9i-anti*ADE8*	$3.6 \pm 1.6 \times 10^{-6}$

5.4.7. Simultaneous integration and assembly of multiple linear DNA fragments

Site-specific genomic integration and simultaneous assembly of multiple fragments is the method of choice to introduce single gene expression cassettes or even whole biosynthetic pathways in metabolic engineering approaches. Several studies could show that support by the CRISPR/Cas9 technology strongly facilitates the introduction of heterologous metabolic pathways [5, 15, 29-31]. A limiting factor for combined assembly and integration of a large number of linear DNA fragments results from the fact that all fragments have to be delivered simultaneously into the same cells. The overall efficiency can suffer from poor individual transformation efficiencies and can get even worse when CRISPR/Cas9 system components would have to be delivered additionally as well.

It should be tested if the plasmid-based system is suitable for such applications and it was tried to integrate and simultaneously reconstitute the previously used loxP-*LEU2*-loxP donor DNA by assembling five individual 500 bp fragments that share 40 bp homology to each other at their 3'- and 5'-ends, respectively (Fig. V-4D). Homology regions of 40 bp were considered as reasonable for a prove of principle experiment since they can be easily added

to any desired PCR product by commercially available and low cost overhang primers. The efficiency of integration and functional loxP-*LEU2*-loxP assembly was determined by a combination of red colony coloring and Leu^+ phenotype, as described before. The pCAS9i-approach (method A) yielded positive transformants with high effectivity even though the number of positive transformants was reduced compared to the integration of a single fragment loxP-*LEU2*-loxP donor DNA (Fig. V-4C). Based on this screening method, 100% efficiency for targeting and assembly in the right locus was found for the applied pCAS9i-based approach. Five randomly selected clones were tested by colony PCR as positive, with no exception (Fig. V-S6).

5.4.8. pCAS9id-mediated genome editing using yeast endogenous donor DNA

Induction of a double strand break followed by homologous recombination-based repair of the cleaved and subsequently partially degraded genomic DNA is the core part of an inherent capacity of homothallic yeast cells to switch from one mating type to the other. Yeast cells either exist as *MAT*a or *MATα* haploids as well as *MAT*a/*MATα* diploids which are generated by the conjugation of two haploid cells with opposite mating types. The molecular basis for developing a mating type specific phenotype is genetically determined by two different alleles of the mating type (*MAT*) locus - *MAT*a and *MATα* [32]. Each *MAT* allele encodes for specific transcription activators and repressors that on the one hand regulate distinct genetic programs that eventually lead to the phenotypic development of a certain mating type in haploid cells and on the other hand repress the development of any mating type specific characteristics in diploid cells [33]. The two *MAT* alleles differ in a ~700 bp sequences, called Ya or Y*α*, that encode for the previously mentioned regulatory factors, whereas the flanking regions, designated as W, X, Z1 and Z2 are identical in both *MAT* alleles. Each haploid cell contains the genetic information of both Y regions (Ya and Yα) that are present in two cryptic and transcriptionally inactive copies of the *MAT*-locus referred to as *HML*α (hidden *MAT* left carrying Yα) and *HMR*a (hidden *MAT* right carrying Ya) whereas only one of both Y regions additionally exists in the transcriptionally active *MAT* locus and determines the mating type of the haploid cell. Mating type switching is caused by replacing the Y region of the *MAT* locus against the opposite one – Ya against Y*α* or vice versa. This process is initiated by a double-strand break next to the Y/Z border mediated by the yeast endogenous HO endonuclease [34, 35]. Exonuclease activity further degrades the DNA of both sides of the cut side thereby eliminating the mating type specific information encoded in the Y region. The resulting gap within the *MAT* locus is repaired by a homologous recombination-based process either using *HML*α or *HMR*a as donor DNA. In this process, the Y region flanking sequences X and Z1 shared by both hidden loci and

the *MAT* locus serve as homology regions for homology directed repair (W and Z2 are additionally shared by *HML*α and *MAT* locus thus expanding homology regions) [32].

Most laboratory strains are unable to switch their mating type because they either do not express a (functional) HO endonuclease [36] or feature so-called stuck mutations [37] within the native recognition sequence of HO. Whereas the first mentioned limitation can be simply overcome by e.g. plasmid-based expression of native HO [38], the letter case poses a more severe problem when mating type switching is desired for e.g. experimental purposes.

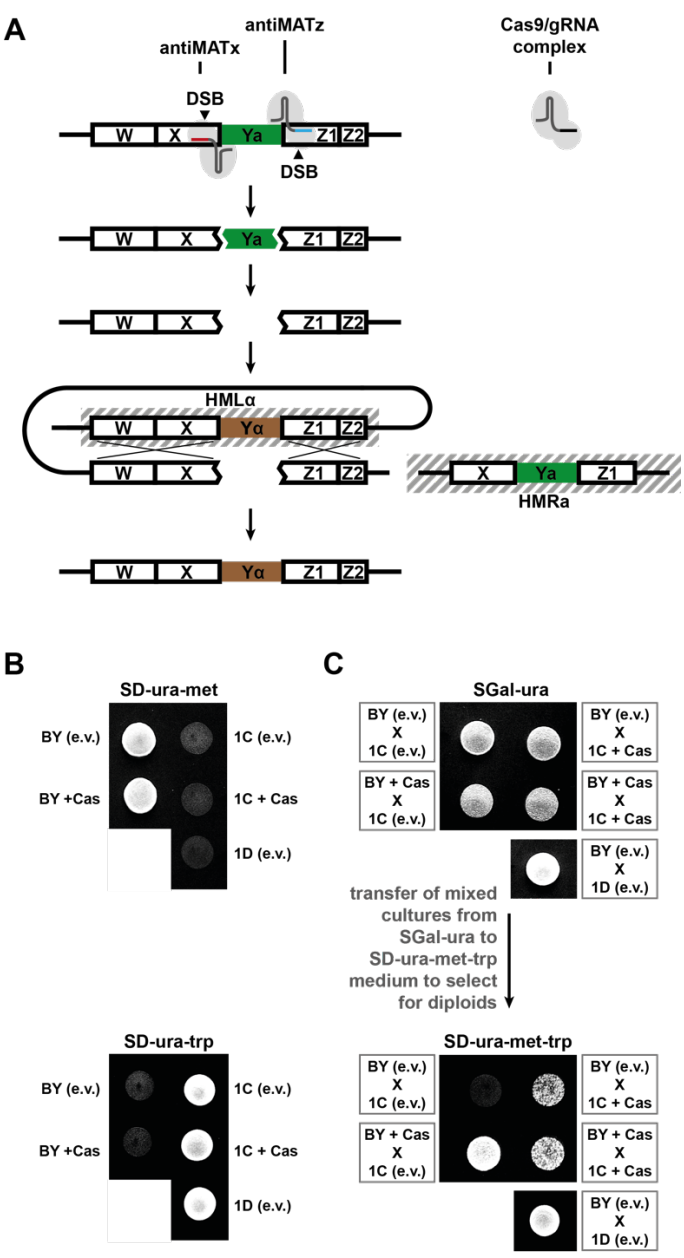

Fig. V-5: Cas9 induced double strand breaks within the *MAT* locus are sufficient to induce mating type switching. (A) The schematic shows the organization of the mating type (*MAT*) locus containing the constant W, X, Z1 and Z2 regions as well as the mating type specific Y region. Plasmid pCAS9id-antiMATx/MATz encodes for two different gRNAs targeting the X and Z1 region, respectively. Cas9-mediated DSB complete excise the Y region resulting in a gap within the *MAT* locus that can be repaired by HDR. Hidden *MAT* loci can be used as donor templates for HDR thus leading to mating type switching. **(C)** Mating assays demonstrate that CRISPR/Cas9-mediated DSBs within the *MAT* locus successfully lead to mating type switching in CEN.PK2-1C (1C; *MAT*a) and BY4741 (BY, *MAT*a). Generation of diploids in a mixed culture (X) of both strains was only possible when at least one both expressed Cas9 from plasmid pCAS9id-MATx/MATz (+Cas) on galactose medium (SGal-ura). Generation of diploids was tested by transferring mixed cultures to SD–ura-met-trp medium that selects for the combination of prototrophies (Met^+ and Trp^+) originating from one of the haploid strains, respectively **(B)**. Empty vectors (e.v.) did not support mating type switching.

The yeast endogenous mechanism of mating type switching resembles the aforementioned CRISPR/Cas9 experiments in many aspects: Double-strand breaks within genomic DNA are repaired by homologous recombination using specific donor DNA as template for HDR.

However, in contrast to the CRISPR/Cas9 experiments described here, HDR involved in mating type switching uses endogenous donor DNA and does not rely on intracellularly delivered external donor DNA. The inducible double-cleaving CRISPR/Cas9 system was tested to replace the native function of HO in Δ*ho* strains. Thus, mating type switching in genetic backgrounds featuring stuck mutations within the *MAT* locus (such as in S288c derived strains) should be enabled due to the easy adaptability of CRISPR/Cas9 cleavage sites.

To induce double-strand breaks within the *MAT* locus, two different protospacer sequences were selected that address sequences of the invariable X (antiMATx) and Z1 (antiMATz) regions present in both *MAT* alleles, thereby mediating a complete excision of the respective Y region (Fig. V-5A). To test if the resulting gap within the *MAT* locus is repaired by the endogenous HDR using *HML*α or *HMR*a as donor sequences, a mating assay was performed. For that, two different strains that have the same mating type, BY4741 (*MAT*a) and CEN.PK2-1C (*MAT*a), and that are therefore unable to mate with each other, were employed. Each of both strains possesses an auxotrophic mutation which does not apply to the other, thus featuring a unique growth phenotype, respectively – BY4741 grows on the medium lacking methionine (-met) (Fig. V-5B, top) whereas CEN.PK2-1C grows on medium freed from tryptophan (-trp) (Fig. V-5B, bottom). The generation of diploids from both different strains requires mating type switching in at least one of both strains. To test for a successful CRISPR/Cas9-mediated mating type switching, mixtures of both strains harboring either pCAS9id-anti*MAT*x/*MAT*z or an empty vector (e.v.; pGREG506) were plated on medium that selects for both plasmids and supports plasmid-based expression of Cas9 were applicable (SGal-ura) (Fig. V-5C, top). Resulting diploids might be subsequently selected on SD-ura-met-trp triple drop-out medium (Fig. V-5C, bottom). Indeed, diploids resulted from all combinations involving at least one strain that harbors a functional pCAS9id-anti*MAT*x/*MAT*z, thus clearly indicating that CRISPR/Cas9 induced DSB within the *MAT* locus can result in successful mating type switching. A negative control that used strains harboring empty vectors did not yield diploids whereas the positive control that used strains already featuring different mating types, BY4741 (*MAT*a) and CEN.PK2-1D (*MAT*α), led to mating and formation of diploids, as expected. Inducing DSB by CRISPR/Cas9 also helped to bypass impaired HO-mediated *MAT* cleavage due to stuck mutations as demonstrated by successful switching the mating type of S288c-derived BY4741. These results clearly indicate that CRISPR/Cas9-mediated DSB can be also repaired by using genomically encoded donor DNA for HDR and depends not on the delivery of external linear donor DNA elements.

5.5. Conclusions

Here, a new set of all-in-one CRISPR/Cas9 plasmids is introduced that allow for a simple and convenient application of the technology in *S. cerevisiae* by combining beneficial features of different existing approaches in one system. Introduction of a desired gRNA protospacer sequence into these plasmids is possible via PCR-based methods or as in case of the inducible single gRNA system, it can be simply obtained by the assembly and integration of single-stranded oligonucleotides in a homologous recombination-mediated process. Cells that are preloaded with the inducible vectors express a functional gRNA-Cas9 complex upon galactose induction. These cells just have to be transformed with a desired donor DNA to obtain highly efficient and effective genome editing without the need of co-introducing any of the CRISPR/Cas9 system components. Thus, the inducible CRISPR/Cas9 systems presented here can easily be integrated into established workflows for marker-based genome editing approaches that are commonly used in the community. The inducible system for preloading cells with CRISPR/Cas9 plasmids can also help to overcome problems that might result from low transformation efficiencies that have been observed for many industrial strains [31, 39], since delivery of CRISPR system DNA elements and donor DNA is sequentially separated. Furthermore, cells once preloaded with the inducible CRISPR/Cas9 vectors can serve as a universal platform for applications were genomic integrations of different DNA fragments or even whole DNA libraries into the same locus is required [39]. The easy architecture of the plasmids that has been disclosed in detail moreover allows to tailor the vectors for individual personal requirements e.g. by changing the selectable marker or the promoter driving Cas9 expression. Easy and simple Cas9 nickase applications would be furthermore enabled by introducing the nCAS9 (nicking) encoding sequence into the successfully tested all-in-one multiplex vectors.

5.6. References

1. **Stovicek V, Holkenbrink C, Borodina I**. CRISPR/Cas system for yeast genome engineering: advances and applications. *FEMS Yeast Res* 2017.
2. **Mans R, van Rossum HM, Wijsman M, Backx A, Kuijpers NG et al.** CRISPR/Cas9: a molecular Swiss army knife for simultaneous introduction of multiple genetic modifications in Saccharomyces cerevisiae. *FEMS Yeast Res* 2015;15(2).
3. **Ryan OW, Cate JH**. Multiplex engineering of industrial yeast genomes using CRISPRm. *Methods Enzymol* 2014;546:473-489.
4. **Generoso WC, Gottardi M, Oreb M, Boles E**. Simplified CRISPR-Cas genome editing for Saccharomyces cerevisiae. *J Microbiol Methods* 2016;127:203-205.
5. **Reider Apel A, d'Espaux L, Wehrs M, Sachs D, Li RA et al.** A Cas9-based toolkit to program gene expression in Saccharomyces cerevisiae. *Nucleic Acids Res* 2017;45(1):496-508.
6. **Bao Z, Xiao H, Liang J, Zhang L, Xiong X et al.** Homology-integrated CRISPR-Cas (HI-CRISPR) system for one-step multigene disruption in Saccharomyces cerevisiae. *ACS Synth Biol* 2015;4(5):585-594.
7. **Laughery MF, Hunter T, Brown A, Hoopes J, Ostbye T et al.** New vectors for simple and streamlined CRISPR-Cas9 genome editing in Saccharomyces cerevisiae. *Yeast* 2015;32(12):711-720.
8. **Gibson DG**. Synthesis of DNA fragments in yeast by one-step assembly of overlapping oligonucleotides. *Nucleic Acids Res* 2009;37(20):6984-6990.
9. **Entian K-D, Kötter P**. 25 Yeast Genetic Strain and Plasmid Collections. *Methods in Microbiology* 2007;36:629-666.
10. **Mirzayan C, Copeland CS, Snyder M**. The NUF1 gene encodes an essential coiled-coil related protein that is a potential component of the yeast nucleoskeleton. *J Cell Biol* 1992;116(6):1319-1332.
11. **Brachmann CB, Davies A, Cost GJ, Caputo E, Li J et al.** Designer deletion strains derived from Saccharomyces cerevisiae S288C: a useful set of strains and plasmids for PCR-mediated gene disruption and other applications. *Yeast* 1998;14(2):115-132.
12. **Gari E, Piedrafita L, Aldea M, Herrero E**. A set of vectors with a tetracycline-regulatable promoter system for modulated gene expression in Saccharomyces cerevisiae. *Yeast* 1997;13(9):837-848.
13. **DiCarlo JE, Norville JE, Mali P, Rios X, Aach J et al.** Genome engineering in Saccharomyces cerevisiae using CRISPR-Cas systems. *Nucleic Acids Res* 2013;41(7):4336-4343.
14. **Jansen G, Wu C, Schade B, Thomas DY, Whiteway M**. Drag&Drop cloning in yeast. *Gene* 2005;344:43-51.
15. **Jakociunas T, Rajkumar AS, Zhang J, Arsovska D, Rodriguez A et al.** CasEMBLR: Cas9-Facilitated Multiloci Genomic Integration of in Vivo Assembled DNA Parts in Saccharomyces cerevisiae. *ACS Synth Biol* 2015;4(11):1226-1234.
16. **Gueldener U, Heinisch J, Koehler GJ, Voss D, Hegemann JH**. A second set of loxP marker cassettes for Cre-mediated multiple gene knockouts in budding yeast. *Nucleic Acids Res* 2002;30(6):e23.
17. **Guldener U, Heck S, Fielder T, Beinhauer J, Hegemann JH**. A new efficient gene disruption cassette for repeated use in budding yeast. *Nucleic Acids Res* 1996;24(13):2519-2524.
18. **Da Silva NA, Srikrishnan S**. Introduction and expression of genes for metabolic engineering applications in Saccharomyces cerevisiae. *FEMS Yeast Res* 2012;12(2):197-214.
19. **Boeke JD, LaCroute F, Fink GR**. A positive selection for mutants lacking orotidine-5'-phosphate decarboxylase activity in yeast: 5-fluoro-orotic acid resistance. *Mol Gen Genet* 1984;197(2):345-346.
20. **Ugolini S, Bruschi CV**. The red/white colony color assay in the yeast Saccharomyces cerevisiae: epistatic growth advantage of white ade8-18, ade2 cells over red ade2 cells. *Curr Genet* 1996;30(6):485-492.
21. **Frankenberg-Schwager M, Frankenberg D**. DNA double-strand breaks: their repair and relationship to cell killing in yeast. *Int J Radiat Biol* 1990;58(4):569-575.
22. **Weiffenbach B, Haber JE**. Homothallic mating type switching generates lethal chromosome breaks in rad52 strains of Saccharomyces cerevisiae. *Mol Cell Biol* 1981;1(6):522-534.
23. **Mortimer RK**. Evolution and variation of the yeast (Saccharomyces) genome. *Genome Res* 2000;10(4):403-409.
24. **Replansky T, Koufopanou V, Greig D, Bell G**. Saccharomyces sensu stricto as a model system for evolution and ecology. *Trends Ecol Evol* 2008;23(9):494-501.

25. **Mortimer RK, Romano P, Suzzi G, Polsinelli M**. Genome renewal: a new phenomenon revealed from a genetic study of 43 strains of Saccharomyces cerevisiae derived from natural fermentation of grape musts. *Yeast* 1994;10(12):1543-1552.

26. **Storchova Z**. Ploidy changes and genome stability in yeast. *Yeast* 2014;31(11):421-430.

27. **Koopman F, Beekwilder J, Crimi B, van Houwelingen A, Hall RD et al.** De novo production of the flavonoid naringenin in engineered Saccharomyces cerevisiae. *Microb Cell Fact* 2012;11:155.

28. **Zhang GC, Kong, II, Kim H, Liu JJ, Cate JH et al.** Construction of a quadruple auxotrophic mutant of an industrial polyploid saccharomyces cerevisiae strain by using RNA-guided Cas9 nuclease. *Appl Environ Microbiol* 2014;80(24):7694-7701.

29. **Horwitz AA, Walter JM, Schubert MG, Kung SH, Hawkins K et al.** Efficient Multiplexed Integration of Synergistic Alleles and Metabolic Pathways in Yeasts via CRISPR-Cas. *Cell Syst* 2015;1(1):88-96.

30. **Jakociunas T, Bonde I, Herrgard M, Harrison SJ, Kristensen M et al.** Multiplex metabolic pathway engineering using CRISPR/Cas9 in Saccharomyces cerevisiae. *Metab Eng* 2015;28:213-222.

31. **Stovicek V, Borodina I, Forster J**. CRISPR–Cas system enables fast and simple genome editing of industrial Saccharomyces cerevisiae strains. *Metabolic Engineering Communications* 2015;2:13-22.

32. **Haber JE**. Mating-type genes and MAT switching in Saccharomyces cerevisiae. *Genetics* 2012;191(1):33-64.

33. **Herskowitz I**. Life cycle of the budding yeast Saccharomyces cerevisiae. *Microbiol Rev* 1988;52(4):536-553.

34. **Nickoloff JA, Chen EY, Heffron F**. A 24-base-pair DNA sequence from the MAT locus stimulates intergenic recombination in yeast. *Proc Natl Acad Sci U S A* 1986;83(20):7831-7835.

35. **Strathern JN, Klar AJ, Hicks JB, Abraham JA, Ivy JM et al.** Homothallic switching of yeast mating type cassettes is initiated by a double-stranded cut in the MAT locus. *Cell* 1982;31(1):183-192.

36. **Meiron H, Nahon E, Raveh D**. Identification of the heterothallic mutation in HO-endonuclease of S. cerevisiae using HO/ho chimeric genes. *Curr Genet* 1995;28(4):367-373.

37. **Fukuda N, Matsukura S, Honda S**. Artificial conversion of the mating-type of Saccharomyces cerevisiae without autopolyploidization. *ACS Synth Biol* 2013;2(12):697-704.

38. **Herskowitz I, Jensen RE**. Putting the HO gene to work: practical uses for mating-type switching. *Methods Enzymol* 1991;194:132-146.

39. **Ryan OW, Skerker JM, Maurer MJ, Li X, Tsai JC et al.** Selection of chromosomal DNA libraries using a multiplex CRISPR system. *Elife* 2014;3.

5.7. Supporting information

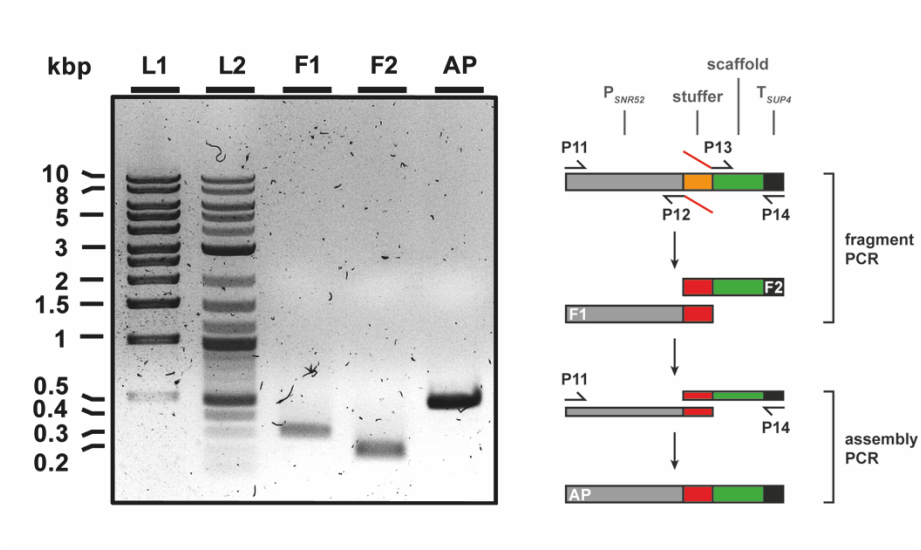

Fig. V-S1: Gel-electrophoretic analysis of assembly PCR intermediates and the final assembly product. At first, both fragments that should be assembled were amplified individually. The *SNR52* promoter containing fragment (F1; 311 bp) was amplified by using primers P11 and P12. The gRNA-scaffold and *SUP4* terminator containing fragment (F2; 211 bp) was amplified by using primers P13 and P14. Overhang primers P12 and P13 introduced the anti-*ADE2* protospacer sequences (red) to the fragments, respectively, that function as overlapping regions in the following assembly PCR step. The assembly product (AP; 502 bp) was amplified with the outer primers P11 and P14. L1 = 1 kbp DNA ladder (Carl Roth); L2 = 2-Log DNA ladder (NEB).

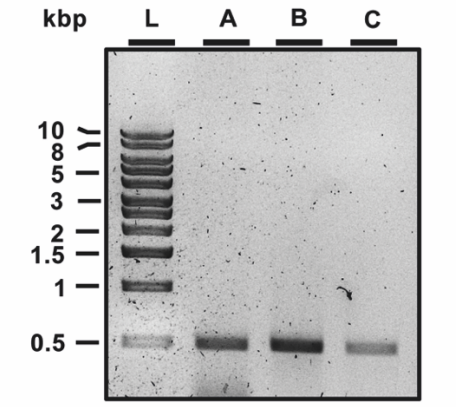

Fig. V-S2: Colony PCR products for confirming proper introduction of anti-*ADE2* protospacer sequence in plasmid pCAS9i analyzed by agarose gel electrophoresis. The anti-*ADE2* protospacer sequence was introduced into PmlI & KpnI cleaved plasmid pCAS9i by method A (one-step *in vivo* HR-mediated assembly of overlapping oligonucleotides P12 and P13; A), by method B (*in vivo* HR-mediated integration of *ADE2* protospacer containing gRNA assembly PCR product; B) or method C (PCR amplification of pCAS9i backbone with primer P12 and P13 and subsequent *in vivo* HR-mediated recircularization of the plasmid; C). Positive transformants yield a PCR product of 508 bp. L = 1 kbp DNA ladder (Carl Roth).

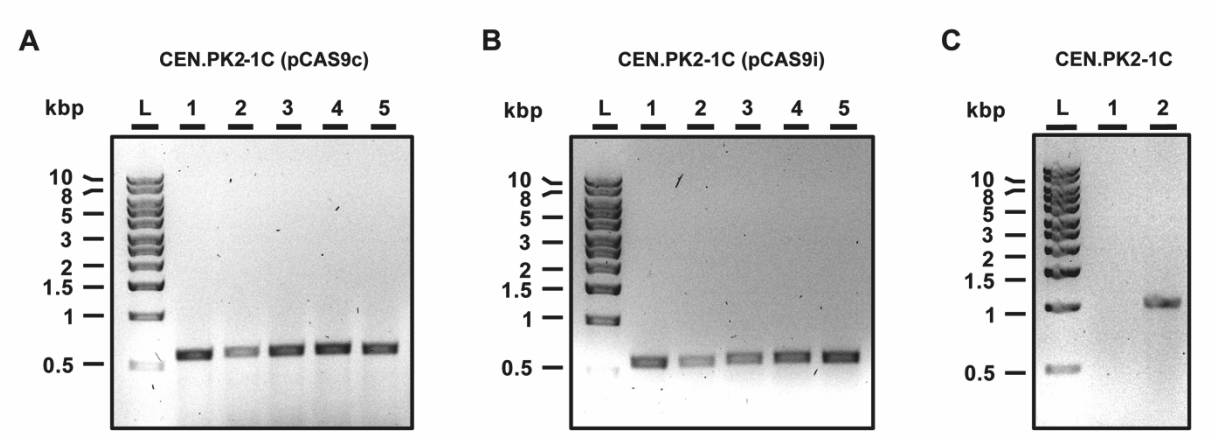

Fig. V-S3: Colony PCR products for confirming the disruption of *ADE2* by integration of loxP-*LEU2*-loxP donor DNA in an CEN.PK2-1C background analyzed by agarose gel electrophoresis. (A) Confirmation of pCAS9c-supported donor DNA integration of five randomly selected transformants (1-5). **(B)** Confirmation of pCAS9i-supported donor DNA integration of five randomly selected transformants (1-5). Positive transformants yield a PCR product of 598 bp. **(C)** PCR-negative control. Primers that were used to confirm the integration of loxP-*LEU2*-loxP into the *ADE2* locus do not yield a PCR product for unmodified CEN.PK2-1C cells (1). The presence and quality of genomic DNA was checked by amplifying a 1 kbp fragment of the *S. cerevisae* genome (2). L = 1 kbp DNA ladder (Carl Roth).

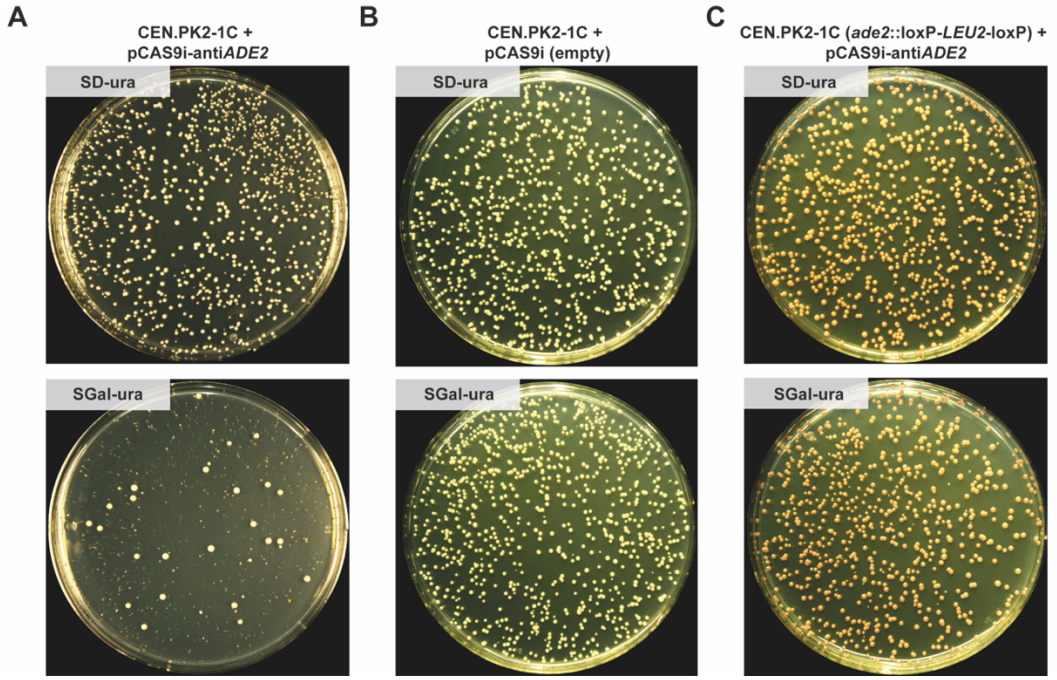

Fig. V-S4: A functional *ADE2*-targeting CRISPR/Cas9 system expressed from pCAS9i is toxic for yeast. Images show representative agar plates. The identical number (100 µL of OD_{600} = 0.002) of pCAS9i-anti*ADE2* harboring CEN.PK2-1C cells **(A)** was plated on uracil-free glucose (SD-ura) or galactose (SGal-ura) containing agar media. Glucose containing media (SD-ura) do not promote the expression of Cas9 from P_{GAL1} and cells grew unimpaired. On galactose containing media (SGal-ura) cells express a functional *ADE2*-targeting CRISPR/Cas9 system. Colonies with the same size as on SD media recovered only from a small percentage of plated cells, whereas the majority of cells showed strongly impaired growth. Reference strains that do not express a functional *ADE2*-targeting gRNA **(B)** or that do not provide a genomic protospacer sequence that could be addressed by the gRNA-Cas9 complex **(C)** grew unaffected on galactose media. Colonies recovered from all plated cells with the same size as on glucose containing media.

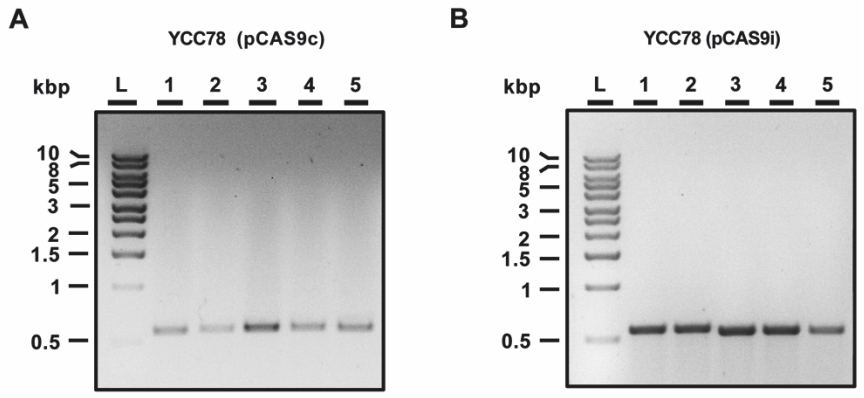

Fig. V-S5: Colony PCR products for confirming the disruption of ADE8 by integration of loxP-kanMX-loxP donor DNA in an YCC78 background analyzed by agarose gel electrophoresis. **(A)** Confirmation of pCAS9c-supported donor DNA integration of five randomly selected transformants (1-5). **(B)** Confirmation of pCAS9i-supported donor DNA integration of five randomly selected transformants (1-5). Positive transformants yield a PCR product of 575 bp. L = 1 kbp DNA ladder (Carl Roth).

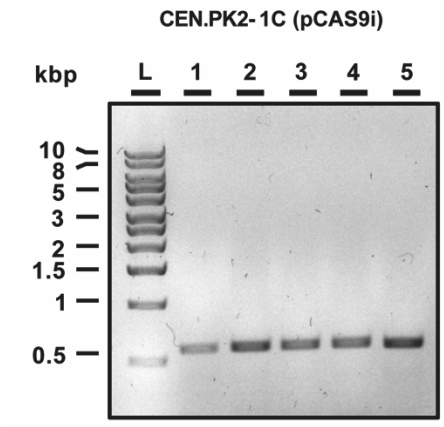

Fig. V-S6: Colony PCR products for confirming the disruption of *ADE2* by integration and proper assembly of fragmented loxP-*LEU2*-loxP donor DNA in an CEN.PK2-1C background analyzed by agarose gel electrophoresis. Confirmation of pCAS9i-supported donor DNA integration of five randomly selected transformants (1-5). Positive transformants yield a PCR product of 598 bp. L = 1 kbp DNA ladder (Carl Roth).

Tab. V-S1: Plasmids used in this study. The table summarizes basic characteristics and properties of indicated plasmids.

Plasmid	description	reference
p425-SNR52p-gRNA.HIS3-SUP4t	is equivalent to p426-SNR52p-gRNA.CAN1.Y-SUP4t [13] but with pRS426 backbone and anti*HIS3*-gRNA	Dr. C. Schneider
p414-TEF1p-Cas9-CYC1t	-	[13]
pC188	-	[12]
pCM188(2µ)	CEN/ARS sequence of pCM188 was replaced by the 2µ-ORI from plasmid pRS425	This study
pUG73	-	[16]
pUG6	-	[17]
pGREG504	-	[14]
pCAS9c	2µ; *URA3*; amp^R; expression of Cas9 endonuclease from *S. pyogenes* from constitutive *TEF1* promoter and gRNA from SNR52 promoter, gRNA expression cassette contains protospacer stuffer	This study
pCAS9i	*TEF1* promoter of plasmid pCAS9c was replaced by the inducible *GAL1* promoter	This study
pCAS9cd	identical to pCASc but contains a second gRNA expression cassette	This study
pCAS9id	identical to pCASi but contains a second gRNA expression cassette	This study
pGREG506	-	[14]

Tab. V-S2: Primers used in this study. Underlined sequence parts represent homology regions of overhang primers used recombination-based cloning approaches.

primer	sequence (5' → 3')	amplicon
P1 (fw)	CACAAATTGCAAAATTTAATTGCTTGCAAAAGGTCACATGCTGTATGATCCAATATCAAAGGAAATGATAGC	2-micron
P2 (rv)	GGAACTCGATTTCTGACTGGGTTGGAAGGCAAGAGAGCCCCGAGCCTGAACGAAGCATCTGTG	2-micron
P3 (fw)	CATGTGACCTTTTGCAAGCAATTAAATTTTGCTGATATCGAATTCGCTGGAGC	P_{SNR52}
P4 (rv)	GGTACCCTCGCAGATGTTGCTGATGTCGTCGTTTAAACGATCATTTATCTTTCACTGCGGAG	P_{SNR52}
P5 (fw)	GACGACATCAGCAACATCTGCGAGGGTACCGTTTTAGAGCTAGAAATAGCAAGTTAAAATAAG	scaffold – T_{SUP4}
P6 (rv)	CGTCGTGACTGGGAAAACCCTGGCGTTACCCAATTAACCCTCACTAAAGGG	scaffold – T_{SUP4}
P7 (fw)	CATTATACTGAAAACCTTGCTTGAGAAGGTTTTGGGACGCTCGAAGGCTTTAATTTGCGGAGGCGTATCACGAGGCCC	*URA3*-2µ-gRNA cassette
P8 (rv)	GAATGTATTTAGAAAAATAAACAAATAGGGGTTCCGCGCACATTTCCCCGAAAAGTGCCACCGGGAACAAAAGCTGGAGCTC	*URA3*-2µ-gRNA cassette
P9 (fw)	CCCTCACTAAAGGGAACAAAAGCTGGAGCTGTACGGATTAGAAGCCGCC	P_{GAL1}
P10 (rv)	GTACTTCTTGTCCATTTTTCCCGGGGGATCCCGGGGTTTTTTCTCCTTGACG	P_{GAL1}
P11 (fw)	TGATATCGAATTCGCTGGAGC	Assembly PCR; F1
P12 (rv)	TGTGGATAGTCTCTACAATTGATCATTTATCTTTCACTGCGGAG	*ADE2* oligo; F1
P13 (fw)	AATTGTAGAGACTATCCACAGTTTTAGAGCTAGAAATAGCAAGTTAAAATAAG	*ADE2* oligo; F2
P14 (rv)	CGCAATTAACCCTCACTAAAGGG	Assembly PCR; F2
P15 (fw)	CGGTTTAGTGTTTTCTTACCCAATTGTAGAGACTATCCCAGCTGAAGCTTCGTACGCTGCAG	split *LEU2* F1
P16 (rv)	TCATGGTTCTGCCCCAG	split *LEU2* F1; ColPCR Integration *ADE2*
P17 (fw)	GTTAACCTTGTTTGCTGGTAAATCT	split *LEU2* F2
P18 (rv)	TCGTTAGAGAATTGGTTGGTGG	split *LEU2* F2
P19 (fw)	CTTTCACCAAAGTAGATACCACC	split *LEU2* F3
P20 (rv)	GTAAGTACATCTGCTTTAACGCAT	split *LEU2* F3
P21 (fw)	CGAAGCAAATGTAGGAATGCG	split *LEU2* F4
P22 (rv)	CTGAAAATGCGCGAACAAAAC	split *LEU2* F4
P23 (fw)	AAATTTGACGAGTCTTCTTGTTTTG	split *LEU2* F5
P24 (rv)	GCAGGCGCATAACATAAGTCACAAATATTGTCCTTGGCCGCATAGGCCACTAGTGGATCTG	split *LEU2* F5
P25 (fw)	GATCAATTGTAGAGACTATCCACA	ColPCR *ADE2* gRNA
P26 (rv)	CTTCGGGGCGAAAACTCTC	ColPCR *ADE2* gRNA
P27 (fw)	CCGGAAGCTTTGGAAGTACTG	ColPCR Integration *ADE2*

primer	sequence (5' → 3')	amplicon
P28 (fw)	GAGAACAAGCCTCTGACGGCGTTTTAGAGCTAGAAATAGCAAGTTAAAATAAG	*ADE8* oligo
P29 (rv)	GCCGTCAGAGGCTTGTTCTCGATCATTTATCTTTCACTGCGGAG	*ADE8* oligo
P30 (fw)	GCATGGCGCAAATGTCAGGACGAGAACAAGCCTCTGACCAGCTGAAGCTTCGTACGCTGCAG	kanMX
P31 (rv)	CGACCTCCTCGATGACATAGTGCACCATGCATCCGGGGCCGCATAGGCCACTAGTGGATCTG	kanMX
P32 (fw)	GTTTCGATGGTACCACACACGC	ColPCR Integration *ADE8*
P33 (rv)	CGGCCTCGAAACGTGAGTC	ColPCR Integration *ADE8*
P34 (fw)	GAGTCATGTAATTAGTTATGTCACGCTCTAGAGCGGCCGCCACCGCTGATATCGAATTCGCTGG	2nd gRNA
P35 (rv)	CCGGGAACAAAAGCTGGAGCTCCACCGCGGTGTTACATGACTCGAAGACATAAAAAAC	2nd gRNA
P36 (fw)	GATACGTTCTCTATGGAGGAGTTTTAGAGCTAGAAATAGCAAGTTAAAATAAG	*CAN1* oligo
P37 (rv)	TCCTCCATAGAGAACGTATCGATCATTTATCTTTCACTGCGGAG	*CAN1* oligo
P38 (fw)	CCGACGAGAGTAAATGGCGAGGATACGTTCTCTATGGCAGGGAAGTCATAACACAGTCC	*HIS3*
P39 (rv)	TCTGTACTTCTCCTTCATCTTCATCACCTATGCCATGTTATTAGGTACCGGCCGC	*HIS3*
P40 (fw)	TCTTCTGTTGTTACACTCTCGTTTTAGAGCTAGAAATAGCAAGTTAAAATAAG	*MAT*x oligo
P41 (rv)	GAGAGTGTAACAACAGAAGAGATCATTTATCTTTCACTGCGGAG	*MAT*x oligo
P42 (fw)	CACTCTACAAAACCAAAACCGTTTTAGAGCTAGAAATAGCAAGTTAAAATAAG	*MAT*z oligo
P43 (rv)	GGTTTTGGTTTTGTAGAGTGGATCATTTATCTTTCACTGCGGAG	*MAT*z oligo

Chapter VI

General discussion

6. Chapter VI: General discussion

6.1. Employing metabolic engineering approaches to alter membrane lipid composition

Systematic manipulation of membrane lipid composition is a challenging endeavor due to a limited set of tools to intervene in the cell's sophisticated and fine-tuned lipid metabolism and lipid homeostasis. Standard approaches to manipulate the cellular lipid composition of both, mammalian cells as well as single-celled eukaryotes such as *S. cerevisiae*, include gene knockouts, drugs that specifically target enzymes involved in the lipid biosynthesis (e.g. fluconazole [1], zaragozic acid [2]) or chemical tools as, for instance, media supplements and lipid chelators [3]. Studies that addressed fatty acid unsaturation of *S. cerevisiae* either used *OLE1* knockout strains or employed a Δ*hem1* background that is defective in the synthesis of δ-aminolevulinate (ALA) which is an essential intermediate of the heme and porphyrin biosynthesis of yeast [4]. Since heme is required as prosthetic group of several enzymes involved in the ergosterol biosynthetic pathway as well as of Ole1p [5], both deletions provide an efficient strategy to impair and interrupt fatty acid unsaturation and the synthesis of sterols simultaneously. Those knockout strains are inviable and cells stop growing after a few cell divisions when cellular concentrations of essential lipids drop to the minimum limit [4] unless the medium is supplemented with unsaturated fatty acids (and ergosterol) or ALA to be able to deal with double-lipid depletion. However, cellular uptake of fatty acids and membrane lipids from the external environment is difficult to control, thus emphasizing that media supplementation provides limited stoichiometric control over lipid composition. Alternative strategies successfully used lipid chelators such as methyl-β-cyclodextrine (MβCD) to remove sterols from biological membranes of *S. cerevisiae* [6, 7] and mammalian cells [8]. Those strategies however feature similar limitations as it is challenging to exactly adjust concentrations of particular lipids *in vivo* with intermediate levels between native conditions and maximal depletion. Additionally, external lipid chelators provide only limited access to internal membrane structures of eukaryotic cells.

The studies presented here used rational genetic manipulations of the expression of enzymes that play key roles in membrane lipid biosynthesis of the eukaryotic model organism *S. cerevisiae* such as Ole1p and Erg9p in order to allow for investigating physiological roles of membrane lipids. These genetic approaches are based on metabolic engineering strategies that help to overcome previously described limitation thus proving a system that allows for adjusting and fine-tuning levels of membrane lipids as shown for the fatty acid unsaturation (Chapter II and Chapter III) and ergosterol (Chapter IV). The

strategies used here only involved components of the yeast endogenous biosynthetic pathways thus manipulating the synthesis of membrane lipids in a system intrinsic way. This way, environmental factors and stimuli that affect physicochemical membrane parameters can be mimicked in an authentic and reliable manner. Depletion of total sterols and reduction of fatty acid unsaturation is e.g. a natural consequence of hypoxic growth conditions and is the only reason why *S. cerevisiae* cannot be grown under anoxic conditions [5]. Oxygen is an essential co-factor of the desaturase reactions catalyzed by Ole1p, Erg1p, Erg11p, Erg3p and Erg5p which is the reason why reduced (dissolved) oxygen concentrations strongly decrease the respective overall enzymatic activities and thus eventually the content of biosynthetic end products [5]. By down-regulating the expression of e.g. Ole1p, it is possible to deduce the effect of hypoxic growth conditions on membrane lipid unsaturation and closely related processes without subjecting cells to hypoxic stress in general. By this means, the interlinkage between oxygen availability, membrane lipid unsaturation and yeast flocculation could be elucidated [9] thereby also emphasizing the diversity of membrane lipid functions in cellular systems.

6.2. Yeast as a model system to investigate physiological roles of membrane lipids

The physiological effects of lipid modifications on cellular functions is very complex and they vary between species and even between different cell types of the same organism [10]. Therefore, it is almost impossible to predict how a cellular system will respond to different changes in membrane lipid composition. The studies presented here addresses fundamental parameters of biological membranes – phospholipid unsaturation, membrane fluidity, lipid packing, sterol content – which are crucial properties of all biological membranous systems thus being relevant for all types of cells and organisms. To study general effects of altered lipid composition and important membrane features on biological processes, model systems have to be employed that are on the one hand simple enough to allow for effectively influencing desired parameters and on the other hand, that are complex enough to provide the native cellular context for processes to be studied. Budding yeast is a valuable model organism to study lipid related cellular processes as it features a relatively simple lipid composition compared to more complex multicellular organisms but major properties are still comparable to the lipidome of other eukaryotic cells [11]. Furthermore, *S. cerevisiae* possesses only a limited diversity of enzymes involved in the synthesis of membrane lipids which reduces the complexity of the metabolic network: yeast e.g. only features one fatty acid desaturase gene in contrast to humans (2 SCD genes [12]) and the mouse model (4 SCD genes [13]) thus representing a minimal system to study effects of altered fatty acid unsaturation, membrane fluidity and lipid packing. This way, recent studies using budding yeast as model have provided new insights in basic principles

of lipid-dependent membrane organization in vivo [14], basic lipid-related cell physiology [15], the eukaryotic lipid metabolism [16, 17] and its interlinkage to other cellular pathways [18].

Large improvements of yeast genetic engineering by employing powerful, simple and affordable CRISPR/Cas9 applications (Chapter V) give easy access to metabolic engineering approaches involving promoter replacement strategies [9], gene deletions to direct the metabolite flux towards alternative or competing pathways [19, 20] and tools for heterologous expression of enzymes that replace functions of endogenous enzymes (Chapter II) or that even expand the yeast lipidome to e.g. unnatural polyunsaturated fatty acids [21-23], cyclopropanated species [24, 25] or cholesterol [26]. This way, limitations of genetic manipulations that result from time consuming, costly strategies and large technical efforts do not any longer apply to the budding yeast model.

6.3. Widespread functions of membranes and membrane lipids in living organisms

From a traditional point of view, cellular lipids fulfil three general functions: (i) lipids, especially triacylglycerols, serve as energy storing molecules, (ii) lipids are the main components of biological membranes, thus exhibiting the well-known barrier function and (iii) phospholipids such as phosphatidylinositol-4,5-bisphosphat (PIP_2) and phosphatidyl-1,4,5-triphosphat (PIP_3) serve as second messengers and are key players of intracellular signaling cascades [10].

However, there is striking evidence that membrane lipids feature much more functions in biological systems as usually expected. Lipids are an omnipresent class of molecules in cellular systems and seem to have big impact on a large variety of cellular processes. The mere fact that 20 – 30% of all ORFs from eubacterial, archaean or eukaryotic organisms are predicted to encode for membrane proteins [27] emphasizes the large influence of membrane lipids and physicochemical membrane properties on various cellular processes, even if only by indirectly influencing the activity [28-30], conformation [31, 32] or subcellular localization [33, 34] of membrane embedded proteins.

Chapter I introduces a novel concept of lipid-depended oxygen sensing in *S. cerevisiae*. In this sensing system, the large pool of ER membrane lipid incorporated fatty acids serves as a “memory device” to integrate a long-term signal for oxygen availability [9, 35]. Short term, acute hypoxic conditions do not influence fatty acid unsaturation to an extend that activates Spt23p- and Mga2p-mediated gene expression as it might be unfavorable to change to an adaptive expression profile when cells are only exposed to hypoxic conditions for a short period of time. In contrast, long-term hypoxic conditions activate the system and activation remains until the membrane composition is diluted by new lipid synthesis.

Therefore, it is proposed that yeast has evolved its lipid homeostasis machinery to adjust enzyme expression levels in accordance to environmental conditions (oxygen availability), but has then adapted these sensors to regulate a wide range of molecular functions that are associated with these conditions. Prominent targets of the membrane fluidity regulon, mediated by Spt23p and Mga2p, were genes whose gene products are involved in the glycolytic metabolism (*TDH1*, *PCK1*, *ENO1*), metal homeostasis (*IZH1*, *IZH2*, *IZH4*, *SIT1*), hypoxic response (*DAN4*), mating [36], the meiotic cell cycle (*CDC4*, *DMC1*), sporulation (*OSW2*, *SPS100*), protein folding (*HSP26*) and flocculation (*FLO1*) – all being cellular processes that are not necessarily linked with each other or involved in the lipid metabolism at first sight nor that are classical membrane-associated cellular processes. This example clearly illustrates the close interlinkage between membrane lipids and a huge variety of cellular processes that is just about to be understood.

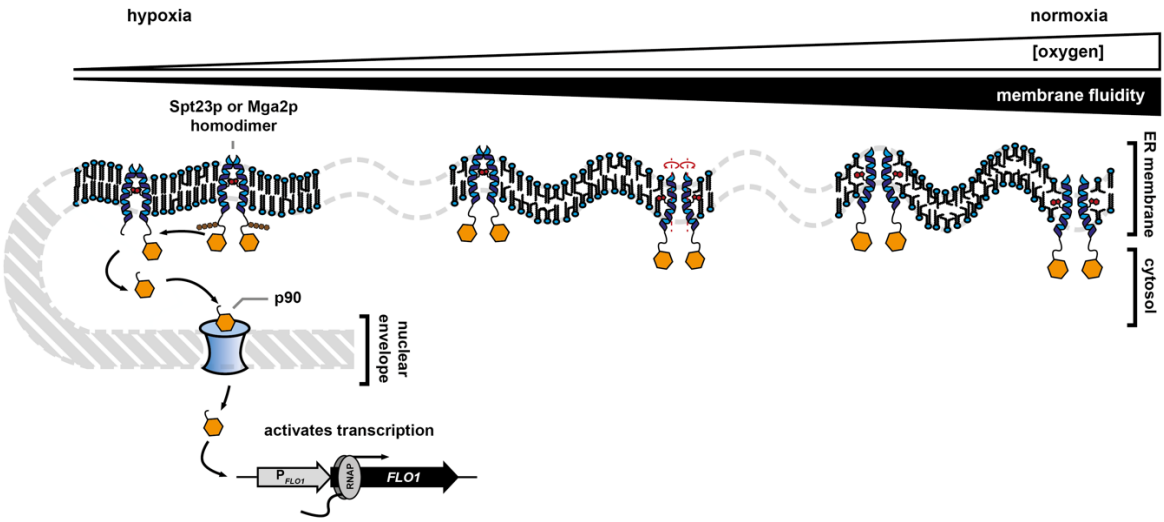

Fig. VI-1: The membrane fluidity regulon adapts budding yeast to hypoxic conditions. Membrane lipid unsaturation drops as molecular oxygen gets limiting and growth conditions switch from normoxic to hypoxic conditions due to reduced Ole1p activity. Decreased membrane fluidity and dense lipid packing activate ER membrane-resident membrane fluidity sensors Spt23p and Mga2p by their rotation-based activation mechanism. Released p90 fragments translocate to the nucleus thus eventually activating a large set of genes. A prominent gene target of Spt23p is, among others, *FLO1* whose gene product is a GPI-anchored cell wall mannose binding protein that induces cell aggregation (flocculation).

6.4. References

1. **Yang H, Tong J, Lee CW, Ha S, Eom SH et al.** Structural mechanism of ergosterol regulation by fungal sterol transcription factor Upc2. *Nat Commun* 2015;6:6129.
2. **Daicho K, Maruyama H, Suzuki A, Ueno M, Uritani M et al.** The ergosterol biosynthesis inhibitor zaragozic acid promotes vacuolar degradation of the tryptophan permease Tat2p in yeast. *Biochim Biophys Acta* 2007;1768(7):1681-1690.
3. **Spector AA, Yorek MA**. Membrane lipid composition and cellular function. *J Lipid Res* 1985;26(9):1015-1035.
4. **Pineau L, Colas J, Dupont S, Beney L, Fleurat-Lessard P et al.** Lipid-induced ER stress: synergistic effects of sterols and saturated fatty acids. *Traffic* 2009;10(6):673-690.
5. **Ishtar Snoek IS, Yde Steensma H**. Factors involved in anaerobic growth of Saccharomyces cerevisiae. *Yeast* 2007;24(1):1-10.
6. **Aresta-Branco F, Cordeiro AM, Marinho HS, Cyrne L, Antunes F et al.** Gel domains in the plasma membrane of Saccharomyces cerevisiae: highly ordered, ergosterol-free, and sphingolipid-enriched lipid rafts. *J Biol Chem* 2011;286(7):5043-5054.
7. **Lagane B, Gaibelet G, Meilhoc E, Masson JM, Cezanne L et al.** Role of sterols in modulating the human mu-opioid receptor function in Saccharomyces cerevisiae. *J Biol Chem* 2000;275(43):33197-33200.
8. **Mahammad S, Parmryd I**. Cholesterol depletion using methyl-beta-cyclodextrin. *Methods Mol Biol* 2015;1232:91-102.
9. **Degreif D, de Rond T, Bertl A, Keasling JD, Budin I**. Lipid engineering reveals regulatory roles for membrane fluidity in yeast flocculation and oxygen-limited growth. *Metab Eng* 2017;41:46-56.
10. **van Meer G, Voelker DR, Feigenson GW**. Membrane lipids: where they are and how they behave. *Nat Rev Mol Cell Biol* 2008;9(2):112-124.
11. **Klose C, Surma MA, Gerl MJ, Meyenhofer F, Shevchenko A et al.** Flexibility of a eukaryotic lipidome--insights from yeast lipidomics. *PLoS One* 2012;7(4):e35063.
12. **Zhang L, Ge L, Parimoo S, Stenn K, Prouty SM**. Human stearoyl-CoA desaturase: alternative transcripts generated from a single gene by usage of tandem polyadenylation sites. *Biochem J* 1999;340 (Pt 1):255-264.
13. **Bai Y, McCoy JG, Levin EJ, Sobrado P, Rajashankar KR et al.** X-ray structure of a mammalian stearoyl-CoA desaturase. *Nature* 2015;524(7564):252-256.
14. **Klose C, Ejsing CS, Garcia-Saez AJ, Kaiser HJ, Sampaio JL et al.** Yeast lipids can phase-separate into micrometer-scale membrane domains. *J Biol Chem* 2010;285(39):30224-30232.
15. **Guan XL, Souza CM, Pichler H, Dewhurst G, Schaad O et al.** Functional interactions between sphingolipids and sterols in biological membranes regulating cell physiology. *Mol Biol Cell* 2009;20(7):2083-2095.
16. **Breslow DK, Collins SR, Bodenmiller B, Aebersold R, Simons K et al.** Orm family proteins mediate sphingolipid homeostasis. *Nature* 2010;463(7284):1048-1053.
17. **Kohlwein SD**. Triacylglycerol homeostasis: insights from yeast. *J Biol Chem* 2010;285(21):15663-15667.
18. **Kurat CF, Wolinski H, Petschnigg J, Kaluarachchi S, Andrews B et al.** Cdk1/Cdc28-dependent activation of the major triacylglycerol lipase Tgl4 in yeast links lipolysis to cell-cycle progression. *Mol Cell* 2009;33(1):53-63.
19. **Paradise EM, Kirby J, Chan R, Keasling JD**. Redirection of flux through the FPP branch-point in Saccharomyces cerevisiae by down-regulating squalene synthase. *Biotechnol Bioeng* 2008;100(2):371-378.
20. **Asadollahi MA, Maury J, Moller K, Nielsen KF, Schalk M et al.** Production of plant sesquiterpenes in Saccharomyces cerevisiae: effect of ERG9 repression on sesquiterpene biosynthesis. *Biotechnol Bioeng* 2008;99(3):666-677.
21. **Yazawa H, Iwahashi H, Kamisaka Y, Kimura K, Aki T et al.** Heterologous production of dihomo-gamma-linolenic acid in Saccharomyces cerevisiae. *Appl Environ Microbiol* 2007;73(21):6965-6971.
22. **Kainou K, Kamisaka Y, Kimura K, Uemura H**. Isolation of Delta12 and omega3-fatty acid desaturase genes from the yeast Kluyveromyces lactis and their heterologous expression to produce linoleic and alpha-linolenic acids in Saccharomyces cerevisiae. *Yeast* 2006;23(8):605-612.
23. **Yazawa H, Iwahashi H, Kamisaka Y, Kimura K, Uemura H**. Production of polyunsaturated fatty acids in yeast Saccharomyces cerevisiae and its relation to alkaline pH tolerance. *Yeast* 2009;26(3):167-184.

24. **Yu XH, Prakash RR, Sweet M, Shanklin J**. Coexpressing Escherichia coli cyclopropane synthase with Sterculia foetida Lysophosphatidic acid acyltransferase enhances cyclopropane fatty acid accumulation. *Plant Physiol* 2014;164(1):455-465.

25. **Yu XH, Rawat R, Shanklin J**. Characterization and analysis of the cotton cyclopropane fatty acid synthase family and their contribution to cyclopropane fatty acid synthesis. *BMC Plant Biol* 2011;11:97.

26. **Souza CM, Schwabe TM, Pichler H, Ploier B, Leitner E et al.** A stable yeast strain efficiently producing cholesterol instead of ergosterol is functional for tryptophan uptake, but not weak organic acid resistance. *Metab Eng* 2011;13(5):555-569.

27. **Wallin E, von Heijne G**. Genome-wide analysis of integral membrane proteins from eubacterial, archaean, and eukaryotic organisms. *Protein Sci* 1998;7(4):1029-1038.

28. **Johannsson A, Smith GA, Metcalfe JC**. The effect of bilayer thickness on the activity of (Na+ + K+)-ATPase. *Biochim Biophys Acta* 1981;641(2):416-421.

29. **Pilot JD, East JM, Lee AG**. Effects of bilayer thickness on the activity of diacylglycerol kinase of Escherichia coli. *Biochemistry* 2001;40(28):8188-8195.

30. **Froud RJ, Earl CR, East JM, Lee AG**. Effects of lipid fatty acyl chain structure on the activity of the (Ca2+ + Mg2+)-ATPase. *Biochim Biophys Acta* 1986;860(2):354-360.

31. **Williamson IM, Alvis SJ, East JM, Lee AG**. Interactions of phospholipids with the potassium channel KcsA. *Biophys J* 2002;83(4):2026-2038.

32. **Eroglu C, Brugger B, Wieland F, Sinning I**. Glutamate-binding affinity of Drosophila metabotropic glutamate receptor is modulated by association with lipid rafts. *Proc Natl Acad Sci U S A* 2003;100(18):10219-10224.

33. **Umebayashi K, Nakano A**. Ergosterol is required for targeting of tryptophan permease to the yeast plasma membrane. *J Cell Biol* 2003;161(6):1117-1131.

34. **Bretscher MS, Munro S**. Cholesterol and the Golgi apparatus. *Science* 1993;261(5126):1280-1281.

35. **Ballweg S, Ernst R**. Control of membrane fluidity: the OLE pathway in focus. *Biol Chem* 2017;398(2):215-228.

36. **Auld KL, Brown CR, Casolari JM, Komili S, Silver PA**. Genomic association of the proteasome demonstrates overlapping gene regulatory activity with transcription factor substrates. *Mol Cell* 2006;21(6):861-871.

7. Appendix

7.1. List of figures

7.2. Cover pictures

- The cover picture of **Chapter I** was adopted from the Lipid Builder 3.0 web page. (http://lipidbuilder.epfl.ch/home).

- The cover picture of **Chapter II** was generated with the QuteMol software using the pdb-file fluid.pdb provided online by H. Heller, M. Schaefer and K. Schulten from the Theoretical Biophysics Group of the Beckman Institute at the University of Illinois, Urbana-Champaign, Illinois, USA.
  (https://heller.userweb.mwn.de/membrane/membrane.html)

  Heller H, Schaefer M, Schulten K. Molecular dynamics simulation of a bilayer of 200 lipids in the gel and in the liquid crystal phase. *The Journal of Physical Chemistry* 1993;97(31):8343-8360.

- The cover pricture of **Chapter III** was generated online with the NGL web viewer using the pdb-file 4YMK.pdb containing information on the crystal structure of the stearoyl-CoA desaturase 1 from *M. musculus*.

  Bai Y, McCoy JG, Levin EJ, Sobrado P, Rajashankar KR et al. X-ray structure of a mammalian stearoyl-CoA desaturase. *Nature* 2015;524(7564):252-256.

- The cover picture of **Chapter IV** was generated with the QuteMol software using the pdb-file LMProj.pdb provided online by Gale Rhodes from the Chemistry Department at the University of Southern Maine, Portland, Maine, USA.
  (https://spdbv.vital-it.ch/TheMolecularLevel/BiochemViews/LipMemb/index.html)

- The cover picture of **Chapter IV** was generated with the QuteMol software using the pdb-file 4oo8.pdb containing information on the crystal structure of *S. pyogenes* Cas9 in complex with guide RNA and target DNA.

  Nishimasu H, Ran FA, Hsu PD, Konermann S, Shehata SI et al. Crystal structure of Cas9 in complex with guide RNA and target DNA. *Cell* 2014;156(5):935-949.

7.3. Declaration of own work

Experiments, data analysis, data representation and writing of the thesis were exclusively performed by myself with exception of:

Chapter II

- Main parts of Chapter II were already published in a similar way in Degreif *et al.*, 2017 (section 7.6). Chapter II was complemented with additional data that could not be considered for the publication (Fig. II-2D; Fig. II-4; Fig. II-6B,C; Fig. II-7; Fig. II-8D; Fig. II-9D) or was published as supplemental information.
- Data presented in Fig. II-7B; Fig. II-10B-E, Fig. II-11 and Fig. II-S1 were provided by Dr. Itay Budin.
- Strains SII-22; SII-23; SII-24 and SII-25 were constructed by Rico Ballmann (Bachelor student) under my supervision.

Chapter III

- Strains SIII-4; SIII-7, SIII-10 and SIII-13 were constructed by Thomas Geiger and Milana Kremenovic (Bachelor students) under my supervision.
- Western blot experiments shown in Fig. III-4B and growth experiments shown in Fig. III-S1 were performed with the help of Thomas Geiger (Bachelor student).
- Dr. Itay Budin helped with the GC-MS analyses shown in Fig. III-S2.

Chapter IV

- GC-MS analyses shown in Fig. IV-2B were done by Dr. Itay Budin according to my instructions and by using my yeast strains.
- Construction of strains SIV-5 and SIV-6 was done by Julian Mahr (diploma student) under my supervision.
- The experiments presented in Fig. IV-8 were performed by Dipl.-Biol. Bayram Cucu by using my strains. Experiments were planned together.
- Construction of strains SIV-17 and SIV-19 and the experiment shown in Fig. IV-9A were done by Sophia Heyde (Bachelor student) under my supervision.
- The experiment shown in Fig. IV-10 was done by Chris Sprengl (diploma student) by using my strain background. Experiments were planned together.
- Construction of strains SIV-18 and SIV-21 was done by Eugenia Korotkova (bachelor student) under my supervision.

Chapter V

- Plasmid pCAS9c and data presented in Fig. V-4C were generated by Milana Kremenovic (Bachelor student) under my supervision.

7.4. Conference contributions

Posters

- Symposium on Enabling Technologies for Eukaryotic Synthetic Biology, (EMBL), Heidelberg (Germany), June 2015:

  "***Altered Membrane Lipid Composition in Genetically Engineered Budding Yeast Reveals a Novel Flocculation Pathway.***"

- 27th International Conference on Yeast Genetics and Molecular Biology, Levico Terme (Italy), September 2015:

  "***A Lipid Engineering Approach Reveals a Non-canonical Yeast Flocculation Pathway Mediated by ER Membrane Fluidity.* "**

  "The role of Clc1p and Chc1p in Endocytosis/Exocytosis in Yeast."

- 13th Yeast Lipid Conference, Paris (France), May 2017:

  "***Lipid Engineering in Budding Yeast Reveals Regulatory Roles for Membrane Fluidity in Flocculation and Hypoxic Growth.***"

- 28th International Conference on Yeast Genetics and Molecular Biology, Prague (Czech Republic), August 2017:

  "***Regulatory Roles for Membrane Fluidity in Yeast Flocculation and Hypoxic Growth.*"**

  Best Poster Prize awarded by Current Genetics (Springer International Publishing AG)

Scientific talks

- 12 édition Levures, Modèles & Outils, Bruxells (Belgium), April 2016:

  "***Engineering of Membrane Lipid Composition in Budding Yeast by Employing Titratable Gene Expression Tools.***"

- 34th Small Meeting on Yeast Transport and Energetics, Chania (Crete, Greece), September 2016:

  "***Lipid Engineering in Budding Yeast for Modifying Physicochemical Membrane Properties.***"

7.5. Curriculum vitae

Daniel Degreif

Address	Lippmannstraße 3, 64295 Darmstadt, Germany
Date of Birth	18/01/1989
Place of Birth	Mainz
Nationality	German

EDUCATION

10/2014 – 1/2018 **Technische Universität Darmstadt,** *Darmstadt (Germany)*

- PhD student in the Department of Biology, Yeast Membrane Biology
- Participation in the project "*Molecular mechanisms of endo- and exocytosis in budding yeast*" supported by the Deutsche Forschungsgemeinschaft

10/2012 – 9/2014 **Technische Universität Darmstadt**, *Darmstadt* (*Germany)*

- M.Sc. in Biomolecular Engineering; GPA 1.0 (very good), passed with honors
- Title of the Master's Thesis: "*Engineering the membrane composition of Saccharomyces cerevisiae*" (Advisors: Dr. Itay Budin & Prof. Dr. Adam Bertl), 1.0 (very good)

10/2009 – 9/2012 **Technische Universität Darmstadt**, *Darmstadt* (*Germany)*

- B.Sc. in Biomolecular Engineering, GPA 1.09 (very good), passed with honors
- Title of the Bachelor's Thesis: „*Functional expression of animal ion channels in Saccharomyces cerevisiae*" (Advisor: Prof. Dr. Adam Bertl), 1.0 (very good)

8/1999 – 4/2008 **Integrierte Gesamtschule "Kurt Schumacher"**, *Ingelheim (Germany)*

- High School Graduation Certificate (Abitur), GPA 1.0 (very good)

PRACTICAL EXPERIENCE

1/2014 – 8/2014 **Joint BioEnergy Institute (JBEI) run by the U.S. Department of Energy (DOE), Lawrence Berkeley National Laboratory (LBNL), and University of California, Berkeley (UCB)**, *Emeryville, CA (United States of America)*

- Practical work for Master's Thesis in the laboratory of Prof. Dr. Jay D. Keasling (Fuel Synthesis Division)

3/2009 – 5/2009 **Department of Neurosurgery at the University Medical Center of the Johannes Gutenberg University Mainz**, *Mainz (Germany)*

- Voluntary internship, participated in the project "*Cellular mechanisms of glioblastoma migration and invasion*"; cultivation of human tumor cells; investigation of tumor cell migration using PET-membranes; application of real-time PCR using the Light-cycler system

SCHOLARSHIPS AND AWARDS

1/2014 – 8/2014 **Study Abroad Scholarship by the German Academic Scholarship Foundation** (Auslandsstipedium der Studienstiftung des deutschen Volkes)

2/2012 – 9/2014 **Scholar of the German Academic Scholarship Foundation** (Studienstiftung des deutschen Volkes)

10/2011 – 9/2012 **Scholar of the Germany Scholarship** (Deutschlandstipendium)

- Funded by the Federal Government and BASF SE

12/2012 **Recipient of the Dr.-Anton-Keller-Foundation Award**

- Awarded by the Department of Chemistry at TU Darmstadt for "excellence in Bachelor's Degree in Biomolecular Engineering".

7.6. Publications

Degreif, D., T. de Rond, A. Bertl, J.D. Keasling, and I. Budin. 2017. Lipid engineering reveals regulatory roles for membrane fluidity in yeast flocculation and oxygen-limited growth. *Metab Eng*. 41:46-56.

Cucu, B., **D. Degreif**, A. Bertl, and G. Thiel. 2017. Vesicle fusion and fission in plants and yeast. *Cell Calcium*. 67:40-45.

7.7. Acknowledgements

Hiermit möchte ich mich ganz herzlich bei allen bedanken, die auf jedewede Art und Weise zum Gelingen dieser Arbeit beigetragen haben – sei es durch tatkräftige Unterstützung im Labor, bei der Planung von Experimenten, Interpretation von experimentellen Ergebnissen, ihre pure Anwesenheit und Verbreitung guter Laune, Hilfe bei Organisatorischem aller Art, alle sonstigen Arten der Unterstützung und der Begutachtung dieser Arbeit.

Vielen herzlichen Dank Euch allen, die sich hierbei angesprochen fühlen möchten!

7.8. Ehrenwörtliche Erklärung

Ich erkläre hiermit ehrenwörtlich, dass ich die vorliegende Arbeit entsprechend den Regeln guter wissenschaftlicher Praxis selbstständig und ohne unzulässige Hilfe Dritter angefertigt habe.

Sämtliche aus fremden Quellen direkt oder indirekt übernommenen Gedanken sowie sämtliche von Anderen direkt oder indirekt übernommenen Daten, Techniken und Materialien sind als solche kenntlich gemacht. Die Arbeit wurde bisher bei keiner anderen Hochschule zu Prüfungszwecken eingereicht.

Darmstadt, den 05. Dezember 2017

_____

Daniel Degreif